Assessing the potential of active treatment to improve the environmental quality of landfill waste using multi surface modelling



Waste of time?

Frank van Raffe

PROPOSITIONS

1. Geochemical models are an essential tool to explore element mobility during landfill waste treatment (this thesis)

2. Understanding the fate of ammonium requires insight in chemical and biological processes (this thesis)

3. Carbon sequestration strategies are not sustainable in polluted environments

4. Striving for perfectly fitting models compromises their reflection of reality

5. Zoos are essential in the urban age to keep in touch with nature

6. Propositions are to stimulate debate, rather than to be right.

Propositions belonging to the thesis, entitled

Assessing the potential of active treatment to reduce the environmental impact of landfill waste using multi-surface modelling: Waste of time?

Frank van Raffe

Wageningen, 8 October 2026

Assessing the potential of active treatment to reduce the environmental impact of landfill waste using multi-surface modelling:

Waste of time?

Frank van Raffe

Thesis committee

Promotor
Prof. Dr. R.N.J. Comans
Professor of Soil Chemistry
Wageningen University & Research

Co-promotors
Prof. Dr. T.J. Heimovaara
Professor of Geoscience & Engineering
Technical University Delft

Other Members
Prof. Dr. H. Rijnaarts, Wageningen University & Research
Prof. Dr. P.E. Holm, University of Copenhagen, Copenhagen, Denmark
Dr. E. van Eynde, Joint research centre of the European Commission, Ispra, Italy
Prof. Dr. J.P. Gustafsson, Swedish University of Agricultural Sciences, Uppsala, Sweden

This research was conducted under the auspices of the Graduate School for Socio-Economic and Natural Sciences of the Environment (SENSE)

Assessing the potential of active treatment to reduce the environmental impact of landfill waste using multi-surface modelling:

Waste of time?

Frank van Raffe

Thesis

submitted in fulfilment of the requirements for the degree of doctor
at Wageningen University
by the authority of the Rector Magnificus,
Prof. Dr. C. Kroeze,
in the presence of the
Thesis Committee appointed by the Academic Board
to be defended in public
on Thursday 8 October 2026
at 3.30 p.m. in the Omnia Auditorium

Frank van Raffe

Assessing the potential of active treatment to reduce the environmental impact of landfill waste using multi-surface modelling: Waste of time?

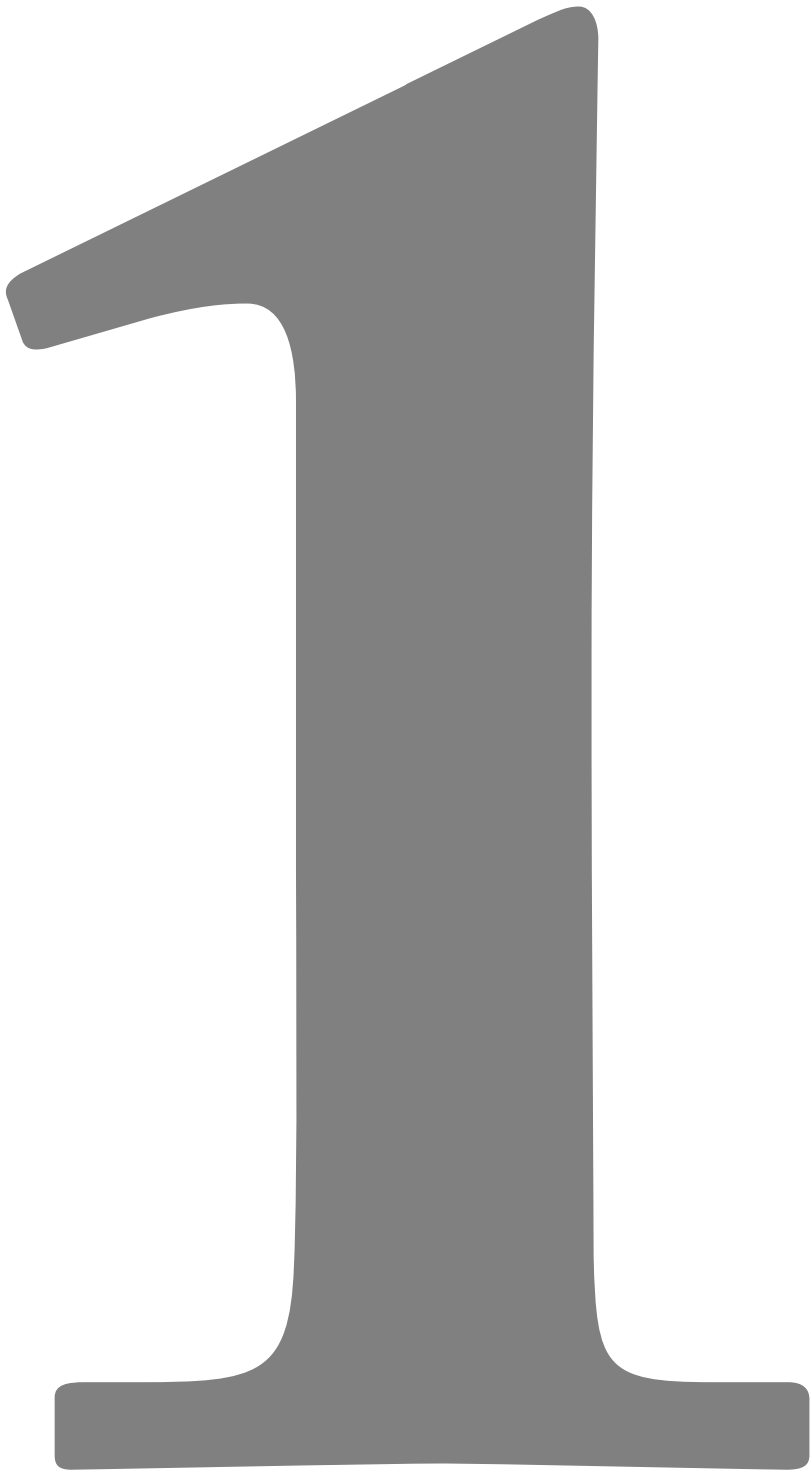
288 pages.

PhD thesis, Wageningen University, Wageningen, the Netherlands (2026)

With references, with summary in English
https://doi.org/10.18174/681159

TABLE OF CONTENTS

Chapter 1	General introduction	7
Chapter 2	Mechanisms controlling the release of inorganic contaminants, organic matter fractions, and ammonium from solid landfill waste: pH dependent leaching experiments and geochemical modelling	23
Chapter 3	Chromium (III) Binding to Purified Fulvic and Humic Acid and its Solid Solution Partitioning and Speciation in Soil	45
Chapter 4	Changing pH, organic matter, and redox state govern contaminant mobility during waste stabilization in landfill simulation reactors	65
Chapter 5	Geochemical processes controlling in-situ contaminant solubility in landfills	87
Chapter 6	General discussion	105
	Supplementary information	127
SI chapter 2		129
SI chapter 3		167
SI chapter 4		189
SI chapter 5		223
Reference list		251
Summary		275
Authorship statement		279
Affiliation of co-authors		281
Acknowledgements		283
About the author		285



Chapter 1

General introduction

Frank van Raffe

1.1. SUSTAINABLE LANDFILLING

Global annual generation of municipal solid waste (MSW) reached 2.1 billion tonnes in 2023, and is estimated to increase to 3.8 billion tonnes by 2050 (United Nations Environment Programme, 2024). The increasing waste production, coupled with a general shift towards sustainability through policy initiatives such as the European Green Deal (Fetting, 2020; Paleari, 2022), has steered governments towards more sustainable waste management options (Scharff, 2014). Governments promote the re-use and recycling of materials rather than incinerating the waste or disposing the waste in landfills (Das et al., 2019; European Parliament and Council of the European Union, 2008), striving towards a circular economy (Pires & Martinho, 2019). Yet problems such as quality degradation (Lee et al., 2014) or concentration of contaminants (Ionas et al., 2014) during material recycling, and the existence of untreatable waste and waste residues, means landfills remain essential as an endpoint for waste. This continuing necessity, and the estimated several 100,000 legacy landfills in Europe alone (J. H. Brand & Spencer, 2024; Nicholls et al., 2021), highlights the importance of sustainable landfill management.

Landfills are the second highest global emitter of the potent greenhouse gas methane (EEA, 2024) and produce leachate with a high concentration of contaminants (Kjeldsen et al., 2002; Moody & Townsend, 2017). Hence, modern sanitary landfills are required to be surrounded by impermeable layers (Council of the European Union, 1999). Gases are thereby captured and either flared or, if of high enough quality, used for energy generation (Yechiel & Shevah, 2016); landfill leachate is captured and, at a cost, treated off-site (J. Gao et al., 2015; Renou et al., 2008). This mode of landfill operation minimizes emissions to the environment, yet the created conditions within the waste body halt waste degradation processes and thereby sustain the environmental threat. Consequently, aftercare costs, i.e. monitoring, leachate treatment, and replacement of impermeable barriers, are passed on to future generations (Scharff et al., 2011; Turner et al., 2017).

To move towards a more sustainable management of landfills, where future generations are no longer burdened by presently generated waste, the Dutch government signed the Green Deal "Sustainable Landfill Management" in 2015 (E. Brand et al., 2016). The Green Deal resulted in three landfill-scale pilot projects to explore active treatment of waste through aeration (Ritzkowski & Stegmann, 2012) or leachate recirculation (Bilgili et al., 2007). Both active treatments aim to accelerate waste stabilization, reducing leachate contaminant concentrations to a level where they adhere to previously derived emission testing values (ETV; (E. Brand et al., 2016; Dijkstra et al., 2018)). At this point, costly aftercare is no longer required, and financial costs are significantly reduced (Berge et al., 2009). The active treatment of the pilot landfills is evaluated via an extensive monitoring programme, including continuous analysis of gas, continuous analysis of leachate quality

and production, and the sampling and characterization of solid waste at the start and end of active treatment.

Reducing leachate contaminant concentrations in the most effective manner requires an understanding of the underlying processes steering the fate of contaminants in the landfill. Acquiring a full understanding is complicated by the complexity of landfills, which are highly heterogeneous in waste composition and contain preferential flow paths (Bareither et al., 2010; Oonk et al., 2013). Consequently, research on landfill-scale active treatment effects focuses mostly on changes in leachate quality (Benson et al., 2007; Brandstätter et al., 2020; L. Liu et al., 2018; Morris et al., 2003). Mechanistic studies, e.g. in landfill simulation reactors, instead have a relatively narrow scope and focus on macro parameters and gas production (Brandstätter et al., 2015a, 2015b; Cerminara et al., 2020; Erses et al., 2008; Fricko et al., 2021a). Mechanistic research on "trace" contaminants such as copper, chromium, or lead is thus largely lacking. To better understand the underlying processes during active treatment, the project "*Coupled multi-process research for reducing landfill emissions*" (CURE) was called into life (Figure 1.1). This thesis specifically focuses on work packages 4 and 5 of CURE, to explore how geochemical models can help better understand the geochemical behaviour of the different contaminants in landfills. In this first chapter, a brief review of relevant background knowledge is given, together with an identification of knowledge gaps that will be further explored in this thesis.

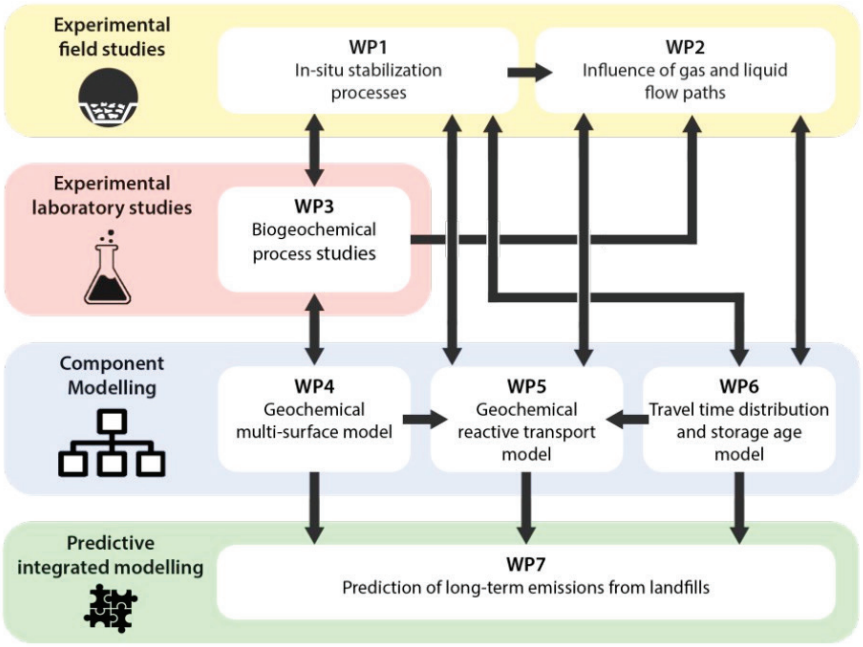


Figure 1.1 Outline of the "Coupled multi-process research for reducing landfill emissions" project which aims to understand the processes underlying reduced landfill emissions via aeration or leachate recirculation of the waste body and in which this thesis is embedded via work package (WP) 4 and 5.

1.2. LANDFILL CONTAMINANTS AND THEIR CHEMICAL SPECIATION

Waste landfill leachate contains a diverse range of contaminants (Eggen et al., 2010), ranging from traditional contaminants such as heavy metals (Baun & Christensen, 2004; Kjeldsen et al., 2002) and well known organic pollutants (Marttinen et al., 2003), to emerging contaminants such as PFAS (Capozzi et al., 2023; Lang et al., 2017; Sabba et al., 2025), microplastics (GodvinSharmila et al., 2023; P. He et al., 2019), and pharmaceuticals (Lu et al., 2016; Masoner et al., 2016). To constrain the scope of this thesis, specific focus will be placed on inorganic contaminants, of which ammonium (NH_4^+) is considered the contaminant of highest concern (Berge et al., 2005; Wijekoon et al., 2022). This scope aligns with the focus of the previously derived ETV (Dijkstra et al., 2018).

The fate of contaminants is linked to their environmental speciation, as contaminants are present in the environment as various chemical species in the dissolved and solid phase (Figure 1.2; Ure & Davidson, 2008). Dissolved species are more mobile (Hemond & Fechner, 2022) and bioavailable (Allen et al., 1980; Parker et al., 1995) and hence pose a larger environmental threat. Knowledge on contaminant speciation additionally provides insights on the steering factors and most prevalent species behind emissions, which can be essential to achieve effective reductions in contaminant emissions. Previous research in soil systems highlighted the importance of pH and the reactive soil surfaces clay, organic matter (OM), and metal (hydr)oxides (Carter et al., 2009; Hernandez-Soriano & Jimenez-Lopez, 2012; Maguire et al., 1981). This importance has been further shown in contaminated matrices, e.g. bottom- and fly ashes (Dijkstra, Van Der Sloot, et al., 2006; Luo et al., 2019; Meima & Comans, 1997, 1998a; Tiwari et al., 2015; H. Zhang et al., 2008), and slags (Loncnar et al., 2016, 2022; Tiwari et al., 2015). The question is whether the same holds true for solid landfill waste.

While the large variety of contaminants in contaminated matrices behaves wildly different, contaminants are typically separated into three distinct groups based on their differences in pH-dependent solubility: non-reactive contaminants, reactive anions, and reactive cations (Hyks et al., 2009; Luo et al., 2019; Van Der Sloot & Dijkstra, 2004; H. Zhang et al., 2008). Non-reactive contaminants, as their name implies, do not react with the solid matrix and hence remain in solution as either a free ion or an inorganic complex. Reactive anionic contaminants preferentially bind to the positively charged surface of metal (hydr) oxides (Adegoke et al., 2013; Cornelis et al., 2008). The binding decreases with increasing pH, as the metal(hydr)oxide surface becomes less positively charged and above the high pH of the point-of-zero charge (~pH 7.5 – 10) turns to an overall negative charge (Kosmulski, 2016). For reactive cationic contaminants binding to (hydr)oxides may similarly be of importance (Dijkstra et al., 2004), yet cations are mostly expected to bind to the pH dependent negatively charged OM (Benedetti et al., 1996). Additionally, (macro) cations

can bind to clay minerals (Barré et al., 2007; Whitworth, 1998), which have a permanent negative charge thanks to isomorphic substitution (Q. Wang et al., 2017). Aside from binding to reactive surfaces, cations and anions are known to form mineral precipitates when the solution is saturated with respect to specific minerals.

All three above-mentioned groups of contaminants are present in landfills, as are the three reactive surfaces. The relatively high OM content of landfills (Östman et al., 2006) means OM binding is likely of high importance compared to more soil-like matrices. Metal (hydr)oxide binding can be of additional high importance even for cationic contaminants, thanks to the generally high pH of landfills (Kjeldsen et al., 2002; Moody & Townsend, 2017). This high pH, together with high contaminant concentrations (Kjeldsen et al., 2002) and CO_2 pressures, also favours the formation of mineral precipitates, including carbonate- and hydroxide minerals (Dijkstra, Van Der Sloot, et al., 2006; Dijkstra, Van Zomeren, et al., 2006; Manning, 2001). Finally, the reducing conditions of landfills likely results in the formation of sulphide minerals (Flyhammar, 1997).

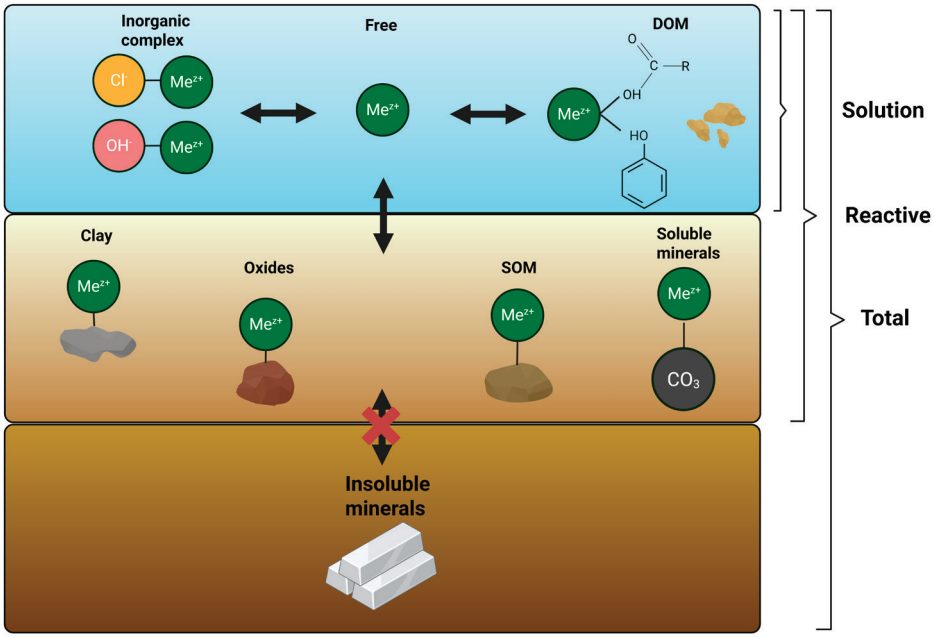


Figure 1.2 An overview of environmental speciation of a metal compound (represented by the green circle "Mez^{+}") between different pools. The solution pool is directly available to organisms and typically considered to pose the biggest environmental threat; the reactive pool contains species which can become available with time or different environmental conditions; the total pool contains species which do not become available.

Landfills often contain high concentrations of NH_4^+, reaching concentrations over 1000 mg/l. The high amounts of OM in the landfill release NH_4^+ upon breakdown (Brandstätter et al., 2015b), which under anaerobic landfill conditions cannot be nitrified and transformed to nitrate (Sahrawat, 2008) and thus accumulate in the leachate. Ammonium is known to bind to clay minerals and specifically the frayed edges of 2:1 clays (Alshameri et al., 2017; Evangelou & Lumbanraja, 2002; Nieder et al., 2011), and to OM (Nommik, 1970; Yin et al., 2022; L. Zhang et al., 2016). The latter may be particularly relevant in the OM dominated landfills, although the binding potential of NH_4^+ to OM is not yet quantified in ion binding models (see section 1.4). In addition to chemical binding, various other processes can be of high relevance in the complex matrix of landfills, among which the precipitation of the mineral struvite (D. Kim et al., 2007; R. Kumar & Pal, 2015), the release of NH_4^+ from waste breakdown (Brandstätter et al., 2015b), nitrification and denitrification (Aharoni et al., 2022; Jianlong & Ning, 2004; Yi et al., 2025), and anaerobic ammonium oxidation (M. Kumar & Lin, 2010; Valencia et al., 2011). These processes have been outlined previously (Berge et al., 2005), but only specific paths have been quantified during active treatment in reactor studies (Brandstätter et al., 2015b; Fricko et al., 2021a), and as such the most effective measures for NH_4^+ reduction remain unknown.

1.3. THE PILOT LANDFILLS AND THE EFFECTS OF ACTIVE TREATMENT

Active treatment of waste landfills has been investigated already for several decades, and its impact on leachate quality and gas production has shown potential. While different forms of active treatment exist, the most common forms are to either re-introduce treated leachate (leachate recirculation) or to introduce air into the landfill (aeration) (Laner et al., 2012). The specific treatments, particularly those of the pilot landfills, and their intended effects will be discussed below. Locations of the pilot landfills, their overall composition, and a graphical depiction of the active treatments are shown in Figure 1.3.

Leachate recirculation is being tested in *the Kragge* landfill, a landfill containing predominantly municipal solid waste. Treated leachate is partly discharged and partly treated in an ANAMMOX water purification system to remove NH_4^+ (Liang & Liu, 2008) before being re-introduced in the landfill together with surrounding groundwater. The system remains anaerobic, and the degradation of waste, and particularly OM, is stimulated via the mixing of microbes present in the landfill and via achieving an optimal moisture content (Reinhart & Al-Yousfi, 1996). During leachate recirculation, gas production has been observed to increase and become enriched in methane (Benson et al., 2007; Erses et al., 2008; L. Liu et al., 2018; Oonk et al., 2013; Šan & Onay, 2001). The improved gas quality increases the efficiency of energy generation, while the enhanced degradation potentially results in an increased reactivity of solid OM and a decrease in dissolved OM concentrations (Olk et al.,

2019). Leachate recirculation stimulates leachate production, which should result in the flushing of (non-reactive) contaminants from the waste body (Benson et al., 2007; Bilgili et al., 2007). While in recirculated landfills NH_4^+ is removed at a more efficient rate due to increased breakdown (Benson et al., 2007), concentrations likely remain high due to the prevailing anaerobic conditions (Berge et al., 2005; Bilgili et al., 2007).

Aeration is being tested in the *Braambergen* landfill (Figure 1.4), a landfill containing predominantly contaminated soil and soil remediation residue, and in the *Wieringermeer* landfill, a landfill containing a mix of commercial, municipal, and construction waste. *Wieringermeer* has continuously been subjected to over-extraction, in which landfill gas is extracted to create a negative pressure and thereby stimulate air entering the landfill; *Braambergen* started with 2 years of overextraction, followed by 2 years of combi-aeration (active gas extraction and ambient air injection), and then continued under overextraction. In both cases, aeration is intended to create aerobic conditions in the landfill, which has known benefits (Rich et al., 2008; Ritzkowski et al., 2006; Ritzkowski & Stegmann, 2012). First and foremost, aerobic degradation of

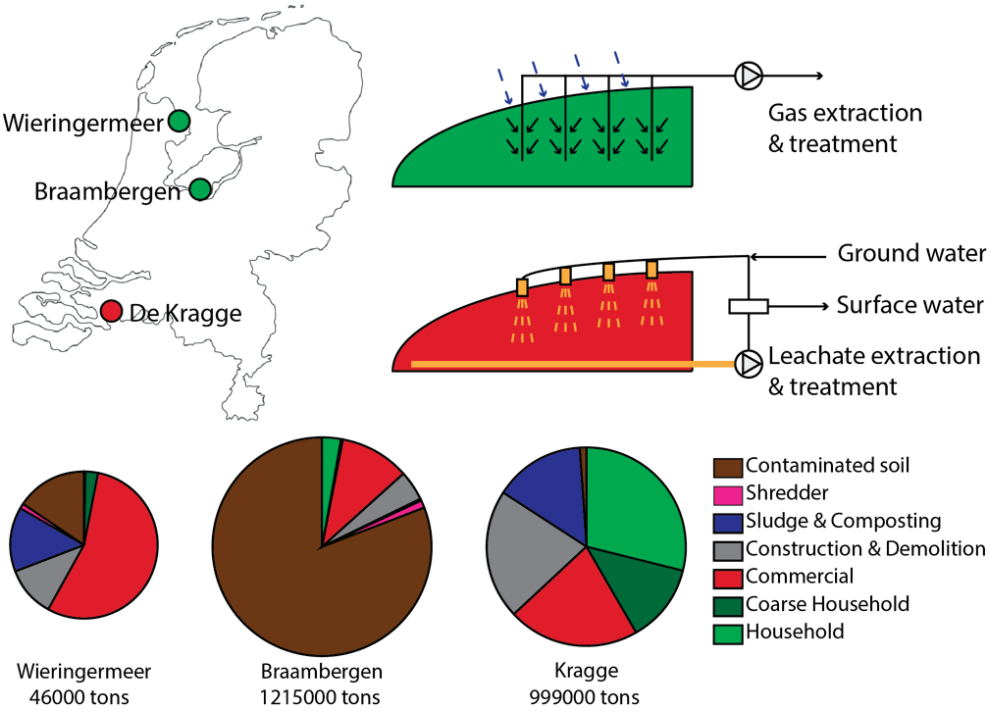


Figure 1.3 a) Locations of the pilot landfills; b) overview of aeration, as applied at Wieringermeer and Braambergen; c) overview of leachate recirculation, as applied at Kragge; d) general composition of the different landfills.

organics is significantly more efficient than anaerobic degradation (Kristensen et al., 1995). An enhanced gas production is thus expected, which for aeration mainly consists of CO_2 instead of methane (Raga et al., 2015; Sohoo et al., 2021). Likewise, an increase in the chemical reactivity of solid OM and a decrease in dissolved OM concentrations can be expected. The enhanced degradation can result in temperature increases up to 70 °C and higher (Raga et al., 2015), potentially enhancing or reducing most biological, physical, and chemical processes. The creation of aerobic conditions dissolves sulphide minerals and thereby releases contaminants into solution, and promotes the formation of metal (hydr)oxides which provide a new binding surface for contaminants (Caille et al., 2003; Dewey et al., 2023; Li et al., 2024). Finally, an important benefit of creating aerobic conditions is the potential to transform NH_4^+ to nitrate via nitrification (Sahrawat, 2008; Zeng et al., 2012). This NH_4^+ transformation, coupled with denitrification in anaerobic zones to transform nitrate to nitrogen gas, means aeration is a potentially efficient method of N removal from landfills (Dang et al., 2023; Hao et al., 2010).

The above effects have been established based either on studies in media other than landfill waste, i.e. soils and sediments, or based on measurements of only gas production and leachate quality in treated landfills or, more commonly, landfill simulation reactors. The exact changes in the solid waste during active treatment therefore remain unknown. Furthermore, while changes in the chemical environment during active treatment are hypothesized and, in part, have been measured previously (P. J. He et al., 2006; Ritzkowski et al., 2006; Sanphoti et al., 2006), their exact influence on the geochemical behaviour of contaminants and their resulting concentrations in landfill leachate is currently unknown.



Figure 1.4 The aeration infrastructure present at the Braambergen landfill.

1.4. GEOCHEMICAL MODELLING OF ENVIRONMENTAL MEDIA

A core component of this thesis is the multi-surface geochemical model (Di Bonito et al., 2024), which is a tool to calculate the environmental speciation discussed in section 1.2. Several geochemical models exist, including VISUAL-MINTEQ (Gustafsson, 2022), PHREEQC (US EPA, 2009), and the software used in this thesis: ORCHESTRA (Meeussen, 2003). Each model has a similar functionality, where separate ion binding models – used to calculate binding to clay, OM, and metal (hydr)oxides – are combined with an underlying thermodynamic database to calculate the formation of inorganic complexes and mineral precipitates.

Various ion binding models exist for each of clay, OM, and metal (hydr)oxides. Ion binding models are typically parameterized by conducting independent adsorption experiments of elements in the presence of a purified material, e.g. illite for clay (Gu & Evans, 2007), humic- or fulvic acid for OM (Oste et al., 2002; Otero-Fariña et al., 2023; J. Xu et al., 2016), and goethite (Antelo et al., 2005) or ferrihydrite (Gustafsson & Antelo, 2022; Mendez & Hiemstra, 2020) for metal (hydr)oxides. The results of these adsorption experiments are subsequently used to derive independent binding parameters. As described below, for most widely studied elements these datasets have typically been combined to derive "generic" parameters which are universally applicable. Although the models mostly function on a similar basis, the underlying theory and purified materials from which their parameters have been derived vary. Calculations on clay binding often assume characteristics of the 2:1 clay illite, which is the most common clay mineral in temperate soils (Barré et al., 2007; Van Der Salm et al., 1998), and binding is often calculated either based on electrostatic interactions using Donnan-type models or via ion-exchange selectivity coefficients (Evangelou & Phillips, 2018). Metal (hydr)oxide binding calculations commonly assume binding solely to iron (hydr)oxides, taking characteristics either of the amorphous ferrihydrite or more crystalline goethite to calculate binding to (de)protonated (hydr)oxide groups. Metal (hydr)oxide ion binding models include the generalized two-layer model (Dzombak & Morel, 1990; Karamalidis & Dzombak, 2010; Mathur & Dzombak, 2006) and the CD-MUSIC model (Hiemstra & Van Riemsdijk, 1996). Finally, models for calculating the binding to OM generally use reactive humic substances (HS) as a model compound: particularly humic acid (HA) and oftentimes fulvic acid (FA). While the existence of HS is a subject of debate due to their operational definition (Hayes & Swift, 2020; Kleber & Lehmann, 2019; Lehmann & Kleber, 2015), their distinct chemical characteristics have proven suitable to predict environmental speciation (e.g. Dijkstra et al., 2009; Gustafsson et al., 2014; Klinkert & Comans, 2020; Otero-Fariña et al., 2023; Xiong et al., 2013). Ion binding models for binding to organic matter include the Stockholm Humic Model (Gustafsson, 2001), Model VI/VII (Tipping, 1998; Tipping et al., 2011), and the NICA-Donnan model (Kinniburgh et al., 1996). All these models consider the heterogeneity inherent to HS by pa-

rameterizing binding to both carboxylic- and phenolic acids together with the existence of either multiple sites or a "non-ideality" parameter for each surface group to represent a distribution in binding affinities.

Multisurface geochemical models have been applied for different environmental media, including (contaminated) soils (Dijkstra et al., 2004; Uddh-Söderberg et al., 2024; Van Eynde et al., 2020; Wiersma et al., 2025), sediments (Canavan et al., 2007), composts (Klinkert & Comans, 2020), ashes (Dijkstra, Van Zomeren, et al., 2006; Luo et al., 2019; Meima & Comans, 1997; H. Zhang et al., 2008), slags (Loncnar et al., 2022), and solid waste (Van Der Sloot et al., 2017). These applications were oftentimes successful, yet samples were characterized *ex*-situ using select chemical extractions. Underlying processes are thus likely disturbed, and relevant aspects, such as the prevailing *in-situ* redox state, are not always adequately considered. Considering that reducing conditions likely prevail in landfills and are expected to be of high importance in the overall contaminant behaviour (section 1.2), the question arises whether *in-situ* characterisation and subsequent modelling is a feasible alternative.

Another important aspect when discussing the quality of geochemical modelling is the quality of the underlying parameter set, as these are intrinsically linked. For a multitude of inorganic contaminants, the parameters for OM binding have been derived from several datasets (Milne et al., 2003) and have been thoroughly evaluated. Yet for two contaminants which currently do not meet the ETV, i.e. NH_4^+ and Cr (Dijkstra et al., 2018), this is not the case. As previously mentioned, NH_4^+ is typically assumed to bind to clay; while binding to HS has been observed this has not yet been quantified. For Cr HS-binding parameters do exist yet are based on limited or no experimental data; this has previously resulted in poor model predictions (Koopmans & Groenenberg, 2011). Hence, these parameters should be improved to better understand the behaviour of NH_4^+ and Cr, particularly in contaminated systems such as landfill leachates where these contaminants are not compliant with environmental limit values.

1.5. THESIS OBJECTIVES

This thesis' objective is to better define the geochemical mechanisms controlling contaminant leaching from solid waste and how these mechanisms can be used to further understand the effects of aeration and leachate recirculation on landfill leachate concentrations. A large knowledge base already exists on mechanisms driving element solubility, yet knowledge on the most relevant mechanisms within solid waste landfill bodies is nearly absent. The intention of this thesis is to first develop this knowledge from controlled laboratory studies, similar to what has been done for other contaminated

matrices, and subsequently apply this to samples that are representative of actual field conditions. The objectives of this thesis are thus as follows:

1. Establish the geochemical mechanisms controlling the leaching of relevant inorganic contaminants, organic matter, and ammonium extracted from solid landfill waste.
2. Improve the binding parameter set of ammonium and chromium, to enable more accurate geochemical modelling and ultimately improve our understanding of underlying processes that control their solubility in landfills.
3. Understand how active treatment of landfill waste via aeration and leachate recirculation affects the mechanisms underlying contaminant solubility and the consequent leaching of contaminants from solid waste.
4. Determine the vertical heterogeneity of contaminant concentrations in landfill pore water, and assess the applicability of lab-derived underlying geochemical mechanisms in predicting the field pore water concentrations.

1.6. THESIS STRUCTURE

To achieve the listed objectives, this thesis is divided into 6 chapters. This includes the current general introduction (**chapter 1**), four content chapters, and a synthesis chapter. Each content chapter constitutes part experimental work and part modelling work and is devoted towards answering one (or several) of the research objectives. An overview of the different content chapters is given in Figure 1.5.

In **chapter 2**, the underlying geochemical mechanisms behind contaminant leaching from untreated waste are explored using pH dependent tests in conjunction with geochemical modelling. Specific focus is placed on the different types of contaminants mentioned in section 1.2, as well as on dissolved organic matter and ammonium. The results of this controlled lab experiment address **objective 1** and form the basis for all subsequent chapters

In **chapter 3**, improved NICA-Donnan binding parameters for Cr are derived to fulfil **objective 2**. Adsorption experiments of chromium to humic- and fulvic acid are conducted and the free ionic chromium species is determined, which was previously discovered to be significantly underestimated by the commonly used generic parameter set. Fitting software is used to derive improved binding parameters, which are validated

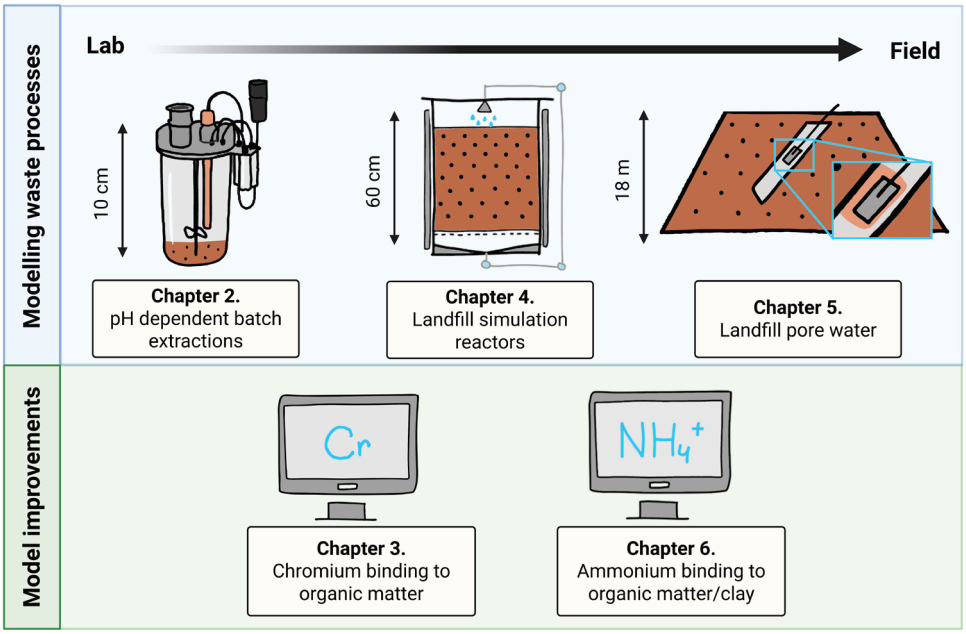


Figure 1.5 An overview of the general thesis, which is separated between investigation of geochemical processes (blue) and improvement of the used geochemical model (green). This graphical overview was created in

against independent data sets of chromium binding to humic acid, free chromium in water extracts, and water extractable chromium.

In **chapter 4**, the changes in contaminant leachate concentrations during aeration and leachate recirculation are investigated in landfill simulation reactors to answer **objective 3**. Results are modelled by defining a set-up in three steps: 1) modelling pH dependent tests, similar to **chapter 2**; 2) modelling water extracts of solid waste sampled from the reactors during operation; 3) modelling leachate flowing out of the landfill simulation reactors. The model approach, initially set up in **chapter 2**, is expanded to better evaluate how contaminant leachate is affected by aeration and/or leachate recirculation.

In **Chapter 5**, pore water in the recirculated *Kragge* landfill is investigated for its chemical composition, to answer **objective 4**. A novel pore water monitoring system is installed to take samples in the saturated and unsaturated zone across a vertical transect. The geochemical model, set up in **chapters 2 and 4**, is applied with assumed properties of the solid waste to establish the relevant geochemical processes of the field situation.

In **Chapter 6**, the content of **chapters 2 to 5** is synthesized and placed in the context of reducing contaminant leachate concentrations during active treatment. A reflection is made of the limitations and implications of the research. **Objectives 3 and 4** are further explored by discussing the trends in leachate concentration from the different actively treated landfills studied in the CURE project. **Objective 2** is completed by discussing an improved modelling description of ammonium. Finally, this thesis' results are outlined against the emission target values (E. Brand et al., 2016; Dijkstra et al., 2018), to evaluate the previously derived values and the feasibility of adhering to the set limits within the foreseen project duration.

2

Chapter 2

Mechanisms controlling the release of inorganic contaminants, organic matter fractions, and ammonium from solid landfill waste: pH dependent leaching experiments and geochemical modelling

Frank van Raffe, Joris J. Dijkstra, Rob N.J. Comans

Published as:

van Raffe, F., Dijkstra, J. J., & Comans, R. N. (2025). Mechanisms controlling the release of inorganic contaminants, organic matter fractions, and ammonium from solid landfill waste: pH dependent leaching experiments and geochemical modelling. *Applied Geochemistry*, 106503.

ABSTRACT

With the intention of making landfilling more sustainable, three full-scale projects have been set up to investigate the effects of leachate recirculation and aeration on the stabilisation of contaminants. Prior to this (an)aerobic stabilisation, solid waste was sampled from all three landfills to identify the mechanisms behind contaminant leaching and stabilization, as a reference point for evaluation of the treatment effects at a later stage of the project. Processes underlying the leaching of a wide range of inorganic contaminants were identified using a combined approach of pH dependent leaching experiments, organic matter fractionation, and geochemical modelling. We additionally focused on organic matter, being an important surface controlling the leaching of inorganic elements, and ammonium, for which compliance with intended environmental limit values for sustainable landfill management is challenging for many landfills. Three types of pH dependent leaching behaviour could be identified for the investigated elements: non-reactive behaviour, anionic behaviour, and cationic behaviour. Reactive elements, including ammonium, showed maximum dissolved concentrations around the upper and lower ends of the pH range, while leaching of non-reactive elements was pH independent. Organic matter became increasingly soluble with increasing pH, while its relative composition became increasingly enriched in fractions reactive for metal binding, most notably humic acid, only for the most organic landfill. The organic signature of the waste samples, together with their varying organic matter content, resulted in distinct differences in leaching behaviour between landfills. These differences result from the seemingly strong influence of organic matter on the pH at which minimum solubility of elements occurs, being lower for elements with higher organic matter binding affinity, an effect being more pronounced for more organic-rich samples. The model, based on independently determined generic sorption parameters, provided adequate descriptions of most elements, yet arsenic and ammonium were poorly described due to mechanisms not captured by the model while chromium was inadequately described due to limitations of the current binding parameters. As the three landfills have been shown to differ strongly with respect to waste properties (e.g. organic versus. inorganic) an important outcome of this study is that landfill-specific combinations of proposed treatment strategies (aeration, leachate recirculation) are necessary to reduce the leaching of specific contaminant groups to below limit values and are anticipated to be most effective for less mature landfills characterized by a lower ratio of solid to dissolved OM.

2.1 INTRODUCTION

In striving towards more sustainable waste management, many governments are striving to decrease the fraction of waste ending up in landfills, e.g. the waste hierarchy of the European Waste Framework directive proclaiming preferring re-use and recycling over disposal (European Parliament and Council of the European Union, 2008). Nevertheless, landfills remain necessary for untreatable waste and residues. Landfills are a long-term environmental threat due to gaseous emissions and the generation of leachate rich in (in)organic contaminants, which – if not properly managed – can enter the underlying soil and pollute ground- and surface waters (Kjeldsen et al., 2002; Moody & Townsend, 2017; Powell et al., 2016; Siddiqua et al., 2022). To prevent this pollution, landfill closure is in many countries followed by legally prescribed "eternal" aftercare, which involves leachate treatment and the placement of artificial barriers to restrict flow (Laner et al., 2012; Scharff et al., 2011). Eternal aftercare is perceived an unsustainable practice, which shifts its associated costs to future generations. In an effort to explore more sustainable practices in the Netherlands, a so-called "Green Deal" was signed between the Dutch government, the Dutch Sustainable landfill Foundation, and landfill operators in 2015 (E. Brand et al., 2016). This agreement instigated three landfill-scale projects in 2016, which investigate the effects of long-term "active treatment" on existing landfills, i.e. leachate recirculation (Reinhart & Al-Yousfi, 1996) and/or aeration (Ritzkowski & Stegmann, 2012). The intended effect of this treatment, which is anticipated to last for 10 years, is to reduce contaminant concentrations in the leachate through flushing, degradation, or retention in the solid phase. If effective, the emission potential of the landfill is expected to be reduced and thus its aftercare period significantly shortened (Berge et al., 2009; Rich et al., 2008). The embedding of the projects within the Green Deal and a large associated research programme ensures an extensive monitoring programme of emissions in the leachate and gas phase, together with sampling and characterization of the solid waste at the beginning and end of the treatment period. This approach results in the acquisition of a large data set, with high temporal resolution, over an extended period of active treatment on a landfill scale. Ultimately, leached contaminant concentrations need to comply with legally derived site-specific emission target values for the projects to be a success and for the landfills to be released from their aftercare (E. Brand, 2014; E. Brand et al., 2016; Dijkstra et al., 2018).

Taking effective steps in reducing contaminant leaching, and having a scientific underpinning that the thus obtained reductions are sustainable, requires an understanding of the underlying processes. The determination of leaching behaviour at different pH levels has proven its value in the identification of leaching processes in both natural materials (Cappuyns & Swennen, 2008; Carter et al., 2009; Dijkstra et al., 2004, 2009; Uddh-Söderberg et al., 2024) and waste materials (Astrup et al., 2006; Cappuyns & Swennen, 2008; Dijkstra, van der Sloot, et al., 2006; Komonweeraket et al., 2015; Quina et al., 2009; Van

Der Sloot et al., 2017; H. Zhang et al., 2008). As shown in several of these studies, further identification of underlying mechanisms can be accomplished through complementary geochemical modelling to calculate the speciation of targeted elements by taking into account mineral formation and adsorption to different reactive surfaces. This complementarity has previously allowed for the distinction of elements showing three different types of environmental behaviour: non-reactive, anionic, and cationic (Hyks et al., 2009; Luo et al., 2019; Van Der Sloot & Dijkstra, 2004; H. Zhang et al., 2008). While elements with non-reactive behaviour are characterized by a limited interaction with the solid matrix and hence no pH dependence, elements with anionic and cationic behaviour both show a maximum in dissolved concentrations at the upper and lower ends of the pH range; the minimum solubility occurs around pH 5 for anions and at variable but higher pH for elements with cationic behaviour. This behaviour is related to the pH dependent charge and solubility of metal (hydr)oxides and organic matter (OM), protonation and hydrolysis of the element, and precipitation of mineral forms. Cations and particularly anions can strongly bind to metal (hydr)oxides (Brandely et al., 2022; Gustafsson & Antelo, 2022; Tiberg et al., 2020), which shift from a positive net surface charge below the point-of-zero charge (PZC) to a negative net charge above the PZC (Hiemstra & Van Riemsdijk, 2009; Kosmulski, 2016), resulting in enhanced cation adsorption and decreased anion adsorption with increasing pH. The solubility of these metal (hydr)oxides increases below pH 5 and above pH 8 (X. Liu & Millero, 1999), where their (partial) dissolution results in a release of adsorbed ions into solution. Cations can furthermore strongly bind to OM, which has a negative charge already at low pH and becomes increasingly negatively charged with increasing pH (Milne et al., 2001; Van Zomeren et al., 2009). The enhanced solubility of OM with increasing pH (Dijkstra et al., 2009) results in an increased solubility at higher pH for cations with an affinity for OM binding. Additionally, protonation of anions at low pH – reducing their negative charge – and increasing complexation of cations with hydroxyl ions (OH^-) at high pH – reducing their positive charge – generally reduces binding for elements of both groups to these reactive surfaces and partially off-sets the aforementioned effects of pH on their adsorption. Finally, potentially solubility controlling mineral phases of several anions typically have a solubility minimum around pH 5, e.g. Wulfenite ($PbMoO_4$; (Conlan et al., 2012; Vlek & Lindsay, 1977)); for cations, the pH at which potentially solubility controlling minerals are stable varies, yet for common hydroxide and carbonate minerals is generally above pH 7.

To our knowledge, the combination of pH dependent leaching, detailed organic matter fractionation as a function of pH, and geochemical modelling has not previously been applied to landfilled solid waste. The high OM content present in landfill waste (Östman et al., 2006) is expected to result in a high importance of OM solubility. The OM solubility is known to be strongly affected by pH (Dijkstra et al., 2004, 2009), yet a thorough investigation of the pH dependent solubility of specific OM fractions relevant for element binding, i.e. humic acid (HA) and fulvic acid (FA) (Hayes & Swift, 2020), has to our knowl-

edge so far only been published for municipal solid waste incinerator bottom ashes (Dijkstra, Van Zomeren, et al., 2006). In addition, geochemical modelling calculations were found to be most sensitive to the description of OM binding properties in soil with varying organic matter contents, ranging from 0.3 – 12 % (Wiersma et al., 2025). Instead, oftentimes general assumptions are made regarding the reactive fraction of OM (e.g. 50% of dissolved OM (DOM) is HA (Dijkstra et al., 2009) or 100% of DOM is FA (Uddh-Söderberg et al., 2024)), while the DOM composition is likely to shift with changing pH considering the differences in pH-dependent solubility between thehumic fractions (Van Zomeren & Comans, 2007). Additionally, there have not yet been any published investigations on the pH dependent solubility of ammonium (NH_4^+) from landfilled waste, despite that it is considered one of the contaminants of highest concern in landfill waste. Ammonium accumulates in the leachate due to constant release during waste degradation and the lack of a removal pathway under anaerobic conditions (Berge et al., 2005). The generally high NH_4^+ concentrations in the leachate require major reductions to comply with the current emission target values (E. Brand et al., 2016). Insights into the mechanisms that control NH_4^+ partitioning between the solid waste and leachate are thus of major importance to enable the development of effective measures to reach the defined target values.

This study explores the underlying geochemical processes governing contaminant release from solid waste of three different landfills, using the combined methodology of pH dependent tests with geochemical modelling. Particular focus is placed on the solubility of OM and its reactive HA and FA subfractions, enabling novel insights in the speciation of these important fractions and enabling a more complete model parametrization as opposed to the commonly made assumptions, as well as on NH_4^+. To this end, waste samples from all three landfills were taken prior to the start of active treatment. Similar sampling will be conducted at the conclusion of the pilot to investigate the development of waste stabilization and improvement of leachate quality. The solid waste was subjected to pH-dependent tests, where underlying mechanisms were further explored using geochemical modelling. Ultimately, the insights gained through the results of this study are linked to prospects of reducing environmental emissions in the three different landfill pilots based on different treatment strategies.

2.2. MATERIALS AND METHODS

2.2.1. Solid waste samples

The sampling procedure developed for this project is outlined in detail in Lammen et al. (2019). In short, waste sampling was conducted at the start of the pilot experiments in 2016 and 2017 for all three pilot landfills, a thorough description of which is given by Yi et al. (2025): Braambergen 11 north (Bra), which was landfilled from 1999 until 2008 with predominantly contaminated soil, soil remediation residues, and construction and

demolition (C&D) waste, and which was subjected to aeration starting from 2017; Kragge (Kra), which was landfilled from 1997 until 2007 with predominantly commercial and domestic waste as well as C&D waste, and which was subjected to leachate recirculation starting from 2018; Wieringermeer (Wie), which was landfilled from 1992 until 2003 with predominantly commercial waste, composting waste, and contaminated soils, and which was subjected to aeration starting from 2017. Due to the large scale of the pilot compartments (4, 5, and 3 ha for Bra, Kra, and Wie, respectively) and the large heterogeneity inherent to landfill waste, large amounts of waste had to be properly sampled, homogenized, and pre-treated to obtain the highest representativeness that was practically achievable. Consequently, 12 boreholes were drilled per landfill compartment in vertical steps of 2 metres using a Sonic Samp drill with a diameter of 88 mm. All landfills are covered with a layer of top soil. For Wie the first two metre drilling was discarded to not include this top soil, whereas for Kra and Bra this drilling was included as the shallower top soil layer of these landfills (~1 metre compared to 2 metres for Wie) meant a significant portion of the first drilling consisted of waste. Inclusion of the cover layer likely slightly "diluted" the top samples of Kra and Bra, as the cover layer has a relatively lower content of inorganic elements and reactive surfaces. The samples were mixed at three different depth intervals (dubbed "top", "mid", and "bot"), resulting in 9 "mixed" samples total (Table 2.1). Data on landfill depth and solid waste characteristics are presented in Table 2.1. After mixing, samples were pre-treated to fulfil experimental criteria – namely a particle size <4 mm – using sieves and a shredder. Portions of 20 kg of the waste were stored at -18 °C until waste characterization and leaching tests as described below.

2.2.2. Waste characterization

2.2.2.1. pH static leaching test

The pH static leaching test (NEN-EN 14997, 2015) characterizes the leaching of contaminants as a function of pH. In short, fresh samples, conserved for 5 years at -18 °C, were extracted with ultrapure water (UPW) at a UPW/waste ratio of 10 L/kg in 8 parallel batches at pre-defined pH values. This was done through continuous automatic addition of acid (HCl) or base (NaOH) to vary the pH between 2 – 12; one batch was extracted at the natural pH (i.e. no acid/base addition). Contrary to preliminary experiments (Lammen et al., 2019; Van Raffe et al., 2021), HCl was used instead of HNO_3 in order to not disturb the speciation of NH_4^+ in the leachates (see Results section). Samples were equilibrated for 48 hours under continuous stirring, and subsequently filtered (0.45 µm) before determining a wide range of inorganic elements using Inductively Coupled Plasma Mass Spectrometry (ICP-MS) and Optical Emission Spectrometry (ICP-OES) in acidified filtrates. Organic and inorganic dissolved carbon (Skalar San++ segmented flow analyser), chloride, and ammonium (Discrete Analyzer) were determined in unacidified filtrates. Dissolved OM was further fractionated into HA, FA, hydrophilic acid (Hy), and hydrophobic neutrals (HON) using the rapid batch fractionation method (ISO 12782-5, 2012; Van Zomeren & Comans,

2007). While only HA and FA are assumed to contribute to element binding, Hy and HON are determined for complete OM characterization.

Table 2.1 Characteristics of the analyzed waste.

Landfill	Layer	Depth	Natural pH	SHA[a]	SFA[a]	HFO[b]	DHA[c]	DFA[c]
		[m - surface]	[-]	[g C/kg]	[g C/kg]	[g/kg]	[mg C/l]	[mg C/l]
Braambergen[d]	Top	0 - 4	7.85	2.26	0.02	17.88	0.03	3.01
Braambergen	Mid	4 - 8	7.5	1.24	0.34	18.75	0.05	10.79
Braambergen	Bot	8 - 12	7.5	0.67	0.36	17.35	0.00	12.08
Kragge[d]	Top	0 - 6	7.5	5.21	0.46	18.75	1.19	15.00
Kragge	Mid	6 - 12	7.5	4.09	0.80	27.72	13.76	51.02
Kragge	Bot	12 - 16	7.45	4.38	1.03	25.53	13.61	66.03
Wieringermeer	Top	2 - 6	7.75	1.76	0.26	14.12	0.08	5.19
Wieringermeer	Mid	6 - 10	7.55	3.80	0.44	15.38	0.42	16.83
Wieringermeer	Bot	10 - 14	7.75	2.80	0.46	12.62	0.55	19.85

[a]Solid humic acid and solid fulvic acid, determined according to (ISO 12782-4, 2012)

[b]Hydrous ferric oxide, calculated using the amount of amorphous (ISO 12782-1, 2012; ISO 12782-3, 2012) and crystalline (ISO 12782-2, 2012) iron and aluminium (hydr)oxides.

[c]Dissolved humic acid and dissolved fulvic acid, measured at natural pH according to (ISO 12782-5, 2012)

[d]Including approximately 1 m of cover soil

2.2.2.2 Solid waste characteristics

The solid phase was further analysed for several parameters required for the geochemical modelling. Solid HA, FA, Hy, and HON were estimated using the rapid batch fractionation method (ISO 12782-4, 2012; Van Zomeren & Comans, 2007). Crystalline and amorphous/nanocrystalline iron (Fe) (hydr)oxides were estimated using a dithionite extraction (DCB) (ISO 12782-2, 2012). Amorphous/nanocrystalline Fe and aluminium (Al) were estimated after an ascorbic acid (asc) extraction (ISO 12782-1, 2012) and an ammonium oxalate (AmOx) extraction (ISO 12782-3, 2012) respectively. Geochemically reactive amounts of contaminants were estimated using the 0.43 M HNO_3 extraction (Groenenberg et al., 2017; ISO 17586, 2016).

2.2.3. Geochemical modelling

Geochemical modelling was conducted akin to the modelling approach of Dijkstra et al. (2004) but with important differences regarding, amongst others, the representation and parameterization of solid and dissolved organic matter, as described below. Element speciation – including binding to DOM, binding to solid reactive surfaces (Fe- and Al (hydr)oxides, OM, clay), and mineral precipitation/dissolution – was calculated in the ORCHESTRA framework (Meeussen, 2003). Specifics on the used binding models and their relevant inputs are outlined below. General inputs consisted of the fixed setpoint pH, pe (assuming pH + pe = 12, implying overall oxidizing conditions based on preliminary evaluation of pH-dependent leaching behaviour of the redox sensitive elements Fe and Mn and the observed absence of sulphidic conditions in most samples), dissolved concentrations of background solutes, and the total reactive concentration of the to-be-modelled element. Compared to Dijkstra et al. (2004) a more elaborate approach was followed in which elements were each modelled in separate model runs, instead of all elements simultaneously in a single model run. This approach allows for more accurately taking competition effects into account between the element under study and other elements competing for sorption sites. To this end, the to-be-modelled element had its input set to the total reactive amount; the background dissolved concentrations of all other major elements and competing elements were fixed to their measured dissolved concentrations.

Adsorption to Fe- and Al (hydr)oxides was modelled using the generalized two-layer model (Dzombak & Morel, 1990). This approach combines the separately measured amounts of Fe/Al (hydr)oxides into one proxy: hydrous ferric oxide (HFO). Al is combined with Fe due to the limited database of binding parameters for Al (hydr)oxides (Meima & Comans, 1999), and is assumed to behave similarly to Fe oxides (Karamalidis & Dzombak, 2010; Mathur & Dzombak, 2006). As such, amorphous Al and Fe (hydr)oxides (as measured using the AmOx and asc extraction, respectively) are recalculated assuming a molar ratio of 95 g Fe/mol HFO and 84 g Al/mol HFO (Hiemstra & Van Riemsdijk, 2009), and assigned a reactive surface area of 600 m^2/g (Dzombak & Morel, 1990). Crystalline oxides are calculated by subtracting the amorphous/nanocrystalline (hydr)oxides from DCB extractable (hydr)oxides, and recalculated assuming a molar ratio of 89 g Fe/mol HFO and 78 g Al/mol HFO, and assigned a reactive surface area of 100 m^2/g (Dijkstra et al., 2009; Van Eynde et al., 2020). Total HFO was subsequently corrected for binding to SOM and DOM, based on separate model calculations, and for mineral dissolution, based on dissolved Fe and Al as measured in the pH dependent test and assuming dissolution of amorphous (hydr) oxides. Alterations of the binding affinities listed by Dzombak & Morel (1990) are adopted from the following studies: for the elements lead (Pb) (Meima & Comans, 1998a), antimony (Sb) (Meima & Comans, 1998b), molybdenum (Mo) (Gustafsson, 2003), Fe(II), and carbonic acid (Appelo et al., 2002).

Adsorption to OM was modelled using the NICA-Donnan model (Kinniburgh et al., 1996). Model inputs consisted of solid HA, solid FA, dissolved HA, and dissolved FA according to their measured concentrations. All fractions were assumed to have a carbon content of 50% (Pribyl, 2010). In general, element binding was calculated using the generic binding parameters derived by Milne et al. (2003, 2001). Fe binding to FA was calculated using the binding parameters of Hiemstra and Van Riemsdijk (2006), Tin (Sn) binding to HA was calculated using the binding parameters of (Dijkstra et al., 2009), and Pb binding to FA and HA was calculated using the binding parameters of Xiong et al. (2013). Furthermore, vanadium (V) was set to only form the reduced V(III), which is known to be prevalent in organic environments and to bind strongly to OM (Gustafsson, 2019).

Controlling mineral phases were determined based on preliminary modelling calculations. In a first step, saturation indices (SI) were calculated for all minerals in the MINTEQV4 database together with additional potentially solubility controlling minerals (see Table S2.1 for a list of added minerals, and their reaction equations in ORCHESTRA) with pH, pe, and dissolved concentrations of elements, HA, and FA as model input. If for at least one pH value the SI was between -1 and 1, the mineral was considered potentially solubility controlling. In a next step, minerals were selected based on their likelihood of presence and/or formation under landfill conditions. Finally, potentially solubility controlling minerals were individually modelled to test how adequately they explained the experimentally observed pH dependent behaviour. An overview of ultimately considered minerals – predominantly carbonate, hydroxide, and silicate minerals – and altered parameter values are given in Table S2.2.

Preliminary modelling, assuming a significantly overestimated clay content of 20% based on unpublished data, and using a Donnan approach according to Dijkstra et al. (2009, 2004), showed clay to be of little importance on modelled pH dependent leaching patterns (Figure S2.1), in agreement with previous studies (Dijkstra et al., 2004). Therefore, electrostatic adsorption to clay was not further taken into account for this study.

2.3. RESULTS & DISCUSSION

2.3.1. Waste homogeneity and vertical heterogeneity

A preliminary experiment, in which pH was adjusted with HNO_3 instead of HCl (Van Raffe et al., 2021), showed chloride (Cl) to remain stable for all landfills and layers across the entire pH range (Figure 2.1). With Cl being a fully mobile element the limited pH dependent effects are expected, yet the relatively invariant concentrations between each of the parallel batches of the pH dependent test are an indication of the effectiveness of the sample homogenization strategy. Additionally, the consistently lower Cl concentration in each landfills' top layer gives first insights into leaching mechanisms. This lowered

concentration may be partly due to inclusion of the relatively Cl-poor cover soil, yet as this soil was discarded for the Wie landfill this is not the sole reason. Presence of older waste of different composition in the deeper layers can be an alternative explanation, yet this would also result in different concentrations in deeper layers for other elements, e.g. Al or Zn, while this is not found. Lower concentrations in the top layers are in some cases also found for other poorly reactive elements, i.e. potassium (K) for Kra and Wie and sulphur (S) for Bra (Figure S2.2), as well as DOM and associated elements (as discussed in the following sections). Based on the above considerations, this feature is interpreted as a depletion from the top layer due to down flushing and subsequent accumulation in deeper layers.

2.3.2. pH-dependent leaching behaviour and speciation

The measured pH-dependent leaching is depicted for major and trace elements together with corresponding modelling predictions (Figures 2.2, 2.6, & S2.3) and for OM fractions (Figure 2.4 & Figure S2.26). The calculated solid- and dissolved phase speciation of selected elements for the Kra landfill is shown in Figure 2.3; solid phase speciation is divided between adsorption to the different reactive solid surfaces and mineral formation; dissolved phase speciation is divided between the free cation or anion in solution, all inorganic species including protonated forms, and adsorption to dissolved HA and FA. Detailed speciation graphs for all elements and all three landfills and their different layers are present in the SI (Figures S2.4 – S2.25). A thorough evaluation of all measured substances shows that the three typical types of leaching behaviour, i.e. non-reactive, anionic, and cationic, can also be distinguished for these landfill samples, as further outlined below.

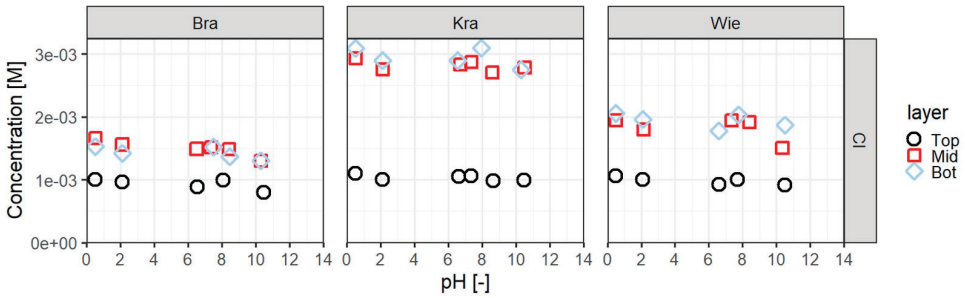


Figure 2.1 Concentration of chloride as a function of pH for all three landfills and all three depth intervals, measured in a preliminary experiment in which HNO_3 instead of HCl was used as acid for pH control.

2.3.2.1. Non-reactive behaviour

Elements with non-reactive behaviour are characterized by a pH independent leaching pattern, which can be observed for Cl (Figure 2.1) and to some extent for K, Li, and S (Figure S2.2). This pH independence is related to the limited interactions of these elements with the solid waste matrix, resulting in only limited differences between the landfills and landfill layers.

2.3.2.2. Anionic behaviour

Anionic behaviour is observed for the elements Mo (Figure 2.2), arsenic (As), phosphorus (P), and Sb (Figure S2.3). The multi-surface model describes this behaviour adequately for Mo and Sb, predicting the formation of Wulfenite ($PbMoO_4$ (Conlan et al., 2012; Vlek & Lindsay, 1977)) at low pH and particularly for Bra and Wie which are characterized by a lower content of reactive surfaces compared to Kra. At higher pH the model predicts the adsorption to Fe/Al (hydr)oxides for both anions, together with a shift between the free ion and inorganic complexes of Mo in the dissolved phase (Figures 2.3, S2.4, and S2.12). The model adequately describes the solubility of P at high pH (Figure S2.3), predicting the precipitation of Ca-phosphate (Figure S2.13), while the pH dependent solubility is inadequately described at low pH. Note that P in Kra shows a more pronounced anionic behaviour compared to Wie and Bra, particularly in the middle and bottom layer. This is likely related to stronger dynamics of OM for these layers, as described below, enhancing competition with P for binding sites and solubilizing organic P (Curtin et al., 2016; McLaren et al., 2015; Y. Yan et al., 2023). For As the model inadequately predicts a cationic behaviour (with a minimum solubility around pH 8) with solely binding to Fe/Al (hydr) oxides (Figure S2.11), instead of the observed anionic behaviour. This cationic behaviour was previously ascribed to the possibly incomplete description of competitive adsorption by other ions such as phosphate and fulvic acids (Dijkstra et al., 2009), the latter being even more likely in these highly organic landfill environments with correspondingly high fulvic acid concentrations, as described below.

2.3.2.3. Cationic behaviour

Cationic behaviour can be observed for Al, barium (Ba), calcium (Ca), cadmium (Cd), cobalt (Co), chromium (Cr), copper (Cu), Fe, magnesium (Mg), manganese (Mn), nickel (Ni), Pb, silicon (Si), Sn, Strontium (Sr), V, and zinc (Zn) (Figures 2.2 and S2.3). The pH at which the concentration minimum occurs is variable; the cationic contaminants in Figures 2.2 and S2.3 are ordered from top to bottom based on the pH at which the solubility minimum is observed. The position of this minimum is the net result of the affinity of the metal for OM, tending to push the solubility minimum to lower pH to follow the pH-dependent solubility of OM (Figure 2.4), as described below, and its tendency to form metal hydroxyl species and (hydr)oxide minerals, pushing the solubility minimum to a higher pH. This apparent interplay is supported by the geochemical model (Figure 2.3), where for example the higher pH solubility minimum of Mg compared to Cu corresponds with a predicted

reduced binding of Mg to OM and a higher prevalence of inorganic hydroxy and carbonate species in the dissolved phase. The influence of OM is further corroborated when comparing the different landfills; the solubility minimum occurs for most elements at significantly lower pH for the Kra landfill compared to the other landfills (e.g. for Cu: pH 7 for Kra, pH 8 for Wie and Bra), related to the relatively high content of OM in the Kra. The Bra landfill, which has a relatively low content of reactive surfaces, instead shows a relatively large importance of mineral dissolution/precipitation, e.g. for Cu (Figure S2.6), which is reflected in the solubility minimum occurring at relatively high pH. The large variation in OM content and OM solubility between the samples in this study allows for a distinction between elements based on their relative OM binding affinity and hydrolysing potential within the cationic group.

The geochemical model mostly predicts the pH dependent leaching behaviour of the elements showing cationic behaviour adequately (Figures 2.2 and S2.3), including the corresponding shift in solubility minimum with changing OM affinity. Chromium, known to strongly bind to OM when present as Cr(III) (Fukushima et al., 1995; Gustafsson et al., 2014; Milne et al., 2003; Wen et al., 2018), i.e. the expected form in the reduced conditions and high OM contents of a landfill (Choppala et al., 2018; Jardine et al., 2011, 2013; Rai et al., 1989), has a solubility minimum around pH 6 (Figure 2.2). The pH dependent behaviour of Cr is, however, poorly predicted by the model. Poor model descriptions for Cr(III) have been observed previously and have been attributed to inadequate OM binding parameters (Koopmans & Groenenberg, 2011). These currently available binding parameters have been derived by linear free energy relationships based on the first hydrolysis constant of Cr, rather than from actual binding experiments (Carbonaro & Di Toro, 2007; Milne et al., 2003) and are currently considered to overestimate the binding affinity (Koopmans & Groenenberg, 2011). While improved binding parameters have been derived for the Stockholm Humic Model (Gustafsson et al., 2014), an adequate Cr binding parameter set for NICA-Donnan does not yet exist. Dijkstra et al. (2009) found an adequate model description of Cr leaching from soil samples, by assuming 50% of DOM consisted of reactive humic substances and assuming that both reactive DOM and particulate OM could be represented by "generic" HA in the model. Contrary to the work of Dijkstra et al. (2009), in the current study the reactivity of DOM is based on measured concentrations of HA and FA. Introducing both HA and FA was previously found to result in an overestimated Cr binding dominated by FA (Koopmans & Groenenberg, 2011). This may also explain our poorer model description compared to Dijkstra et al. (2009). The adequate modelling of other elements preferentially binding to OM, as discussed later, further emphasizes the specific inadequacy of the used Cr-FA binding parameters.

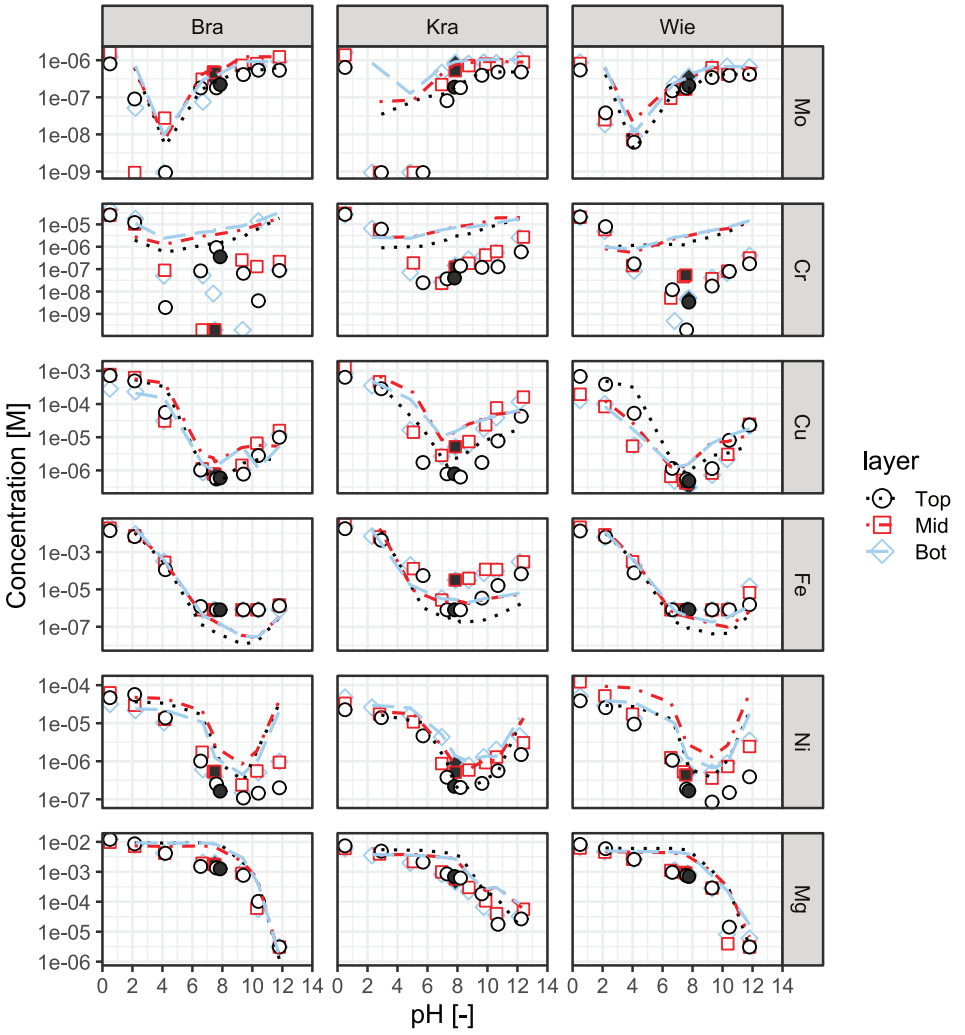


Figure 2.2 Concentration of selected major and trace elements as a function of pH for each landfill and depth interval, measured experimentally (markers) and as calculated through multi-surface geochemical modelling (lines). Samples without pH adjustment are coloured dark grey.

Cu shows a concentration minimum at a pH of around 7, slightly higher than for Cr, which is adequately predicted for Bra and Wie by the model yet slightly overestimated for Kra (Figure 2.2). The predicted solid phase speciation shifts from solely binding to solid OM (SOM) towards binding to metal (hydr)oxides around neutral pH and the precipitation of mineral forms ($Cu(OH)_2$) at high pH (Figures 2.3 & S2.6). The relative contribution of SOM is highest for Wie; while the SOM content is higher for Kra than Wie, the higher reactive Cu concentration of Kra has likely resulted in a higher SOM site occupancy and shift towards lower-affinity sites, which, together with the relatively higher oxide content of Kra, result in the increased contribution of metal (hydr)oxides. Further modelling with a 10 times lower Cu concentration for Kra resulted in a shift toward a higher contribution of SOM binding (data not shown), confirming the significant effect of Cu loading to the relative contribution of these two reactive surfaces. In the dissolved phase, binding to DOM prevails above pH 6 for all landfills (Figures 2.3 & S2.6), and remains key in controlling the pH dependent solubility.

A concentration minimum around pH 8 can be observed for Fe, which in the solid phase is predicted to be predominantly present in the mineral form ferrihydrite and in the dissolved phase predicted to be bound to DOM with inorganic hydroxide species dominating >pH 10 (Figure S2.7). The previously described shift of minimum solubility towards lower pH for Kra is well-pronounced for Fe, owing to its high binding affinity

specifically for FA (Hiemstra & van Riemsdijk, 2006). Ni binds to Fe/Al (hydr)oxides across the pH range in the solid phase, while in solution DOM binding is only of importance for Kra and the other landfills show predominantly inorganic hydroxide species formation (Figure S2.8). In the presence of the higher amounts of DOM and SOM in Kra, the prediction of Ni at high pH is substantially better than in Wie and Bra. Mg shows only limited binding to the solid phase, instead precipitating as the mineral magnesite above pH 8 and brucite above pH 9; in the dissolved phase Mg is predominantly present as free ion (Figure S2.9), except above pH 9-10 where inorganic hydroxide, carbonate, and sulphate species are becoming more important, as well as binding to dissolved HA and FA for Kra. The decreasing binding affinity to OM of these elements again fully reflects the shift in the solubility minimum in Figure 2.2.

2.3.2.4. Organic matter

The pH dependent solubility of OM and its reactive fractions also show anionic behaviour (Figures 2.4 and S2.26). With the reactive fractions of OM having a variable negative charge, the charging behaviour of metal (hydr)oxides and (de)protonation of OM, resulting in decreasing binding with increasing pH, largely explain the observed behaviour. The deprotonation of OM at high pH further results in an increased repulsion between constituent molecules in particulate OM and consequently an increased solubility (Weng, Temminghoff, & Van Riemsdijk, 2002b), while the low calcium (Ca) concentrations at high

pH (Figure S2.3) reduce OM coagulation rates (Kloster et al., 2013; Wall & Choppin, 2003). The increased solubility at high pH is paired with an absolute increase in the "reactive" components of the DOM (Hayes & Swift, 2020; Olk et al., 2019) for Kra, becoming particularly enriched in HA. For Bra and Wie the relative composition of DOM remains rather invariant across the entire pH range except at pH 2, with a slight enrichment in dissolved

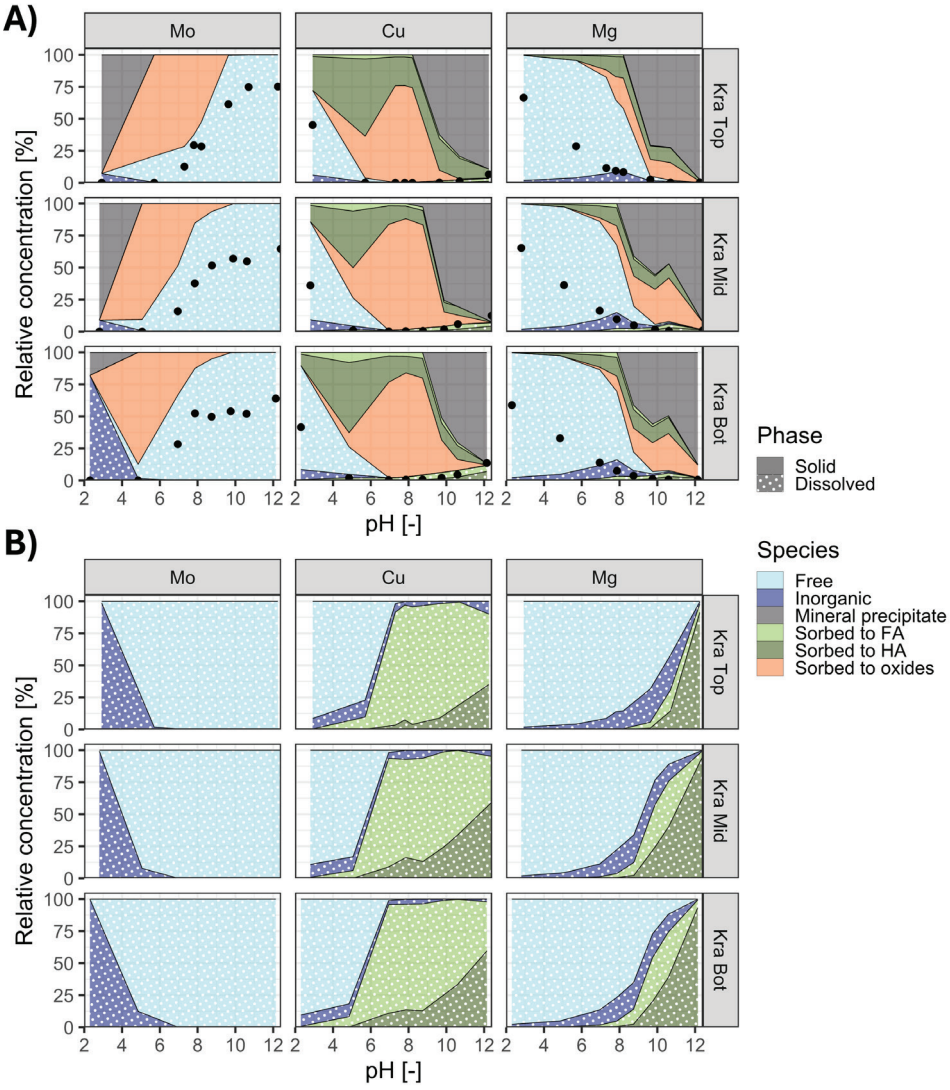


Figure 2.3 A) Model calculated solid and dissolved phase speciation of molybdenum (Mo), copper (Cu), and magnesium (Mg) as a function of pH for the different layers of the Kragge landfill. Measured dissolved concentrations are represented by the black circles; B) Dissolved phase speciation of Mo, Cu, and Mg as a function of pH for the different layers of the Kragge landfill. Solid colours represent solid species, white-dotted colours represent dissolved species. Shown mineral precipitates are PbMoO4 (Mo), Cu(OH)2 (Cu), Magnesite (Mg; pH 9 – 10), and Brucite (Mg; above pH 10).

HA at high pH for Wie. The relative enrichment in HA at high pH is related to its lower charge density compared to FA (Milne et al., 2001; Van Zomeren & Comans, 2009) and its higher susceptibility to Ca-induced coagulation relative to FA, Hy, and HON (Kloster et al., 2013; Weng, Temminghoff, & Van Riemsdijk, 2002b). The increasing concentration of DOM from pH 4 to pH 2 are associated with metal (hydr)oxide dissolution for which HA and FA have a strong binding affinity (Bao et al., 2022; Y. Xu et al., 2020). All landfills show significantly lower DOM concentrations in the top layer, again an indication of potential down-flushing and/or enhanced degradation due to air intrusion.

The observed pH-dependent solubility of OM fractions allows further insight into the validity of often used assumptions for geochemical modelling, e.g. 50% of DOM being HA (Dijkstra et al., 2009) or 100% of DOM being FA (Gustafsson et al., 2014; Uddh-Söderberg et al., 2024). The relatively constant amount of reactive fractions across all pH levels of 40% (Bra) or 50% (Wie) closely follows the assumption of 50% of DOM being reactive, yet considering this reactive fraction to be HA leads to the application of erroneous parameter values as FA was found to be the most prevalent

reactive fraction (Milne et al., 2003). Assuming 100% of DOM to consist of FA would attribute correct parameter values yet instead overestimate DOM reactivity for these samples. Furthermore, the share of reactive fractions is significantly lower for all samples at pH 2, while for Kra at higher pH the share of reactive fractions is significantly higher and dominated by HA. Hence, assuming an invariant reactivity percentage of DOM when modelling across such an extensive pH range is invalid, particularly for more organic rich samples. The implications of using these simplified assumptions are further investigated through two additional modelling scenarios: 1) assuming measured reactive SOM is all HA, and assuming 50% of measured DOM is HA; 2) assuming measured reactive SOM is all HA, and assuming 50% of measured DOM is FA. Results for Cr, Cu, and Pb are highlighted in Figure 2.5, with results for all elements listed in Figure S2.27. The assumption of 50% HA, without consideration of Cr binding to FA, significantly improved predictions of Cr solubility (Figure 2.5), consistent with the observed overestimated Cr binding to FA discussed above. Nevertheless, predictions remain poor relative to Dijkstra et al. (2009), which may be related to the different nature of HA in these waste samples relative to HA in soils. Limited effects were found for Cu (Figure 2.5), and for most other elements (Figure S2.27). Assuming 50% of DOM to be HA resulted in a lower Cu solubility at high pH; assuming 50% of DOM to be FA instead resulted in overestimations. Finally an assumption of 50% of DOM being HA resulted in significantly worsened predictions for Pb (Figure 2.5), as is also the case for Cd and Zn (Figure S2.27); assuming 50% of DOM to be FA instead showed little effects. While the often used assumptions are thus shown to have limited effects only for most elements, for specific elements considerate impacts can be observed. Additionally, assumptions can have consequences on the calculated speciation, e.g. a predicted larger

portion of Cu being bound to reactive surfaces around neutral pH when assuming 50% of DOM is HA compared to assuming 50% of DOM is FA (Figure S2.28).

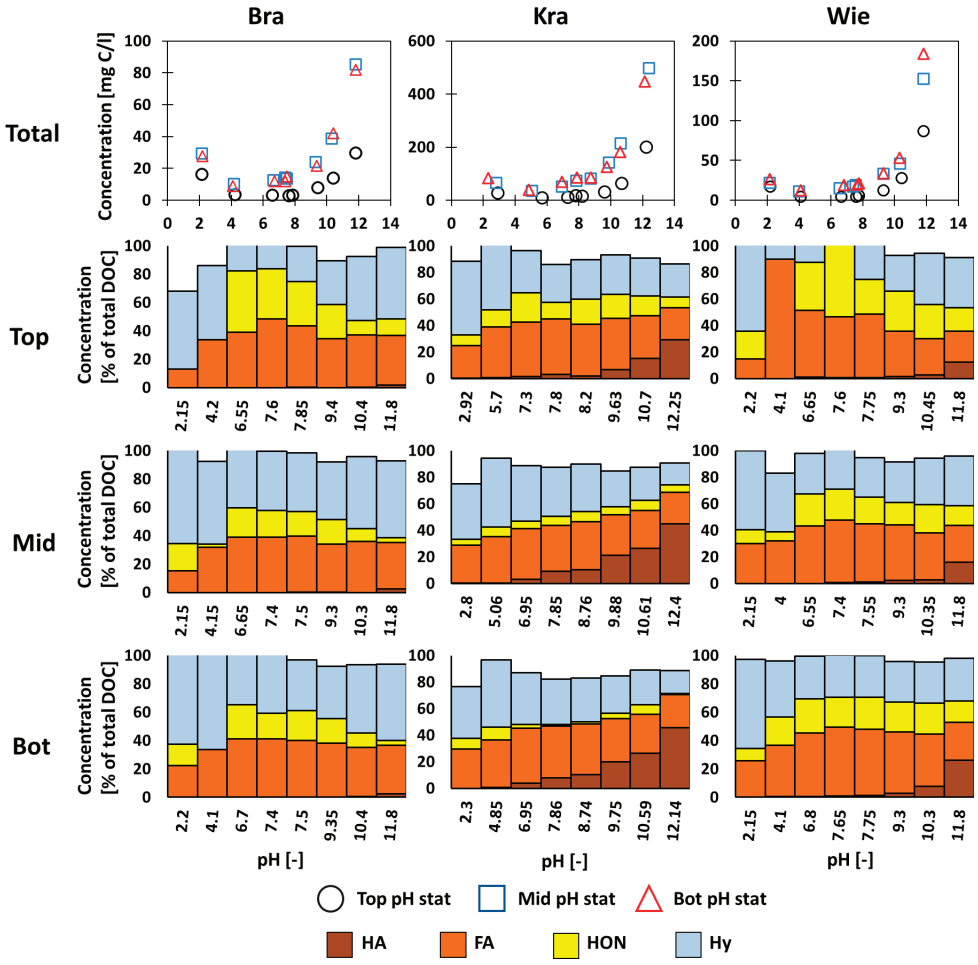


Figure 2.4 Concentration of dissolved organic matter (upper panels) and of its subfractions (as a percentage of total DOC) as a function of pH for each landfill and each depth interval. Note the difference in y-axis scale in the upper panels for total DOC concentrations in the three landfills. Also note that the sum of all DOC subfractions for some samples exceeds 100% relative to separately measured total DOC, or in certain cases is considerably less than 100%; in both cases this is likely due to analytical uncertainty.

2.3.2.5. Ammonium

The pH dependent leaching of NH_4^+ is akin to that of a reactive cation and shows a concentration minimum of generally around pH 7, and around pH 10 for the middle and bottom layer of Kra (Figure 2.6). The most organic layers, i.e. the middle and bottom layer of Kra, have significantly higher NH_4^+ concentrations than Bra and Wie. The top layers of all

three landfills have consistently lower concentrations, a sign of down flushing of NH_4^+ or nitrification due to air intrusion. While a clear pH dependence is observed experimentally, the model predicts non-reactive behaviour (Figure 2.6). Monovalent ions such as NH_4^+ in soils are predominantly associated with clay minerals (Alshameri et al., 2017; Nieder et al., 2011; Nommik & Ahtras, 1982). While electrostatic binding to clay mineral surfaces is not taken into account in the present model, a hypothetical clay content of 20% was found to have little effect on the predicted pH dependent behaviour of NH_4^+ in preliminary model calculations that included electrostatic binding to clay minerals (Figure S2.1).

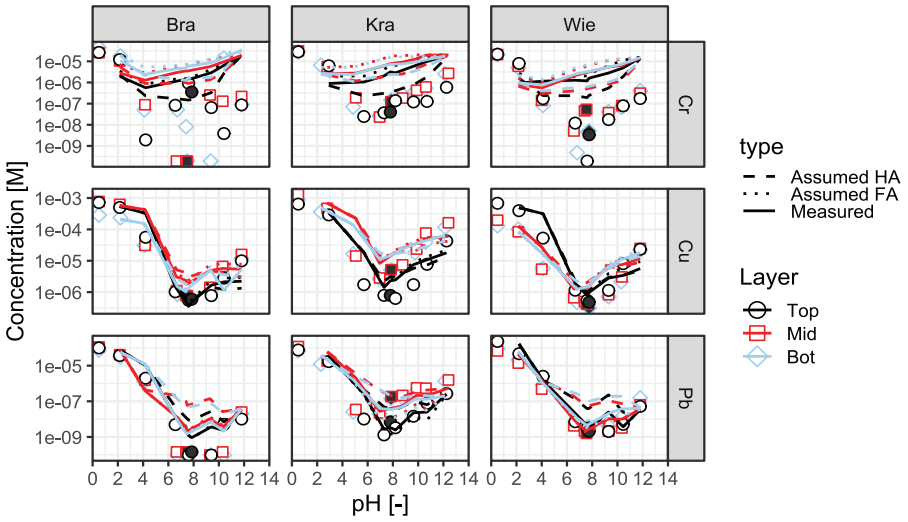


Figure 2.5. Concentrations of chromium, copper, and nickel as a function of pH for each landfill and each depth interval, measured experimentally (markers) and as calculated through multi-surface geochemical modelling using measured dissolved and solid HA and FA as input (solid lines), or assuming 50% of dissolved OM is HA (dashed lines) or FA (dotted lines). Samples without pH adjustment are coloured dark grey.

The discrepancy between model and experiment indicates that processes explaining the NH_4^+ behaviour are not sufficiently incorporated in the model. This can particularly concern potential binding to OM (Nommik, 1970; Nommik & Ahtras, 1982; L. Zhang et al., 2016), selective binding to the frayed edges of 2:1 clay minerals such as vermiculite or illite (Bruggenwert & Kamphorst, 1979; Evangelou & Lumbanraja, 2002; Nieder et al., 2011), or precipitation of minerals other than struvite which was already considered in the current modelling approach (D. Kim et al., 2007; R. Kumar & Pal, 2015). Furthermore, nitrification may play a role, as this process has a maximum potential around pH 8 in soils (Sahrawat, 2008; Shammas, 1986) coinciding with the observed concentration minimum (Figure 2.6). Nevertheless, $NO_3 + NO_2$ concentrations remained constant over the entire pH range (data not shown), suggesting that nitrification during the leaching test is unlikely. The

potential role of nitrification was further investigated through a time-dependent leaching test (section SM2.1 in the SI) of which the results form a further indication that the experimentally observed pH dependent leaching pattern is more likely to be the result of sorption processes than of nitrification (Figure 2.7). If nitrification is the cause of the pH-dependent behaviour, constantly decreasing concentrations with time are expected at neutral pH while concentrations are expected remain constant at high and low pH where nitrification is inhibited. Instead, NH_4^+ concentrations significantly increased at the upper and lower ends of the pH range, and remained relatively unchanged around neutral pH (Figure 2.7). This observation may indicate that rather than nitrification, sorption processes control the pH dependent solubility of NH_4^+ and are currently significantly underestimated by the model. Desorption from the solid phase is observed at conditions unfavourable for sorption, i.e. low and high pH, and the observed increase is consistent with time-dependent concentration patterns previously observed by Dijkstra, Van Der Sloot, et al. (2006).

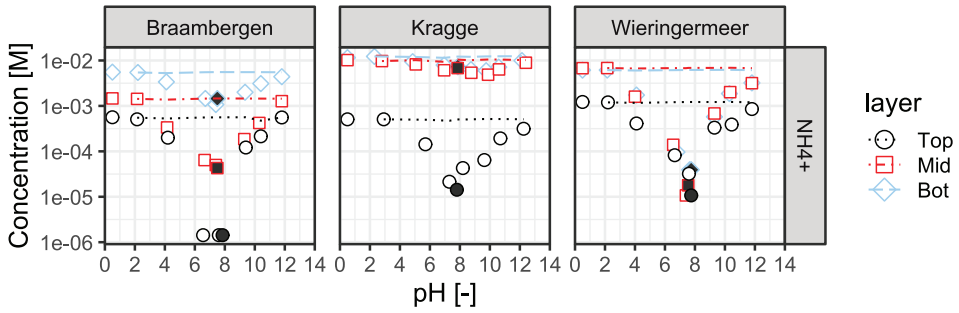


Figure 2.6 Concentration of ammonium as a function of pH for each landfill and each depth interval, measured experimentally (markers) and as calculated through multi-surface geochemical modelling (lines). Clay was not considered in the modelling calculations.

2.3.3. Implications for active treatment of landfill waste

The elaborate characterization of *in-situ* sampled waste from three different depth intervals in the three pilot landfills of this study was conducted to explain observed differences in leaching behaviour between landfills, and identify underlying mechanisms controlling leaching of individual elements. As such, this study is meant to provide a baseline that can give direction on how active treatment can be most effectively used to decrease contaminant concentrations in the leachate. The three categories previously identified in different environmental media, i.e. non-reactive behaviour, anionic behaviour, and cationic behaviour, were also identified here for landfill waste. In general, the two treatment approaches, i.e. active treatment by leachate recirculation or aeration, are expected to affect these three contaminant categories differently. Leachate recirculation promotes the throughflow of water and flushing of non-reactive salts and DOM with associated cations from the major flow paths in the waste body. Observable lower

concentrations in the top layer of these elements (Figure 2.1) already seem to confirm this flushing effect through decades of rainwater infiltration prior to sampling and the start of active treatment. Furthermore, both aeration and leachate recirculation are expected to stimulate degradation of particularly easily degradable OM, being most effective during aeration (Ritzkowski & Stegmann, 2012), and ultimately resulting in more stable and humic-like OM with a relative enrichment in FA and particularly HA and a consequently enhanced reactivity of SOM towards metal binding and reduced DOM concentrations (Olk et al., 2019). Additionally, the enhanced aerobic conditions of the aeration treatment likely result in further Fe(II) oxidation and (neo-)formation of Fe/Al (hydr)oxides (Schwab & Lindsay, 1983). Consequently, both treatments are expected to increasingly stimulate the retention of elements that strongly adsorb to reactive organic and metal (hydr)oxide surfaces in the solid matrix, while their mobilization through adsorption to and competition with DOM (Weng et al., 2011) is reduced e.g. Mo (Figure S2.4), Cu (Figure S2.6), Ni (Figure S2.8), and Pb (Figure S2.17). The magnitude of active treatment effects may differ between landfills based on the relative importance of these reactive surfaces as observed in the present study. The observed ratio of SOM to DOM in the investigated landfills may already represent different maturation stages, where more mature waste is considered to have a relatively high amount of SOM compared to DOM. Based on our results, Kra can be considered the least mature waste, followed by Wie and Bra. The magnitude of active treatment effects may thus decrease in this order, where particularly for contaminants with a high affinity for OM leachate concentrations may decrease proportionally to the achieved enhancement of the SOM/DOM ratio.

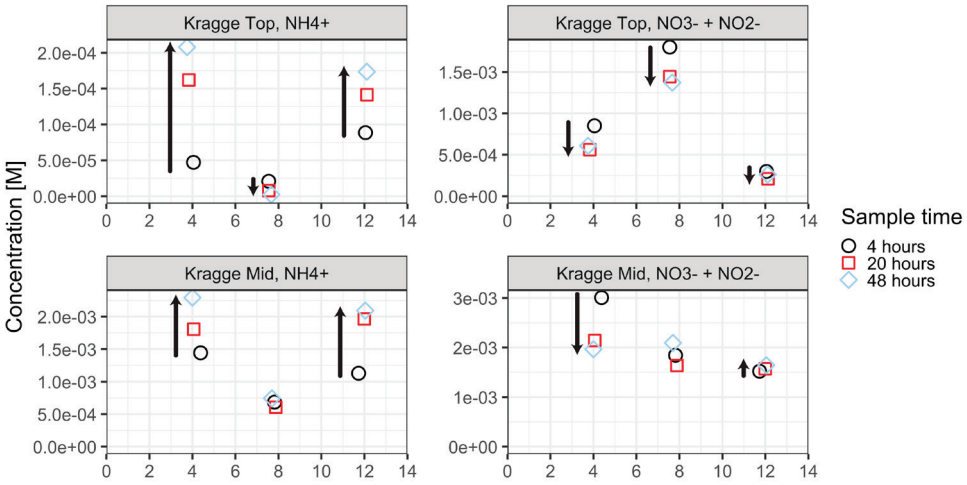


Figure 2.7. Concentrations of ammonium and nitrate + nitrite as a function of pH for the top and middle layer of the Kragge landfill, measured as a function of pH (markers). Arrows indicate the change in concentrations with time at the specific pH levels.

Interpreting these results, particularly in the context of active treatment, does require consideration of the used methodology. In the present study, waste was sampled from the landfill and directly homogenized. While this has proven to be an effective tool to identify geochemical mechanisms, translating results to the field requires consideration of waste heterogeneity and preferential flow paths in the landfill. Assessment of actual in-situ effects of active treatment requires additional temporal monitoring of landfill leachate and pore water composition (Aharoni et al., 2017; Dahan et al., 2009).

2.4. CONCLUSIONS

Landfilled solid waste samples – sampled from three landfills of different waste origins, at three different depth intervals, and homogenized to acquire representative samples – were characterized on their geochemical leaching behaviour. pH static leaching experiments showed reactive elements, including ammonium, had maximum solubility at highest and lowest pH. The pH of the solubility minimum varied for cationic elements, which resulted from the interplay between the binding affinity for organic matter (OM) and the tendency of the element to form hydroxy species and mineral precipitates. This effect was emphasized for more organic-rich landfills. Increasing pH resulted in increased OM solubility, where the dissolved OM of the most organic landfill became increasingly dominated by humic substances and particularly humic acid with increasing pH. The geochemical model mostly adequately predicted this behaviour, however arsenic and ammonium were poorly predicted, presumably due to binding mechanisms not captured by the model. Poor predictions were also obtained for chromium, due to limitations of the currently available generic binding parameters for this metal in the NICA-Donnan model.

The results of this research confirm that a reduction in the concentration of specific contaminant groups require different treatment strategies for different landfills. Non-reactive contaminants can only be removed from the waste body by enhanced flushing with water, which may be a relevant treatment technique to lower the leaching potential of soluble salts for all of the investigated landfills. Our modelling of leaching processes shows that for contaminants that (strongly) associate with reactive organic and/or mineral surfaces, enhancing the reactivity of organic matter and Fe/Al (hydr)oxides in the solid phase, and reduction of dissolved organic matter in the leachate by aeration of the waste body, can be an effective strategy to reduce the leaching of reactive contaminants from landfill waste. This treatment is anticipated to be most effective in less mature landfills characterized by a low ratio of solid OM to dissolved OM and particularly for contaminants with a high affinity for OM binding. Overall, this study has shown that landfill-specific combinations of proposed treatment strategies (aeration, leachate recirculation) may be necessary to reduce the leaching of specific contaminant groups to below limit values.



Chapter 3

Chromium (III) Binding to Purified Fulvic and Humic Acid and its Solid Solution Partitioning and Speciation in Soil

Frank van Raffe, Rob N.J. Comans, Jan E. Groenenberg

Published as:

van Raffe, F., Comans, R. N., & Groenenberg, J. E. (2025). Chromium (III) Binding to Purified Fulvic and Humic Acids and Their Solid-Solution Partitioning and Speciation in Soil. *ACS Earth and Space Chemistry*, *9*(7), 1815-1824.

ABSTRACT

Chromium (Cr) is a metal of high environmental concern which exists as Cr(III) and Cr(VI) in the environment, with Cr(VI) considered most toxic and mobile. Humic substances may reduce Cr(VI) to Cr(III) while simultaneously binding Cr(III), reducing its bioavailability and protecting it against (re-)oxidation. Nevertheless, Cr(III) binding to humic substances is insufficiently quantified, as binding constants in ion binding models are based on limited data and consequently uncertain. In this paper, Cr binding experiments to humic- and fulvic acid were conducted in conjunction with the Donnan membrane technique to determine the free Cr^{3+} concentration. New NICA-Donnan binding parameters were derived using ORCHESTRA-PEST, exploring scenarios with solely Cr^{3+} binding and additionally considering Cr binding in the form of $CrOH^{2+}$ or $Cr_2(OH)_2^{4+}$. Parameters for the scenario of combined Cr^{3+} and $Cr_2(OH)_2^{4+}$ binding were deemed most realistic, yet obtained binding affinities were unexpectedly low, potentially related to the previously suggested overestimated electrostatic contribution particularly for trivalent ions in the NICA-Donnan model. Validating the new parameters showed a significant improvement compared to the generic NICA-Donnan parameters in predicting Cr-HA binding in a synthetic system and in predicting free Cr^{3+} concentrations in soil solution, the most relevant species concerning toxicity and (bio)availability. The new parameters underestimated binding to organic matter however, resulting in inaccurate predictions of solid-solution partitioning in organic-poor deeper soil layers. The new parameters ultimately better reflect the spectroscopically identified mechanisms of Cr binding to humic substances, yet found limitations highlight the incorrect description of electrostatic binding by the Donnan model.

3.1. INTRODUCTION

Chromium (Cr) is a metal of high concern for environmental pollution, being present in high concentrations at polluted sites due to its use in several industries, e.g. tanning, electroplating, and wood-preservation (Coetzee et al., 2020; Tumolo et al., 2020). Effective remediation of these sites and proper protection of the environment requires knowledge on Cr transport and availability.

Cr is present in the natural environment either as Cr(III) or Cr(VI), with the latter being more mobile and more toxic (Choppala et al., 2018) yet the former prevailing at organic matter contents typically present in soils (Jardine et al., 2013). A specific fraction of organic matter, i.e. operationally defined humic substances (HS) (Van Zomeren & Comans, 2007), play an important role in the speciation and availability of Cr. Humic substances reduce Cr(VI) to Cr(III) while simultaneously providing a strong binding surface to prevent reoxidation and reduce the bio-availability of Cr to plants (Jardine et al., 2011, 2013; McGrath, 1982; Ohta et al., 2012; C. Pan et al., 2017; Reijonen & Hartikainen, 2016; Song et al., 2006; Stewart et al., 2003; Z. Yang et al., 2021). Mobility of HS-bound Cr is restricted by HS present in the solid phase, and promoted by HS in the dissolved phase. While HS play a key role in the fate of Cr, binding of Cr(III) to HS has been insufficiently quantified, limiting accurate predictions of Cr behaviour.

Multi-surface geochemical models are a commonly used tool for predicting element speciation, being an assemblage of models for calculating ion binding to different reactive surfaces, i.e. metal (hydr)oxides, clays, and HS (Di Bonito et al., 2024). Models used for calculating binding to HS include the Stockholm Humic Model (Gustafsson, 2001), model VI/VII (Tipping, 1998; Tipping et al., 2011), and the NICA-Donnan model (Kinniburgh et al., 1999). Cr binding parameters used in these models are based on limited experimental data, with the generic parameters used in the NICA-Donnan model being derived solely empirically from linear free energy relations (Carbonaro & Di Toro, 2007; Milne et al., 2003), both resulting in uncertain calculations (Groenenberg & Lofts, 2014). While in several cases the Cr solid-solution partitioning has been adequately described using these parameters (Dijkstra et al., 2009; Groenenberg et al., 2012), significant underestimations of the free Cr species indicate a correct description of underlying mechanisms is currently lacking (Koopmans & Groenenberg, 2011). Understanding these mechanisms is critical for predicting Cr toxicity and availability (Allen et al., 1980; Parker et al., 1995). There is thus a need for improved Cr binding parameters.

Within the NICA-Donnan model, solely monomeric binding of the free metal ion is considered, which in case of Cr is the Cr^{3+} ion. Nevertheless, the tendency of Cr to hydrolyse already at low pH (Rai et al., 1987, 1989) suggests binding of the first Cr-hydroxy species ($CrOH^{2+}$) to be of potential relevance, as is already considered in other HS binding models

(Gustafsson, 2001; Tipping, 1998). Additionally, EXAFS analyses showed that the dimeric Cr species $Cr_2(OH)_2^{4+}$ has an important contribution to Cr-binding to purified fulvic acid, an organic soil (Gustafsson et al., 2014), and a Cr contaminated soil (Löv et al., 2017). Consideration of $CrOH^{2+}$ and/or $Cr_2(OH)_2^{4+}$ in the NICA-Donnan model is thus expected to significantly improve the model description, both in terms of the underlying binding mechanisms and the accuracy of predictions.

The aim of this paper is to derive newly optimized Cr(III) binding parameters for the NICA-Donnan model, investigating the potential improvements by considering potential binding of $CrOH^{2+}$ and/or $Cr_2(OH)_2^{4+}$, and to validate the functionality of these new parameters. To do so, titration-binding experiments of Cr(III) to isolated fulvic- and humic acids (FA and HA respectively) were conducted at three pH levels. The Donnan membrane technique (DMT) (Temminghoff et al., 2000) was used to determine the free Cr^{3+} activity and thereby to better explore the distinction between specific Cr species. The obtained data was used to derive optimised binding parameters, considering binding of Cr^{3+} alone and in conjunction with $CrOH^{2+}$ or $Cr_2(OH)_2^{4+}$. The newly derived parameters were tested on several environmental samples to test their adequacy.

3.2. MATERIALS AND METHODS

3.2.1. Cr-binding experiments

The binding of Cr(III) to FA and HA was studied with titration-binding experiments in which free ionic Cr^{3+} was determined using the Donnan Membrane Technique (DMT) (Temminghoff et al., 2000) in a similar experimental setup as described by Oste et al. (2002). DMT uses a "donor" cell – containing Cr, background electrolytes, and HS – and an "acceptor" cell – containing background electrolytes – which are separated by a negatively charged membrane to prevent the passage of Cr-HS complexes. Through this, DMT distinguishes the "free" fraction, i.e. unbound Cr^{3+} which is only present in the acceptor cell, from total Cr, as present in the donor cell. Due to the known slow equilibration time of strongly hydrolysing trivalent cations such as Cr (Gustafsson et al., 2014) or aluminium (Al)(Weng, Temminghoff, & Van Riemsdijk, 2002a), a pre-experiment was conducted to establish the required equilibration time within the DMT system. In this pre-experiment the acceptor and donor cell were both kept at pH 3 and contained a background electrolyte concentration of 30 mM $NaNO_3$ and 2 mM $CaCl_2$; the calcium (Ca) was added to reduce Cr-membrane interactions (Janot et al., 2021) and the required time for equilibration (Weng et al., 2005). The donor solution additionally contained 10^{-7} M $Cr(NO_3)_3$ without HS, or $5x10^{-5}$ M $Cr(NO_3)_3$ with 167 mg L^{-1} Tongbersven humic acid (THA)(Kalis et al., 2006; Temminghoff et al., 1997). The acceptor cell was sampled after 1, 2, 4, and 8 days of equilibration.

The actual Cr-binding experiments were conducted using THA and Suwannee River Fulvic Acid (SRFA, IHSS). A donor solution containing either 167 mg L^{-1} THA or 334 or 1002 mg L^{-1} SRFA was titrated with $Cr(NO_3)_3$ at three pH levels, with a background electrolyte concentration of 30 mM $NaNO_3$ and 2 mM $CaCl_2$ for the THA experiment, which was adapted to 30 mM $NaNO_3$ and 2 mM $Ca(NO_3)_2$ for the SRFA experiment to omit Cl and thereby simplify the system. For the THA experiments, Cr concentrations ranged from $3x10^{-7}$ to $5x10^{-3}$ M with an intended pH of 3, 4.5, and 6; for the SRFA experiments Cr concentrations ranged between $1x10^{-7}$ and $5x10^{-3}$ M with an intended pH of 3, 4, and 5. Precise intended and actual conditions of the experiments can be found in Tables S3.1 and S3.2; important to note that all titrations were conducted in duplicate, with two DMT systems running parallel to each other. Formation of insoluble Cr-hydroxides resulted in detection problems for Cr in the acceptor cell at pH 6 in the HA experiments, hence for the FA experiment lower pH levels were used. Donor and acceptor cell were sampled after 4 days for every titration step and analysed for pH, Cr on the Inductively Coupled Plasma – Mass Spectrometer (ICP-MS Element 2, *Thermo Fisher Scientific Inc., Waltham,*), Ca, potassium (K), and sodium (Na) on the Inductively Coupled Plasma – Optical Atomic Emission Spectrometer (ICP-OES iCAP 6500 DUO, *Thermo Fisher Scientific Inc., Waltham,*); the donor cell was further analysed for dissolved organic carbon (DOC) to check the final HA/FA concentration on the Segmented Flow Analyser (SFA San++, *Skalar Analytical B.V., Breda, The Netherlands*).

3.2.2. Calculation of free and bound Cr

The activity of Cr^{3+} and Na^+ in the acceptor cell was calculated in ORCHESTRA (Meeussen, 2003), using the Davies equation for activity corrections and accounting for inorganic speciation using the reaction equations present in the MINTEQV4 database. Inputs in the model consisted of measured concentrations (Cr, Ca, Na) and pH in the acceptor cell, and theoretical chloride (Cl) and nitrate (NO_3^-) concentrations based on the background electrolyte and varying additions of $Cr(NO_3)_3$ (Tables S3.1 and S3.2). The Na^+ activity was similarly calculated in the donor cell, ignoring the presence of HS. The thus obtained activities of Na^+ were used to estimate the Cr^{3+} activity in the donor cell according to (Temminghoff et al., 2000):

$$\frac{(Cr^{3+})_{donor}}{(Cr^{3+})_{acceptor}} = \left(\frac{(Na^{+})_{donor}}{(Na^{+})_{acceptor}} \right)^3 \quad (3.1)$$

The concentration of total non-bound inorganic Cr in the donor cell was subsequently calculated using ORCHESTRA, again considering the inorganic speciation reactions present in the MINTEQV4 database. Finally, the amount of Cr adsorbed to HA/FA was determined from the difference between the calculated non-bound inorganic Cr and the total measured Cr concentrations in the donor solution.

3.2.3. Optimization of NICA-Donnan parameters for HA and FA

Optimized binding parameters of Cr(III) to HA and FA were derived for the NICA-Donnan model (Kinniburgh et al., 1999). An extensive description of the model is given elsewhere (Groenenberg et al., 2010; Kinniburgh et al., 1999); in short, binding of a component *i* is considered for two distinct sites (representing carboxylic and phenolic groups), with their own affinity distributions. The total amount bound (Q_i) at a given concentration (c_i) is calculated according to:

$$Q_i = \frac{n_{i1}}{n_{H1}} Q_{max1,H} \frac{\left(\widetilde{K}_{i1}c_i\right)^{n_{i1}}}{\sum_i \left(\widetilde{K}_{i1}c_i\right)^{n_{i1}}} \frac{\left[\sum_i \left(\widetilde{K}_{i1}c_i\right)^{n_{i1}}\right]^{p_1}}{1+\left[\sum_i \left(\widetilde{K}_{i1}c_i\right)^{n_{i1}}\right]^{p_1}} + \frac{n_{i2}}{n_{H2}} Q_{max2,H} \frac{\left(\widetilde{K}_{i2}c_i\right)^{n_{i2}}}{\sum_i \left(\widetilde{K}_{i2}c_i\right)^{n_{i2}}} \frac{\left[\sum_i \left(\widetilde{K}_{i2}c_i\right)^{n_{i2}}\right]^{p_2}}{1+\left[\sum_i \left(\widetilde{K}_{i2}c_i\right)^{n_{i2}}\right]^{p_2}} \quad (3.2)$$

The parameters in equation 3.2 are both intrinsic to the humic material ($Q_{max1,\ H}$ and $Q_{max2,\ H}$ describe the maximum proton densities; p_1 and p_2 describe the width of the affinity distributions) and specific to the component *i* ($\widetilde{K}_{i,1}$ and $\widetilde{K}_{i,2}$ describing the median binding affinities of the component to the humic; $n_{i,1}$ and $n_{i,2}$ describing the non-ideality of the component). Charge of the humic is neutralized by co-ion exclusion and counter-ion attraction within the Donnan volume V_D. This volume is calculated according to (Kinniburgh et al., 1996):

$$logV_D = b\,(1 - \log I) - 1 \quad (3.3)$$

Where parameter b is an empirical constant and I is the ionic strength.

Optimized NICA-Donnan parameters were derived by fitting the model to experimental data using a coupling of ORCHESTRA to PEST (Doherty, 2023) in a similar fashion to Janot et al. (2017). Ion specific parameters $\widetilde{K}_{Cr,1}$, $\widetilde{K}_{Cr,2}$, $n_{Cr,1}$ and $n_{Cr,2}$ were fitted until calculated Cr-HS binding best approximated measured Cr-HS binding based on sum of least squares, taking into account inorganic complexation and Ca competition for HS binding based on experimental conditions (Tables S3.1 and S3.2). The optimization was conducted in different scenarios. Initially, the binding of Cr was explored using proton parameters specific for THA and SRFA (Table S3.3) in 3 steps: 1) fitting all four ion specific parameters for Cr^{3+}, constraining n values between 0.1 and 0.99 and with no constraints on K values; 2) fitting all four ion specific parameters for Cr^{3+} and additionally introducing and fitting four ion specific parameters for the first Cr-hydroxy species ($CrOH^{2+}$); 3) fitting all four ion specific parameters for Cr^{3+} and additionally introducing and fitting four ion specific parameters for the dimeric Cr species ($Cr_2(OH)_2^{4+}$). A detailed description of these scenarios within ORCHESTRA-PEST is described in the SI (SM3.1), with the constants of Cr hydrolysis and formation of the Cr dimer listed in Table S3.4.

The most appropriate of the three scenario's was selected based on several aspects (highest R^2 value; lowest root mean square error (RMSE; (Bennett et al., 2013)); visual goodness of fit; whether fitted parameter values are deemed realistic, as described in the results section). The selected scenario was once more conducted, yet using the generic proton parameters of Milne et al. (2001) (Table S3.3) instead of proton parameters specific for the used humic material. Thereby new NICA-Donnan Cr parameters are derived, which can be used in generic speciation calculations based on the generic parameter sets of Milne et al. (2001, 2003).

3.2.4. Parameter assessment for soil samples

Adequacy of the final derived Cr parameters was assessed through modelling the Cr speciation of various datasets using both the newly derived parameters and the original "Milne" Cr parameters (Milne et al., 2003) and comparing model calculations with measurements. Assessments on model 'accuracy' are based on calculated RMSE (Bennett et al., 2013) and a visual comparison between modelled and measured Cr concentrations and species. The assessment was conducted in three steps, the first step using the dataset of Fukushima et al. (1995), the second step using the dataset of Koopmans & Groenenberg (2011), and the third step using dataset NB from Groenenberg et al. (2012).

The first parameter assessment used the dataset of Fukushima et al. (1995) to model Cr binding to a peat HA. The total amount of Cr, total amount of Cl, total amount of HA (40 mg L^{-1}), pH, and a constant background electrolyte concentration of 0.01 M Na and 0.01 M formic acid were used as model inputs and the amount of unbound Cr and Cr bound to HA was calculated; a summary of used input data as well as measured bound Cr are listed in Table S3.5. The MINTEQV4 database was expanded to include the formation of Cr^{3+}-formic acid complexes, based on the values listed by Vinokurov & Bondar' (2003). The RMSE was subsequently calculated from the difference between calculated and measured unbound Cr.

The 2nd parameter assessment used the dataset of Koopmans & Groenenberg (2011) to calculate the free Cr^{3+} species in 2 mM $Ca(NO_3)_2$ soil extracts, which were compared against free Cr^{3+} concentrations measured using DMT. Specifics on the soil extracts and available data can be found in the original paper, with a summary of data listed in Tables S3.6 and S3.7. Modelling was conducted in a similar fashion to Koopmans & Groenenberg (2011), using pH, total dissolved concentration of Cr, total dissolved concentrations of competing elements (Al, Ca, cadmium (Cd), Cl, copper (Cu), iron (Fe), K, magnesium (Mg), manganese (Mn), Na, nickel (Ni), NO_3^-, lead (Pb), phosphate (PO_4^{3-}), sulphate ($SO4^{2-}$), and zinc (Zn)) and HA as model inputs, yet deviating from the original paper by inputting measured FA rather than FA + hydrophobic organic neutrals (HON) as input for FA. Metal binding was calculated solely considering binding to HS, using generic parameters (Milne et al., 2003) for most competing elements and the parameters of Hiemstra & Van Riems-

dijk (2006) for Fe binding to FA. Binding of Cr^{3+} was calculated using both the original generic parameters (Milne et al., 2003) and the newly derived parameters.

The 3rd parameter assessment used the dataset from Groenenberg et al. (2012) to calculate the solid-solution partitioning of Cr in different soils rather than free Cr^{3+}. Available data, summarized in Tables S3.8 and S3.9, is similar to the 2nd assessment round, yet excludes DMT measurements and instead uses total pore water concentrations and 2 mM $CaCl_2$ extractable concentrations at different depths of a soil profile to validate model results. Calculating the solid-solution partitioning rather than only the solution speciation requires the model to be extended to include additional solid reactive surfaces. Binding to clay was calculated using the Donnan model, whereas binding to Fe/Al (hydr) oxides was calculated using the generalized two-layer model (Dzombak & Morel, 1990). Inputs consisted of total amount of Cr determined using the 0.43 M HNO_3 extraction (Groenenberg et al., 2017), total dissolved concentrations of competing elements (Al, As, barium (Ba), Ca, Cd, Cl, cobalt (Co), Cu, Fe, molybdenum (Mo), Ni, Pb, PO_4^{3-}, S, antimony (Sb), selenium (Se), tin (Sn), vanadium (V), and Zn), pH, total dissolved and solid HA and FA, total hydrous ferric oxide (using Fe oxides as a proxy for aluminium oxide, similar to Dijkstra et al., 2009), and total clay content. Calculated dissolved Cr concentrations were compared with measured dissolved Cr concentrations to test model accuracy.

3.3. RESULTS

3.3.1. Equilibration time

The conducted equilibration experiments showed equilibrium within the acceptor cell to be approximated after ~2 days in the absence and ~4 days in the presence of HA (Figure S3.1); a slightly longer equilibration time for Cr(III) than the 30 hours of Fukushima et al. (1995), around the same time as the 3 – 4 days found for Al by Weng et al. (2002), yet significantly shorter than the equilibrium time for Cr(III) of over 211 days observed by Gustafsson et al. (2014). Yet the long equilibrium times of the latter were found at a particularly low pH of 2.3 and at high Cr concentrations of 10^{-3} M, while the conditions of Weng et al. (2002) and Fukushima et al. (1995) were more similar to the present study. Consequently, the found equilibrium time of 4 days is considered well in line with previous studies and the 4 days of equilibration used in our Cr binding experiments were therefore considered appropriate.

3.3.2. Titration measurements

A marked difference in data quality is observed between the results of Cr binding to THA and SRFA (Figure S3.2): significant scatter is found for THA, whereas for SRFA there is a continuous relation between bound Cr and free Cr^{3+} for all pH levels. This significant scatter of THA has several potential causes: 1) potential precipitation of $Cr(OH)_3(s)$ for the

samples at pH 6 obfuscating results (Papassiopi et al., 2014); 2) larger deviation and variation in measured pH from the intended pH (Table S3.1 & S3.2); 3) a larger difference in pH between donor and acceptor compared to the SRFA data (Table S3.1 & S3.2). The more scattered measurements may result in a worse fit for THA compared to SRFA, which needs to be considered when interpreting the derived binding parameters.

3.3.3. Parameter optimization

3.3.3.1. Fulvic acid

The unconstrained fit of ion specific Cr^{3+} binding parameters using specific SRFA proton parameters resulted in a relatively good description (R^2 = 0.987, RMSE = 0.231; Table 3.1). In spite of the good fit, Cr binding is underestimated by the model at pH 5, particularly towards higher Cr concentrations (Figure 3.1a). This is potentially the result of the increasing prevalence of $CrOH^{2+}$ and $Cr_2(OH)_2^{4+}$ with increasing pH and increasing Cr concentration (Figure S3.3). As both forms potentially contribute to Cr binding, solely accounting for Cr^{3+} complexation appears to provide an incomplete description with larger discrepancies at higher pH. Including the binding of $C_rOH_2^+$ or

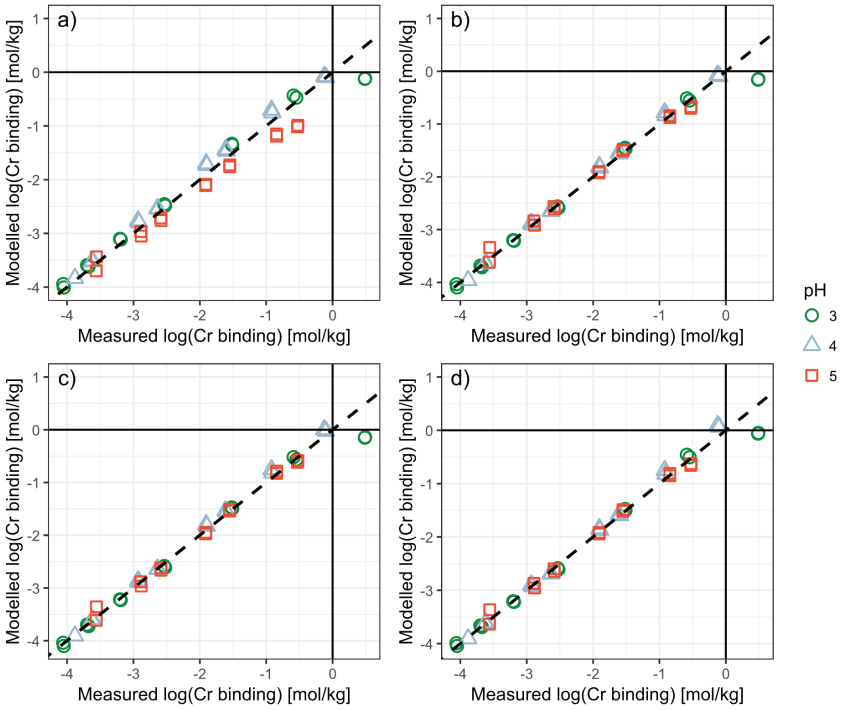


Figure 3.1 Optimized fits of Cr binding to SRFA using specific properties: a) fit solely considering Cr^{3+} binding; b) fit including binding of $CrOH^{2+}$; c) fit including binding of $Cr_2(OH)_2^{4+}$. Optimized fit of Cr binding to SRFA using generic proton properties, including binding of Cr2(OH)24+ (d).

Table 3.1 Optimized parameters for the different fitting scenarios of Cr binding to SRFA. Value x represents parameters values either of the hydroxy or the dimeric species, depending on the scenario. Fits used proton parameters specific to SRFA, as listed in Table S3.3, except for the fit of "Generic $Cr_2(OH)_2^{4+}$"for which generic proton parameters (Milne et al., 2003) were used.

	Cr^{3+}	Cr^{3+} & $CrOH^{2+}$	Cr^{3+} & $Cr_2(OH)_2^{4+}$	Generic Cr^{3+} & $Cr_2(OH)_2^{4+}$
$logK_{1,Cr}$	1.75 ± 0.31	1.59 ± 0.44	1.55 ± 0.4	-0.82 ± 5.36
$n_{1,Cr}$	0.99 ± 0.15	0.94 ± 0.27	0.95 ± 0.25	0.99 ± 2.71
$logK_{2,Cr}$	6.44 ± 2.24	5.39 ± 20.2	6.01 ± 6.8	5.64 ± 0.94
$n_{2,Cr}$	0.79 ± 0.65	0.55 ± 7.47	0.58 ± 2.7	0.75 ± 0.84
$logK_{1,x}$	-	0.38 ± 223.7	0.3 ± 10.16	0.13 ± 1.05
$n_{1,x}$	-	0.99 ± 63.22	0.46 ± 0.6	0.56 ± 0.43
$logK_{2,x}$	-	6.34 ± 2.9	8.01 ± 5.91	1.56 ± 8462.22
$n_{2,x}$	-	0.99 ± 1.11	0.71 ± 0.94	0.44 ± 358.37
R^2	**0.987**	**0.993**	**0.993**	**0.994**
RMSE	**0.231**	**0.171**	**0.169**	**0.155**

$Cr_2(OH)_2^{4+}$ does for both complexes indeed result in an improved fit (Table 3.1). This improvement is mainly related to a better description of Cr binding at pH 5 (Figure 3.1b,c), where the additional species indeed contributes stronger to the dissolved Cr speciation (Figure S3.4b,c). The observed improvements in the R^2 and RSME are similar for both scenario's, making selection of the most relevant scenario not unambiguous. While binding of $CrOH^{2+}$ is considered in both model VI/VII and SHM, the actual occurrence of this binding mechanism has not been experimentally demonstrated. Conversely, EXAFS analyses have shown an association between $Cr_2(OH)_2^{4+}$ and humic substances (Gustafsson et al., 2014; Löv et al., 2017). Furthermore, speciation analysis of the obtained fits showed that type 1 sites (carboxylic acids) were of significant importance across the experimental pH range for the $Cr_2(OH)_2^{4+}$ fit, but less so for the $CrOH^{2+}$ fit at pH 5, where type 2 sites (phenolic acid groups) became most significant (Figure S3.4b,c). Type 1 sites are expected to be of highest importance for Cr binding across the experimental pH range, as deduced from the previously observed limited competition between Cr and Al in the pH range of 3 - 7 and Cr concentration range of 1 – 100 µg L^{-1} (Gustafsson et al., 2014; M. Yan et al., 2016) and the preferential binding of Al to type 2 sites (M. Yan et al., 2016). Based on the above considerations, the fit based on Cr^{3+} and $Cr_2(OH)_2^{4+}$ binding is considered the most realistic representation.

Using generic FA proton parameters (Milne et al., 2001) rather than specific SRFA parameters to fit the scenario of Cr^{3+} and $Cr_2(OH)_2^{4+}$ binding resulted in a surprisingly further yet small statistical improvement (R^2 = 0.994, RMSE = 0.155, Table 3.1). Binding is accurately predicted for all pH levels and Cr concentrations (Figure 3.1d), where solely at the highest Cr concentration at pH 3 calculated Cr binding is significantly lower than measured. Under

these conditions the model predicts saturation of FA, while the measured binding data do not yet level off at this Cr loading (Figure S3.2). As this phenomenon is also observed for all scenario's using specific SRFA proton parameters, it is unlikely to be related to inaccurate proton parameters. Instead, the calculated low binding may point to the formation of trimeric species at this pH and particularly this high Cr concentration (Stuenzi et al., 1989) which the model does not account for.

Based on LFER calculations, K values for Cr are expected to fall between those of Al and Fe (Gustafsson et al., 2014). The K_1 values of the generic fit are between those of Fe and Al, yet derived K_2 values are significantly lower than for both Fe (Hiemstra & Van Riemsdijk, 2006) and Al (Weng, Temminghoff, & Van Riemsdijk, 2002a). This difference may point towards a too low Cr affinity for the type 2 sites, yet it should be noted that comparison may not be appropriate due to the included contribution of $Cr_2(OH)_2^{4+}$ to total Cr binding in our study, whereas no hydrolysed species were included in the parameter derivation of the similarly readily hydrolysable Fe and Al (Stefánsson, 2007; Xiao et al., 2008). The derived K values of our generic fit are further significantly lower compared to the fit with SRFA-specific proton parameters (Table 3.1), particularly for the K_1 of the Cr^{3+} species and K_2 of the $Cr_2(OH)_2^{4+}$ species. A low K_1 value has previously been derived for Al (Weng, Temminghoff, & Van Riemsdijk, 2002a), being significantly lower than those of divalent ions (Milne et al., 2003) and substantially lower than K_1 values predicted with LFER (Otero-Fariña et al., 2023; Wiersma et al., 2025). These low K_1 values are related to the low generic $K_{1,H}$ value of FA (2.70, see Table S3.3), which is in turn related to the unrealistically high negative electrostatic potential calculated with the present Donnan model, including the relation of the Donnan volume with ionic strength (Equation 3.3) for small humic particles (L. K. Koopal et al., 2025; Pinheiro et al., 2021; Town et al., 2019). The overestimation of the negative electrostatic potential results in a too high contribution of the electrostatic binding, which becomes particularly problematic for ions of higher valency and ultimately results in lower specific binding affinities. The same effect applies to the obtained low K_2 value of the dimer. This finding is contrary to that of Gustafsson et al. (2014), who found an increased importance of dimeric Cr binding at higher pH where the contribution of phenolic acids becomes more important. The low $K_{1,Cr}$ and $K_{2,dim}$ values result in high standard deviations (Table 3.1), which are the result of the fitted higher affinity of $K_{1,dim}$ and $K_{2,Cr}$ controlling binding to these sites.

Based on the current uncertain binding parameters, the NICA-Donnan model predicts that for pH 3 Cr is predominantly present in the Donnan phase across all Cr activities, while for pH 4 & 5 a shift in Cr species (Cr^{3+} to dimeric Cr) from low to high Cr activity corresponds with a shift in site binding (from the 2 sites to the 1 sites) related to the respective affinities of the different species. The high importance of type 2 sites in this study differs from the findings of Gustafsson et al. (2014), and together with predominance of the Donnan phase at pH 3 is again an indication of an underestimated K_1 value.

The fitted n values for the scenario considering binding of both Cr^{3+} and $Cr_2(OH)_2^{4+}$ and using generic proton parameters closely follow the relation of $n_2 = 0.76 * n_1$ listed by Milne et al. (2003) (Table 3.1). Nevertheless, derived n values are much higher than those found for Al and Fe (0.2 – 0.4 (Hiemstra & Van Riemsdijk, 2006; Weng, Temminghoff, & Van Riemsdijk, 2002a)), with $n_{1,Cr}$ reaching the upper boundary of 0.99. Constraining these n values to the 0.2 – 0.4 range resulted in a significantly worse fit (Figure S3.5); hence these constraints were ultimately not implemented and the predictions based on the here-derived parameter set were considered most accurate. Based on the previously noted uncertainty of the Fe and Al binding parameters this was deemed acceptable.

3.3.3.2. Humic acid

As a result of the lower quality of the titration data (Fig. S3.2), unconstrained fitting of Cr^{3+} to THA resulted in a significantly less accurate prediction compared to that of SRFA (R^2 = 0.892, RMSE = 0.787; Table 3.2). Similar to the SRFA fit the model calculated Cr binding is signifcantly lower than measured Cr binding, most likely again the result of an incomplete description of relevant Cr species binding to the HA (Figure 3.2). Contrary to SRFA, an overestimation of Cr binding is found at pH 3 and 4.5 at low Cr activities. Both the predicted over- and underestimation are reduced when considering binding of $CrOH^{2+}$ (R^2 = 0.923, RMSE = 0.623, Table 3.2) or $Cr_2(OH)_2^{4+}$ (R^2 = 0.924, RMSE = 0.62, Table 3.2). Similar to SRFA, the analytical evidence of

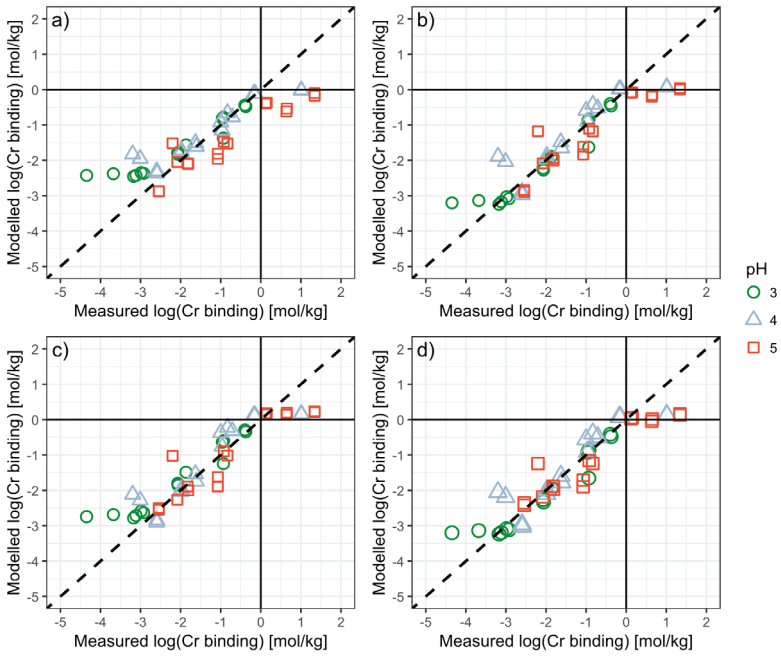


Figure 3.2 Optimized fits of Cr binding to THA using specific properties: a) fit solely considering Cr^{3+} binding; b) fit including binding of $Cr(OH)^{2+}$; c) fit including binding of $Cr_2(OH)_2^{4+}$; d) optimized fit of Cr binding to THA using generic proton properties, including binding of $Cr^2(OH)_2^{4+}$.

dimeric Cr binding to humic substances (Gustafsson et al., 2014; Löv et al., 2017) led us to select the scenario of Cr^{3+} and $Cr_2(OH)_2^{4+}$ for the derivation of generic parameters.

When fitting using generic proton parameters (Milne et al., 2001) and considering binding of both Cr^{3+} and $Cr_2(OH)_2^{4+}$, a further unexpected yet small statistical improvement is again found (R^2 = 0.933, RMSE = 0.582, Table 3.2). Nevertheless, the overestimation of Cr binding at low pH and underestimation at high pH remain visible (Figure 3..2d). Comparison of the obtained K values with those of Al and Fe (Hiemstra & Van Riemsdijk, 2006; Weng, Temminghoff, & Van Riemsdijk, 2002a) and n values with those of Milne et al. (2003) leads to similar observations as for SRFA, i.e. lower than expected K values and higher than expected n values. The common trend of $n_2 = 0.76 * n_1$ is however no longer followed; instead the n_2 value of both the Cr^{3+} and $Cr_2(OH)_2^{4+}$ species reaches the lower boundary of 0.1. Restricting n_1 and n_2 to the 0.2 – 0.4 range (Milne et al., 2003) again resulted in less-accurate predictions and was not implemented. Contrary to FA, use of generic proton parameters resulted in increased K_1 values for HA. This is related to the higher $K_{1,H}$ of the generic HA proton parameters (log $K_{1,H}$ = 2.93) relative to the specific THA proton parameters (log $K_{1,H}$ = 2.21, Table S3.3), resulting in an increased competition of the proton which needs to be compensated for by higher $K_{1,Cr}$ values to properly model the measured Cr binding. Consequently, Cr binding to THA is predicted to occur predominantly to type 1 sites (Figure S3.6d), which is in agreement with previous findings on limited competition between Cr and Al for Cr binding to organic matter (Gustafsson et al., 2014; M. Yan et al., 2016).

3.3.4. Optimized parameter application

3.3.4.1. NICA-Donnan predictions of chromium binding to humic acid

Calculating Cr-HA binding based on the dataset of Fukushima et al. (1995) shows a significantly improved description when using the newly optimized parameters (RMSE = 0.25) compared to when using the generic parameters of Milne et al. (2003) (RMSE = 1.87; Figure 3.3). The model description using the newly optimized parameters is considered adequate, particularly in the absence of precise information on background electrolyte concentrations and pH, which are not listed by Fukushima et al. (1995), and the differences in properties between the HA used for our parameter derivation and used in the experiments of Fukushima et al. (1995).

Where application of the generic parameters consistently results in a predicted too high binding, the newly optimized parameters predict a too high binding for pH 3.25 and 3.79, a too low binding at pH 4.3, and a consistently adequate binding for pH 3.48. Additionally, higher pH and higher Cr concentrations are marked by more binding to type 1 sites and particularly more binding of the dimeric Cr species (Figure S3.7), while at low pH Cr is relatively more present in the Donnan phase. Hence, the observed overestimated Cr-

HA binding could be an indication of an overestimated electrostatic potential, where the underestimated Cr-HA binding at high pH could be an underestimated binding affinity particularly of the dimeric Cr species.

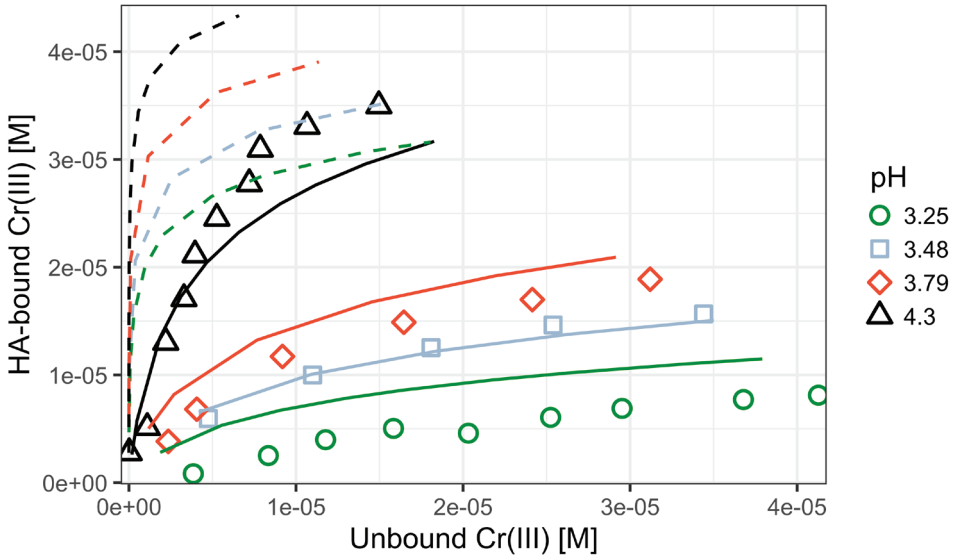


Figure 3.3 Cr^{3+} bound to humic acid at varying pH and an ionic strength of 0.01 M as a function of unbound Cr^{3+} as measured by Fukushima et al. (1995)(points); as modelled with the NICA-Donnan model using our newly optimized parameters (solid lines); as modelled with the NICA-Donnan model using the generic parameters of Milne et al. (2003) (dashed lines).

3.3.4.2. NICA-Donnan predictions of free chromium in a contaminated soil

Modelling the data of Koopmans & Groenenberg (2011) to predict free Cr^{3+} in a 2 mM $Ca(NO_3)_2$ soil extract resulted in a poor description when using the generic parameters of Milne et al. (2003) (RMSE = 2.57). No clear trend can be found between measured and modelled free Cr^{3+}, and the consistently lower than measured free Cr^{3+} calculations indicate an overestimated Cr-HS binding (Figure 3.4). Applying the newly optimized parameters listed in Tables 3.1 & 3.2 resulted in a major improvement (RMSE = 1.53), with a clear trend between measured and modelled free Cr^{3+} yet with predicted free Cr^{3+} concentrations consistently 10 times higher than measured (Figure 3.4). Hence Cr binding to HS appears to be consistently underestimated by our optimized parameters. As noted during the parameter derivation, use of generic proton parameters statistically improved fits yet resulted in an unrealistically high importance of type 2 sites and an unexpectedly low K_1 value for FA. Translating such results to a soil system consequently resulted in a poor description of actual binding. This finding highlights the importance of adequately capturing the underlying mechanisms when deriving parameters, and for

the NICA-Donnan model stresses the importance of improving the electrostatic model, the previously demonstrated shortcomings of which are exacerbated when investigating ions with higher valencies.

It is important to note that most Cr is calculated to be bound to FA, with negligible binding to HA (Figure S3.8), which results from the predicted lower affinity of Cr binding to HA than FA, and the relatively high fraction of FA in the analysed samples. The above observations thus particularly reflect the Cr-FA binding parameters; evaluation of both the new Cr-HA and Cr-FA binding parameters requires comparison with measurements in soil extracts with a higher proportion of HA.

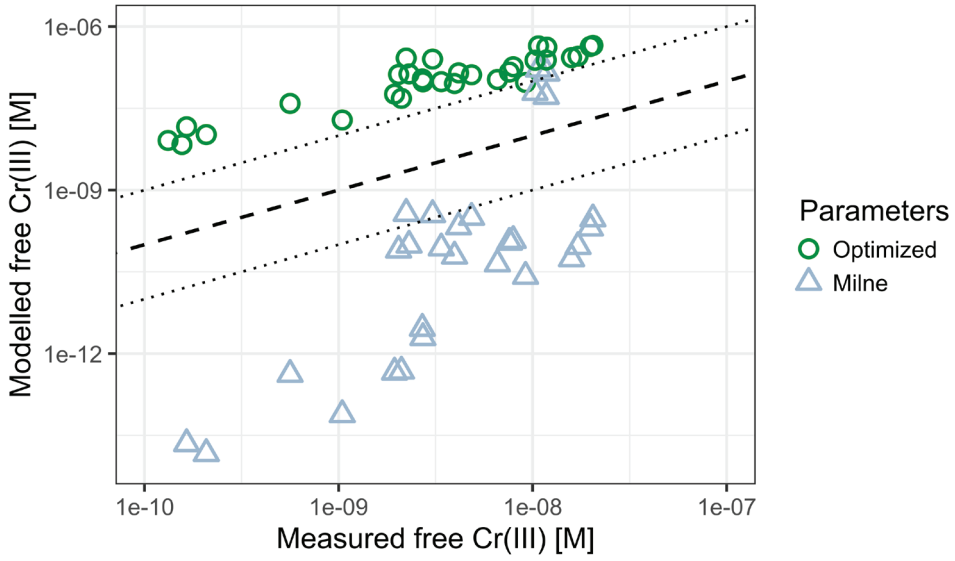


Figure 3.4 Measured free Cr^{3+} concentrations in 2mM $Ca(NO_3)_2$ soil extracts against the calculated free Cr^{3+} concentration as calculated using the generic parameters of (Milne et al., 2003) (blue triangles) and as calculated using the newly derived parameters of this paper (green circles). The dashed line represents the 1:1 line, with the dotted lines representing a factor 10 higher or lower predictions.

3.3.4.3. Multi-surface model predictions of dissolved chromium in a contaminated soil profile

Total dissolved Cr, i.e. free ionic Cr and Cr bound to DOM, in the pore water and in 2 mM $CaCl_2$ extracts of a contaminated soil profile (Groenenberg et al., 2012) can be relatively well predicted using a multi-surface model approach including NICA-Donnan with the binding parameters of (Milne et al., 2003) (Figure 3.5, left; RMSE = 0.645). Predicted dissolved Cr is consistently higher than measured in the collected pore water, whereas no consistent over- or underestimation is observed for $CaCl_2$-extracted Cr. Speciation calcula-

tions predict the solid-solution partitioning to be fully controlled by HS, with an increased contribution of metal (hydr)oxides at lower depths (Figure S3.9); predicted Cr partitioning is hence purely a reflection of FA and HA solid-solution partitioning. Applying the newly derived parameters resulted in a decreased accuracy (RMSE = 1.34), particularly in the deeper parts of the soil profile where dissolved Cr is consistently underestimated by the model (Figure 3.5, right). Samples at these depths are characterized by a higher pH (up to pH 6) and a reduced amount of both solid and dissolved HS, together with a reduced ratio of solid/dissolved HS (Table S3.8) and, similar to the 4 aberrant points in Figure 3.4, high amounts of HON. The high amounts of HON point towards an inconsistency in the fractionation, yet including HON in the modelling was found to have limited effects only (results not shown); the inaccurate description is hence a result of the used parameters. The low HS content of these lower samples means adequately describing binding to dissolved HS becomes increasingly important, yet this is inadequately captured by the model and instead Cr predominantly

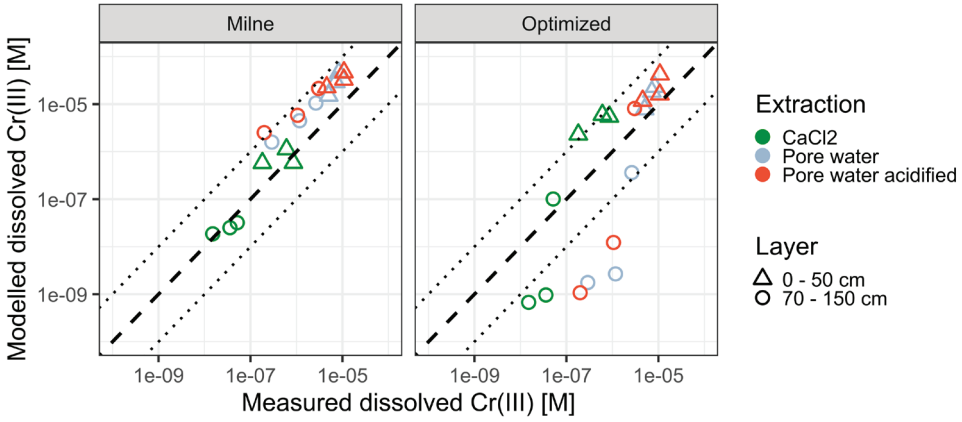


Figure 3.5 Measured total dissolved Cr concentrations in a contaminated soil profile, in solutions obtained by 1) a 2 mM $CaCl_2$ extraction; 2) pore water extraction, and 3) pore water extraction from an adjacent artificially acidified soil profile (Groenenberg et al., 2012), plotted against Cr concentrations predicted with a multi-surface model (see text for details). The left panel shows model predictions based on the generic parameters of Milne et al. (2003), the right panel predictions based on the newly optimized parameters.

binds to metal (hydr)oxides (Figure S3.9). A stronger control of HS is expected, as the modelling using the generic Milne parameters showed HS solid-solution partitioning likely controls Cr solubility; this again indicates the newly derived Cr-HS binding affinity is too low. This may further be the result of the newly derived high n values, reducing the prevalence of high affinity sites which become increasingly important at low HS concentrations (i.e., in the deeper layers of the soil profile) and further underscore the

underestimated Cr-HS binding. It should thus be emphasized that care should be taken in applying these parameters to environments with low amounts of HS.

3.4. DISCUSSION

Within the present study, new NICA-Donnan parameters have been derived for Cr binding to HA and FA, based on new Cr binding experiments in which free Cr^{3+} was measured with DMT. While the generic parameters derived by Milne et al. (2003) adequately predicted Cr solid-solution partitioning (Dijkstra et al., 2009; Groenenberg et al., 2012), they strongly underestimated free Cr^{3+} concentrations (Koopmans & Groenenberg, 2011), a key species for understanding Cr toxicity and availability, and strongly overestimated Cr^{3+} binding to HA. The newly derived parameters significantly improved predictions of Cr-HA binding and free Cr^{3+}, and provided a similarly adequate description of Cr-HS binding in the upper parts of a soil column compared to the generic parameters, yet low K values and high n values likely resulted in too low Cr-FA binding. This consequently led to an inadequate description of Cr solid-solution partitioning in the HS-poor lower parts of the soil column, where accurate description of the heterogeneity of Cr binding becomes increasingly important. The potential causes of these limitations are described below.

The complexity of Cr, particularly regarding its strong hydrolysis, required certain concessions to be made to ensure the obtained parameters were as robust as possible. These concessions were in particular related to the limited range in pH, i.e. only up to pH 6 for HA and pH 5 for FA. The higher pH for HA resulted in more scattered titration data and consequently less-reliable derived parameters. It should be considered that potentially relevant mechanisms that could contribute to Cr binding outside the applied pH range, such as an increasing importance of phenolic acids or the formation of further hydrolyzed Cr species, may not have been captured in the derived binding parameters. Consequently, these parameters may result in a decreased accuracy of predicted Cr binding at higher pH values.

The model FA used for this experiment (SRFA) may not fully represent Cr-FA interactions in soil environments, as it has an aquatic rather than terrestrial origin. SRFA is characterized by smaller and more soluble molecular compounds relative to FA extracted from soil (Schellekens et al., 2017), with a higher binding capacity and proton affinity of type 1 sites than generic FA, and for one (out of two) SRFA samples a higher capacity of type 2 sites (Milne et al., 2001). These deviations would be expected to be suppressed by using specific proton parameters during the parameter estimation for Cr, yet surprisingly better fits were obtained when using the generic proton parameters of Milne et al. (2001). The small size of SRFA may further exacerbate the problems associated with the currently used electrostatic model (L. K. Koopal et al., 2025; Pinheiro et al., 2021), and hence have

resulted in an overestimated importance of the Donnan phase (Town et al., 2019) and an underestimation of the specific Cr-FA binding affinity. In addition, the small size of SRFA is likely to lead to a lower polydispersity, leading to a lower heterogeneity which may explain the high n values found in this study. The limited representativeness of the originally aqueous SRFA for the soil system became apparent during the validation steps, where Cr-binding to soluble FA in $CaCl_2$ extracts was more accurately predicted than Cr binding to both solid and dissolved FA in soil profiles. This difference in properties may also have contributed to the underestimated dissolved Cr in the deeper soil layers, where soluble FA became increasingly sparse. Hence, use of SRFA may at least partly explain observed limitations of the presently derived parameter set, yet it also highlights recently identified limitations of the representation of electrostatic binding in the current NICA-Donnan model and the need for proper humic substances characterization to adequately describe the behaviour of multivalent ions such as Cr in the environment.

While validation of the newly optimized Cr-HA binding parameters showed significant improvements compared to the generic parameters, there are indications that the electrostatic contribution is again higher than realistic. The effects nevertheless appear smaller than for FA, as can be expected from the significantly larger particle size of THA (Pinheiro et al., 2021).

3.5. CONCLUSION

In this study, new Cr binding experiments to Suwannee River fulvic- and Tongbersven humic acid were conducted at three pH levels, with analysis of free Cr^{3+} concentrations using the Donnan membrane technique. These measurements were subsequently used to calculate new Cr binding parameters for the NICA-Donnan model using a coupling of ORCHESTRA-PEST. Fits were firstly conducted using proton parameters specific to the humic- and fulvic acid used in the experiments. Different scenarios were explored in the derivation of the binding parameters, with only Cr^{3+} binding and with inclusion of the binding of $CrOH^{2+}$ or $Cr_2(OH)_2^{4+}$. This approach, and added insights from previous experimental observations, resulted in a final best fit by using generic proton parameters and considering binding of both Cr^{3+} and $Cr_2(OH)_2^{4+}$ to derive the new Cr binding parameters. The obtained parameters resulted in a high statistical significance, yet a likely underestimation of K values and unrealistically high n values. The newly derived binding parameters were tested against different datasets of Cr binding to purified humic acid and in soil systems, showing that Cr-HA binding in a synthetic systems, free Cr^{3+} concentrations in pore water and $CaCl_2$ extracts, and predictions on the Cr solid-solution partitioning in the top layers of a soil profile were all improved, yet predictions of Cr solid-solution partitioning in the deeper layers with low concentrations of humic substances worsened. The validations indicate a likely underestimated binding of Cr to humic substances,

potentially the result of the overestimated contribution of the Donnan phase in the NICA-Donnan model. While an improvement of the Cr binding parameters is found, our results highlight that even when fits provide a good description of experimental data, an inaccurate description of underlying mechanisms potentially limits the generic quality of model predictions. It should hence be stressed that known limitations of the electrostatic component of the NICA-Donnan model should be addressed to more adequately describe metal-HS binding, particularly when concerning higher valency ions such as Cr.



Chapter 4

Changing pH, organic matter, and redox state govern contaminant mobility during waste stabilization in landfill simulation reactors

Nick Quist*, Frank van Raffe*, Joris J. Dijkstra, Rob N.J. Comans
***These authors contributed equally**

Published in a revised form as:

Quist, N., van Raffe, F., Dijkstra, J. J., & Comans, R. N. (2026). Changing pH, organic matter, and redox state govern contaminant mobility during waste stabilization in landfill simulation reactors. *Journal of Hazardous Materials*, 142532.

ABSTRACT

Landfills remain an important endpoint for waste and waste residues, yet current management in the Netherlands requires eternal aftercare to protect public health and the environment. Enhanced waste stabilization in landfills through active treatment, i.e. aeration and leachate recirculation, has potential as a sustainable alternative to current landfill management. However. the influence of active treatment on solid waste properties and subsequent leaching of hazardous contaminants has only been limitedly investigated. This study investigates these influences in landfill simulation reactors containing 30 kg of waste from different origins and that are treated using aeration, leachate recirculation, and their combination. Large differences in leachate contaminant concentrations were found between treatments. A shift from leachate recirculation to aeration changed prevailing redox conditions from anaerobic to aerobic and decreased pH and dissolved organic- and inorganic carbon. Consequently, concentrations of ammonium and inorganic contaminants with a high organic matter binding affinity decreased, whereas other inorganic contaminants first increased in concentration due to mineral dissolution followed by a decrease due to mineral precipitation or binding to reactive surfaces. The underlying mechanisms of these trends could be identified based on geochemical modelling. The observed changes during aeration were accelerated when aeration was prefaced by leachate recirculation, and concentrations rebounded when anaerobic conditions were re-introduced. Our findings ultimately demonstrate that active treatment of landfills requires careful consideration of the most effective strategy, as trade-offs in contaminants leaching mean their potential risks should be weighed against each other.

4.1. INTRODUCTION

A continuous increase in global waste generation (Hoornweg & Bhada-Tata, 2012; United Nations Environment Programme, 2024) has led governments to explore sustainable alternatives to landfills for waste management (Das et al., 2019; European Parliament and Council of the European Union, 2008; Scharff, 2014). Nevertheless, landfills remain a necessary waste endpoint due to the existence of untreatable waste and waste residues. Landfills are a source of hazardous emissions, posing a risk to public health and the environment through the generation of greenhouse gases, namely methane (EEA, 2024; Manheim et al., 2021), and contaminant-rich leachate (Dagwar & Dutta, 2024; Kjeldsen et al., 2002; Teng et al., 2021). These emissions are prevented by encapsulating the waste in artificial barriers (Council of the European Union, 1999), yet this approach delays waste decomposition and retains the waste emission potential. As a result, the so-called "aftercare" period, i.e. the period following waste acceptance in which landfills are thoroughly monitored, can be lengthy and in certain cases indefinite, leading to high societal costs (Scharff et al., 2011).

The need for more sustainable landfill management has led to the signing of a "green deal" between the Dutch government, landfill operators, and knowledge institutes (E. Brand et al., 2016). This green deal initiated three landfill-scale pilot projects to assess the potential of aeration and leachate recirculation as active treatment for reducing contaminant emissions to comply with legally accepted emission target values (ETV) (E. Brand et al., 2016; Dijkstra et al., 2018). In conjunction with a large associated research programme, an extensive monitoring programme has been developed to quantify active treatment effects on gaseous and leachate emissions (Van Raffe et al., 2023).

Assessing the true potential of long-term active treatment to reduce leachate contamination requires knowledge of both the changes in leachate contaminant concentrations and the geochemical evolution of the solid waste and the corresponding effects on contaminant transport. Studies of the latter are however scarce, as *in-situ* monitoring of solid waste is challenging and costly. A feasible laboratory-scale alternative for determining solid phase changes are Landfill Simulation Reactors (LSRs), which provide the additional benefit of an accelerated stabilization rate compared with field treatment to give insights on shorter timescales. While LSRs are well established, previous research has primarily focused on gas production, chemical and biological oxygen demand, pH, nitrogen, carbon, and macro ions (Brandstätter et al., 2015a, 2015b; Cerminara et al., 2020; Erses et al., 2008; Fricko et al., 2021a; Long et al., 2018; Nikolaou et al., 2010; Šan & Onay, 2001; Tong et al., 2015). Crucially, existing studies on inorganic contaminants have largely overlooked the role of organic matter (OM) (Erses & Onay, 2003; Giannis et al., 2008; Hrad et al., 2013; H. Kim et al., 2011; Sinan Bilgili et al., 2007), a key factor governing the solid/solution partitioning of heavy metals (Groenenberg et al., 2012; Kalbitz & Wennrich, 1998; Weng,

Temminghoff, Lofts, et al., 2002). Furthermore, studies modelling the mechanisms underlying contaminant mobility are scarce, and has to our knowledge been limited to gas production and trends in pH and macro ions (van Turnhout et al., 2018). Consequently, the underlying geochemical processes driving the leachability of inorganic contaminants during active treatment in LSRs remain underexplored.

To address this gap, geochemical mechanisms can be elucidated by coupling dedicated leaching experiments with "multi-surface" geochemical modelling. This modelling framework calculates chemical interactions – including binding to reactive surfaces, inorganic complexation, and mineral precipitation (Di Bonito et al., 2024) – and thereby offers a comprehensive view of chemical speciation. These models have successfully identified underlying processes in batch extractions of landfill waste (Dijkstra et al., 2009; Van Der Sloot et al., 2017; van Raffe, Dijkstra, et al., 2025) and in landfill pore-water (van Raffe et al., 2026) and thus are a promising tool for exploring contaminant partitioning in LSR studies.

This study investigates the mechanisms underlying ammonium (NH_4^+) and inorganic contaminant leaching from actively treated waste in LSRs. While the broader experimental design included 16 LSRs representing the three Dutch pilot landfills, this paper focuses on eight LSRs operated under three distinct conditions: leachate recirculation under anaerobic conditions, aeration, and a combination of both. The LSRs were operated for 682 days, with frequent leachate sampling for the analyses of OM and contaminant concentrations. Observed contaminant leaching trends were interpreted by applying a mechanistic geochemical model based on established chemical release mechanisms in landfilled waste (van Raffe, Dijkstra, et al., 2025). The model was parametrized using pH and *in-situ* redox measurements, alongside reactive surface data derived from independent selective extractions. By coupling the analysis of a broad range of contaminants with geochemical modelling, our approach offers a more complete mechanistic understanding of contaminant leaching than previous LSR studies. Furthermore, our findings reveal the complex trade-offs between contaminant leachability and the time required for effective treatment, providing essential data for validating active treatment as a sustainable landfill management strategy.

4.2. MATERIALS AND METHODS

4.2.1. Landfill solid waste sampling

Solid waste samples were collected from the three Dutch pilot landfills: Braambergen 11N (Bra), containing contaminated soil, remediation residues, and construction and demolition (C&D) waste; Kragge (Kra), containing commercial, domestic, and C&D waste; and Wieringermeer (Wie), containing commercial waste, composting residues, and contaminated soils (Yi et al., 2025). Sampling was conducted approximately five years after

the initiation of active treatment at each site: September 2022 (Bra), October 2022 (Wie), and March 2023 (Kra).

The sampling strategy prioritized obtaining sufficient bulk volume for the LSR experiments (see section 4.2.2) rather than establishing spatial representativeness of the pilot sites. Vertical drilling was performed using a sonic samp drill at multiple locations (Bra: 7; Kra: 11; Wie: 3). Drilling proceeded in two-meter intervals until an impenetrable layer or the basal drainage was reached (maximum depths: 12 m at Bra, 18 m at Kra, and 14 m at Wie).

To minimize preferential flow paths in the reactors, the collected waste was sieved to <36 mm (<10% of the LSR inner diameter, to limit preferential flow (ISO 21268-3, 2019)) and thoroughly homogenized prior to filling the LSRs. A subsample was dried at 105 °C to determine moisture content and characterized for parameters relevant for contaminant leaching (section 2.3), and to evaluate the pH dependent leaching of contaminants (see SM1 in the SI).

4.2.2. Landfill simulation reactors

4.2.2.1. General set-up

A schematic overview of the LSRs is provided in Figure 4.1. Briefly, the LSRs consisted of polypropylene (PP) cylinders (60 cm height, 38 cm diameter). A perforated disc (10 mm thickness, 10 mm pore size) separated the waste from the leachate reservoir. An aeration ring was positioned on top of this disc to introduce nitrogen or compressed air; to prevent clogging, this ring was sandwiched between layers of 1 mm PP mesh. Leachate was recirculated using an impeller pump (Modified F2P10-19, Johnson Pump, Sweden) and distributed evenly via a custom 3D-printed PP divider. All reactors were insulated with foam rubber and heated via mats to maintain an internal temperature of 34 °C.

The LSRs were filled with moist waste equivalent to 27 kg dry matter (DM) for Kra and 30 kg DM for Bra and Wie. Subsequently, 1 L of demineralized water was added to non-recirculation LSRs (final moisture content: Bra 38%, Kra 75%, Wie 41%). Recirculation LSRs required higher volumes of water were required to ensure pump functionality, with variable amounts added due to differing waste water retention capacity (added water: Bra 9 L, Kra 5 L, Wie 8 L; final moisture contents: Bra 68%, Kra 90%, Wie 62%). Redox potential of the waste was logged hourly using an in-situ redox probe (ORP 40-4-B, Swap Instruments, NL) and a separate reference electrode (Ag/AgCl, KCl, 3 M, REF-12-0-A, Swap Instruments, NL), at 7.5, 17.5, 27.5, and 37.5 cm (measured from the bottom of the waste). The redox potential was recalculated from mV to pe, correcting for the reference electrode (Wolkersdorfer, 2008).

4.2.2.2. Experimental conditions

The experimental treatment conditions are detailed in Table 4.1. This study evaluates three distinct operation regimes: i) Recirculation, with leachate recirculation under anaerobic conditions; ii) Aeration, with aeration and no leachate recirculation. For Bra and Kra, aeration was followed by an anaerobic period; iii) Recirculation-Aeration, with a period of leachate recirculation under anaerobic conditions followed by a period of aeration without leachate recirculation. Prior to the start of above treatments, all LSRs had a 139-day anaerobic initialization period without gas input.

Table 4.1 Operational conditions of the landfill simulation reactors (LSR). Anaerobic conditions are annotated as An. Aeration is annotated as Ae. All treatments were prefaced by a 139-day anaerobic initialization period without gas input

Operational name	**Condition (An/ Ae)**	**Anaerobic period**	**Aerobic period**	**Gas input**	**Recirculation**
-		**[days]**	**[days]**	**[ml/min]**	**[l/w]**
Recirculation	An	543	-	2 (N_2)	1
Aeration[a]	Ae – An	108	435	2 (N_2) + 10 (Air)	-
Recirculation-Aeration	An – Ae	252	291	2 (N_2) + 10 (Air)	1[b]

a The aeration LSR of Wie was not returned to anaerobic conditions and was kept under aeration.

b Recirculation was applied only under anaerobic conditions, and stopped under aeration.

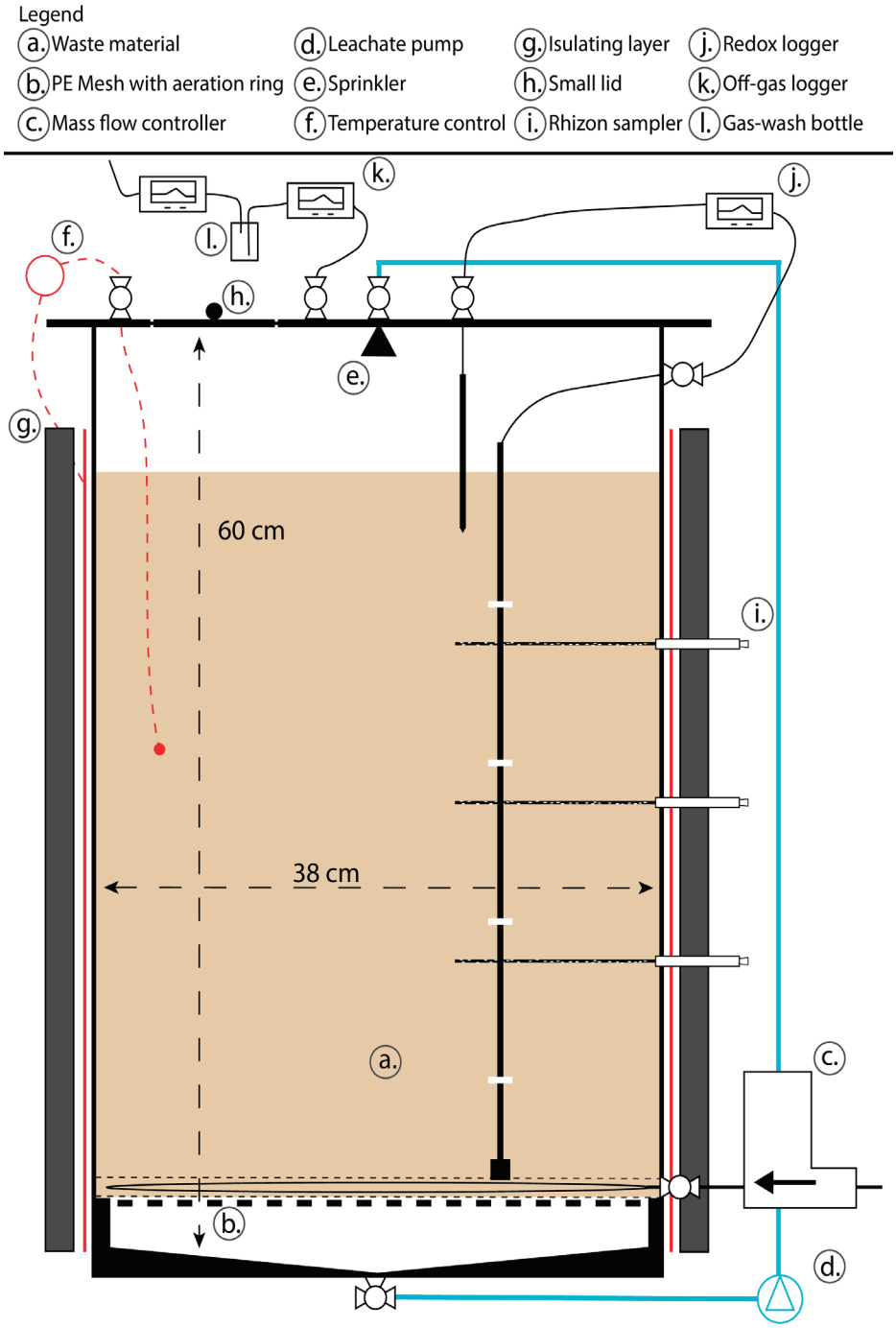


Figure 4.1 Schematic overview of the landfill simulation reactors used in this study.

Anaerobic conditions were maintained by continuous N_2 gas injection (2 ml/min). Leachate recirculation was applied at a rate of 1 L/week (approx. 20 times the field intensity at

Kra). Aeration was achieved using compressed ambient air with a continuous flow of 10 ml/min (five times the target field rate for Bra and Wie).

For the Recirculation-Aeration LSRs, the operational mode switched to aeration after 139 days of initialization and 252 days of recirculation. To ensure effective aeration, accumulated leachate was gravimetrically drained prior to the switch. The aeration LSRs of Bra and Kra were reverted to anaerobic conditions (2 ml N_2/min) after 139 days of initialization and 435 days of aeration. Thus, potential leachate quality changes following the termination of aeration and the return of anaerobic conditions could be investigated.

To simulate rainfall, 500 ml of demineralized water was added every 2-3 weeks 500 to all non-leachate recirculation LSRs; for anaerobic LSRs this water was purged with N_2 prior to addition to prevent oxygen ingress.

4.2.2.3. Leachate sampling

A 5 cm reservoir between the perforated disc and LSR base (Figure 4.1) allowed for leachate accumulation between sampling events. At each sampling round, 100 ml of leachate was collected. To ensure that samples represented the specific time interval between sampling rounds, all remaining leachate was gravimetrically drained from the non-recirculation LSRs following sample collection (implemented from the second sampling round onwards). Samples were stored at 4°C prior to analyses.

4.2.2.4. Solid phase sampling

To monitor solid phase changes, six sacrificial PP mesh bags (~250 g wet waste, 3 mm PP mesh) were embedded in each LSR. At three intervals during operation, a mesh bag was retrieved through the small lid on top of the LSRs, sieved (4 mm), and stored at 4°C prior to pre-treatment and analyses.

4.2.3. Sample analyses

4.2.3.1. Leachate analyses

The pH and electrical conductivity were measured immediately upon collection. Samples were subsequently filtered through 0.45 µm cellulose filters and split into three aliquots. Chloride and NH_4^+ were analysed on a discrete analyser (Skalar Bluvision, Analytical B.V., Breda, *The Netherlands*). From round 7 onwards, NH_4^+, NO_2^- + NO_3^-, and total N were measured using a segmented flow analyser (SFA, San++, Skalar Analytical B.V., Breda, *The Netherlands*). Other inorganic contaminants were, after acidification to a concentration of 0.14 M HNO_3, analysed on an Inductively Coupled Plasma – Optical Atomic Emission Spectrometer (ICP-OES iCAP 6500 DUO, Thermo Fisher Scientific Inc., Waltham, *MA, USA*) (Al, Ca, Cu, Fe, K, Mg, Mn, Na, P, Si, Z) and High Resolution – Inductively Coupled Plasma – Mass Spectrometry (HR-ICP-MS Element 2, Thermo Fisher Scientific Inc., Waltham,

MA, USA) (Al, As, Ba, Cd, Co, Cr, Cu, Fe, Mn, Ni, Sb, Sr, V, Zn). The remaining aliquot was used to determine organic C (OC) by measurement of total and inorganic C (TC and IC respectively, where OC = TC - IC) using a SFA. In addition, this aliquot was subjected to rapid batch fractionation (Van Zomeren & Comans, 2007) to determine dissolved humic substances (HS: humic acid (HA), fulvic acid (FA), hydrophilic acid (Hy), and hydrophobic neutrals (HON)).

4.2.3.2. Chemical extractions of solid waste

Reactive solid phases were characterized using selective extractions on the mesh bag samples. Amorphous Al- and Fe (hydr)oxide contents were estimated via ammonium oxalate (ISO 12782-3, 2012) and ascorbic acid (ISO 12782-1, 2012) extractions, respectively; crystalline Al- and Fe (hydr)oxides were estimated using the dithionite extraction (ISO 12782-2, 2012). Concentrations of Al and Fe in the extracts were measured with an ICP-OES. The total amount of HS and its subfractions (HA, FA, Hy, HON) was determined through acid-base extraction followed by rapid batch fractionation (Van Zomeren & Comans, 2007) and subsequent OC determination with a SFA. Clay content was measured via the sieve and pipette method (Houba et al., 1995), yet not for the mesh bag samples. Finally, total reactive contaminant contents were determined by 0.43 M HNO_3 extraction (Groenenberg et al., 2017) and water-extractable concentrations by ultrapure water (UPW) extraction (L/S 10) followed by analysis via ICP-OES and HR-ICP-MS for macro- and trace elements (see section 4.2.3.1 for specific elements).

4.2.4. Geochemical modelling

Geochemical modelling was conducted in the modelling framework ORCHESTRA (Meeussen, 2003) in a similar set-up as van Raffe, Dijkstra, et al. (2025). This approach included modelling adsorption to reactive surfaces (HA, FA, Al- and Fe (hydr)oxides, clay) together with the formation of inorganic complexes and precipitation/dissolution of mineral phases based on the thermodynamic constants in the MINTEQV4 database (US EPA, 1999). Adsorption to HA and FA was modelled using the NICA-Donnan model (Kinniburgh et al., 1996), considering the generic parameters of Milne et al. (2001, 2003) and taking the measured dissolved (section 4.2.3.1) and solid (section 4.2.3.2) HA and FA as input with an assumed carbon content of 50% (Pribyl, 2010). Adsorption to Al- and Fe (hydr) oxides was modelled using the generalized two-layer model and generic parameters of Dzombak & Morel (1990) taking hydrous ferric oxide (HFO) as a singular proxy for metal (hydr)oxides due to the limited database of Al (hydr)oxides (Meima & Comans, 1999). The content of HFO was based on the measured quantities of amorphous and crystalline Al- and Fe (hydr)oxides (section 4.2.3.2). For amorphous (hydr)oxides a molar ratio of 84 g Al/mol HFO, 95 g Fe/mol HFO (Hiemstra & Van Riemsdijk, 2009), and a reactive surface area of 600 m^2/g (Dzombak & Morel, 1990) was assumed. For the crystalline (hydr) oxides a molar ratio of 78 g Al/mol HFO, 89 g Fe/mol HFO, and a reactive surface area of 100 m^2/g (Dzombak & Morel, 1990; Van Eynde et al., 2020) was assumed. In line with van

Raffe, Dijkstra, et al. (2025), calculated HFO was corrected for binding to solid OM and dissolved OM based on separate model calculations and for dissolution of amorphous (hydr)oxides based on measured dissolved Al and Fe concentrations in solution. A further correction was made to account for sulphides in the anaerobic LSRs, as part of the initially determined oxides likely dissolved and formed sulphides and as during pretreatment of the waste in the mesh bags these sulphides may have partly dissolved and reformed as oxides; both instances result in an overestimation of the oxide content. To this end, HFO contents were halved based on the model-predicted relevance of Fe-sulphide formation (pH + pe < 8). Contrary to van Raffe, Dijkstra, et al. (2025), adsorption to clay was modelled using a Donnan model, taking measured clay content as input and assuming all clay to be illite with a Donnan volume of 1 L/kg (Weng et al., 2001). Additional inputs consisted of a calculated liquid:solid ratio (L/S), measured leachate pH, pe, dissolved concentrations of IC and competing elements, and reactive element concentration (0.43 M HNO_3 extraction) of the element of which the dissolved concentration is to be predicted, based on the aforementioned input parameters and in a similar fashion to van Raffe, Dijkstra, et al. (2025). The model was used to calculate the solid-solution partitioning and speciation of all analysed elements in both the solid and solution phase for three distinct datasets: LSR leachate (section 4.2.3.1), the pH-dependent test (section SM4.1, SI), and the mesh bag extracts (section 4.2.3.2). Findings from the latter two experiments were used to build the modelling framework of the LSR leachate modelling and are described in the SI (section SM4.2); the LSR leachate modelling is described below.

The LSR leachate was modelled as a well-mixed batch system. While the LSRs are dynamic systems, we believe this batch equilibrium approach was appropriate as the leachate was collected on average over a period of one month between sampling rounds, following which leachate was fully drained from the LSRs. Each leachate sample was thus a representation of the entire LSR for the entire period between sampling rounds. The L/S ratio was calculated based on a mass balance approach, with total liquid calculated from added (initial water and added e.g. through rain simulation) and removed water (drainage and leachate sampling), and the solid weight being the initial dry weight minus the dry mass removed with the mesh bags. Dissolved element and OM concentrations together with pH were measured in the leachate samples. The redox potential (pe) measured at 7.5 cm from the bottom of the waste was used as model input. The solid reactive surfaces and reactive elements content was set to those determined in the mesh bags extractions; for leachate sampling rounds where mesh bags were not sampled, inputs were set equal to the last round in which mesh bags were analysed. Assumed mineral forms in the modelling were based on van Raffe, Dijkstra, et al. (2025) and listed in Table S4.2.

4.3. RESULTS

4.3.1. General parameters

Operational conditions (Table 4.1) significantly influenced the redox potential (Figure 4.2). Under leachate recirculation, strongly reducing conditions (pe ≈ -7.5) prevailed irrespective of waste origin. In contrast, continuous aeration led to a steady increase in redox potential, stabilizing at different plateaus for the different wastes: pe ≈ 0 for Kra, pe ≈ 3 for Bra, and a two-step increase for Wie (pe ≈ -1 then ≈ 3). The Recirculation-Aeration treatment resulted in a more rapid oxidation for Kra and Wie compared with continuous aeration. Here Kra exhibited a two-step increase (pe ≈ 0 then ≈ 5), while Wie directly increased to stabilize at the same level as for continuous aeration (pe ≈ 3). This accelerated response is likely due to the drainage step performed before switching the operational conditions, which effectively removed dissolved reductants. Unexpectedly, the Bra Recirculation-Aeration LSR showed no distinct increase of the redox potential after the switch to aeration. This absence is probably due to compaction of the finer, clay-rich waste during leachate recirculation restricting gas permeability, as this compaction was observed during waste sampling upon LSR termination.

Leachate pH increased slightly during recirculation, exceeding above 8.0 (Figure 4.2), a value characteristic of methanogenic or stable phase landfills (Sanphoti et al., 2006). Conversely, aeration caused a pH decrease, consistent with previous LSR studies (Raga & Cossu, 2013; van Turnhout et al., 2018). This acidification is likely driven by the production of organic acids during stimulated OM degradation (Sundberg et al., 2004) and proton release during nitrification (Nag et al., 2018; Rasmussen, 1990).

Reactive organic matter fractions (HA and FA) increased in concentration during recirculation (Figure 4.2), correlated with the observed increased pH (van Raffe, Dijkstra, et al., 2025). The lower HA and FA concentrations under aeration are attributed to stimulated microbial degradation and the observed decreasing pH (Figure 4.2).

4.3.2. Inorganic contaminants

Inorganic contaminant concentrations in the LSR leachate showed a strong dependence on operational conditions (Figures 4.3 & S4.7), driven by the previously described shifts in redox potential, pH, and dissolved HS. Based on mechanisms identified in the pH-dependent leaching tests (section SR4.1) and mesh bag extracts (Figures S4.4 & S4.5), contaminants were categorized as anionic and two cationic subdivisions based on i) redox sensitivity and ii) the observed pH of minimum solubility (Figure S4.2). The geochemical model generally captured the observed leaching trends (Figure S4.9), yet root mean square error (RMSE) (Bennett et al., 2013) values frequently exceeded 1 (Figure S4.10), indicating strong deviations between model calculations and measurements which are discussed below.

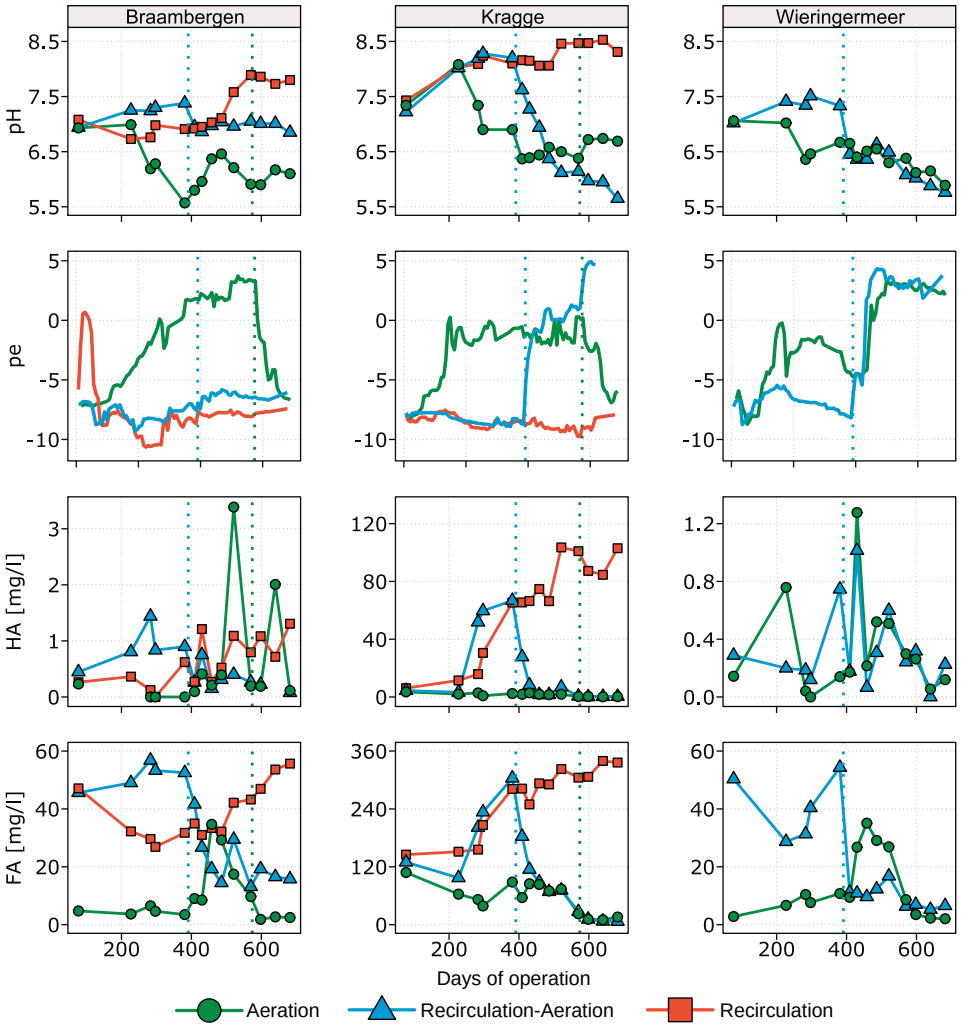


Figure 4.2 Measured changes in general parameter in the landfill simulation reactors during the operation under different operational conditions. The vertical dotted lines indicate the date at which the Recirculation-Aeration LSR switched from recirculation to aeration (blue) and when the aeration LSRs of Braambergen and Kragge switched from aeration to anaerobic conditions (green).

4.3.2.1 Reactive anions

Anionic contaminant concentrations, represented by As (Figure 4.3), generally remained stable under recirculation and decreased under aeration. The geochemical model adequately predicts these trends, identifying adsorption to Fe/Al (hydr)oxides as the controlling mechanism for all operational conditions (Figure 4.4). The observed decrease in As leachate concentrations during aeration is attributed to increased anion adsorption to these Fe/Al (hydr)oxides at the lower pH (Hiemstra & Van Riemsdijk, 1999; Kosmulski, 2016). This pH-dependency was clearly demonstrated in the pH-dependent test (Figure

S4.2) and best exemplified by the Bra aeration LSR, where a minor pH increase around day 500 (Figure 4.2) triggered a simultaneous spike in anionic concentrations (Figures 4.3 and S4.7). In addition to changing pH, the oxidation

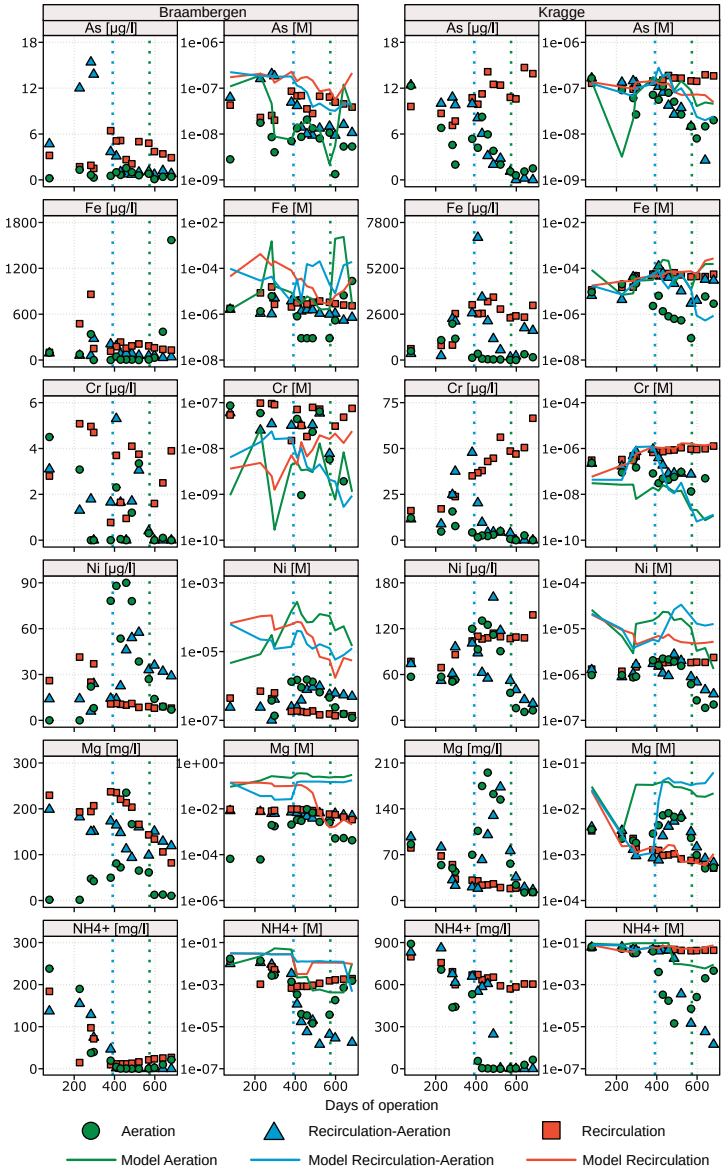


Figure 4.3 Measured (symbols) and modelled (lines) concentrations of contaminants in the LSR leachates during LSR operation under different operational conditions. The vertical dotted lines indicate the date at which the Recirculation-Aeration LSR switched from recirculation to aeration (blue) and when the aeration LSRs of Braambergen and Kragge switched from aeration to anaerobic conditions (green).

of Fe-sulphides during aeration may have induced the (neo)formation of metal (hydr) oxides (Couture et al., 2013) and thereby provide additional binding sites, which further explains the observed reduced anion mobility during aeration.

The other anionic contaminants (Mo, Sb, and P) all showed a similar decrease in concentrations during aeration, albeit with an initial increase in Mo and Sb concentrations (Figure S4.7). This was again predicted to be predominantly controlled by Fe/Al (hydr)oxide binding and a predicted formation of calcium-phoshate minerals for P (Figure S4.12). Under leachate recirculation Mo and Sb concentrations decrease and P concentrations increase, with the contrary result of the latter potentially related to organic P mineralization, as was previously found under anaerobic conditions (Vink et al., 2010), or due to a stronger pH dependence of P at a pH of 8 (Figure S4.2).

4.3.2.2. Reactive cations

Cationic contaminants can be distinguished based on their response to a changing redox potential (via changes in their valency or changes in the stability of sulphide minerals) and their pH of minimum solubility (section SR4.1).

Redox sensitive cationic contaminants

Concentrations of redox sensitive cations, represented by Fe, were stable under leachate recirculation and initially increased and subsequently decreased under aeration (Figure 4.3). The geochemical model predicted Fe to be present as a sulphide mineral under the anaerobic conditions of leachate recirculation (Figure 4.4). Upon aeration, sulphide oxidation and mineral dissolution released Fe to solution, following which Fe concentrations decreased due to the precipitation of first carbonate and then (hydr)oxide minerals (Figure S4.13). This order of mineral precipitation is consistent with predicted Fe behaviour in anaerobically deposited soils (Vink et al., 2017).

The reversibility of the above mechanisms can be observed for the Bra and Kra Aeration LSRs, which return to anaerobic conditions on day 591 caused a spike in leachate Fe concentrations (Figure 4.3) as formed Fe-(hydr)oxides re-dissolved as Fe^{2+}. The model captured this dissolution, yet predicted a rapid re-formation of Fe-sulphides and a corresponding drop in Fe concentrations (Figure 4.4 & Figure S4.13). This drop is not yet observed in the measurements, suggesting a kinetic lag.

Other redox sensitive metals (Cd, Cu, Mn, and Zn) similarly increased and then decreased during aeration. The initial increase is for all predicted to be a result of sulphide mineral dissolution, while the subsequent decrease is either a result of mineral formation (Mn) or binding to reactive surfaces (Cd, Cu, Zn) (Figure S4.12). Notably, the mesh bag extracts only showed a clear redox sensitivity for Fe and Cu (Figure S4.5), which could only be

modelled accurately by adjusting pe + pH values upwards to account for oxidation during sampling and storage (see section SM4.2).

Reactive cations a with solubility minimum below pH 8

Cationic elements with a solubility minimum below pH 8, exemplified by Cr (Figure 4.3), generally increased in concentration in the recirculation LSRs and decreased in concentration in the aeration LSRs. These trends parallel trends in HS solubility (Figure 4.2), consistent with model predictions that identify binding to dissolved HS (Figure 4.4) as the primary control mechanism for Cr (van Raffe, Comans, et al., 2025; H. Wang et al., 2024). Similar behaviour was observed for Sn and Al in Kra LSRs, which are similarly characterized by a high affinity for OM binding (Milne et al., 2003; Weng, Temminghoff, & Van Riemsdijk, 2002a).

Reactive cations a with solubility minimum between pH 8 and 10

For cationic elements with a solubility minimum between pH 8 and 10, represented by Ni (Figure 4.3), concentrations generally increased (Kra) or remained stable (Bra & Wie) in the recirculation LSRs. During aeration, concentrations initially increased and later decreased. The model poorly predicted these dynamics, predicting Ni to be predominantly bound to Fe/Al (hydr)oxides and OM (Figure 4.4 & S4.11) yet with a high uncertainty considering the poor predictions. The observed differing behaviour of Ni during leachate recirculation for the different waste is in likelihood related to the different pH of minimum solubility. For Kra this pH of minimum solubility is decidedly lower than for Bra and Wie (Figure S4.2), related to its higher OM content (van Raffe, Dijkstra, et al., 2025); the increasing pH under recirculation thus moves away from minimum solubility and results in increasing concentrations. For Bra and Wie the pH hovers around the minimum, resulting in stable concentrations.

The initial Ni concentration increase observed during aeration likely resulted from an increased competition for surface binding sites following mineral dissolution of other elements, specifically the release of Fe upon sulphide dissolution and the to-be-discussed Ca release upon carbonate dissolution. This influx of competing ions displaces Ni, temporarily increasing the leachate concentration. The subsequent decline in Ni aligns with the eventual decrease of these competing elements, alongside a decrease in pH and dissolved HS concentrations (Figure 4.2). The inability of the model to capture this 'peak' trend suggest that the assumed system equilibrium may not be valid during rapid geochemical shifts. Si and Co showed similar trends (Figure S4.7), although Si is predicted to be controlled by the formation of silicate minerals rather than surface complexation (Figure S4.12).

Reactive cations a with solubility minimum above pH 10

Cationic elements with a solubility minimum above pH 10, exemplified by Mg (Figure 4.3), decreased in concentration in the recirculation LSRs and increased before subsequently decreasing in the aerated LSRs. The geochemical model predicts these trends to be predominately steered by mineral precipitation as either struvite or sepiolite (Figure 4.4). Under leachate recirculation, the elevated pH (Figure 4.2) promotes mineral precipitation (van Raffe, Dijkstra, et al., 2025), thereby reducing leachate concentrations. Conversely, the release of Mg during aeration likely stems from mineral dissolution at lower pH and reduced availability of co-precipitating elements. The subsequent decrease under aerated conditions was not captured by the model. Potentially this is the result of a disconnect between the waste mass (where mineral precipitation occurs) and the leachate (on which calculations are based. Other contaminants in this group include Ba, Sr, and Ca, all of which followed similar patterns(Figure S4.7), yet with differing controlling minerals (sulphates for Ba, carbonates for Sr and Ca) (Figure S4.12).

4.3.2.3. Ammonium

Ammonium (NH_4^+) tends to accumulate in landfill leachate due to the absence of nitrification as a removal pathway under anaerobic conditions (Berge et al., 2005; Zhao et al., 2024), making it the contaminant of primary concern (Dijkstra et al., 2018; Kjeldsen et al., 2002). In the LSRs NH_4^+ concentrations decreased under both leachate recirculation and aeration, with a more pronounced decline during aeration (Figure 4.3) related to differences in underlying mechanisms. During leachate recirculation the observed decrease is likely driven by struvite precipitation, as pH increased towards the struvite solubility minimum (around pH 8.5 (R. Kumar & Pal, 2015)) and P concentrations were elevated under leachate recirculation (Figure S4.7). The geochemical model only predicted struvite formation for Kra (Figure 4.4 and S4.17), however here model predictions of NH_4^+ were also most accurate (Figure 4.3). Under aerated conditions the observed decrease of NH_4^+ is attributed to nitrification, where NH_4^+ is oxidized to nitrate (NO_3^-) by nitrifying bacteria, a pathway well-documented in aerobically treated waste (Mertoglu et al., 2006; Wu et al., 2014; Zeng et al., 2012).

The role of competing reductants and growth lag period

A multitude of studies – varying in LSR size, waste composition, and aeration intensity – have similarly demonstrated the potential of aeration to reduce NH_4^+ concentrations (Bolyard & Reinhart, 2016; Borglin et al., 2004; Brandstätter et al., 2015b; Fricko et al., 2021; Hrad et al., 2013; Morello et al., 2016; Nag et al., 2018; Prantl et al., 2006; Ritzkowski et al., 2006; Slezak et al., 2009, 2015). Remarkably, the required aeration period before NH_4^+ concentrations decreased was relatively consistent across studies at approximately 100 days. Considering the vast range of aeration intensities applied (from 22 ml/kg/h in this study to 4800 ml/kg/h (Nag et al., 2018)), this consistency suggests that the oxidation of competing reductants (e.g. OM and sulphides (Borch et al., 2010)) and the growth of ni-

trifying bacteria (Prosser, 2007) are rate-limiting steps for nitrification, rather than oxygen availability. This hypothesis explains why Cossu et al. (2016) did not observe a decrease in NH_4^+ despite applying an aeration rate of 208 ml/kg/h for 90 days; the duration was likely insufficient to exhaust the competing reduced species and facilitate the growth of nitrifying bacteria. This is further supported by studies where aeration was not preceded by an anaerobic initialisation phase or where, instead of sampled landfill waste, synthetic waste was used. In such cases reduced species did not accumulate, and the aerobic microbial community did not switch their metabolism to a very low rate to survive anaerobic conditions (Diab et al., 1993). Correspondingly, aeration allowed for an immediate oxidation of and steep decline in NH_4^+ (Borglin et al., 2004; Slezak et al., 2009, 2015). Nitrification inhibition by sulphides may have further obstructed the removal of NH_4^+ (Iván et al., 2013; Schalk et al., 2019). This effect is well illustrated by the Recirculation-Aeration LSRs in this study: the drainage of leachate removed a significant load of dissolved reductants, facilitating more effective aeration and oxidation of sulphides which resulted in a more rapid decline of the NH_4^+ concentrations (Figure 4.3).

Rebound effects

The efficiency of aeration for NH_4^+ removal is widely recognized (Hao et al., 2010; Ritzkowski & Stegmann, 2007), yet to adhere to legislation criteria the permanence of this removal is critical. A return of the Aeration LSRs of Bra and Kra to anaerobic conditions resulted in a rebound of NH_4^+ concentrations due to ongoing (anaerobic) OM degradation (Figure 4.3). This rebound effect has been noted previously (Fricko et al., 2021a), but was deemed limited and related to a significantly increased NH_4^+ sorption capacity of aerated waste. We found no indication of an increased sorption capacity but rather determined a reduced reactive surface area for our aerated waste (Quist et al., in prep). As such, achieving a permanent reduction of NH_4^+ concentrations via aeration requires the complete removal of the degradable waste fraction, rather than temporary aeration.

4.4. DISCUSSION

4.4.1. Identifying mechanisms underlying contaminant solubility

The present study aimed to elucidate the mechanisms governing contaminant leaching from actively treated waste in LSRs. Multi-surface modelling, underpinned by initial pH-dependent leaching tests of untreated solid waste and UPW extracts of solid waste sampled from the LSR during experimental operation, allowed the identification of key solubility controlling mechanisms – namely mineral precipitation, binding to reactive surfaces, and the importance of redox conditions.

The here identified mechanisms aligned closely with those observed in the pore water of a leachate recirculation landfill (van Raffe et al., 2026). This consistency highlights the

value of controlled ex-situ LSR set-ups in interpreting complex in-situ processes, as the LSRs allow for a detailed analysis of the solid-phase and the use of measured, rather than assumed, redox potentials. This approach revealed the redox sensitivity of Mn and Cd, which was not identified by van Raffe et al. (2026). This discrepancy suggests that the importance of redox conditions may be obscured by sample transport and handing, as could also be noted by the limited redox sensitivity in the results of the mesh bag extracts and the pH dependent test (section SR4.1).

4.4.2. Achieving effective reductions in contaminant concentrations

The operational conditions employed in this study highlighted the importance of the hydrological conditions in active landfill treatment. In the Recirculation-Aeration LSRs, the intermediate drainage of leachate rich in reduced species resulted in rapid changes in redox conditions, thereby accelerating the onset of nitrification and NH_4^+ removal. This suggest that the implementation of aeration as an active treatment strategy could be significantly optimized by actively controlling the hydrological conditions within landfill bodies, draining the waste of moisture to remove competing reductors and improve gas permeability and thereby increase aeration efficacy.

Nonetheless, this study also demonstrated that aeration involves a distinct trade-off. The reduction in NH_4^+ was counterbalanced by the mobilisation of other contaminants, where parallel sulphide oxidation resulted in concentration peaks for several redox-sensitive elements, including Cd, Cu, Fe, Mn, and Zn. Thus, while aeration effectively targets NH_4^+, it risks elevating other contaminants above established target values (Dijkstra et al., 2018).

4.4.3. Implications of active treatment termination

The ultimate goal of active treatment is to reduce contaminant concentrations below the established ETV, ensuring that residual emissions do not pose environmental harm (E. Brand et al., 2016; Dijkstra et al., 2018). The current ETV determination assumes a 'worst-case' scenario where emissions remain constant upon the termination of active treatment. However, our results challenge this assumption.

In the aeration LSRs of Bra and Kra, conditions were reverted to anaerobic after 574 days. Within days, concentrations of NH_4^+ and Fe rebounded. This return to anaerobic conditions is a likely scenario in full-scale landfill bodies once active aeration ceases and residual oxygen is consumed. Consequently, reliance on leachate concentrations alone is insufficient for determining safe active treatment termination. A comprehensive assessment of the 'emission potential', i.e. the total amount of potential releasable contaminant, is required. A full understanding of the emission potential should not be derived only from developments in leachate concentrations, as discussed in this paper, but also requires the development of the solid phase characteristics that steer contaminant mobility.

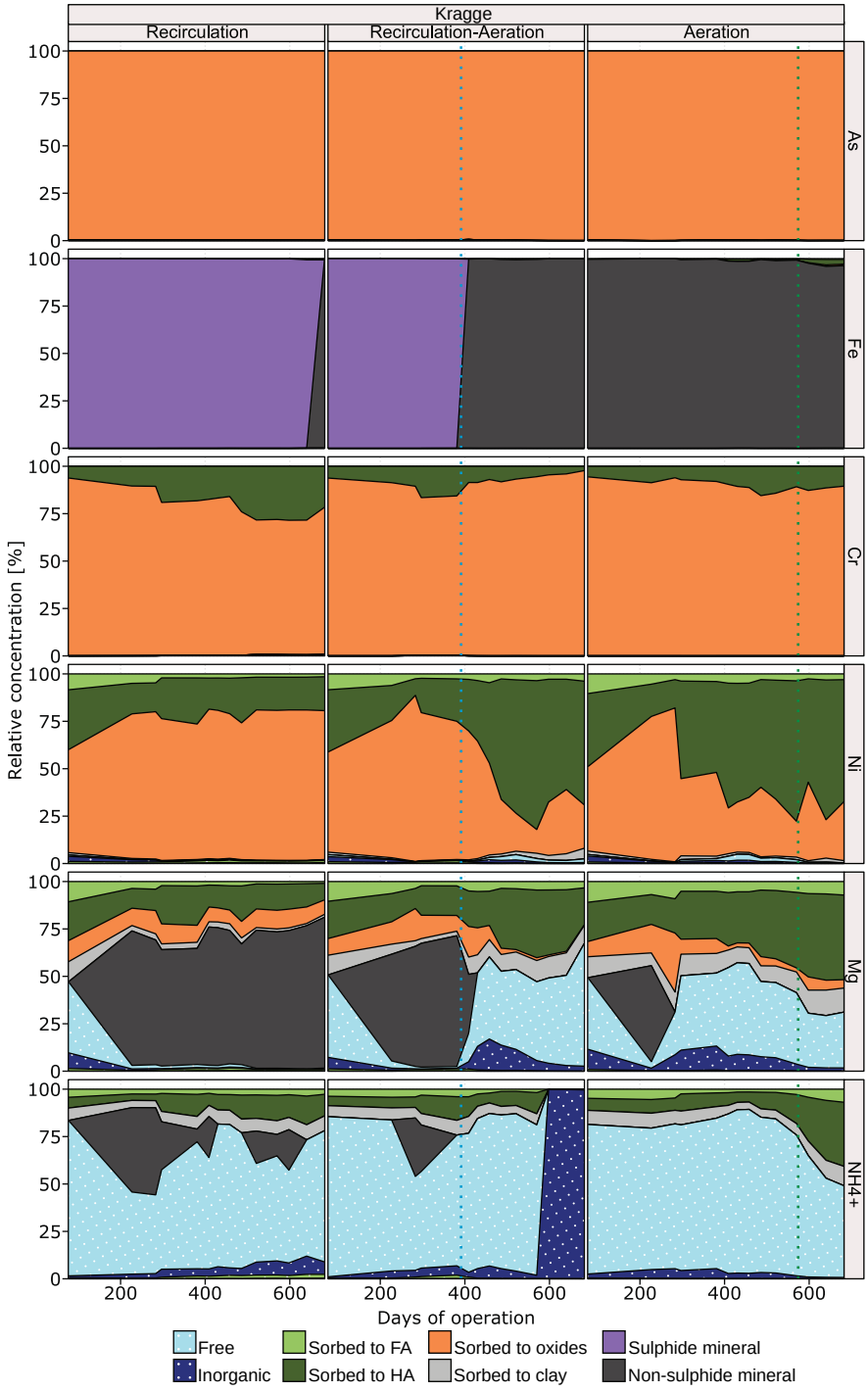


Figure 4.4 Model calculated solid and dissolved phase speciation of contaminants in the Kragge LSRs as a function of time. The vertical dotted lines indicate the date at which the Recirculation-Aeration LSR switched from recirculation to aeration (blue) and when the aeration LSRs of Braambergen and Kragge switched from aeration to anaerobic conditions (green).

4.5. CONCLUSION

This study elucidated the geochemical mechanisms governing hazardous contaminant leaching from landfill waste, demonstrating how these mechanisms drive changes in contaminant mobility during active treatment via aeration and leachate recirculation. By coupling landfill simulation reactors and pH-dependent leaching test with state-of-the-art multi-surface geochemical modelling, we quantified the critical roles of pH, redox potential, mineral formation/dissolution and organic matter leaching in controlling contaminant solubility.

The impact of treatment conditions was distinct. Leachate recirculation maintained strongly reducing conditions, stable humic substances concentrations, and generally increased pH. Consequently, multiple contaminant concentrations increased due to pH-driven solubility increases, while sulphide mineral precipitation controlled the solubility of redox-sensitive elements. Aeration lowered pH and decreased concentrations of both organic and inorganic carbon as the system became more aerobic. This resulted in an initial increase in contaminant concentrations due to mineral dissolution, followed by a decrease driven by binding to reactive surfaces and the formation of new mineral precipitates (e.g. metal (hydr)oxides). Crucially, the efficiency of aeration was improved when preceded by leachate recirculation and subsequent gravimetric leachate drainage. This Recirculation-Aeration strategy effectively removed dissolved reductants prior to aeration, highlighting the importance of adequate landfill drainage to accelerate active treatment.

Aeration proved most effective for the decrease of NH_4^+ and dissolved OM, yet did introduce a critical trade-off in the temporary mobilization of redox-sensitive contaminants which at peak levels exceeded emission target values. Furthermore, a return of the aerated LSRs to anaerobic conditions resulted in a rebound in contaminant (NH_4^+, Fe) concentrations, challenging the assumption that aeration as active treatment results in permanent stability. Therefore, environmentally safe termination of active treatment cannot rely solely on leachate monitoring. It requires a robust characterisation of the solid waste's emission potential to ensure the return to anaerobic conditions does not lead to a future exceedance of emission target values.



Chapter 5

Geochemical processes controlling in-situ contaminant solubility in landfills

Frank van Raffe*, Nick Quist*, Tristan C. Rees-White, Rob N.J. Comans
***These authors contributed equally**

Reproduced with permission from:

van Raffe, F., Quist, N., Rees-White, T. C., & Comans, R. N. (2026). Geochemical Processes Controlling In Situ Contaminant Solubility in Landfills. *ACS ES&T Water*, *6*(3), 1481-1490.

Copyright © 2026 American Chemical Society

ABSTRACT

Sustainable management of landfills through actively reducing contaminant emissions requires knowledge on underlying geochemical processes, which is currently limited. To this end, pore water was sampled across a vertical transect from a landfill subject to leachate recirculation with an *in-situ* collection system. The samples were analysed for pH and the concentration of inorganic contaminants and dissolved organic matter fractions; all showed similar distributions with depth. The underlying mechanisms of this analogous behaviour were identified using geochemical modelling, which captured measured concentrations adequately for most contaminants. While non-reactive contaminant concentrations were best predicted considering limited interaction with the solid matrix and reactive anions were best predicted by metal (hydr)oxide binding, adequate predictions for reactive cations with a high organic matter binding affinity required a description of humic substance fractions. Predictions of other reactive cations were steered by the formation of carbonate or sulphide minerals. The importance of mineral precipitates deviates from previous lab experiments on sampled solid waste, highlighting the importance of modelling *in-situ* samples to explore processes in complex systems such as landfills. The obtained understanding can be used to test landfill simulation reactor results, to aid in understanding impacts of proactive waste management strategies and ultimately facilitate their implementation.

5.1. INTRODUCTION

Worldwide, governments move towards more sustainable waste management, yet increasing waste generation together with remaining untreatable waste and waste treatment residues implies that landfills remain necessary (Hoornweg & Bhada-Tata, 2012; Scharff, 2014). Landfills threaten the environment both through the emission of greenhouse gases (EEA, 2024) and the production of contaminated leachate, which under improper management can be transported to the underlying soil and pollute ground- and surface water (Kjeldsen et al., 2002; Siddiqua et al., 2022; Vaverková, 2019). As per the EU landfill directive, landfilled waste is isolated from the environment through the placement of engineered barriers and the capture and permanent treatment of generated leachate (Council of the European Union, 1999); an effective yet unsustainable practice in which the burden of current waste management is transferred to future generations (Laner et al., 2012).

Exploring more sustainable waste management practices in the Netherlands has been furthered by the signing of a "Green deal" in 2015, which initiated three landfill-scale pilots with the necessary infrastructure to test and understand the effectiveness of aeration and leachate recirculation as active treatment to promote landfill waste stabilization (E. Brand et al., 2016). If this approach can reduce contaminant concentrations in the leachate sufficiently to meet pre-determined and legally defined emission target values (ETV; (E. Brand et al., 2016; Dijkstra et al., 2018)), use of protective top liners and their costly replacement may no longer be necessary, while aftercare of the generated leachate can be reduced (Berge et al., 2009). The Dutch municipal solid waste (MSW) landfill *The Kragge* is subjected to leachate recirculation, with the goal to promote the mixing of nutrients and microbiota and thereby increase organic matter (OM) stabilization and reduce contaminant emissions (Reinhart & Al-Yousfi, 1996; Sinan Bilgili et al., 2007; White et al., 2011).

Although extensive research has been carried out on the effects of leachate recirculation in landfill simulation reactors (LSR; (Ma et al., 2021; van Turnhout et al., 2018)), research on full landfill-scale recirculation is limited (Benson et al., 2007; Chung et al., 2015; L. Liu et al., 2018). Additionally, for both LSRs and landfill scale pilots previous research was limited to overall gas composition and general leachate quality. Yet the large heterogeneity in both the chemical composition and the physical/hydrological accessibility of the waste inherent to a MSW landfill (Konstantaki et al., 2016) makes effective treatment challenging. Moreover, the existence of inevitable preferential flow paths can lead to discrepancies between the composition of waste body pore water and the collected landfill leachate (Aharoni et al., 2020). Consequently, the actual effects and processes occurring within the waste body remain largely unknown, while essential to understand for the development of effective and sustainable waste management strategies.

The mobility and release of contaminants is steered by degradation of the landfilled waste (Brandstätter et al., 2015a; Slezak et al., 2015), hydrological flows (Kosson et al., 1996), and the chemical environment. Solubility of contaminants is significantly impacted by parameters such as pH (Dijkstra et al., 2009; Dijkstra, Van Der Sloot, et al., 2006; van Raffe, Dijkstra, et al., 2025), the concentration of competing ions (Antelo et al., 2005; Hongshao & Stanforth, 2001; Qin et al., 2006), and the quantity and characteristics of reactive organic and mineral surfaces (Bao et al., 2022), particularly solid- and dissolved OM (SOM and DOM) and its subfractions (humic acid (HA), fulvic acid (FA), hydrophilic acid (Hy), and hydrophobic neutrals (HON)) (Van Zomeren & Comans, 2007). The exact controls behind contaminant leaching, i.e. inorganic complexation, adsorption to reactive surfaces, and/or mineral precipitation, can be explored through geochemical modelling (Di Bonito et al., 2024) as has been done successfully among others in soils (Dijkstra et al., 2009; Uddh-Söderberg et al., 2024) and waste (Astrup et al., 2006; Dijkstra, Van Der Sloot, et al., 2006; van Raffe, Dijkstra, et al., 2025).

This paper presents the composition of pore water samples obtained via an in-situ vadose monitoring system (VMS) in *The Kragge*, focusing particularly on the vertical heterogeneity of DOM and associated inorganic contaminants. To our knowledge this is the first time that DOM and its composition along with a wide range of inorganic contaminants is investigated in in-situ pore water across a vertical transect in a landfill subjected to leachate recirculation. With this characterization, supported with geochemical modelling, we aim to elucidate processes controlling in-situ dissolved contaminant concentrations which were previously only indirectly deduced (Aharoni et al., 2017, 2022) or investigated *ex-situ* (van Raffe, Dijkstra, et al., 2025). This study can thus provide important added value to regular leachate monitoring to understand contaminant mobility in landfills during active treatment, in support of evaluating the feasibility to obtain compliance with emission target values (E. Brand et al., 2016; Dijkstra et al., 2018).

5.2. MATERIALS AND METHODS

5.2.1. Site description

In-situ pore water samples were collected from *The Kragge* landfill near *Bergen op Zoom* in the Netherlands. The landfill cell of interest has been in operation from 1997 until 2007 and is filled with predominantly MSW (Yi et al., 2025). The waste has been subject to leachate recirculation since 2017; prior to the leachate recirculation the waste has been sampled and characterized for three different depth intervals (van Raffe, Dijkstra, et al., 2025). An additional solid waste sampling was performed one year after installation of the VMS described in the following section, for a characterization that more closely coincides with the collected pore water samples.

5.2.2. Pore water sampling

The vadose zone of the landfill was sampled through two VMS (Dahan et al., 2009), referred to as VMS A & B. Both VMS are made of polyvinyl chloride liners and were installed at a 45-degree decline in October 2021. Sampling cells were located at ~0.4 metre intervals between 3 – 6.5 metres and between 9.6 – 13 metres below the surface (Figure 5.1). A detailed description of VMS installation and operation can be found elsewhere (Stringfellow et al., 2023). Contact between the sampling cells and the surrounding waste body was ensured by pumping a grout (5:1:0.8, water:cement:bentonite, Table S5.2) bottom-up into the VMS. The two sampling rounds (October 2022 & May 2023) presented in this paper were part of a three-monthly pore water sampling campaign (July 2022 – March 2024) and selected as representative depth profiles to illustrate identified geochemical processes, specifically regarding pH trends as described in the results section. Samples were collected in PET bottles and stored at 4 ^{0}C prior to pre-treatment and analysis. The sampling campaigns also include samples from a common leachate collection pit, representing the overall leachate flowing out at the base of the landfill.

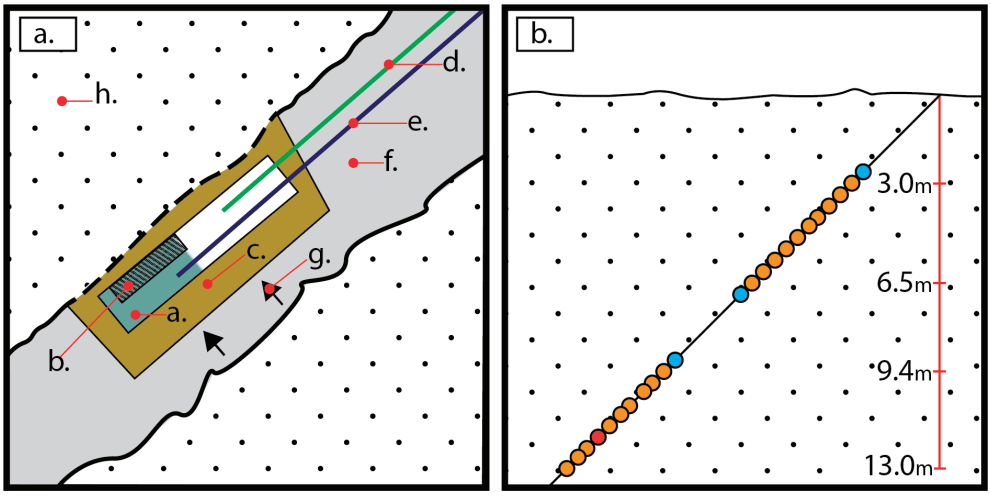


Figure 5.1 Schematic depiction of (a.) a vadose monitoring system (VMS) sampling port: with the sampled pore water (a.), collected through a porous ceramic unit (b.), surrounded by quartz flour (c.). Pore water is sampled via application of under-pressure in the sampling port (d.) and transported to the surface via a second tube (e.) by applying overpressure. Grout (f.) was pumped into the VMS during installation to ensure good connection between the sampling port and surrounding waste (h.) via attachment pressure (g.). The VMS was installed at a 45-degree incline (b.). The sampling ports, depicted by the orange circles, are situated in two 10-port clusters with depths from the landfill surface of 3.0 to 6.5m and 9.4 to 13.0m. The blue circles represent Flexible Time-Domain Reflectometry probes to monitor water content at three different depths. For VMS A, the sample port at 11.9m below the landfill surface did not function and is depicted with a red circle.

5.2.3. Sample pre-treatment and analysis

On the day of sampling, pH and electrical conductivity were measured in unfiltered samples using their respective electrodes. The pore water samples were subsequently filtered over a 0.45 µm cellulose nitrate filter pre-rinsed with ultrapure water (UPW). Part of the filtrate was acidified to a concentration of 0.14 M HNO_3 and analysed on an Inductively Coupled Plasma – Optical Atomic Emission Spectrometer (ICP-OES iCAP 6500 DUO, *Thermo Fisher Scientific Inc., Waltham,*) and an Inductively Coupled Plasma – Mass Spectrometry (ICP-MS Element 2, *Thermo Fisher Scientific Inc., Waltham,*) for Aluminium (Al), Arsenic (As), Barium (Ba), Calcium (Ca), Cadmium (Cd), Cobalt (Co), Chromium (Cr), Copper (Cu), Iron (Fe), Potassium (K), Lithium (Li), Magnesium (Mg), Manganese (Mn), Molybdenum (Mo), Sodium (Na), Nickel (Ni), Phosphorus (P), Lead (Pb), Sulfur (S), Antimony (Sb), Silicon (Si), Tin (Sn), Strontium (Sr), Vanadium (V), and Zinc (Zn). A second part of the samples was analysed non-acidified on a Segmented Flow Analyser (SFA San++, *Skalar Analytical B.V., Breda, The Netherlands*) for total carbon (TC) and inorganic carbon (IC) which gives dissolved organic carbon (DOC) via TC-IC = DOC, Ammonium (NH_4^+), Nitrite and Nitrate (NO_3^- + NO_2^-), and total Nitrogen (Nts); and on a discrete analyser (Skalar Bluvision, *Analytical B.V., Breda, The Netherlands*) for Chloride (Cl). The DOC in the remaining filtrate was further separated into HA, FA, Hy, and HON through rapid batch fractionation (Van Zomeren & Comans, 2007).

5.2.4. Geochemical modelling

Geochemical modelling of the inorganic contaminants was conducted in the modelling environment ORCHESTRA (Meeussen, 2003), in a similar setup to van Raffe, Dijkstra, et al. (2025). This modelling approach calculates inorganic complexation in solution and formation of possibly-occurring mineral precipitates based on thermodynamic equilibrium constants present in the MINTEQV4 database, adsorption to HA and FA using the NICA-Donnan model (Kinniburgh et al., 1996), and adsorption to metal (hydr)oxides using the generalized two-layer model (Dzombak & Morel, 1990). Modelling is conducted in separate model runs, using total reactive concentrations of the to-be-modelled element and measured dissolved concentrations of all other elements to better represent potential competition effects. The present modelling set-up deviates from the approach of van Raffe, Dijkstra, et al. (2025) in the addition of clay adsorption as calculated using a Donnan model, the use of an improved NICA-Donnan parameter set for Cr (van Raffe, Comans, et al., 2025), Cu, Cd, and Zn (Wiersma et al., 2025), and an adapted set of possible minerals due to the reducing conditions and higher than atmospheric CO_2 pressure occurring within the landfill. All deviations from the generic binding parameter sets for NICA-Donnan (Milne et al., 2001, 2003) and GTLM (Dzombak & Morel, 1990), together with possibly-occurring minerals, are listed in Table S5.3.

The large heterogeneity inherent to waste, together with the limited available information regarding the environment surrounding individual sampling ports, makes geochemical

modelling of solid waste/pore water partitioning processes challenging. To characterize the waste surrounding the sampling ports, waste was sampled at 11 locations on the landfill in vertical steps of one to two metres and separated into three depth intervals (0 – 6 m, 6 – 12 m, 12 – 18 m). Waste characterisation for each of these layers was based on various solid phase extractions as outlined below, and layer characteristics were assigned to sampling ports based on their depth in the landfill. An overview of the extracted amounts of reactive organic and mineral surfaces is listed in the SI (Table S5.1). Solid HA & FA were determined using rapid batch fractionation (ISO 12782-4, 2012; Van Zomeren & Comans, 2007), and quantified on a weight basis by assuming an OM carbon content of 50% (Pribyl, 2010). Hydrous ferric oxide (HFO) was used as a proxy for Al/Fe (hydr)oxides (Meima & Comans, 1999). Amorphous Al- and Fe (hydr)oxides were measured through ammonium oxalate (ISO 12782-3, 2012) and ascorbic acid (ISO 12782-1, 2012) extractions respectively, assuming molar masses of 84 g Al and 95 g Fe per mol HFO (Dijkstra et al., 2009), and a reactive surface area of 600 m^2/g (Dzombak & Morel, 1990). Crystalline Al- and Fe (hydr)oxides were measured using a dithionite extraction (ISO 12782-2, 2012), assuming molar masses of 78 g Al and 89 g Fe per mol HFO (Van Eynde et al., 2020) and a reactive surface area of 100 m^2/g. Clay content was determined using the sieve and pipette method (Houba et al., 1995), yet only for a mixed sample which was not separated based on sampled depth; hence the clay content was considered constant with depth. Total reactive metal contents were measured in 0.43 M HNO_3 extracts (Groenenberg et al., 2017; ISO 17586, 2016) using ICP-OES and ICP-MS. Further model inputs were the measured pH, a liquid:solid (L/S) ratio of 1 based on the three-layer measured moisture content of ~100% (dried at 105°C for 24 hours), and measured dissolved concentrations of HA, FA, inorganic carbon (IC), and competing ions. A pH + pe of 6 was assumed, representative of a reducing environment, based on preliminary modelling of the redox sensitive elements Cu, Fe, Mn, and Zn and in line with redox measurements of sampled *Kragge* waste in a landfill simulation reactor study. This assumption was made as ex-situ redox measurements were unstable and not representative due to sample exposure to the atmosphere. The distribution and speciation of the targeted contaminants between the solid and dissolved phase was calculated. Overall modelling adequacy was determined based on the root mean square error (RMSE; (Bennett et al., 2013)) of the logarithm of measured and modelled dissolved concentrations. Two additional modelling runs were conducted to show the uncertainty of this modelling approach, and particularly the uncertainty of solid phase characteristics surrounding specific sampling cells: a run using the highest measured reactive surface contents and lowest reactive concentrations of each element (being the condition with lowest calculated dissolved concentrations), and vice versa (being the condition with highest calculated dissolved concentrations).

5.3. RESULTS

5.3.1. pH and non-reactive contaminants

The pH of the pore water increases with depth in both VMS (Figure 5.2a, b), with the pH in the lower regions exceeding the pH found in the leachate. While for both VMS a similar slight increase in pH with depth can be observed in the upper part, the VMS deviate in the lower region; for VMS A the trend of a slight increase in pH with depth continues, whereas in October 2022 strongly elevated pH values of up to 13 are found in VMS B. This strong increase is attributed to leaking of grout used during the installation of the VMS, corroborated by the elevated ratio of Na/Cl for these samples (> 5, Figure S5.1) which approach those of the grout (~10, Table S5.2). Pore water samples influenced by the grout thus deviate from the original surrounding waste environment. Nevertheless, the elevated pH, and its effects on OM as discussed later, does provide additional insight in processes that control the distribution and speciation of contaminants, in a similar way as pH-dependent leaching experiments in the laboratory (van Raffe, Dijkstra, et al., 2025). Moreover, these conditions provide insights relevant for landfills that are more dominated by cement(like) materials such as construction & demolition waste (Butera et al., 2014).

Contaminants considered as non-reactive are Cl (Figure 5.2c, d), K, Li, and Na (Figure S5.2), all of which are indeed predicted by the geochemical model to have limited interaction with the solid matrix. Consequently, pore water concentrations are determined by their initial concentration, water flow, and transport through the waste. The model predictions for these contaminants are adequate except for Cl, for which the RMSE slightly exceeds 1 (Table S5.4, Figure S5.3). These adequate predictions show that both the extractions and the moisture content determination of sampled waste represent the waste surrounding the VMS and provide reliable input for the geochemical model. All non-reactive contaminants increase in concentration with depth, potentially due to downward transport from the top layer and/or waste compaction leading to a lower L/S and accompanying higher concentration of elements. The concentration of non-reactive elements is variable for the lowest five sampling ports of VMS B, which can be linked to the previously noted leakage of grout as elements with a high content in the grout (i.e. Na, Li; Table S5.2) are elevated in the pore water (Figure S5.2). For VMS A the lowest two sampling ports have reduced concentrations for all non-reactive elements and dissolved inorganic carbon (DIC) (Figure S5.4). The reduced concentrations could be an indication of an impermeable layer above these sampling ports, limiting downflow and thus these pore water samples represent a waste environment that is distinct from the samples above it. This is further supported by field observations during waste sampling and VMS installation, where a sudden change from no to several metres of standing water was encountered around 12 metres depth.

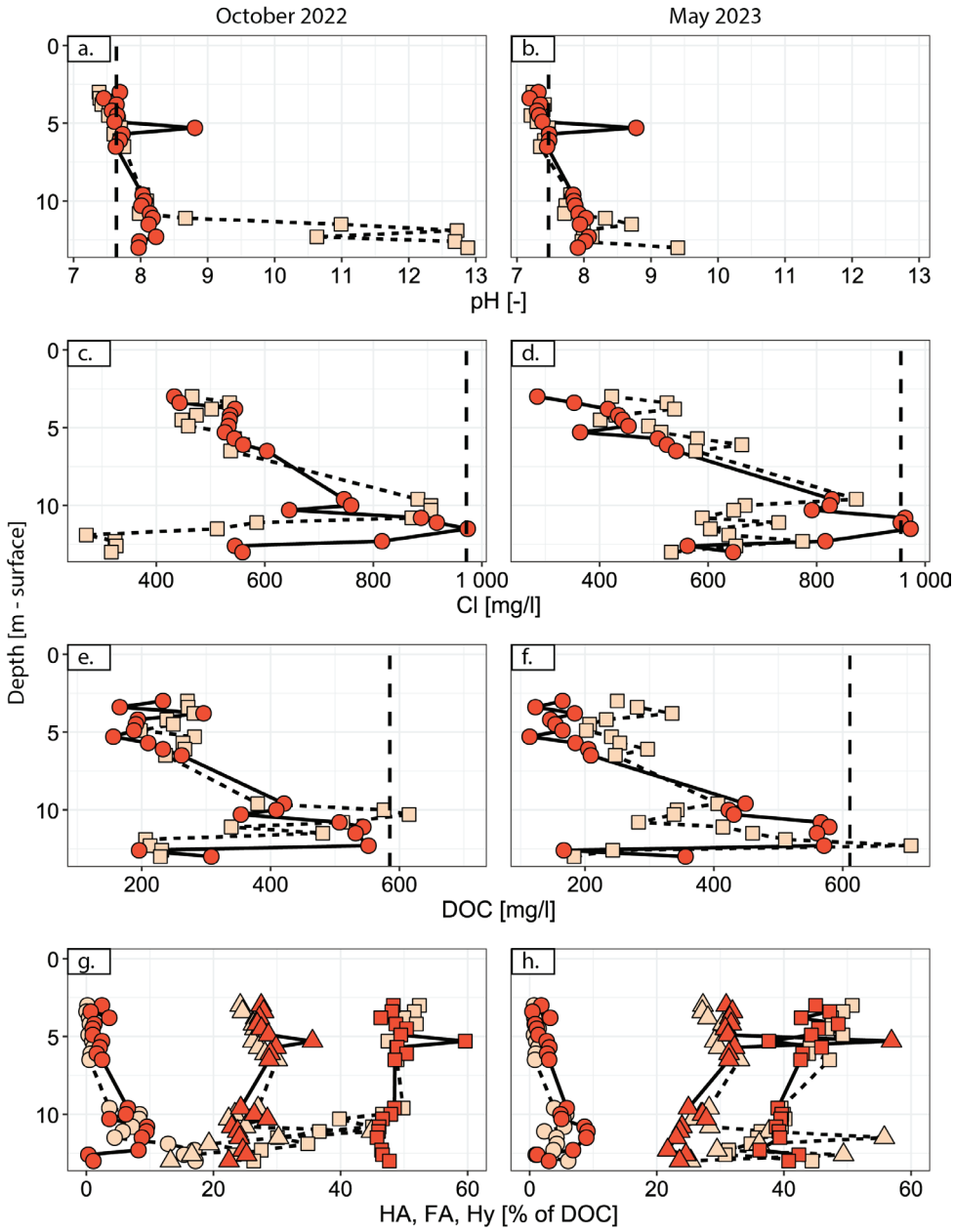


Figure 5.2 The pH of landfill pore water as a function of depth in VMS A (red circles), VMS B (beige squares), and measured simultaneously in the leachate collected from a leachate collection pit (dashed lines) in a.) October 2022 and b.) May 2023. The chloride concentration of landfill pore water in c.) October 2022 and d.) May 2023. The DOC concentration of landfill pore water in e.) October 2022 and f.) May 2023. The relative contribution of humic substance fractions in DOC of landfill pore water in VMS A (red) and VMS B (beige), humic acid (circles), fulvic acid (squares) and the hydrophilic fraction (triangles) in g.) October 2022 and h.) May 2023.

5.3.2. Organic matter

The DOC concentrations generally increased with depth (Figure 5.2e, f), corresponding with higher water-extractable DOC concentrations in the bottom layer of the same landfill (van Raffe, Dijkstra, et al., 2025). The relative composition of the DOC in VMS A shows a small decrease of FA and Hy and an increase of HA with depth, except for the two lowest sampling ports where the DOC concentration drops and the contribution of HA is limited (Figure 5.2g, h). The lower DOC concentration in these sampling ports coincides with the observed reduced concentrations of contaminants (non-reactive as observed in Figure 5.2 and reactive as discussed below), DIC, and a slightly lower pH. As previously mentioned, these lowest two sampling ports are potentially below an impermeable layer and likely to be subject to a different hydrological regime and surrounded by less reactive waste both in terms of contaminants and OC.

In VMS B, the elevated pH values (>10) found in October 2022 in the five lowest sampling ports coincide with a drop in DOC concentrations for these sampling ports (Figure 5.2e), contrary to an expected increase in OC solubility above pH 10 (van Raffe, Dijkstra, et al., 2025). The characteristics of the DOC also change; the relative contribution of HA increases while it decreases for both FA and Hy (Figure 5.2g). In May 2023, the elevated pH values in the bottom section of VMS B reduced (Figure 5.2b), and DOC concentrations increased again (Figure 5.2f), with a lower relative contribution of HA and higher FA and Hy contributions, similarly as in VMS A (Figure 5.2h).

The unexpected pH-DOC relation found in grout-influenced sampling ports was further explored on waste samples extracted at a similar depth as these sampling ports. Experiments in which the pH of a 1:10 waste to water solution was raised (pH > 12) by addition of the same grout used to fill the VMS, showed a suppressing effect on DOC solubility and only a slight increase of the HA contribution (section SM5.1, Figure S5.5a, b). Compared to pH dependent tests on similar waste without grout and standard pH-adjustment with 0.1 M NaOH, the contribution of FA, Hy and specifically HA to DOC is clearly suppressed by the grout (Figure S5.5c, d). At the high pH of the grout-influenced sampling ports, DOC concentrations are expected to be dependent on the (de)coagulation of OM (H. Gao et al., 2025). Yet, a reduced solubility of OM due to increased coagulation by polyvalent cations (Wall & Choppin, 2003; Weng, Temminghoff, & Van Riemsdijk, 2002b) in the grout was tested and found to hold no ground, as addition of a high concentration of Al (15 mg/l) to isolated HA and FA solutions was found to have only a limited effect on HA and FA coagulation at the high pH of 12 that was observed in VMS B (section SM5.1, Table S5.3). The DOC reduction may also be caused by adsorption on reactive mineral surfaces in the grout, possibly through (multivalent) cation bridging, rather than by direct cation-induced coagulation reactions. It is also interesting to note that a grout-induced conversion of HA and FA to HON is apparent, leading to molecular associations that bind irreversibly to the resin used in the fractionation procedure (Figure S5.5). The elevated

HON contribution to DOC is not found for in-situ sampled pore water; a possible explanation may be that HON adsorbs onto inner tubing of the VMS system during sample transport to the surface; this interaction is absent in the pH-dependent tests.

5.3.3. Reactive contaminants and major ions

The vertical trends of inorganic contaminants, major ions, and DOC correlate strongly, with generally increasing concentrations with depth (Figures 5.3, S5.6, S5.7). Geochemical modelling calculations for most contaminants predicted this distribution in soluble concentrations adequately (RMSE <1), particularly for the sampling ports not influenced by grout (Figures 5.4, S5.8, S5.9; Table S5.4). Below we will present and discuss the speciation of compounds for which the model adequately captured the vertical trends in the pore water. Based on the speciation calculations three groups of compounds with similar behaviour could be identified, consistent with their pH-dependent leaching in laboratory extractions of the same waste (van Raffe, Dijkstra, et al., 2025): the previously introduced non-reactive contaminants, reactive anions, and reactive cations. Speciation diagrams of representatives of these groups are shown in the SI (Figures S5.11 – S5.16).

5.3.3.1. Reactive anions

Contaminants and major ions that can be grouped as reactive anions are As, Mo, P, S, and Sb, which all increase in concentration with depth and show elevated concentrations when influenced by the grout (Figures 5.3 and S5.6). The model only captured these trends adequately for As and S, while P showed a calculated trend independent with depth yet with an adequate RSME of 0.77 when omitting grout-influenced samples (Figure 5.4 and S5.8, Table S5.4) and hence its speciation in the influenced samples will not be further discussed. The model predicts As to be present as both As(III) and As(V), as previously encountered in landfill leachates (Ponthieu et al., 2006) and column experiments (Ghosh et al., 2006), and to bind to metal (hydr)oxides (Figure S5.11), for which both As(III) and As(V) have a high affinity (Dixit & Hering, 2003). Mineral precipitates are predicted to control the solubility of P (Ca-phosphates, with a best description when allowing brushite to precipitate (Frost & Palmer, 2011)) and S (Barite (Hanor, 2000) and Chalcocite (L. W. Wang, 2012)).

5.3.3.2. Reactive cations

Reactive cations can be subdivided based on their calculated affinity for organic matter binding and the vertical trends in their dissolved concentrations, corresponding with their pH of minimum solubility as previously established with pH-dependent tests (van Raffe, Dijkstra, et al., 2025).

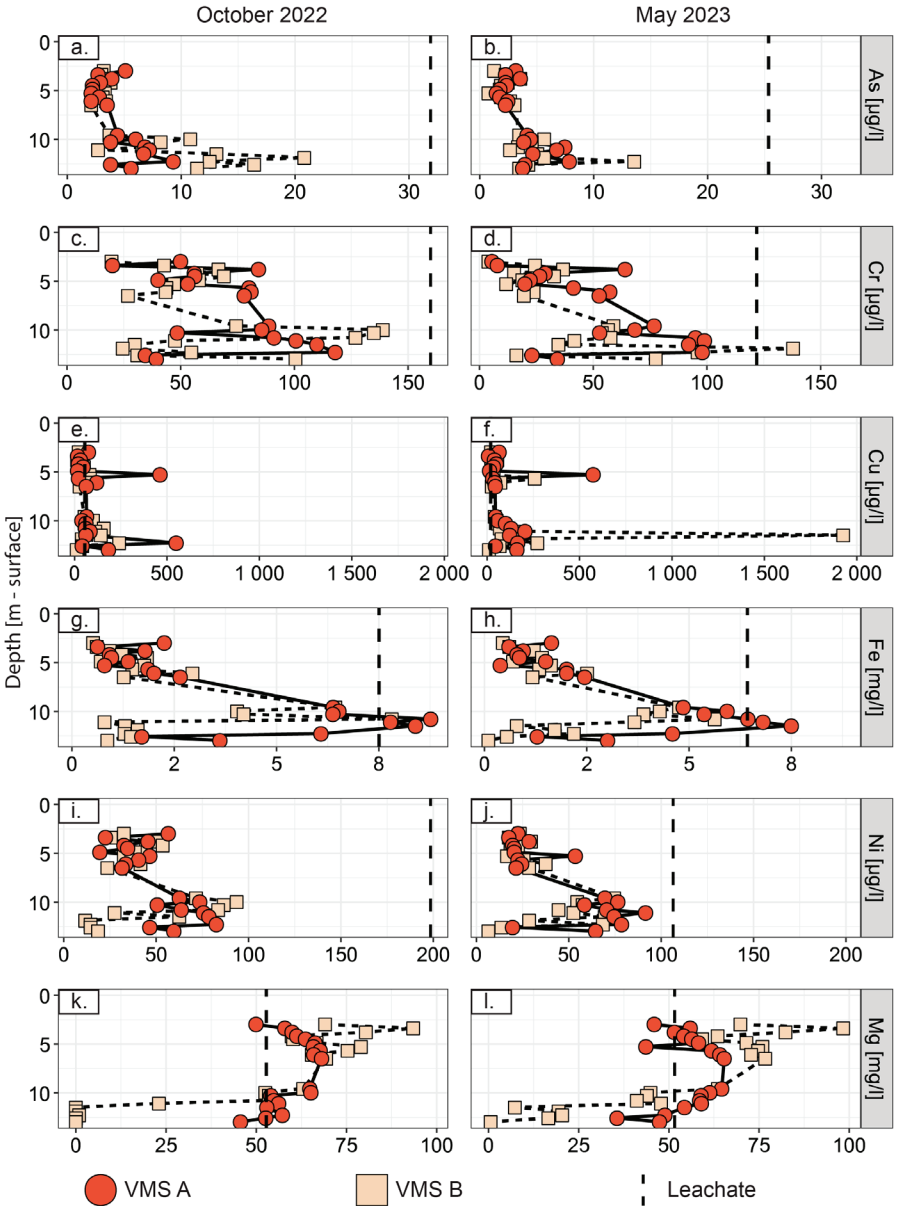


Figure 5.3 Measured pore water concentrations in VMS A (red circles), VMS B (beige squares), and as measured simultaneously in the leachate collected from a leachate collection pit (dashed lines), of As in a.) October 2022 and b.) May 2023; Cr in c.) October 2022 and d.) May 2023; Cu in e.) October 2022 and f.) May 2023; Fe in g.) October 2022 and h.) May 2023; Ni in i.) October 2022 and j.) May 2023; Mg in k.) October 2022 and l.) May 2023.

Reactive cations with solubility minimum below pH 8

Reactive cations with a solubility minimum between pH 5 – 8, i.e. Sn, V, Cr, Cu, Fe, Al, and Pb (van Raffe, Dijkstra, et al., 2025), increase in concentration with

depth and were predicted to associate with DOM in the dissolved phase across the entire depth of the landfill. An exception is Sn, which due to its high hydrolysing potential (Séby et al., 2001) is predicted to be predominantly present as inorganic hydroxyl species. The model adequately describes V, Cu, and Fe; adequately describes Sn when not considering grout-influenced samples; closely describes the trend of Cr yet with a RMSE above 1; and inadequately describes Al and Pb (Figures 5.4 and S5.8, Table S5.4). All DOM-associated cations except Cr are calculated to bind predominantly to FA (Figures S5.12 – S5.14). While Cr is known to bind to FA (Gustafsson et al., 2014), the presently used binding constants underestimate its OM binding affinity (van Raffe, Comans, et al., 2025), resulting in an underestimated Cr solubility (Figure S5.8). Cations associated with DOM in pore water are in the solid phase predicted to be either predominantly bound to SOM (V, as expected in organic systems (Gustafsson, 2019)), bound to Fe/Al (hydr)oxides (Cr), or precipitated as a mineral (Sn, Cu, Fe). Mineral species that provided the best description of analytical results were Sn hydroxide ($Sn(OH)_4$) for Sn (Séby et al., 2001), Cu sulphide (Chalcocite) for Cu (L. W. Wang, 2012), and a combination of Fe hydroxide (Ferrihydrite; (Hiemstra, 2013)) and Fe carbonate (Siderite; (Koo & Kim, 2020)) for Fe. Precipitation of Fe sulphide (pyrite) at a pH + pe of 4 further improved Fe predictions, yet significantly worsened predictions of Cu (Figure S5.9); while a pH + pe of 6 ultimately resulted in a best description, potential formation of Fe sulphide minerals in reducing pockets is likely.

Reactive cations with solubility minimum between pH 8 and 10

Reactive cations with a minimum solubility from pH 8 - 10, i.e. Ni, Zn, and Co (van Raffe, Dijkstra, et al., 2025), increase in concentration with depth yet only have a limited association with DOM due to their relatively low binding affinities (Milne et al., 2003). All three ions are inadequately described; however, the description of Co improves substantially when not considering the grout-influenced sampling ports (Table S5.4). The model predicts Co binding to metal (hydr)oxides, to which it is known to bind particularly above pH 7 (Ponthieu et al., 2006). Modelling predictions for Zn significantly improved and approximated the measurements most closely when considering a pH + pe of 4 and precipitation of Zn sulphide (Sphalerite). While Sphalerite commonly forms at high temperatures around hydrothermal vents (Keith et al., 2014), sphalerite formation has also been observed in the biofilm of sulphate reducing bacteria (Labrenz et al., 2000), which are likely to be found in reducing landfill environments (Jin et al., 2020).

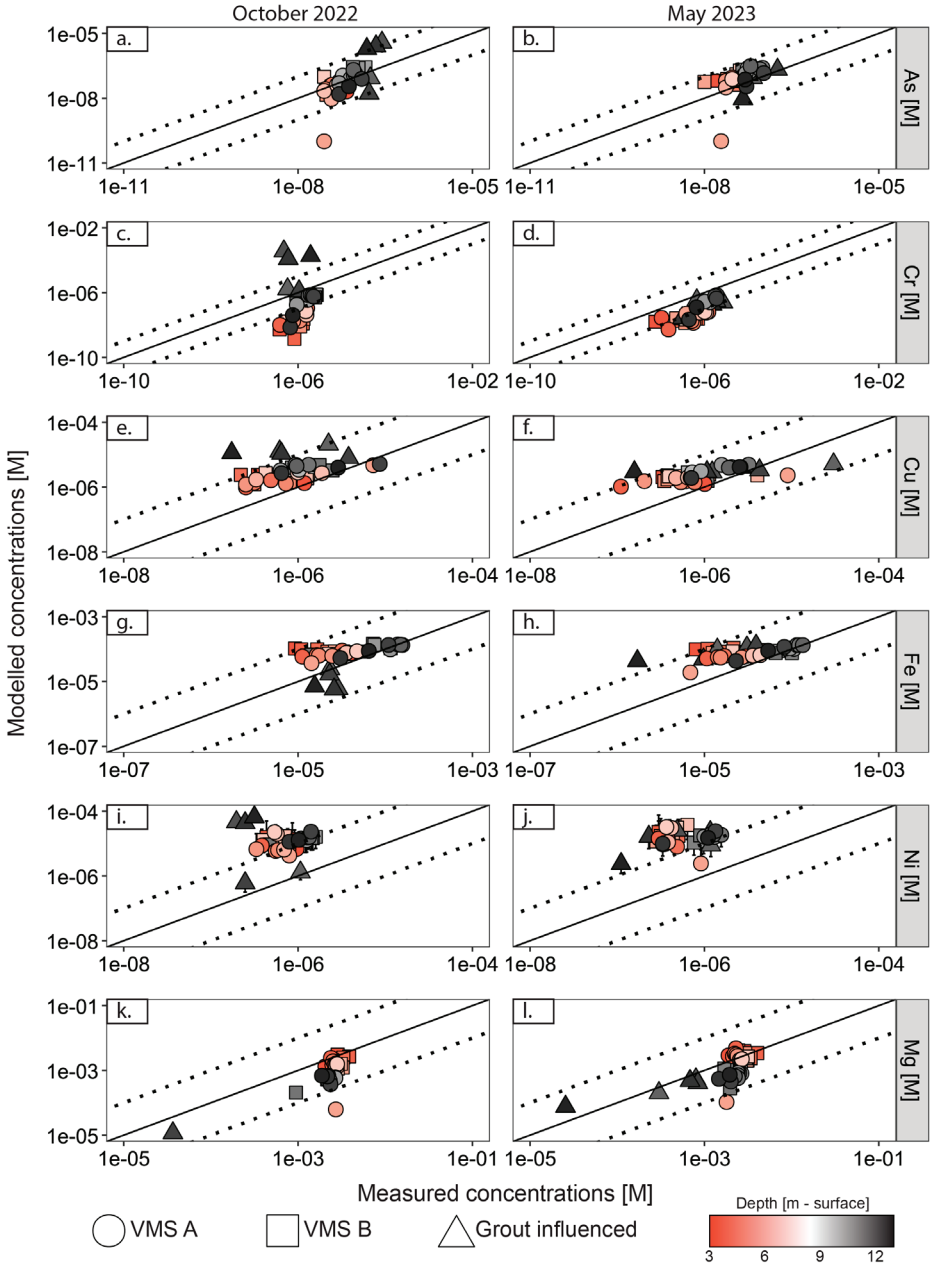


Figure 5.4 Measured pore water concentrations in VMS A (circles) and VMS B (squares) against model results of As in a.) October 2022 and b.) May 2023; Cr in c.) October 2022 and d.) May 2023; Cu in e.) October 2022 and f.) May 2023; Fe in g.) October 2022 and h.) May 2023; Ni in i.) October 2022 and j.) May 2023; Mg in k.) October 2022 and l.) May 2023. The 1:1 line is represented by the solid line; 10 times higher and 10 times lower predicted concentrations are represented by dashed lines. VMS B ports influenced by grout leakage are marked by triangles. Sampling ports close to the surface are coloured red, deeper ports are coloured black.

Reactive cations a with solubility minimum above pH 10

Reactive cations with a minimum solubility above pH 10, i.e. Si, Mn, Ba, Sr, Ca, and Mg (van Raffe, Dijkstra, et al., 2025), are all characterized by a decrease in concentration with depth (Figures 5.3 and S5.6). All these ions are described adequately by the model except Ca (Table S5.4), the trend of which is nevertheless described correctly (Figure S5.8). All these ions are weakly-to-not associated with DOM, binding only in the lower layer where HA becomes more prevalent (Mn) or only binding at the high grout-influenced pH where DOM is strongly negatively charged (Ba, Sr, Ca, Mg) (Figure S5.16). All the above ions can also form mineral precipitates, and their trend with depth appears to be determined by the type of mineral formed (Figures 5.3, S5.6, and S5.16). For Si, which is predicted to form the silicate Sepiolite (Baldermann et al., 2018; Jones & Conko, 2011), concentrations do not vary strongly with depth. For Ba, which is predicted to form the sulphate mineral Barite (Hanor, 2000), concentrations more clearly decrease with depth yet with fluctuating concentrations in the lower layer concurrent with opposite trends in the concentrations of S. Finally, Ca, Sr, Mn, and Mg can all form carbonate minerals (respectively Calcite (Manning, 2001), Strontianite (Helz & Holland, 1965; Mavromatis et al., 2017), Rhodochrosite (Jensen et al., 2002; Sternbeck, 1997), and Magnesite (Power et al., 2017; Qafoku et al., 2015)) with Mg and Mn additionally forming hydroxide minerals at the high grout-influenced pH (respectively Brucite (Pokrovsky & Schott, 2004) and Pyrochroite, which have a similar mineral structure (Burns & Burns, 1979) and with pyrochroite typically forming under reducing conditions (Roy, 1968)). The observed vertical trends of these elements, i.e. decreasing with depth, are consistent with carbonate precipitation induced by both the higher pH (Figure 5.2a, b) and DIC (Figure S5.4) in the deeper layers of the landfill. Except for Mn, model predictions of these elements are improved or remain similar for the grout-influenced sampling ports, contrary to all other contaminants (Table S5.4). The elevated pH values due to the grout leakage thereby provide further insights in underlying leaching mechanisms for these contaminants.

5.3.3.3. Ammonium

Particular consideration should be given to NH_4^+, as it is a priority contaminant in (anaerobic) landfills (Berge et al., 2005) and farthest from compliance with the ETV (leachate concentrations: ~1100 mg/l; ETV: 50 mg/l; (Dijkstra et al., 2018)). The model describes the dissolved NH_4^+ concentrations adequately (Figure S5.10, Table S5.4), predominantly predicting limited interactions with the solid matrix yet with improved model predictions at higher pH when formation of struvite is predicted (Figure S5.17), which is commonly found in landfill and wastewater treatment systems (Tansel et al., 2018). Nevertheless, the pH dependent leaching tests of these waste samples (van Raffe, Dijkstra, et al., 2025) suggest that relevant processes are unaccounted for by the current geochemical model, which include release of NH_4^+ upon breakdown of SOM (Ladd & Jackson, 1982), potential adsorption to OM (Nieder et al., 2011; Nommik, 1965), and specific binding to the frayed edges of 2:1 clays (Bruggenwert & Kamphorst, 1979; Evangelou & Lumbanraja, 2002).

5.4. DISCUSSION

This research highlights the power of combining pore water sampling and geochemical modelling to elucidate in-situ geochemical processes underlying contaminant leaching from complex engineered systems such as landfills or heavily contaminated sites. The pore water samples showed a strong variation in parameters that govern contaminant solubility, i.e. pH, DOC, and IC, with consequently strongly varying contaminant concentrations in which groups with similar behaviour could be identified. Adapting the geochemical modelling set-up from previous pH dependent leaching experiments on solid waste samples from van Raffe, Dijkstra, et al. (2025) provided an adequate description of these vertical trends for most contaminants. Building upon previous ex-situ mechanistic explorations of the same waste to investigate in-situ pore water samples allowed us to capture the effects of the elevated CO_2 pressure and the sulphidic environment in the landfill, resulting in a model-predicted important contribution of carbonate minerals (Fe, Mg, Sr, Mn, Ca) and sulphide minerals (Cu, Fe, Zn) to contaminant solubility. The presence of these minerals in municipal solid waste has previously been determined experimentally (Fannin & Roberts, 2006; Flyhammar, 1997; Östman et al., 2008), yet the exact control of these minerals on contaminant mobility has not been shown. The extent of this control as shown in our findings aligns with geochemical modelling of other anaerobic environments, including sediments (Vink et al., 2017), paddy soils (Y. Pan et al., 2014), and leachate plumes (Van Breukelen et al., 2004).

While the model provides an adequate prediction for most contaminants, additional processes may well have been missed in the heterogeneous and complex landfill system, particularly given that the applied geochemical multi-surface model has primarily been developed and tested for aerobic natural and waste environments. Firstly, redox conditions were estimated rather than measured. Considering the importance of redox conditions for contaminant leaching (Borch et al., 2010), we recommend direct redox measurements in future pore water research. Secondly, specific solubility-controlling minerals may have been missed, while the non-included DOM competition for anionic contaminant binding to metal (hydr)oxides is likely of particular relevance in the organic-rich environment of the landfill. Lastly there is an uncertainty in solid phase model inputs. By implementing a three-layer average parametrization per 6-m rather than per individual sampling port, reactive surface contents assigned to specific ports could have been more precise, particularly in light of the large heterogeneity inherent to landfills. Assigning to specific ports was however not feasible given that sampling was conducted every 2 metres, and the three-layer distinction was considered optimal as it aligns with previous analyses of the waste (van Raffe, Dijkstra, et al., 2025) and it captures the transition between the observed two distinct regions around 12 metres depth. Further inaccuracy of the solid phase is introduced by assuming a reactive surface of 600 m^2/g for the metal (hydr)oxides in this model calculation, based on assumed average soil conditions,

while metal (hydr)oxides present in the waste are probably largely newly formed and thus have higher surface areas. Nevertheless, the model is relatively insensitive to these uncertainties and model uncertainties are more so related to uncertainty in OM binding parameters (Wiersma et al., 2025). This is reflected in a RMSE above 1 for certain elements, e.g. Al, Ni, Zn (Table S5.4), of which OM binding parameters are known to be less accurate (Milne et al., 2003).

Applying the VMS unveiled contaminant concentrations changing with depth, and these changes differing between contaminants. The geochemical model provided insights into the differing contaminant behaviour, and underlying mechanisms were steered by the prevailing redox state, pH, and DOC concentrations. These insights could not be obtained by solely monitoring the bulk leachate, where detailed trends are obscured. In addition, our results provide an *in-situ* benchmark of contaminant mobility controlling processes against which LSR experiments testing the impact of active treatment strategies can be validated. This benchmark can facilitate the implementation of effective aftercare strategies to reduce long-term landfill after-care.

5.5. CONCLUSIONS

In this study, pore water samples were taken across a vertical transect from a landfill which has been subject to leachate recirculation using a vadose monitoring system. Samples were analysed for pH, the concentration of dissolved organic matter and its subfractions, and concentrations of inorganic contaminants. Most parameters increased with depth, with a sharp decrease for the lowest sampling ports likely due to the presence of an impermeable layer. Geochemical modelling predicted pH, dissolved organic matter, and redox state as steering parameters. Contrary to lab studies, reactive cations were predicted to be largely controlled by the formation of carbonate minerals, and the formation of sulphide minerals for copper, zinc and iron. These differences showcase the potential of combining in-situ sampling pore water across a vertical transect with geochemical modelling to better understand contaminant solubility. The obtained insights can be used to validate laboratory experiments testing active treatment as a more sustainable management strategy, and ultimately facilitate effective implementation of active treatment.

6

Chapter 6

General Discussion

Frank van Raffe

6.1. INTRODUCTION

Global generation of waste is continuously increasing (United Nations Environment Programme, 2024), and while governments steer towards a circular economy (Pires & Martinho, 2019) with a focus on waste re-use and recycling (Das et al., 2019; European Parliament and Council of the European Union, 2008), landfills remain an essential waste endpoint (B. Kumar, 2025). Landfills pose a threat to human health and to the environment via the generation of the potent greenhouse gas methane (EEA, 2024) and leachate rich in traditional (Baun & Christensen, 2004; Christensen et al., n.d.; Kjeldsen et al., 2002; Marttinen et al., 2003) and emerging contaminants (Capozzi et al., 2023; GodvinSharmila et al., 2023; P. He et al., 2019; Lang et al., 2017; Lu et al., 2016; Masoner et al., 2016). These emissions are restricted in modern landfills via the placement of impermeable barriers (Council of the European Union, 1999), yet this halts waste degradation and stabilization. The environmental threat of the waste is consequently retained, and environmental protection costs are shifted to future generations.

The Dutch government signed a "Green Deal" in 2015 to investigate a more sustainable alternative (E. Brand et al., 2016), where waste stabilization is accelerated via leachate recirculation or aeration in an attempt to reduce leachate concentrations until they adhere to previously derived emission testing values (ETV) (Dijkstra et al., 2018). This "Green Deal" sparked three landfill-scale pilots to investigate this active treatment and extensively monitor changes in gas production and quality, leachate quality, and solid waste characteristics. While there are previous indications of the potential of active treatment on a landfill scale, these indications are mainly related to changes in gas quality (Reinhart, 1996; Ritzkowski & Stegmann, 2012) or focus on specific (macro) contaminants (Brandstätter et al., 2020). Studies focusing on more detailed landfill simulation reactors (LSRs) had a relatively narrow focus on macro parameters (Brandstätter et al., 2015a; Cerminara et al., 2020; Fricko et al., 2021a), and knowledge on the underlying mechanisms behind potential reductions of contaminants and an underpinning of the sustainability of the achieved reductions remained lacking. As such, the large research program CURE (coupled multi-process research for reducing landfill emissions) was called into life, to provide insights in the changes incurred during landfill treatment.

This thesis is a part of CURE and intended to investigate the geochemical mechanisms underlying contaminant leaching from landfills, and how an understanding of these mechanisms can help explain how active treatment may reduce contaminant leaching. In this general discussion, I will first synthesise the main findings of this thesis and place them in the context of sustainable landfilling (**section 6.2**). Following this synthesis, derived conclusions will be used to:

1. Reflect on the used methodologies (**section 6.3**), to illustrate the limitations and strengths of the taken approaches.

2. Further discuss the mechanisms of ammonium solubility (**section 6.4**), as this is considered the contaminant of highest priority in landfills.
3. Reflect on the implications for active treatment (**section 6.5**), specifically with regards to the previously derived emission testing values and current developments in leachate quality. This places the thesis findings in the context of the feasibility of sustainable landfilling.
4. Give recommendations on future research (**section 6.6***)*.

6.2. MAIN FINDINGS

The primary objective of this thesis was to **define the geochemical mechanisms controlling contaminant leaching from solid waste and how these mechanisms can be used to further understand the effects of aeration and leachate recirculation on landfill leachate concentrations**. This objective has been explored from the lab to the field, and in this section I will synthesise the obtained results. Later sections place these results in context to discuss this research' limitations and implications.

In the most well-defined lab set-up, the pH-dependent test combined with geochemical modelling in **chapter 2**, three distinct groups of contaminants could be identified based on their pH-dependent solubility: non-reactive contaminants, reactive anions, and reactive cations. Non-reactive contaminants had only limited interaction with the solid matrix and hence did not show any pH dependence, while reactive ions had a maximum solubility around the upper and lower ends of the pH range. Reactive anions had a minimum solubility around pH 5, steered by binding to metal (hydr)oxides; for reactive cations minimum solubility occurred at varying pH, based on the tendency of the cations to hydrolyse (pushing the solubility minimum to a higher pH) and their affinity for organic matter (OM) binding (pushing the solubility minimum to a lower pH). Mechanisms behind cation solubility were diverse, including binding to OM, binding to metal (hydr)oxides, and the formation of minerals. Ammonium (NH_4^+) surprisingly showed behaviour akin to a reactive cation with a solubility minimum around pH 8. A geochemical model was applied to calculate the chemical speciation of the elements based on inorganic complexation, formation of mineral precipitates, and binding to reactive surfaces (OM and metal (hydr) oxides). The model was capable of describing the pH dependent behaviour of most elements, except for the cationic behaviour of ammonium, due to the absence of binding parameters, and chromium (Cr), likely due to poor OM-binding parameters.

New OM-binding parameters for Cr were derived in **chapter 3,** to improve the inadequate geochemical model predictions of Cr identified in **chapter 2**. Adequate modelling of Cr is of particular importance as it is one of the few elements currently not adhering to the ETV (see section 6.5). The strong tendency of Cr to hydrolyse (Rai et al., 1987, 1989) meant

experimental data of the conducted Cr adsorption experiments could only be adequately described when considering the binding of $Cr_2(OH)_2^{4+}$ in addition to the free Cr^{3+} species. As $Cr_2(OH)_2^{4+}$ binding to OM was previously spectroscopically identified (Gustafsson et al., 2014), this was considered a likely hypothesis. Evaluating the new parameters against three independent datasets showed significantly improved predictions compared to using the generic parameters of (Milne et al., 2003). The lower binding affinity of the new parameters resulted, however, in an underestimated Cr-OM binding, with consequently worsened predictions of dissolved Cr in environments with low OM. While these implications are of lower importance in the OM-rich landfills, its effects could still be noted in **chapter 4**: the pH-dependent solubility of Cr was significantly more accurately described using the new parameters compared to the results of **chapter 2**, yet improvements were less pronounced for the OM poor samples originating from the *Braambergen* landfill.

The improved model set-up was applied to identify effects of active treatment on contaminant solubility in landfill simulation reactors in **chapter 4**. Under leachate recirculation, strongly reducing conditions were maintained, with stable humic substance concentrations and an increased pH. The increased pH led to increased contaminant concentrations due to hydrolyzation and mineral dissolution, while sulphide mineral precipitation was identified to control the solubility of several redox sensitive elements, i.e. Cd, Cu, Fe, Mn, and Zn. Under aeration, aerobic conditions were induced, while dissolved OM concentrations and pH both decreased. The changes in redox conditions and pH resulted in an initial dissolution of minerals and a corresponding increase in contaminant concentrations. This increase was followed by a subsequent decrease upon the predicted formation of (oxide) minerals or the binding to reactive surfaces. Ammonium concentrations decreased strongly during aeration, likely due to nitrification transforming NH_4^+ to nitrate. Investigating the contaminant solubility under these significantly different treatments revealed mechanisms that were not captured in the pH-dependent tests of **chapter 2**, particularly the importance of redox conditions. The LSR results reveal a precarious balance of actively aerating the waste, where a decrease in NH_4^+ concentrations coincided with an concentration increase of contaminants which were present as sulphide minerals.

Obtained insights were ultimately combined to determine solubility and fate of contaminants on a landfill scale for the landfill subjected to leachate recirculation using vadose monitoring systems (VMS) in **chapter 5**. The geochemical model set-up was once more applied to determine mechanisms underlying contaminant solubility, considering the insights from the previous chapters and by estimating solid waste properties based on distinct extractions of solid waste sampled near the VMS. The measured pore water concentrations showed a high covariance, with concentrations of contaminants and organic matter increasing with depth and with a sharp decrease below 12 meters depth. This sharp decrease was likely due to the presence of an impermeable layer. The trends in pore

water concentrations could be disentangled based on the earlier derived mechanisms: the formation of specific minerals and the binding to reactive surfaces as determined in the pH-dependent tests in **chapter 2**, and the importance of sulphide minerals as determined in the LSRs in **chapter 4**. Even with limited information of the waste surrounding the pore water, an estimate based on solid waste samples, together with a thorough description of the sampled water, proved sufficient to adequately predict pore water concentrations. This highlights the power of geochemical modelling to provide insights on contaminant speciation in such complex systems.

6.3. REFLECTION ON THE USED METHODOLOGIES

6.3.1. Investigating different scales

In this thesis, contaminant leaching from solid waste was investigated from the detailed and well-defined lab scale to the complex field scale. The complementarity of the experiments provided important insights. This section discusses the benefits and drawbacks of each experiment, to provide reference for data interpretation and for what experiments best fit potential future research questions.

The lab scale pH-dependent tests in **chapters 2 and 4** were conducted in a well-defined system, as samples were thoroughly analysed on solid phase properties, equilibrated, and fully mixed to ensure measured concentrations and pH were homogenous and attributable to the entire system. By additionally stretching the pH range from 2 to 12, mechanisms such as metal (hydr)oxides and OM dissolution or the formation of mineral precipitates became apparent and could be accurately modelled. This clearly defined system meant controlling mechanisms underlying contaminant leaching could be identified, and hence why pH-dependent tests are a part of leaching assessment frameworks (Garrabrants et al., 2021b, 2021a) and have been used to characterize samples of varying origins (Astrup et al., 2006; Carter et al., 2009; Dijkstra et al., 2004; Dijkstra, Van Der Sloot, et al., 2006; Komonweeraket et al., 2015; Loncnar et al., 2022; Meima & Comans, 1997). The analysing conditions are however far from landfill conditions. Waste had to be sampled, pre-treated to 4 mm size, and extracted at high liquid:solid ratios (10:1), at room temperature, and under atmospheric aerobic conditions. While specific mechanisms could be clearly identified, e.g. the formation of hydroxide minerals and binding to OM and metal (hydr)oxides, other mechanisms could not be identified which were shown to be highly relevant in the other experiments, e.g. redox dependent processes.

The LSR experiments in **chapter 4** have a larger scale and complexity than the pH-dependent tests, while the system remains relatively well defined. Being "landfill simulation reactors", the LSRs more closely approximated landfill conditions than the pH-dependent tests, and results are thus more directly applicable to actual processes ongoing in a

landfill. Conditions in the LSR could be controlled well and measured directly, and the waste could be more efficiently actively treated compared to in the field. Mechanisms such as the formation and dissolution of sulphides were consequently identified, and active treatment effects could be analysed without need for large scale waste sampling and observed on a shorter timescale than the landfill-scale experiments thanks to the higher active treatment intensity. While the LSRs were relatively well-defined and similarly characterized to the pH-dependent tests, the larger particle size (3.6 cm mesh size sieves compared to 4 mm for the pH-dependent tests), larger volumes (30 kg compared to 100 g in the pH-dependent tests), and the non-mixing of the LSRs meant leaching and modelling results were more variable and at times required the prior knowledge obtained from the pH-dependent tests for full interpretation. Landfill simulation reactors additionally still do not fully translate to the field, as the small scale of the LSRs cannot capture the complexity and heterogeneity of full-scale landfills (Hrad et al., 2013; Ritzkowski & Stegmann, 2012). This could, among others, be observed in the redox conditions. The LSRs were either fully aerobic or anaerobic thanks to the introduction of respectively compressed air or nitrogen gas; a switch from one gas to the other resulted in a rapid transition of redox states. In contrast, full-scale landfills simultaneously contain aerobic and anaerobic pockets (Konstantaki et al., 2016) and are thereby subject to complex interplays of reducing and oxidizing mechanisms. The used rates of aeration and leachate recirculation in the LSRs were also significantly higher than field application rates, complicating exact analysis of how treatment affects the waste in the field. While LSR experiments are thus significantly closer to reality than the pH-dependent tests and lend themselves well for exploratory studies, they do not fully represent landfill conditions and translation to the real system has substantial limitations.

The pore water samples taken using vadose monitoring systems in **chapter 5** represent actual landfill conditions and the identified mechanisms can be directly linked to mechanisms occurring in the landfill. The landfill system is also the most complex, which makes mechanistic interpretations difficult. This was further complicated by the unknown nature of the waste that influenced individual sampling ports and the absence of an *in-situ* measured redox potential; the former could however be approximated from solid phase characterization of solid waste at different depths near the monitoring systems; the latter could be approximated based on the redox potentials observed in the LSRs. Yet this complexity means knowledge on mechanisms steering solid-solution partitioning is required before detailed interpretation as was done in **chapter 5** is possible. Hence, previous VMS studies where this knowledge was not available focused either solely on the vertical distribution of contaminants and its effect on underlying soil concentrations (Aharoni et al., 2017, 2020) or more specifically on transformation of nitrogen based on isotopic analysis (Aharoni et al., 2022). The requirement of prior knowledge can be (partly) alleviated by better characterisation of the system, e.g. by analysing the waste extracted during sleeve installation and/or by installing redox sensors at various depths.

6.3.2. Equilibrium modelling of dynamic systems

Geochemical models calculate speciation and solid-solution partitioning assuming a system is in chemical equilibrium (L. Koopal et al., 2020). This assumption likely holds true for the pH-dependent tests in **chapters 2 and 4**, as the used equilibration time of 48 hours previously showed to approximate equilibrium for most elements (Dijkstra, Van Der Sloot, et al., 2006). The studies on the LSR leachate (**chapter 4**) and landfill pore water (**chapter 5**), however, deal with a dynamic system with changing waste properties and ongoing water flow during active treatment.

In the LSRs, changing waste properties were captured by analysing the solid waste throughout LSR operation and through this considered in the modelling. Generated leachate was allowed to accumulate for an extended period prior to sampling, which was likely sufficient to achieve a (quasi-)equilibrium. Yet for the non-recirculated LSRs, this accumulated water only had limited contact with the waste during the vertical downflow. This downflow started as clean water at the top of the LSR, and likely gradually became enriched with contaminants due to desorption from reactive surfaces and dissolution of minerals within the waste mass. In case of rapid transport and a quasi-equilibrium, this desorption/dissolution would be lower than in equilibrium and consequently the model would overestimate dissolved concentrations. This overestimation for the aerated reactors can indeed be observed in **chapter 4** for Zn, Cd, Pb, Co, Si, Ni, and Mg. For the recirculated LSRs, the leachate is constantly recirculated and hence there is a significantly longer contact time between waste and water; predictions of the recirculated LSRs were consequently more adequate. This could be indicative that the equilibrium assumption for the non-recirculated LSRs is not valid and is the basis of the poorer model descriptions. This could be further tested for example by analysing recirculated leachate across different time steps to investigate when full equilibrium is reached and how this affects model prediction quality. An alternative explanation for the poorer model descriptions could be changing leachate quality during its accumulation phase, as for an extended period the leachate was no longer in contact with the waste yet potentially subject to changes in pH and DOM. This would not have an effect on the actual solubility of the contaminants, yet may have affected the model predictions.

The flow within landfills is relatively complex, with a mix of preferential flow paths and stagnant zones (Fellner & Brunner, 2010; Oonk et al., 2013). Based on the yellow to dark brown colours and the measurable high concentrations of all pore water samples in **chapter 5**, the occurrence of a preferential flow path feeding the sampling ports is unlikely. In the case of preferential flow, there would only be brief contact with the waste and thus a more diluted solution with lighter colours is expected. It was hypothesized that there is an impermeable layer in the lower layers sampled by the VMS, around which there is either horizontal or limited flow. For these layers contact times between waste and water can be significant, considering travel times within landfill bodies can be several

years (L. Wang & Heimovaara, 2025) and contact times are likely significantly longer in recirculated landfills such as *the Kragge* where the VMS were installed. Under such conditions, the equilibrium assumption is likely to be valid. In the higher layers, where sample colours were observably lighter and concentrations between ports were similar, a higher connectivity is likely and may have resulted in lower residence times. Indeed, again an overestimated solubility of Zn, Pb, Cd, Ni, and Co by the model can be observed, particularly for the higher sampling ports. Nevertheless, the model predictions are significantly more adequate for all ports relative to the LSR predictions.

6.3.3. Geochemical modelling of solid waste

Multi-surface geochemical models have been developed to calculate the chemical speciation of elements in soils and waters (Di Bonito et al., 2024). Application on various contaminated materials previously was successful, e.g. for contaminated soils (Carter et al., 2009; Dijkstra et al., 2004), slags (Loncnar et al., 2016, 2022), and municipal solid waste bottom- and fly ash (Meima & Comans, 1997; H. Zhang et al., 2008), and has been successfully applied to characterize solid landfill waste in my thesis. There are several important aspects of waste that were noteworthy in the modelling results that are here further discussed.

The investigated systems, i.e. laboratory batch extractions, landfill simulation reactors, and field pore water, were all either reduced or aerobic with a high content of OM to serve as electron donor (Aeschbacher et al., 2010, 2011; Chen et al., 2003; Pham et al., 2012) and reduce elements such as chromium (Jardine et al., 2011) and vanadium (Gustafsson, 2019). Previous research in paddy soils showed poor predictions of trace metal solubility under reduced conditions (Y. Pan et al., 2016), yet redox sensitive elements were relatively well described both in the LSRs (**chapter 4**) and in the pore water (**chapter 5**). The strongly reduced conditions over prolonged periods likely resulted in the formation of sulphide minerals, a process which the model captured relatively well. Other processes which could influence the model predictions appeared not to significantly influence model results, e.g. the reduction of metal (hydr)oxides (Suter et al., 1991), the formation of poorly defined sulphur clusters enhancing contaminant solubility (Luther & Rickard, 2005), adsorption to minerals stable under reduced conditions (Charriau et al., 2011; Jean & Bancroft, 1986), or a change in OM reactivity due to an increase in sulphur groups (Yu et al., 2016).

Particularly for the pore water samples of **chapter 5**, the solid waste surrounding the sampling ports was only limitedly characterized. This was expected to be challenging particularly considering the highly heterogeneous nature of landfills, yet the modelling prediction proved surprisingly adequate and trends were captured for most elements. Parameters that were directly measured for each sampling port, i.e. pH and dissolved OM fractions, were thus sufficient to achieve a successful model description for most ele-

ments. Overall, geochemical models can be an important tool to understand geochemical speciation even for complex systems with limited characterization.

Contrary to soils, metal (hydr)oxides were predicted to be the predominant binding surface for most cations in landfill waste (as identified in **chapters 2, 4, and 5**). This was for instance the case for copper, which in soils typically associates with OM (Dijkstra et al., 2004) yet in this thesis was found to be preferentially bound to metal (hydr)oxides. Similar observations have been made for municipal solid waste incinerator bottom ashes (Dijkstra, Van Der Sloot, et al., 2006; Meima & Comans, 1999), which unlike the landfill waste are oxide-rich and OM-poor and a high predicted importance of metal (hydr)oxide can thus be expected. The high importance of metal (hydr)oxides for organic matter rich landfill waste could be due to a combination of: 1) high contaminant concentrations, as high contaminant/OM ratios reduce their OM binding affinity (Craven et al., 2012) and as high concentrations result in high ionic strengths and a smaller Donnan volume of the OM (L. K. Koopal et al., 2005); 2) a general pH above 8, which nears the point-of-zero charge of oxides (Kosmulski, 2016) and thereby makes them negatively charged and more relevant to bind cations.

Throughout the experiments in this thesis, higher concentrations and consequently higher ionic strengths were encountered than typical in soils and waters. The effects on OM binding were described above, yet the high ionic strengths additionally impact the compound activities in solution. This is typically corrected for in geochemical modelling via the Davies equation (Davies, 1938), which has been shown to accurately calculate activities in concentrated electrolyte solutions up to 500 mM (Samson et al., 1999). The highest observed total electrolyte concentrations were observed in the pH-dependent tests at pH 2, with a highest total electrolyte concentration of 467 mM for the *Braambergen* sample in **chapter 4**. Hence, applying the Davies equation is justified to model element solubility in these samples. When modelling systems of a higher ionic strength, an adjusted Davies equation should be used.

6.3.4. Used ion binding parameters

The used ion binding models use generic parameters to calculate ion binding to their respective reactive surfaces. The strength of this approach is that parameters have been derived independently on purified surfaces and the calculated behaviour is based solely on well-studied and understood mechanisms, contrary to more simplified calculations using partition functions (Groenenberg et al., 2012). However, the quality of the used parameters dictates the quality of the model outputs, particularly those of OM (Wiersma et al., 2025), which can have significant consequences for model results. NICA-Donnan uses the proton parameters of Milne et al. (2001) and element binding parameters of Milne et al. (2003) to calculate binding. For several elements these parameters have been derived from a large number of datapoints and are relatively reliable. Other element parameters

are based on smaller datasets, or are derived from linear free energy relationships (LFER) (Carbonaro & Di Toro, 2007) when no data was available. Consequently, derived binding parameters are significantly less reliable. Elements investigated in this thesis which are considered to have a low reliability are Ba, Cr, Fe, Mg, Mn, Sr, Sn, V, and Zn. The uncertainty of these parameters is particularly prolific for strongly hydrolysing ions. This could be observed in **chapter 2** for Cr, which required an improved parameter set (**chapter 3**) to adequately describe the pH-dependent solubility in **chapter 4**. Vanadium (V) is another element known to strongly hydrolyse (Gustafsson, 2019) and which has LFER derived parameters (Milne et al., 2003); similar to Cr in **chapter 2**, modelling its pH dependent solubility resulted in an overestimation which is improved when assuming 50% of dissolved OM was humic acid (HA) (Figure 6.1). For such strongly hydrolysing ions, the LFER derived binding parameters strongly overestimate actual OM binding. Assuming all OM is present as HA, which binding affinities are lower than FA, results in an assumed binding which is closer to the "actual" binding. The similar overestimation in binding when using LFER parameters for Cr and V shows that for such strongly hydrolysing ions, binding experiments need to be conducted to adequately derive a binding affinity.

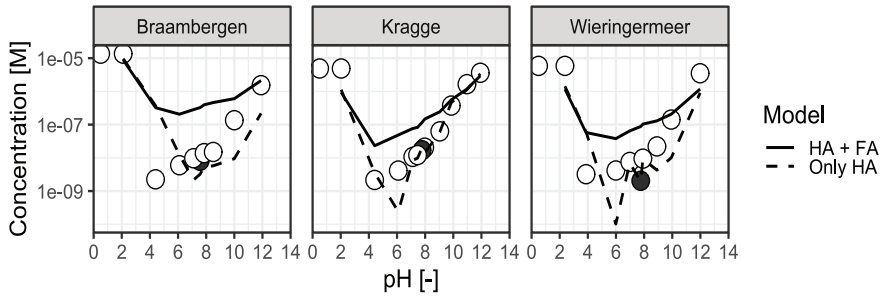


Figure 6.1. Measured (markers) and modelled (lines) concentrations of V as a function of pH in ultrapure water extracts of solid waste sampled after 6 years of active treatment. Modelling input consisted of measured HA and FA concentrations (solid line), or only taking HA which is set to 50% of DOM (dashed line).

Additionally, the used generic parameters have been derived under oxidized conditions, and carboxylic- and phenolic acid are considered the predominant reactive groups for metal binding (Shi et al., 2016). Under the reducing conditions in which (part of) the experiments in this thesis were conducted, OM is likely to transform and increase in the amount of reactive sulphide groups (Yu et al., 2016) to which elements can bind (Smith et al., 2002). The generic parameters may thus not fully represent the reactivity of the organic material.

6.4. MECHANISMS OF AMMONIUM SOLUBILITY

With NH_4^+ considered the contaminant of highest concern in landfills (Berge et al., 2005), additional focus went to its geochemical behaviour in **chapters 2, 4, and 5**. Ammonium concentrations decreased during LSR aeration in **chapter 4**, which was likely a result of nitrification (Brandstätter et al., 2015b; Fricko et al., 2021b). While this was not a considered mechanism in the geochemical model, the observed decrease was still captured by the model due to a decrease in the input values for total reactive NH_4^+ taken from measured 1 M KCl extractable NH_4^+ concentrations. Contrary to the LSRs, in the landfill pore water (**chapter 5**) insights in underlying mechanisms were obtained as NH_4^+ concentrations were predicted to be steered by struvite precipitation, an important precipitate in waste water treatment (D. Kim et al., 2007; R. Kumar & Pal, 2015). This was however not predicted in the pH dependent tests (**chapters 2 and 4**), where the reactive cationic behaviour of NH_4^+ was inadequately captured. The NH_4^+ kinetics test (**chapter 2**) showed a kinetic (de-)sorption at high and low pH resembling that of reactive divalent cations rather than a monovalent cation (Dijkstra, Van Der Sloot, et al., 2006). This suggests that in addition to the considered formation of struvite and the electrostatic binding to clay and OM, other mechanisms steer this pH-dependent solubility. Thus, additional tests were conducted to identify the potential relevance of specific binding to organic matter (Nommik, 1970; Rodrigues et al., 2007; L. Zhang et al., 2016) and/or to the frayed edges of 2:1 clays (Alshameri et al., 2017; Linggi et al., 2021). These results are presented below.

Experiments investigating NH_4^+ binding to isolated HA and FA showed that, across a range of NH_4^+ concentrations and pH levels, consistently 10% of NH_4^+ was bound to OM (Figure 6.2). Modelling the system without any specific binding to HA and FA resulted in a significant overestimation of binding by the model, with most NH_4^+ being bound electrostatically. The overestimated binding considering solely electrostatics is surprising, yet measurements via both SFA (as depicted in Figure 6.2) and ion selective electrode corroborate the low adsorption. The measured low NH_4^+ adsorption and the overestimated modelled binding already when solely considering electrostatics shows that specific binding to OM is likely not the main mechanism behind the pH dependent solubility of NH_4^+.

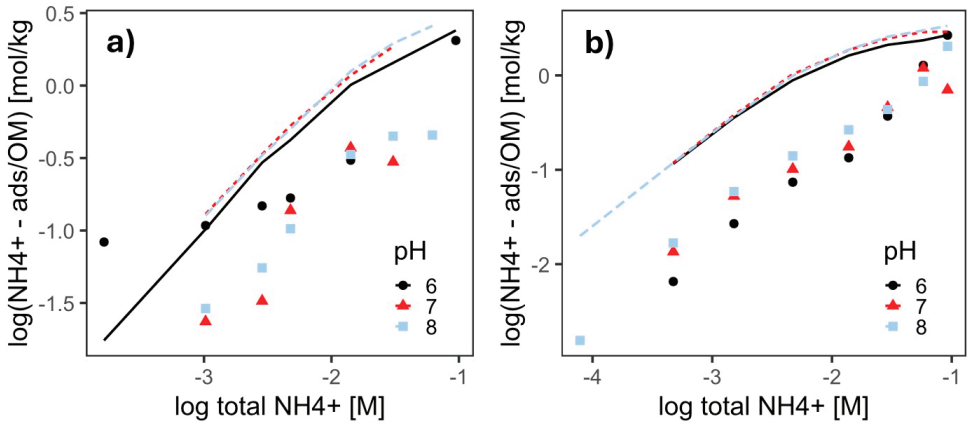


Figure 6.2 Results of the ammonium binding experiment to a) isolated fulvic acid from groundwater; b) isolated Tongbserven Humic acid (Kalis et al., 2006). Both fractions were isolated using the adapted IHSS protocol adopted from Swift (1996). Batches with only NH_{4+} (blanks) and NH_4^+ together with HA/FA (4 g/l) were brought to pH via addition of NaOH, put under N2 atmosphere to prevent nitrification, and equilibrated for 48h. Further addition of NaOH after 2, 4, 8, and 24 hours was necessary to establish wanted pH. Samples were filtered after 48 hours (0.45 µm) and free NH_4^+ was measured using a segmented flow analyser, which is geared towards colorimetric detection of free NH_4^+. The concentration difference between NH_4^+-HA/FA batches and blanks was used to calculate adsorption (symbols). NICA-Donnan binding parameters were fitted using a coupling of ORCHESTRA-PEST (Janot et al., 2017) (lines).

Specific binding to clay was further investigated via additional model runs on the pH-dependent experiments of **chapter 2,** using a Gaines-Thomas ion exchange model rather than a Donnan model to calculate clay binding. Results in Figure 6.3 show a marked improvement in the predictions of both NH_4^+ and K^+ behaviour when using Gaines-Thomas. Solubility of NH_4^+ is indeed predicted to decrease above pH 5 due to a reduced competition with protons for clay binding, and increase above pH 8 due to the transformation of NH_4^+ to NO_2^-. While the absolute concentrations are not predicted accurately, potentially related to uncertainties discussed below, the captured trend shows that (selective) clay binding is a likely mechanism steering the pH-dependent solubility of NH_4^+. These results imply that previously assumed binding of NH_4^+ (Dijkstra et al., 2018) is underestimated and selective binding to clay minerals drive NH_4^+ solubility and transport within waste landfills and in the underlying soil (Bruggenwert & Kamphorst, 1979; S. Yang & Yang, 2024). This is affirmed by the improved predictions of K^+ (Figure 6.3), where the use of Gaines-Thomas exchange also results in significantly improved descriptions compared to the Donnan model. Modelling of monovalent cations with a (relatively) high selectivity for clay binding should thus use exchange coefficients rather than the Donnan model for an adequate evaluation.

While the modelling predictions improved when using Gaines-Thomas, the absolute soluble concentrations of NH_4^+ were not adequately described. This may be related due to uncertainties in the clay measurements, as measured clay contents were relatively low and the used methodology may not be fully applicable for waste samples. An additional cause may be uncertainties in the used coefficients. Traditionally model set-ups assume binding to illite, including the calculations applying the Donnan model in this thesis, owing to its relative prevalence in temperate soils. Yet for the exchange calculations presented in Figure 6.3 I instead selected parameters for montmorillonite, because of a significantly larger database of selectivity coefficients in literature (Bruggenwert & Kamphorst, 1979). Both illite and montmorillonite are 2:1 clays, and their selectivity coefficients are comparable yet with a slightly higher NH_4^+ selectivity for illite. As the exact clay mineral composition of the waste is unknown, use of the selectivity coefficients for montmorillonite rather than for illite was deemed acceptable. If illite clays do dominate waste mineral fractions, the higher NH_4^+ selectivity of illite compared to montmorillonite means the calculated NH_4^+ binding may have been underestimated and the predicted dissolved concentrations overestimated. This makes further characterizing the waste clay composition and potential improvement of NH_4^+-illite selectivity coefficients an important follow-up research question.

6.5. IMPLICATIONS FOR ACTIVE TREATMENT

In this thesis I investigated the mechanisms behind contaminant solubility to 1) understand the mechanisms behind observed changes in leachate quality during active treatment; 2) assess whether observed changes are sustainable. Throughout the thesis I predominantly focused on the mechanisms governing solubility, and here I will place these results in the context of leachate quality developments to further discuss the 2nd objective. I will compare leachate quality developments as measured from the full-scale landfills against the LSR results of **chapter 4**, and give a perspective of the potential to fulfil the previously derived emission testing values (ETV)(Dijkstra et al., 2018).

6.5.1. Developments in leachate quality

The key environmental parameters controlling contaminant solubility, i.e. pH and DOM and its subfractions, fluctuated throughout the active treatment period and showed a distinct seasonality (Figure 6.4). The pH in the leachate of the aerated landfills (*Braambergen* and *Wieringermeer*) slightly increased over time, opposite to the decrease observed in the aerated

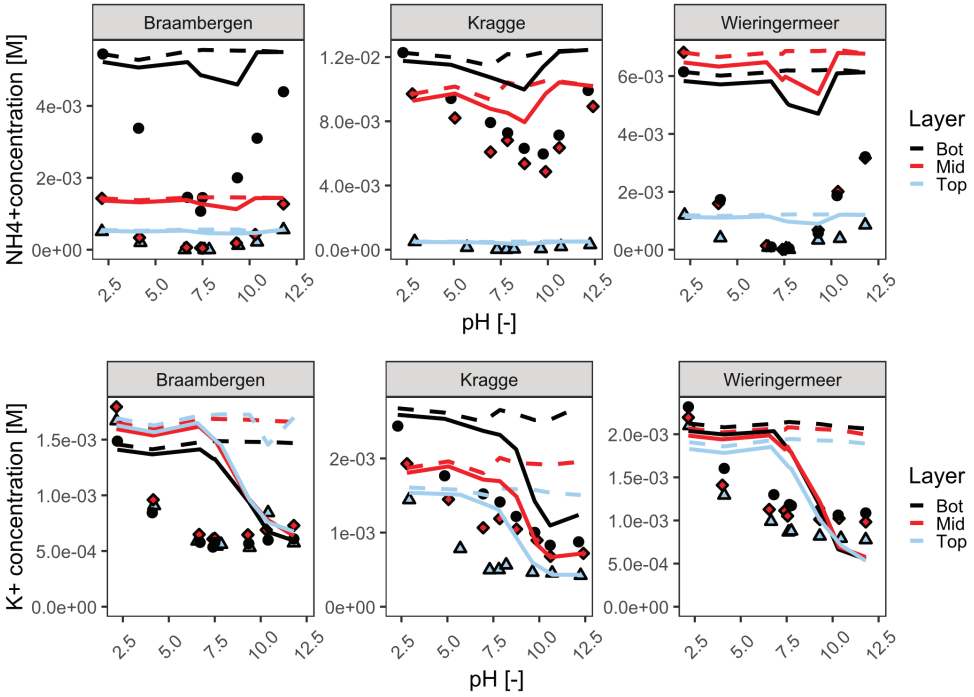


Figure 6.3 pH-dependent leaching of ammonium (top) and potassium (bottom) as measured in waste sampled prior to the start of active treatment at three different depths, as shown in chapter 2. Leaching was modelled considering binding with a donnan model (dashed lined) or using Gaines-Thomas exchange coefficients to model selective binding to clay (solid lines). Gaines-Thomas exchange coefficients were based on the average coefficient values listed for Montmorillonite in Bruggenwert & Kamphorst (1979), with log K values of respectively 0, 0.6, 0.5, and 0.7 for Na, K, Ca, and NH_4^+ with respect to proton binding, in good agreement with parameters used in PHREEQC (US EPA, 2009).

LSRs. This is likely due to the higher temperatures in the landfill, which inhibits nitrification and enhances ammonification (Ritzkowski & Stegmann, 2012). A reverse trend between the aerated landfills and LSRs can likewise be observed for DOC, which concentrations increase in the landfill leachate. This increase points towards an enhanced degradation of the solid waste and consequent solubilization of OM. The more efficient aeration in the LSRs likely resulted in subsequent breakdown of the DOC, yet this does not occur in the landfills. The DOC in the leachate of the aerated landfills has become relatively enriched with HA, pointing towards waste maturation. Under leachate recirculation (*Kragge*) the leachate pH remains stable, similar to the LSRs. The DOC concentrations decrease – likely due to a combination of flushing and DOC in the ANAMMOX reactors, which are used to reduce leachate NH_4^+ concentrations (Pereira et al., 2017) – while the relative DOC composition remains unchanged.

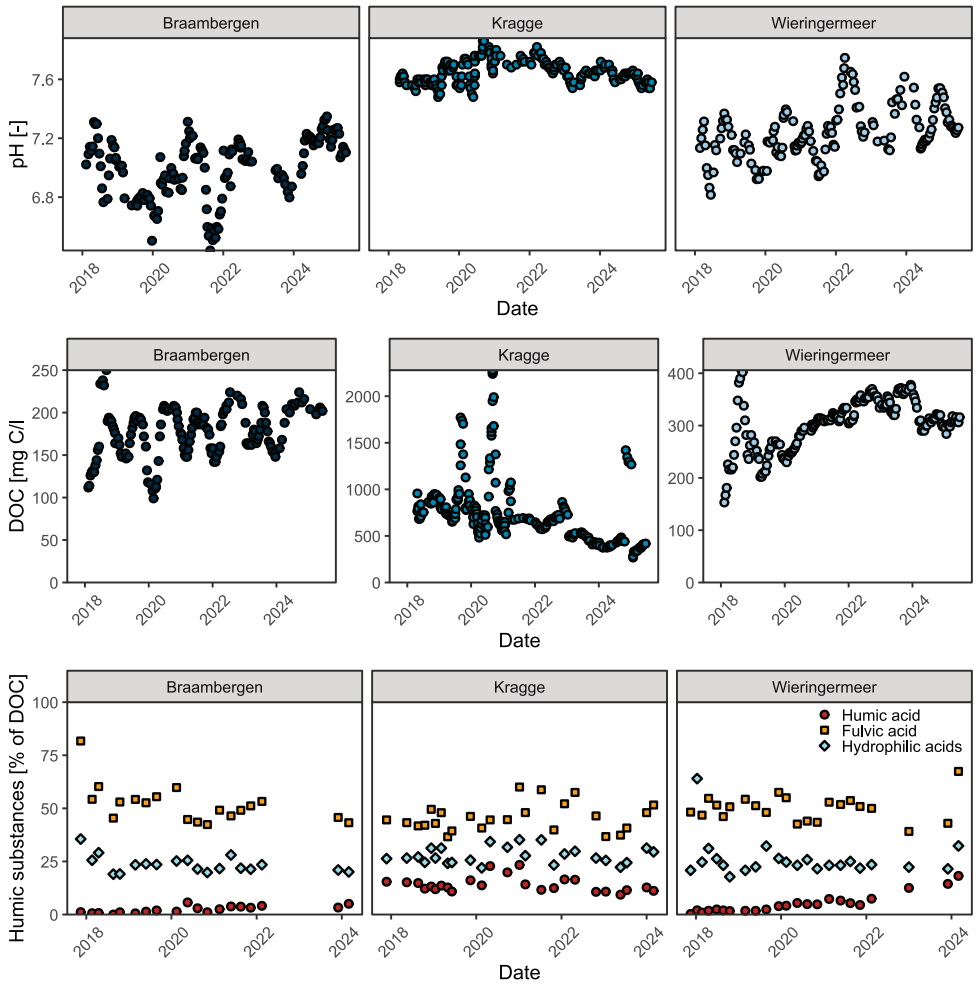


Figure 6.4 Developments in pH and dissolved organic matter during the active treatment of the different landfills. Braambergen and Wieringermeer are subjected to aeration, Kragge is subjected to leachate recirculation.

The contrasting trends in DOC and pH between the leachate of the aerated landfills and the aerated LSRs also result in contrasting trends in contaminant concentrations (Figure 6.5). The mechanisms identified throughout this thesis hold true and can be used to understand leachate contaminant concentrations. Arsenic and Cr increase in the aerated landfills and decrease in the *Kragge* landfill with leachate recirculation, following trends in DOC. This is due to the similar negative charge of As and DOC (Groenenberg et al., 2012; Qiao et al., 2020), and the high binding affinity of Cr to DOC as identified in the LSRs (**chapter 4**) and spectroscopically shown previously in landfill leachate (H. Wang et al., 2024). Iron concentrations decrease for the aerated landfills and remain relatively stable in the landfill subject to leachate recirculation, in agreement with the LSRs where decreas-

ing Fe under aeration was the result of Fe (hydr)oxide precipitation while under anaerobic conditions Fe is likely present as a sulphide mineral with a corresponding stable dissolved Fe concentration. Nickel concentrations slightly increase in aerated landfills and decrease for *Kragge*, following DOC concentrations in agreement with the LSR results. Magnesium concentrations remain relatively stable and slightly decrease for *Wieringermeer*, with the latter likely resulting from the slight increase in pH and consequent formation of mineral precipitates as suggested from the LSRs. Finally, NH_4^+ concentrations decrease in the *Kragge* leachate, in agreement with the observed decrease in the recirculation LSRs. The decreased concentration in the *Kragge* leachate is likely related to struvite precipitation at the higher pH, as identified in the LSRs, together with the removal of NH_4^+ from the leachate in the ANAMMOX reactors prior to their re-introduction into the landfill waste body and the possible binding to clay minerals as identified in section 6.4. In the aerated landfills NH_4^+ leachate concentrations are relatively unchanged, while a decrease in NH_4^+ concentrations due to nitrification is expected based on the aerated LSRs. The apparent absence of a reduction of NH_4^+ can have several possible reasons. Firstly, the presence of other reducing agents, e.g. reduced Fe and organic matter (Van Breukelen & Griffioen, 2004), likely consume the introduced oxygen and prevent sufficiently oxidized conditions to induce nitrification. Nitrification did occur in the aerated LSRs due to the higher aeration rates (20x higher than the landfills), yet even so required more than a year of effective aeration before levels were noticeably reduced (see Figure 4.4). Secondly, oxidation of OM and NH_4^+ is likely reduced in hard-to-reach anaerobic pockets (Konstantaki et al., 2016), which are less prominently present in LSRs containing sieved waste. Thirdly, there are signs of N_2 fixation occurring within the landfills (Yi et al., 2025), which may partly off-set potential reductions due to nitrification. Finally, previously mentioned high temperatures occurring within landfills may inhibit nitrification (Stark, 1996).

6.5.2. Achieving waste 'completion'

The goal of the accelerated waste stabilization ultimately lies in the previously derived ETV (E. Brand et al., 2016; Dijkstra et al., 2018), which establish the allowable contaminant concentrations in the leachate to protect the surrounding environment for the next 500 years in case of free outflow of leachate. The ETV of the different contaminants, together with their average and maximum concentration from June 2024 to June 2025, are listed in Table 6.1. Most elements are relatively far below the ETV for most or all landfills, and hence can be considered to no longer pose an environmental threat. The ETV are exceeded for a singular measurement for Cd and Zn (*Wieringermeer)* and S (*Kragge)*. While the average values of S in *Kragge* and Zn in *Braambergen* are relatively low and hence the high concentration likely does not pose

a threat, for *Wieringermeer* the Cd concentration greatly exceeds the ETV and it should be assessed whether this measurement is a short spike or a longer term emission before it can be declared safe or not. Four contaminants exceed the ETV for (nearly) all sites and

should be considered a potential environmental threat: Cl (except for *Wieringermeer*), Cr, Ni, and NH_4^+. Chloride concentrations are strongly decreasing for all landfills and may well reach the ETV even for *Kragge* within 5 years. Chromium and Ni concentrations decrease for *Kragge* and are nearing the ETV, yet *Braambergen* and *Wieringermeer* concentrations are continuously increasing to further stray from the ETV. Considering this increase is linked with an increase in DOC concentrations caused by the accelerated waste degradation, the concentrations are reasonably likely to reduce below the ETV once active treatment is concluded and accelerated degradation is halted. Finally, NH_4^+ concentrations are a factor 10 – 20 higher than the ETV, and are only decreasing for *Kragge*. As seen in the LSRs, reaching concentrations which adhere to the ETV required creating fully aerobic conditions, which appears not to be possible in the actual landfills. Additionally, even when such concentrations were reached in the LSRs, switching from aeration back to anaerobic conditions resulted in NH_4^+ concentrations increasing once more due the continued degradation of waste and no further NH_4^+ transformation (**Chapter 4**). Thus, while decreasing NH_4^+ concentrations to an environmentally safe level in itself is already difficult, this is further complicated by the fact that a permanent reduction to environmentally safe levels can only be ensured by full stabilization of the degradable waste, as otherwise a re-increase of NH_4^+ to above ETV levels may be expected. Within two year of LSR operation, at 20x higher treatment rates that those in the landfill, this stable phase was not yet reached. This implies the treatment period of a full-scale landfill is likely to be vast, and in terms of achieving stable low concentrations of NH_4^+ may well not be feasible, even if the signs are more positive for other contaminants. For further studies the feasibility may potentially be improved by treating the waste during the active landfilling period, as Berge et al. (2009) already indicated this to more effective.

6.5.3. A note on the environmental testing values

The ETV form an important basis for quantifying effects of active treatment, yet several notes should be made based on the knowledge gained during this thesis. Firstly, the ETV assume that leachate concentrations remain constant following release from active treatment. As already noted for NH_4^+, this assumption may be invalid as aerated pilots may return to anaerobic conditions and lead to a consequent re-increase of NH_4^+, particularly in the presence of significant amounts of OM. Similarly for leachate recirculation, air intrusion into the waste body following the gravimetric drainage of water and the degradation of impermeable barriers may lead to a return of aerobic conditions, which is potentially followed by an increase in elements which are present as sulphides, as noted in the LSRs (**chapter 4**). Yet in contrast, a reduced reactivity and 500 years of flushing may result in decreasing concentrations of non-reactive elements and dissolved OM and its associated contaminants. The potential trends in contaminant release from the waste following release from active treatment should be further evaluated for individual, potentially problematic contaminants to provide better risk assessment.

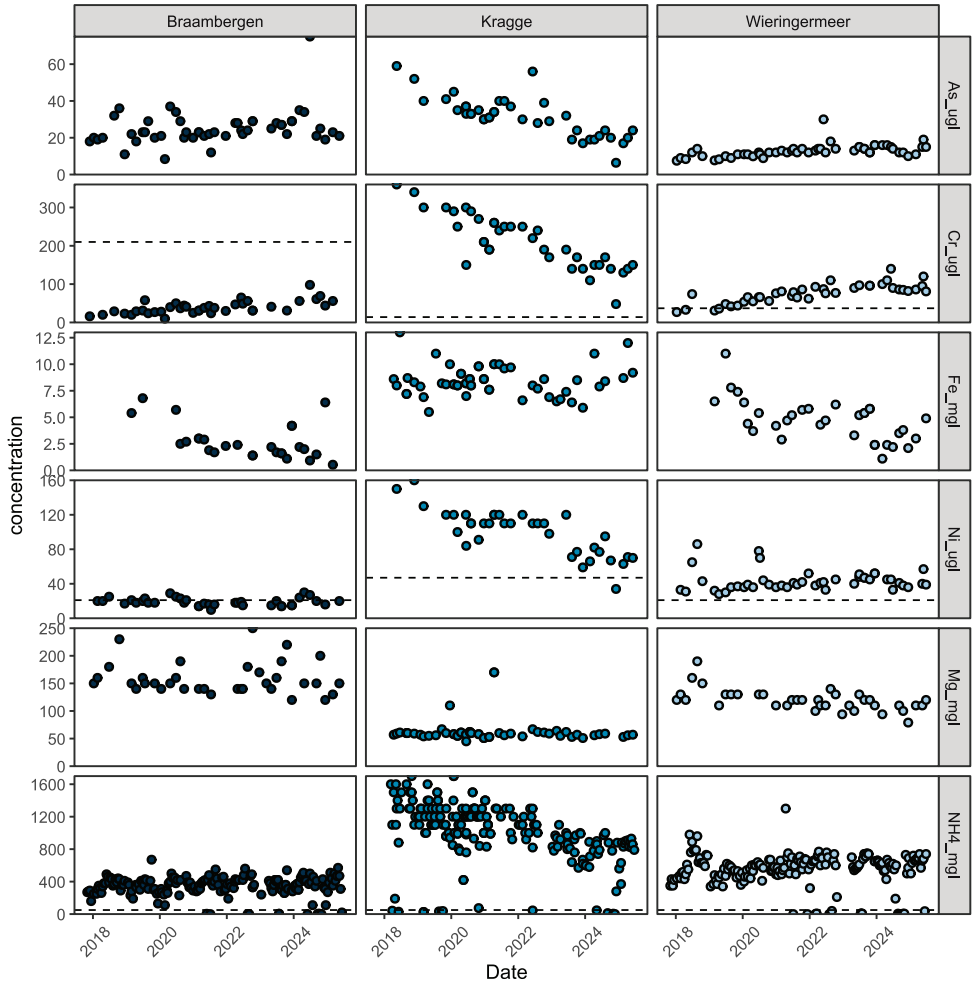


Figure 6.5 Element concentrations in the bulk leachate as a function of time. Emission testing values (ETV) are depicted by the black dashed line; ETV were not derived for iron, and have been omitted for arsenic as leachate concentrations trends were obscured by the high ETV values (190 µg/l for Braambergen and Wieringermeer, and 100 µg/l for Kragge), related to their strong binding potential in the soils underlying the landfill (Dijkstra et al., 2018).

A second note regarding the ETV is the fact that they have been calculated considering the parameters that were available at the time. In my thesis I evaluated the geochemical modelling specifically of NH_4^+ and Cr, and noted an overestimated importance of Cr-OM binding and an underestimated binding of NH_4^+ with clay surfaces. With the original parameters, Cr and NH_4^+ solubilities were consistently overestimated, and it is likely that their transport through the subsurface was also overestimated during the derivation of the ETVs. This may further be the case for NH_4^+, where biological processes that may further reduce NH_4^+ concentrations, e.g. nitrification, were not considered yet are likely to

occur in the underlying soil. Hence, derived ETV of these elements are likely stricter than necessary.

Table 6.1 *Emission testing values and the average and maximum leachate concentration measured June 2024 – June 2025 for the landfill sites investigated in this thesis.*

	Braambergen			Kragge			Wieringermeer		
	ETV	Average	Max	ETV	Average	Max	ETV	Average	Max
Chloride [mg/l]	450	**599**	**719**	160	**630**	**899**	2400	580	950
Arsenic [µg/l]	190	32	75	100	19	24	190	13	19
Cadmium [µg/l]	6.4	0	0	3.6	0	0	1.3	**8**	**58**
Chromium [µg/l]	210	67	98	14	**133**	**150**	37	**87**	**95**
Copper [µg/l]	50	5	5	64	16	21	19	7	12
Nickel [µg/l]	21	**21**	**27**	47	**63**	**77**	21	**38**	**57**
Lead [µg/l]	130	5	5	130	0	0	130	19	73
Zn [µg/l]	160	10	11	120	33	53	39	22	**61**
Sulphur [mg/l]	233	91	150	67	14	**76**	467	17	34
Ammonium [mg/l]	50	**400**	**570**	50	**830**	**930**	50	**550**	**740**

6.6 RECOMMENDATIONS FOR FUTURE RESEARCH

Considering my research ultimately had to be constrained, here are additional recommendations of paths future research could take to further improve our understanding of contaminant behaviour and making waste environmentally safe.

- Measure local redox conditions directly when investigating the total leachate flowing from the landfill or when sampling landfill pore water. Through this, achieve a better indication of underlying mechanisms behind contaminant solubility and the importance of redox potential.
- Improve modelling of element speciation under reduced conditions by deriving parameters from experiments executed specifically under reduced conditions and using material isolated from reduced environments.

- Improve description of NH_4^+ behaviour in landfills by characterizing the (clay) mineral composition of the landfill waste, thereby either adopting selectivity coefficients from minerals that best describe the landfill situation, or deriving new selectivity coefficients for the relevant minerals.
- Evaluate the generic binding parameters of strongly hydrolysing elements, as the current linear free energy relation (LFER) derived parameters likely significantly overestimate binding as these were theoretically derived due to a lack of available/ reliable experimental data. Preferably a hydrolysed species should be additionally be considered to bind to organic matter, as this will significantly improve model predictions. Most important candidates are vanadium and tin, due to their poor binding parameters and their strong tendency to hydrolyse.
- Expand the scope of assessing active treatment effects beyond inorganic contaminants. Evaluate the potential reduction of emerging pollutants, such as PFAS, pharmaceuticals, microplastics, for which landfills are a known significant source. The changing reactivity of organic matter within landfills as observed in CURE can be of use particularly in evaluating pollutants with an affinity towards OM binding, notably PFAS with a long hydrophobic tail and pharmaceuticals with known high K_{oc} values.

6.7 CONCLUDING REMARKS

In this thesis I set out to better understand how contaminants behave within landfill systems, and if this knowledge can be used to reduce their emissions from landfills and ultimately keep the environment safe. My research showed the complexity underlying these contaminant emissions, and the different factors that come into play when tackling a matrix contaminated with a multitude of contaminants. The dominant factors are the solution pH, redox state of the system, and the solubility and composition of organic matter. Their effects on contaminant leaching differ depending on which contaminant is looked at, which makes achieving a reduction in contaminant emissions not straightforward: a change in these factors may reduce the leaching of one contaminant yet increase the leaching of another. My research helps untangle this complexity by giving insights into how changing factors influence each individual contaminant, to ultimately make actively reducing landfill contaminant emissions a more realistic prospect. It however needs to be stated that directly influencing environmental factors on a landfill scale was shown to be difficult. A more feasible option would have been to instigate accelerated stabilization at an earlier stage and on a smaller scale.



Supplementary Information

2

Supplementary information Chapter 2

Controlling mechanisms behind contaminant release in solid landfill waste prior to (an)aerobic stabilization: pH dependent leaching experiments and geochemical modelling

Supplementary descriptions

SM2.1 Methodology of the time-dependent ammonium leaching test

To investigate the potential underlying mechanisms behind the observed pH dependent leaching behaviour of ammonium (NH_4^+), an additional test was conducted where the Kragge top and middle layer were extracted in a similar fashion to the original pH dependent test yet only at pH 4, 12, and without altering the sample pH. The extracts were equilibrated through constant stirring and after 4, 20, and 48 hours pH was directly measured and 20 ml of solute was sampled and replaced with 20 ml ultrapure water. Samples were filtered over 0.45 µm cellulose filters and analysed for NH_4^+ and nitrate + nitrite using sequential flow extraction (Skalar San++ segmented flow analyser).

Supplementary Figures

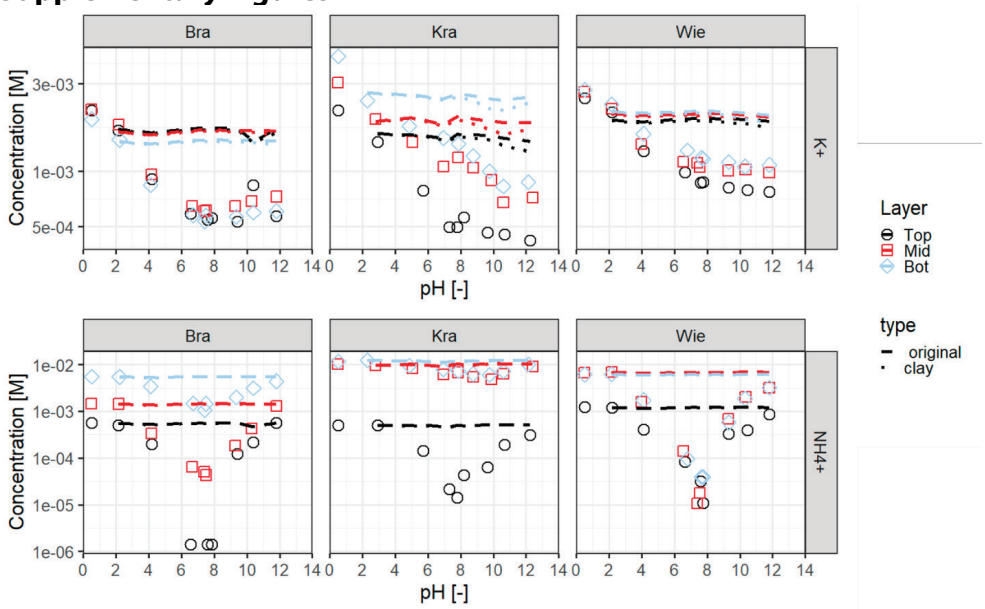


Figure S2.1. Leachable concentrations (markers) and geochemical model predictions (lines) of potassium (top) and ammonium (bottom) as a function of pH for three different landfills at different depths. Modelling is conducted without clay (dashed lines) and assuming 20% clay content (dotted lines).

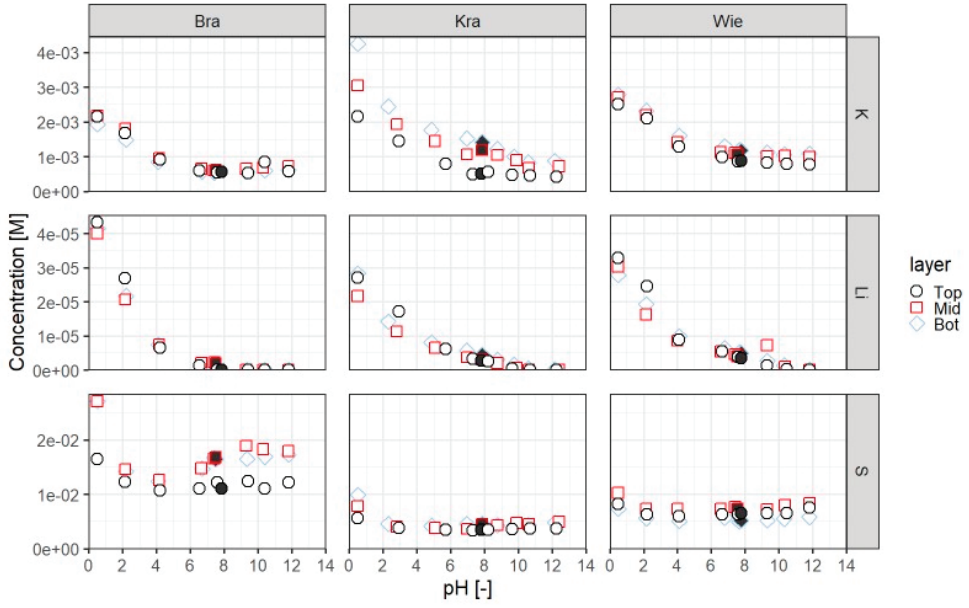


Figure S2.2 Concentrations of potassium, lithium, and sulphur as a function of pH for the three landfills at different depths. Unmanipulated samples are coloured dark grey.

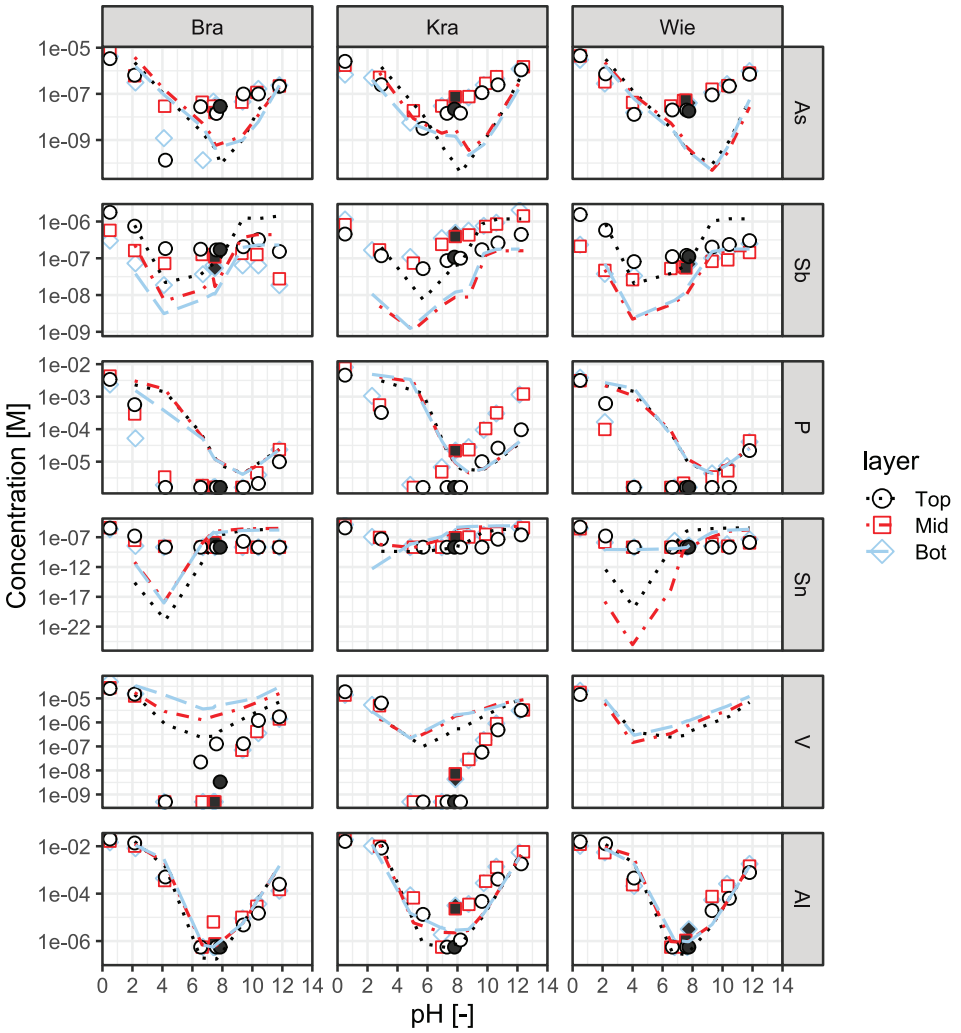


Figure S2.3 Concentration of remaining elements as a function of pH for each landfill and each depth, measured in a pH dependent test (markers) and as calculated through multi-surface geochemical modelling (lines). Clay was not considered in the calculations. Unmanipulated samples are coloured dark grey.

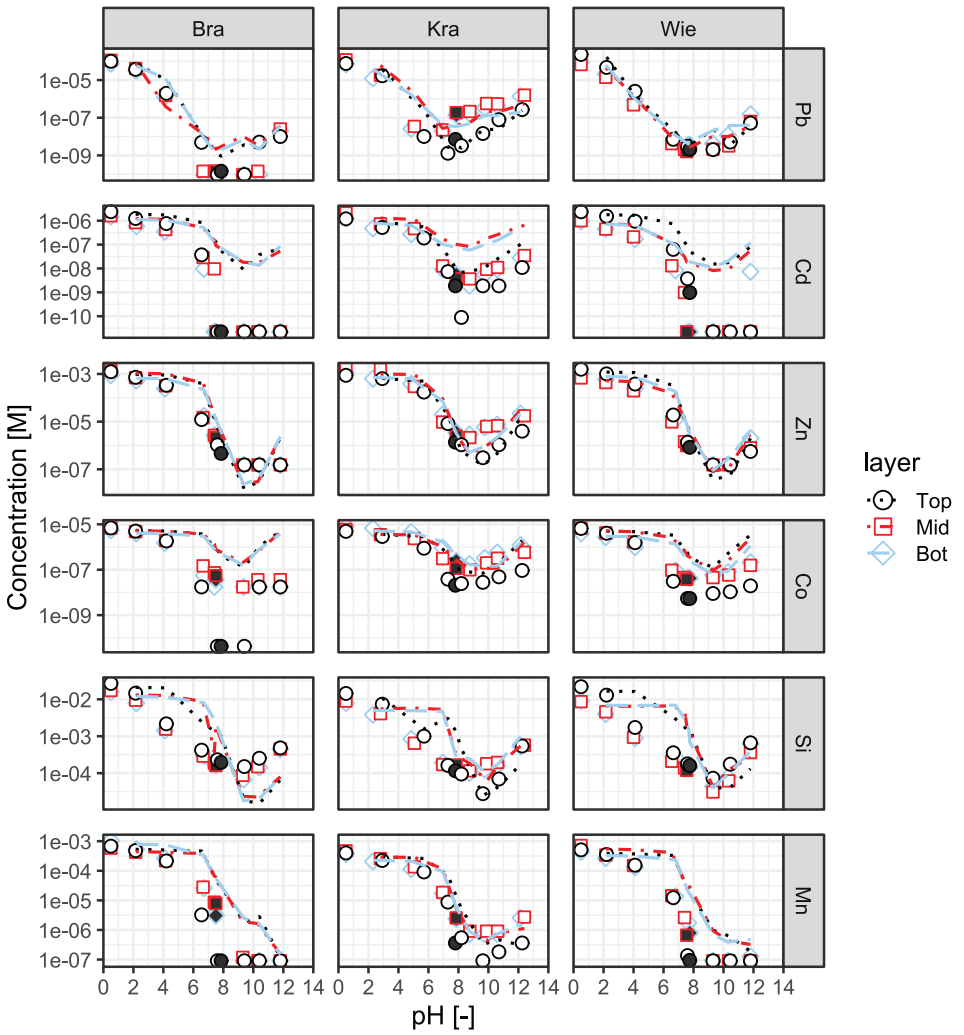


Figure S2.3 (continued)

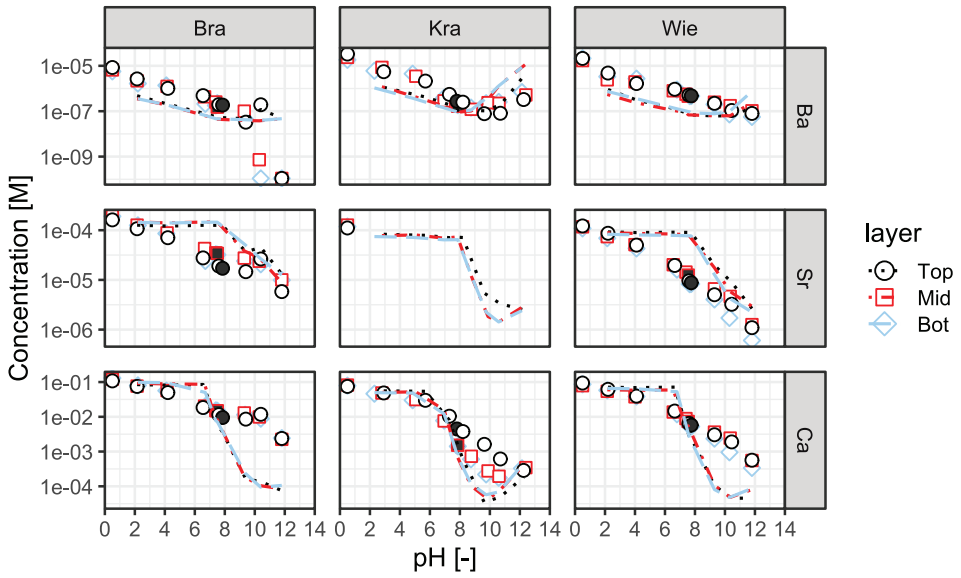


Figure S2.3 (continued)

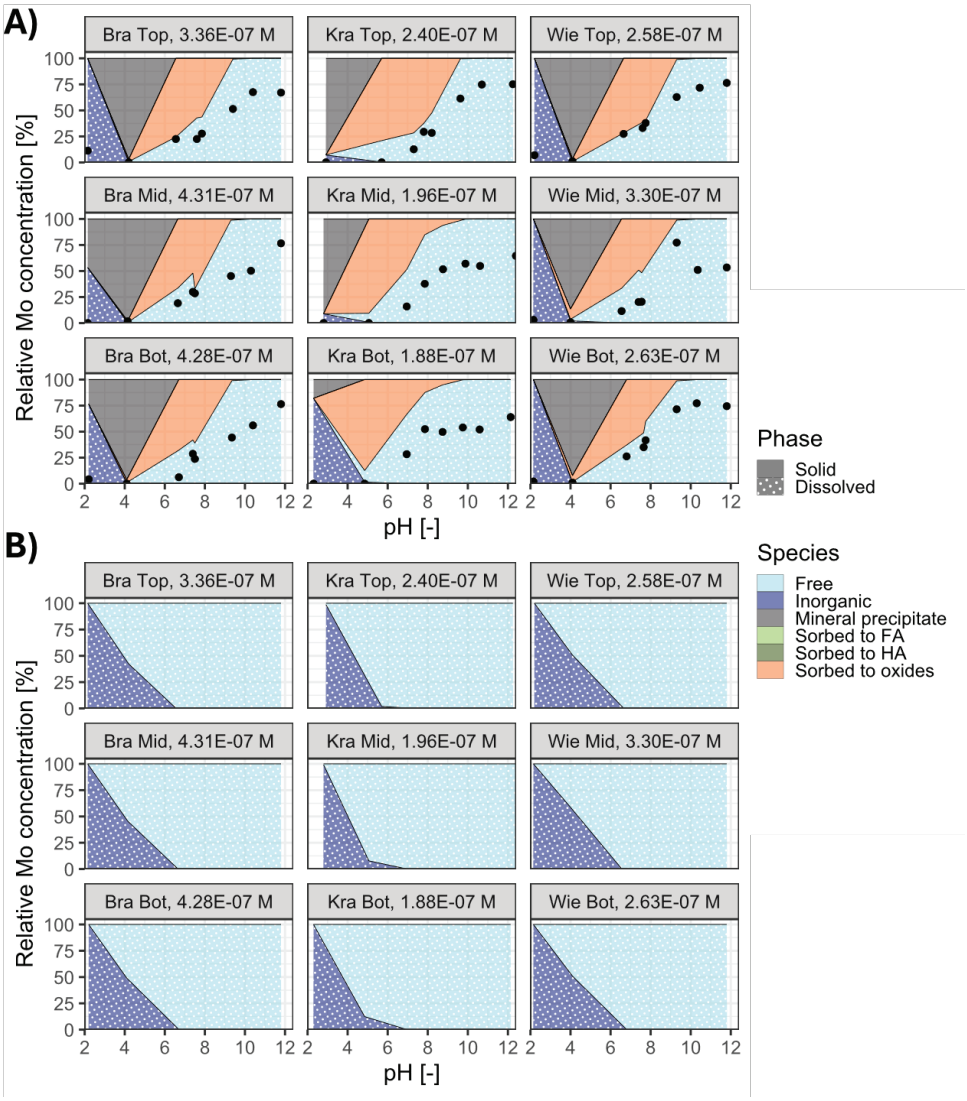


Figure S2.4 A) Model calculated solid and dissolved phase speciation of molybdenum as a function of pH for all landfills and landfill layers. Measured dissolved concentrations are represented by the black circles; B) Dissolved phase speciation of molybdenum as a function of pH for all landfills and landfill layers. Solid colours represent solid species, white-dotted colours represent dissolved species. Total concentrations used as model input are above each graph. Shown mineral precipitate is PbMoO4; shown inorganic species are predominantly H2MoO4 (pH 2 – 4) and HMoO4 (pH 4 – 6).

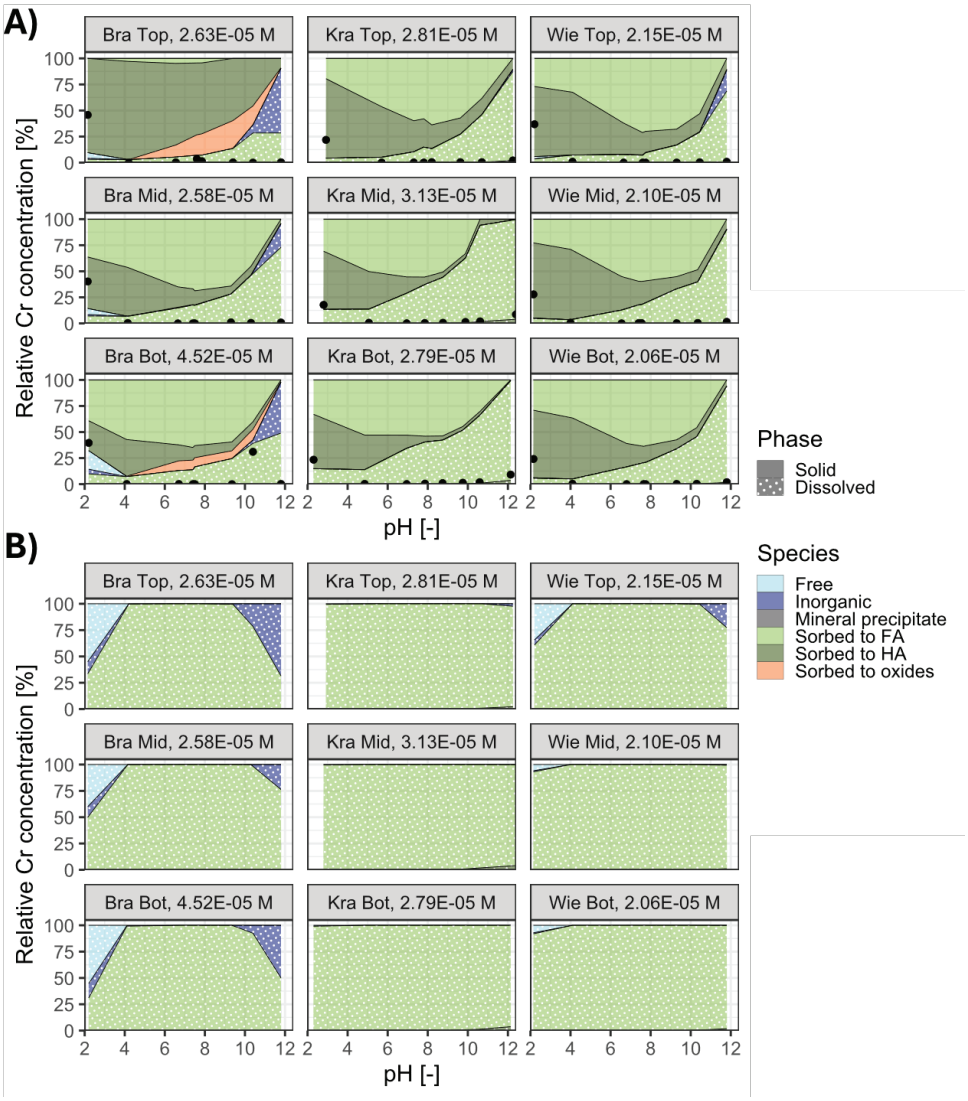


Figure S2.5 A) Model calculated solid and dissolved phase speciation of chromium as a function of pH for all landfills and landfill layers. Measured dissolved concentrations are represented by the black circles; B) Dissolved phase speciation of chromium as a function of pH for all landfills and landfill layers. Solid colours represent solid species, white-dotted colours represent dissolved species. Total concentrations used as model input are above each graph. Shown inorganic species are predominantly CrO2- and Cr(OH)4- in approximately equal share.

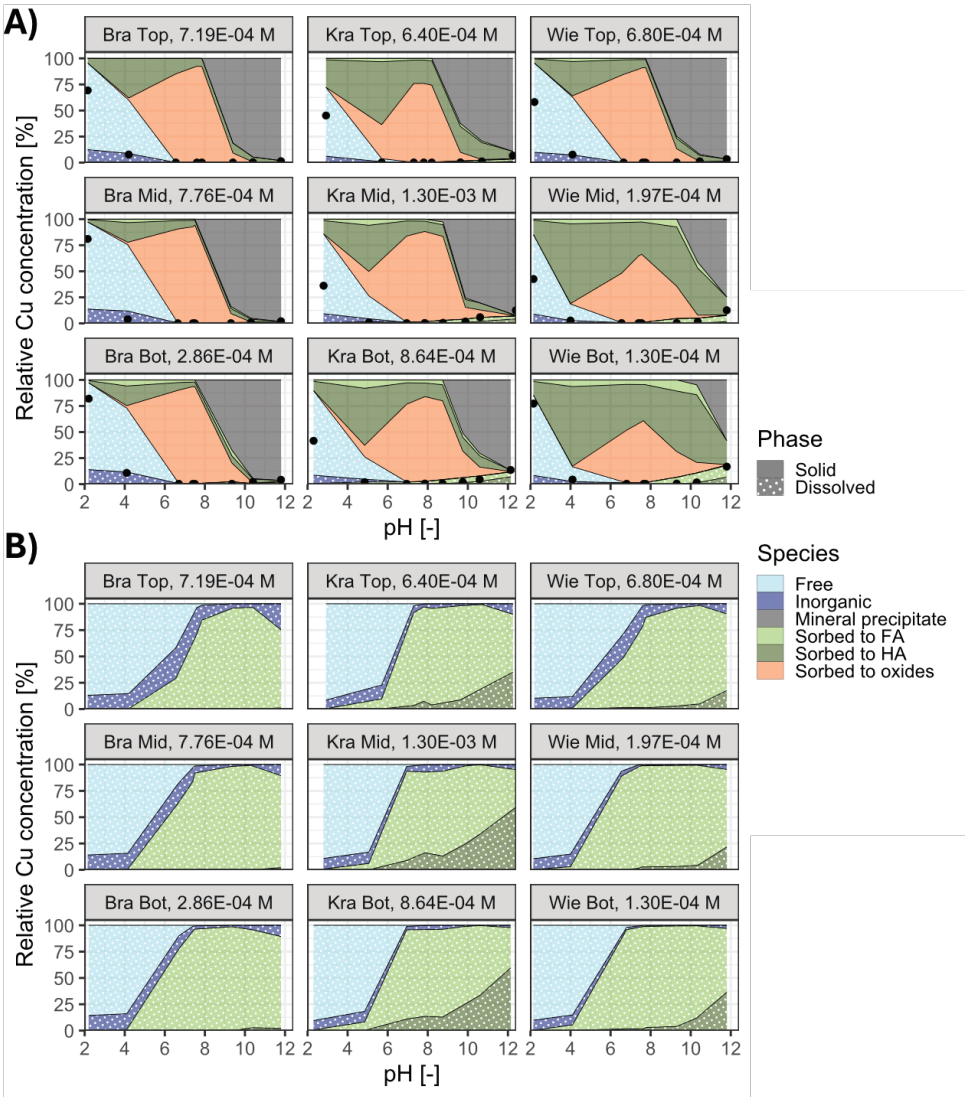


Figure S2.6 A) Model calculated solid and dissolved phase speciation of copper as a function of pH for all landfills and landfill layers. Measured dissolved concentrations are represented by the black circles; B) Dissolved phase speciation of copper as a function of pH for all landfills and landfill layers. Solid colours represent solid species, white-dotted colours represent dissolved species. Total concentrations used as model input are above each graph. Shown mineral precipitate is Cu(OH)2.

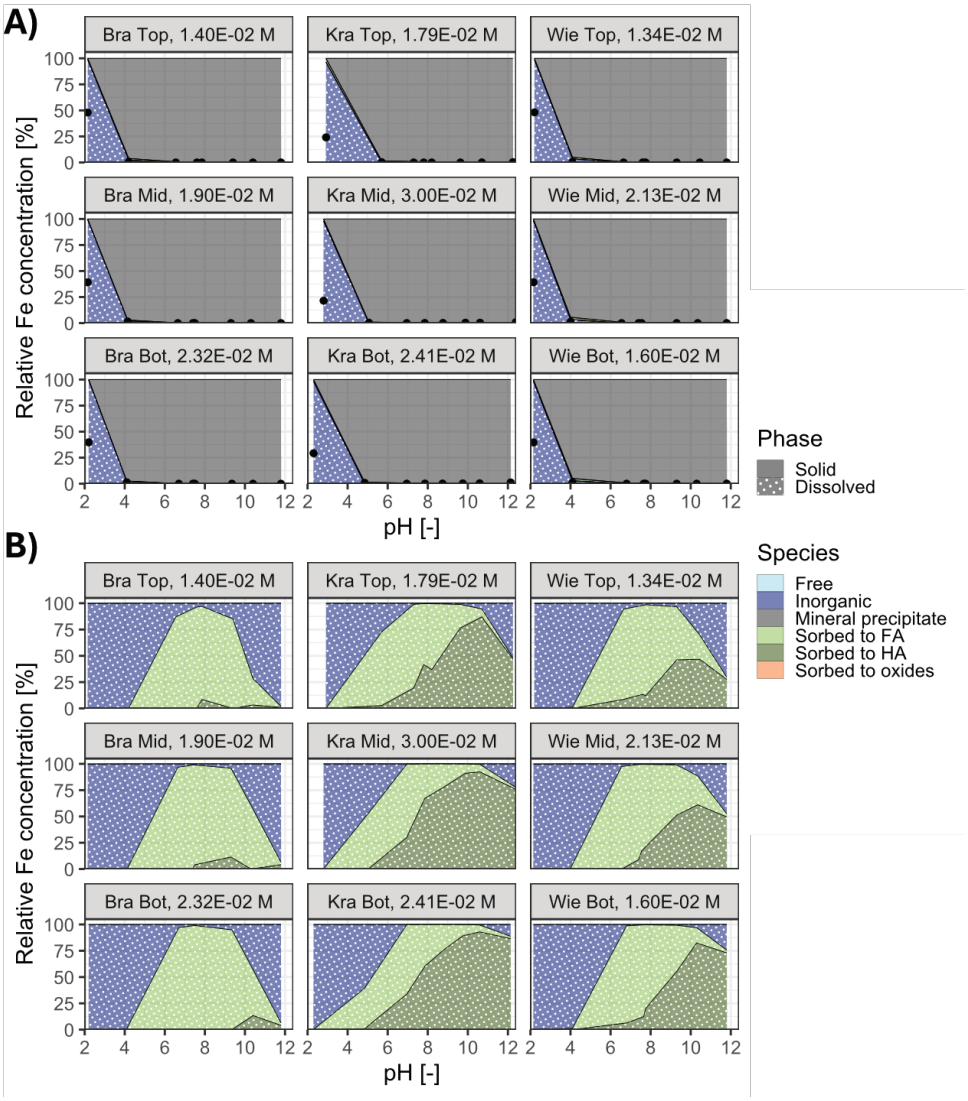


Figure S2.7 A) Model calculated solid and dissolved phase speciation of iron as a function of pH for all landfills and landfill layers. Measured dissolved concentrations are represented by the black circles; B) Dissolved phase speciation of iron as a function of pH for all landfills and landfill layers. Solid colours represent solid species, white-dotted colours represent dissolved species. Total concentrations used as model input are above each graph. Shown mineral precipitate is ferrihydrite; shown inorganic species are predominantly Fe2+ (low pH) and Fe(OH)4- (high pH).

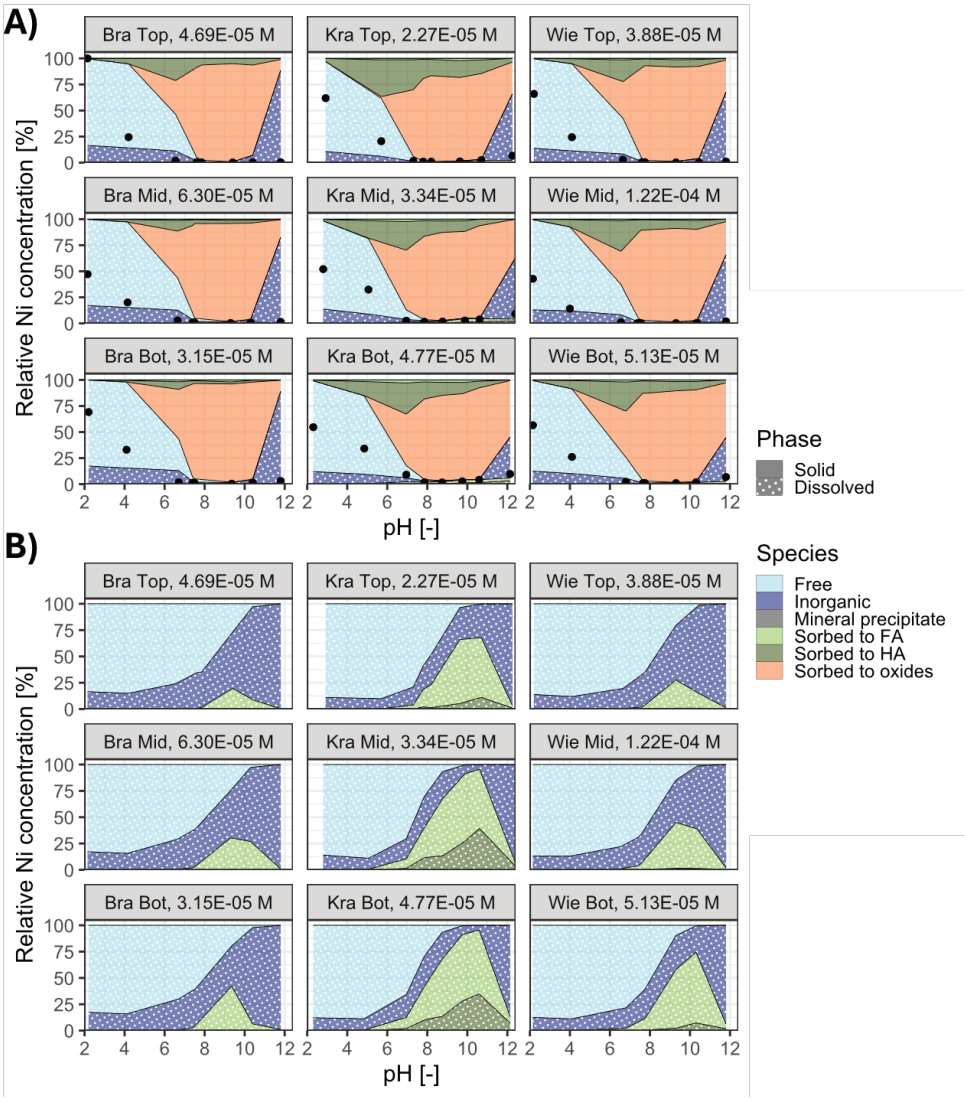


Figure S2.8 A) Model calculated solid and dissolved phase speciation of nickel as a function of pH for all landfills and landfill layers. Measured dissolved concentrations are represented by the black circles; B) Dissolved phase speciation of nickel as a function of pH for all landfills and landfill layers. Solid colours represent solid species, white-dotted colours represent dissolved species. Total concentrations used as model input are above each graph. Shown inorganic species are predominantly NiCl+ (pH 2 - 4), NiCO3 (pH 4 – 6), NiOH (pH 6 – 9), Ni(OH)2 (pH 9 – 11), and Ni(OH)3 (above pH 11).

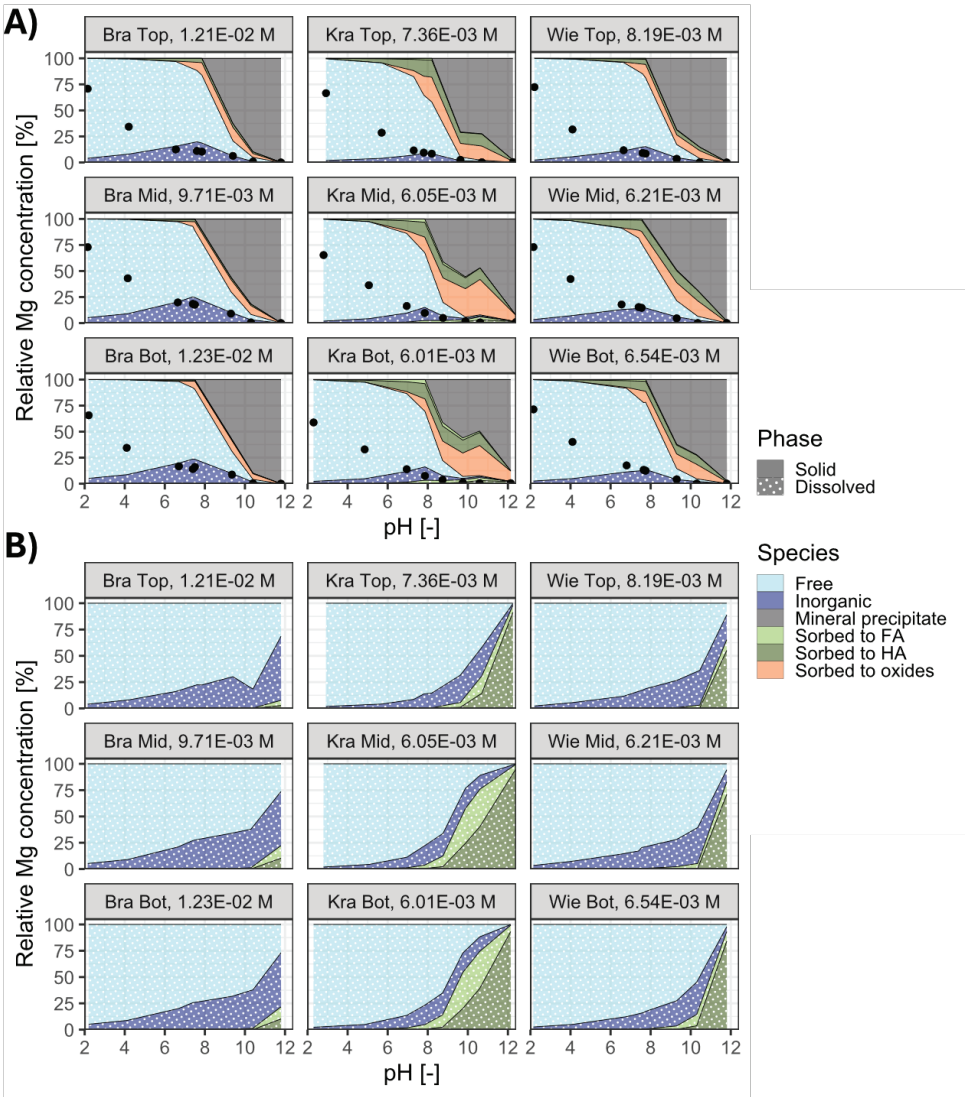


Figure S2.9 A) Model calculated solid and dissolved phase speciation of magnesium as a function of pH for all landfills and landfill layers. Measured dissolved concentrations are represented by the black circles; B) Dissolved phase speciation of magnesium as a function of pH for all landfills and landfill layers. Solid colours represent solid species, white-dotted colours represent dissolved species. Total concentrations used as input are above each graph. Shown mineral precipitates are Magnesite (pH 9 – 10) and Brucite (above pH 10); shown inorganic species are predominantly MgSO4 (pH 2 – 9), MgCO3 (pH 9 – 10), and MgOH+ (above pH 10).

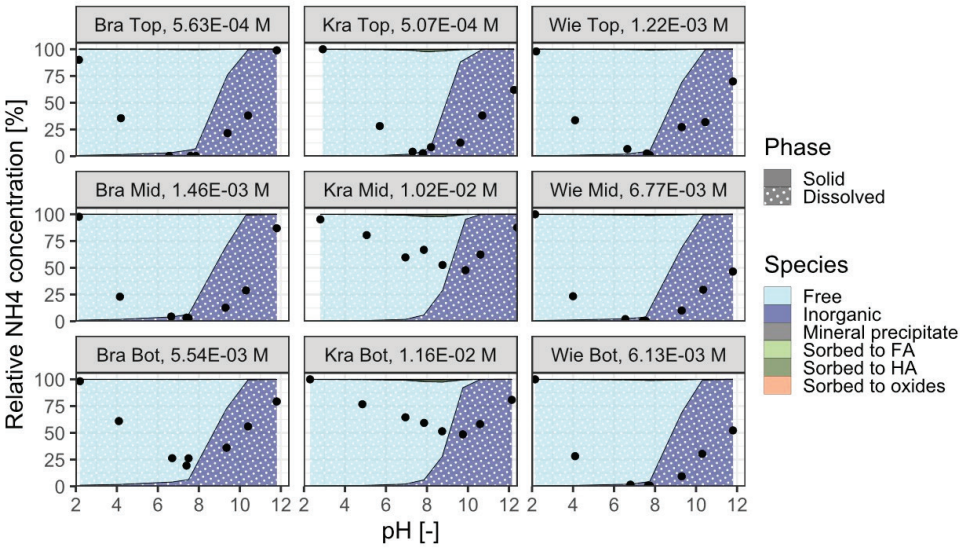


Figure S2.10 Model calculated solid and dissolved phase speciation of ammonium as a function of pH for all landfills and landfill layers. Measured dissolved concentrations are represented by the black circles. Binding to clay is not taken into account in this Figure. Total concentrations used as model input are above each graph. Shown inorganic species are predominantly NH3 (until pH 9.5) and NO2- (above pH 9.5).

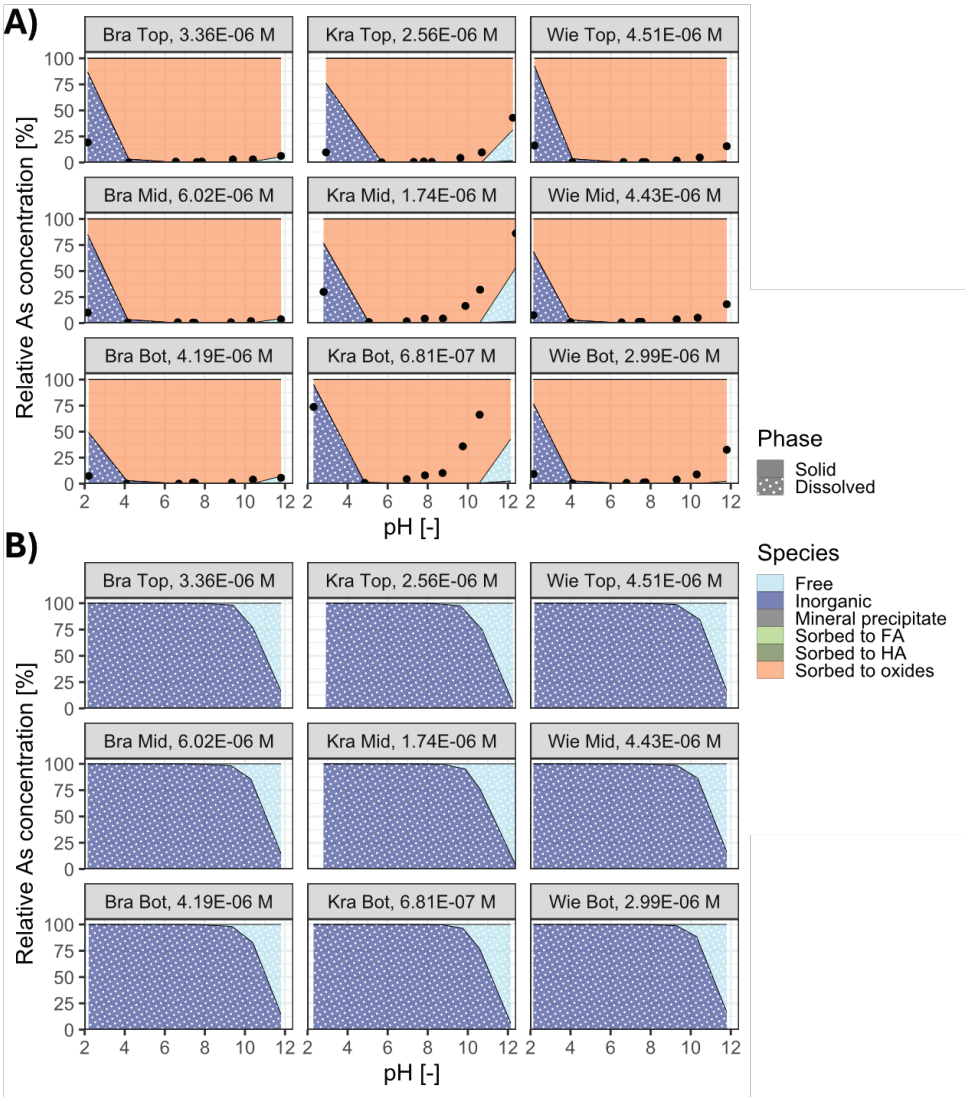


Figure S2.11 A) Model calculated solid and dissolved phase speciation of arsenic as a function of pH for all landfills and landfill layers. Measured dissolved concentrations are represented by the black circles; B) Dissolved phase speciation of arsenic as a function of pH for all landfills and landfill layers. Solid colours represent solid species, white-dotted colours represent dissolved species. Total concentrations used as model input are above each graph. Shown inorganic species are predominantly H2AsO4- (pH 2 – 7) and HAsO42- (pH 7 – 11).

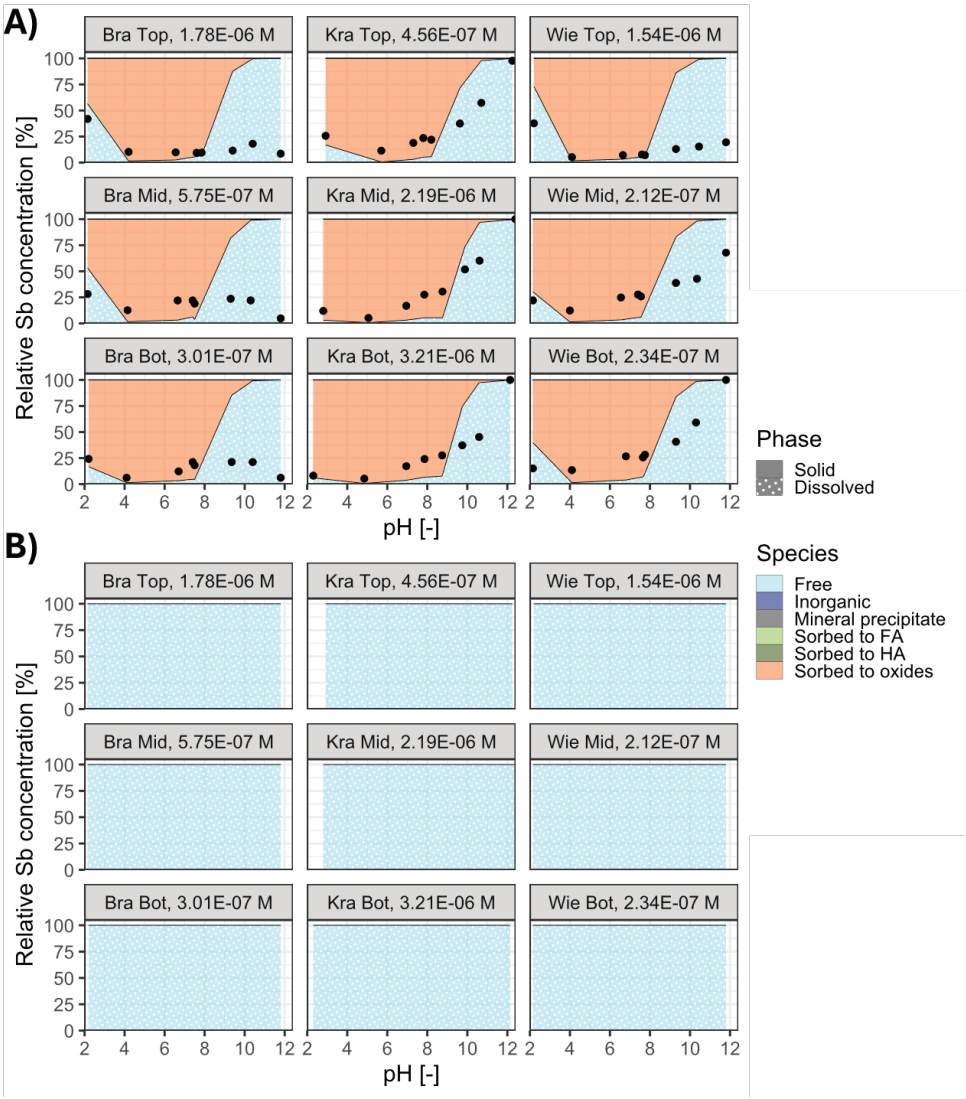


Figure S2.12 A) Model calculated solid and dissolved phase speciation of antimony as a function of pH for all landfills and landfill layers. Measured dissolved concentrations are represented by the black circles; B) Dissolved phase speciation of antimony as a function of pH for all landfills and landfill layers. Solid colours represent solid species, white-dotted colours represent dissolved species. Total concentrations used as model input are above each graph.

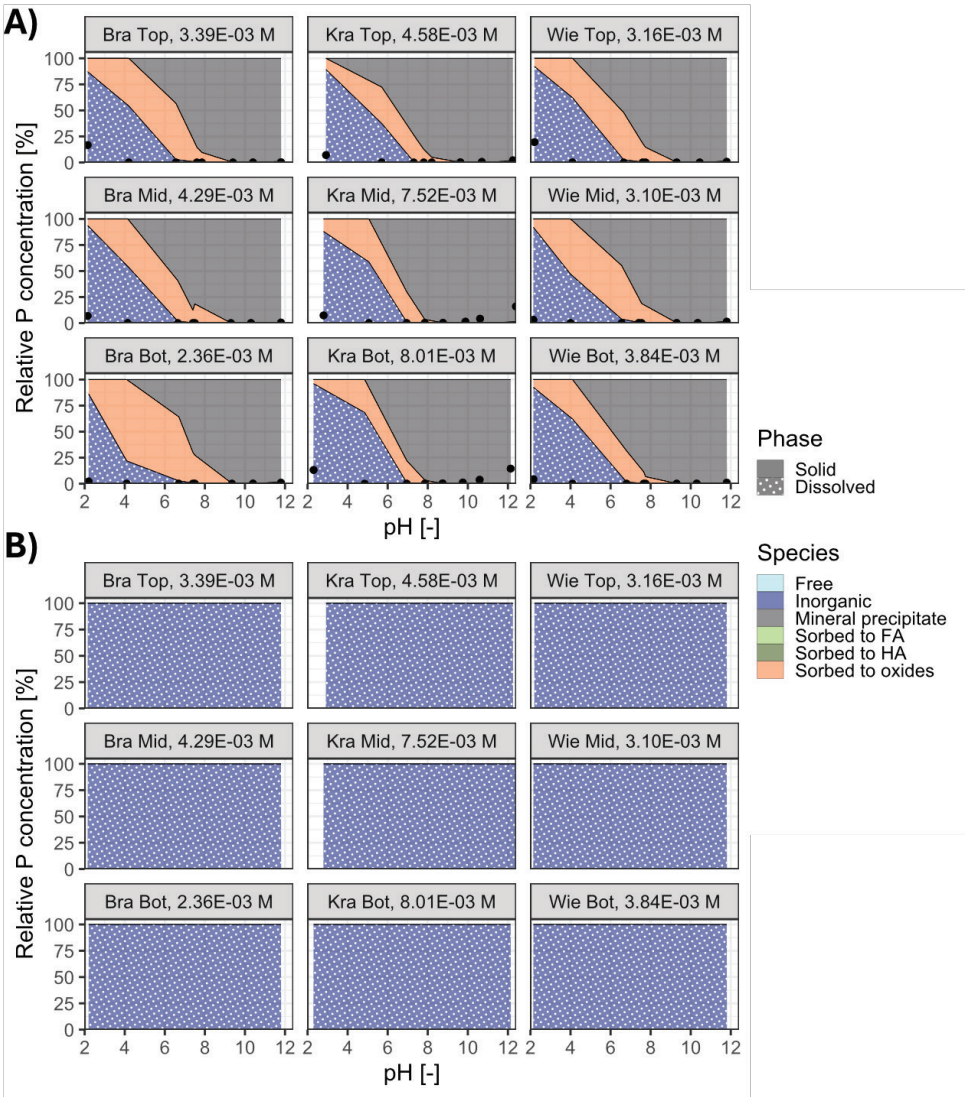


Figure S2.13 A) Model calculated solid and dissolved phase speciation of phosphorus as a function of pH for all landfills and landfill layers. Measured dissolved concentrations are represented by the black circles; B) Dissolved phase speciation of phosphorus as a function of pH for all landfills and landfill layers. Solid colours represent solid species, white-dotted colours represent dissolved species. Total concentrations used as model input are above each graph. Shown mineral precipitate is Ca4H(PO4)3; shown inorganic species are predominantly FeH2PO4+ (pH 2) and calcium phosphates (above pH 4).

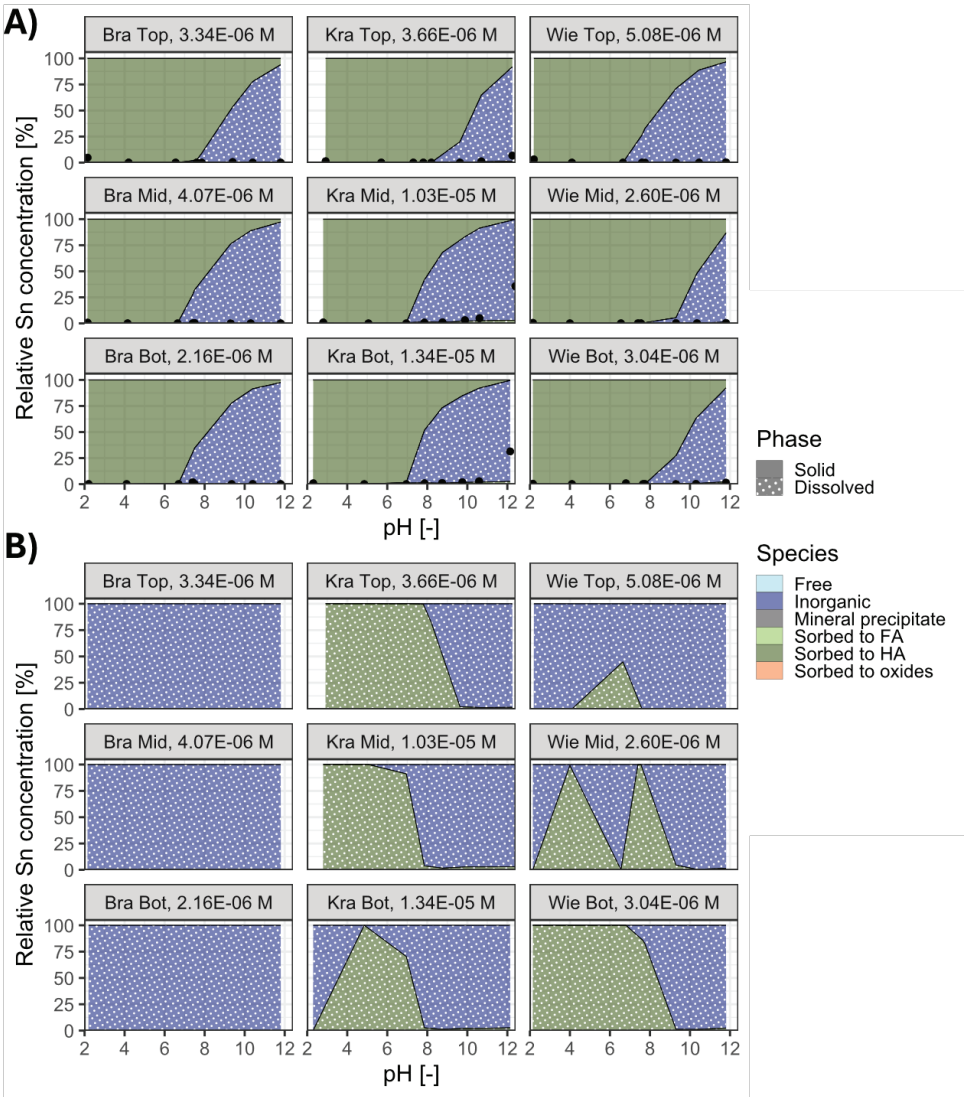


Figure S2.14 A) Model calculated solid and dissolved phase speciation of tin as a function of pH for all landfills and landfill layers. Measured dissolved concentrations are represented by the black circles; B) Dissolved phase speciation of tin as a function of pH for all landfills and landfill layers. Solid colours represent solid species, white-dotted colours represent dissolved species. Total concentrations used as model input are above each graph. Shown inorganic species is predominantly Sn(OH)6-2.

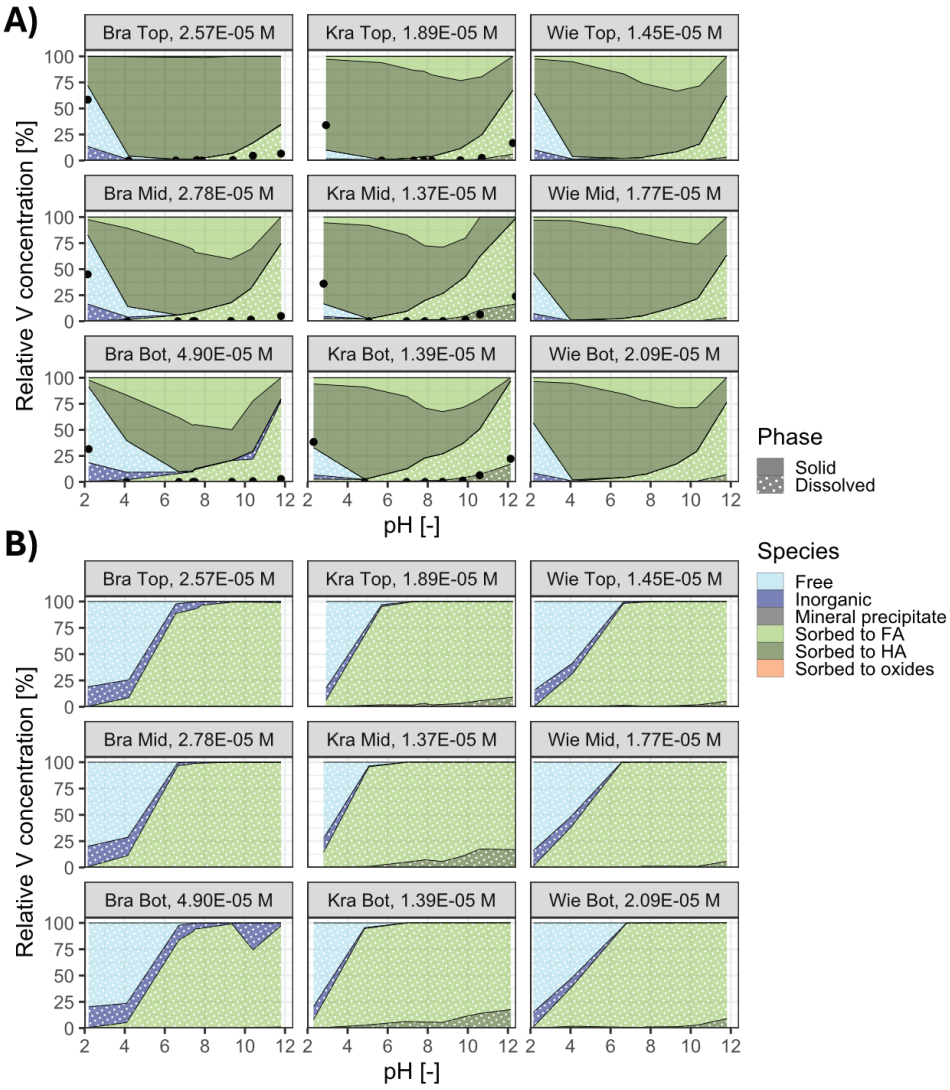


Figure S2.15 A) Model calculated solid and dissolved phase speciation of vanadium as a function of pH for all landfills and landfill layers. Measured dissolved concentrations are represented by the black circles; B) Dissolved phase speciation of vanadium as a function of pH for all landfills and landfill layers. Solid colours represent solid species, white-dotted colours represent dissolved species. Total concentrations used as model input are above each graph.

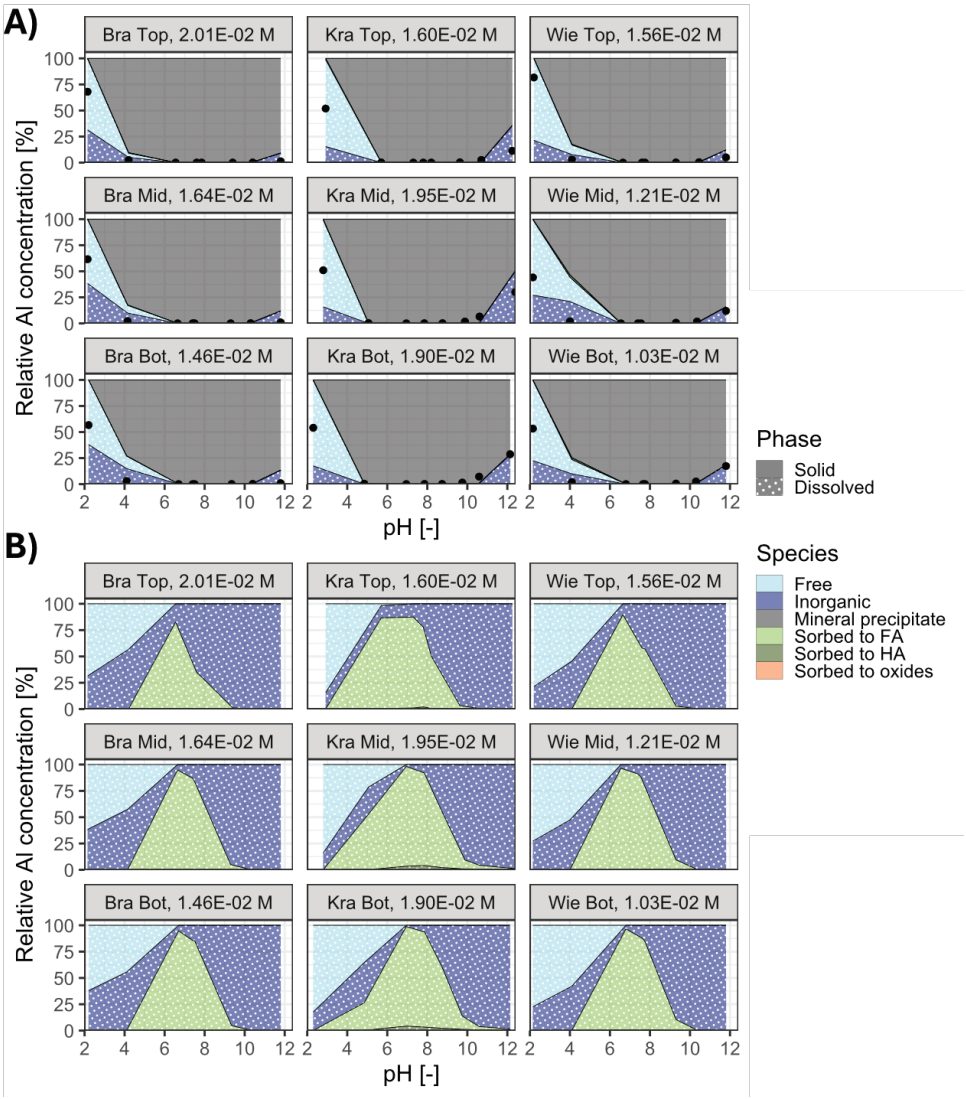


Figure S2.16 A) Model calculated solid and dissolved phase speciation of aluminium as a function of pH for all landfills and landfill layers. Measured dissolved concentrations are represented by the black circles; B) Dissolved phase speciation of aluminium as a function of pH for all landfills and landfill layers. Solid colours represent solid species, white-dotted colours represent dissolved species. Total concentrations used as model input are above each graph. Shown mineral precipitate is gibbsite; shown inorganic species are predominantly AlSO4+ (low pH) and Al(OH)4- (high pH).

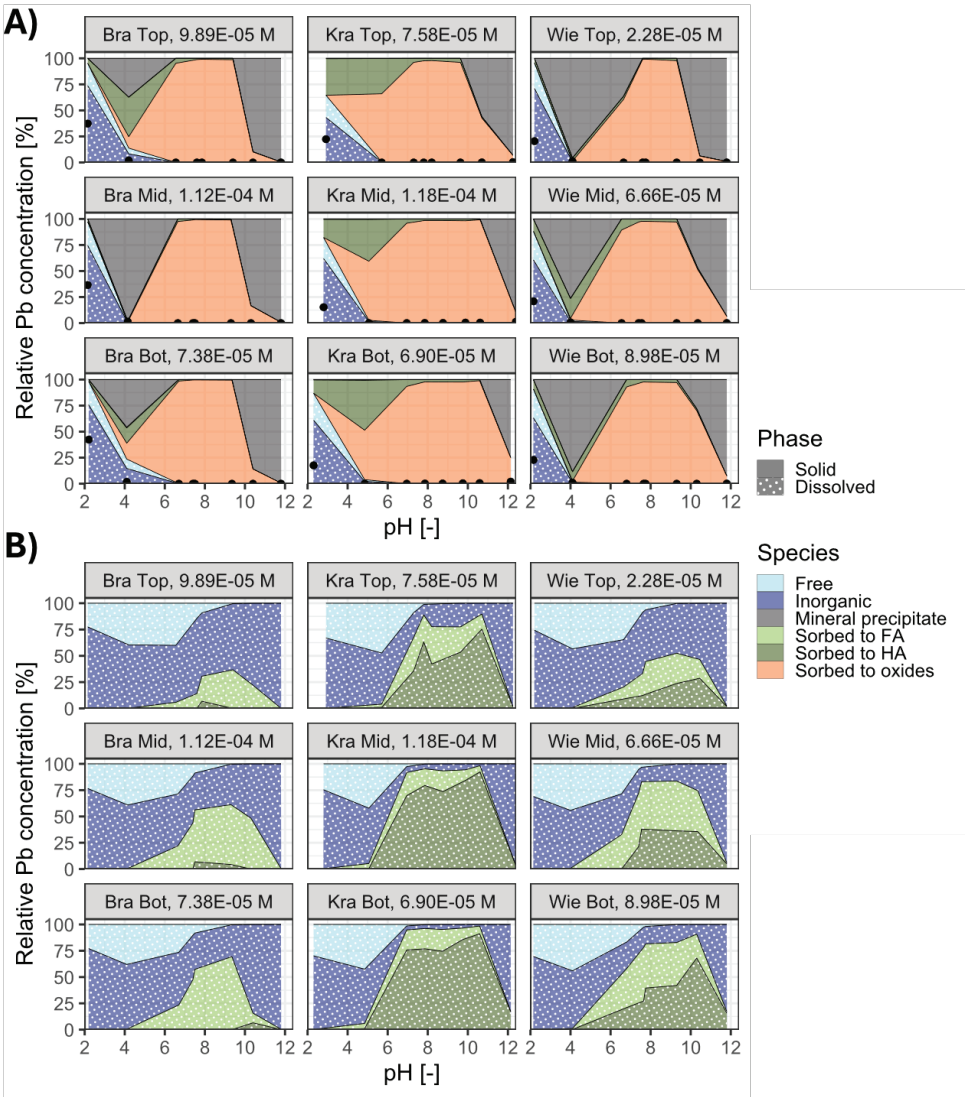


Figure S2.17 A) Model calculated solid and dissolved phase speciation of lead as a function of pH for all landfills and landfill layers. Measured dissolved concentrations are represented by the black circles; B) Dissolved phase speciation of lead as a function of pH for all landfills and landfill layers. Solid colours represent solid species, white-dotted colours represent dissolved species. Total concentrations used as model input are above each graph. Shown mineral precipitates are PbMoO4 (low pH) and Pb(OH)3 (high pH); shown inorganic species are predominantly PbCl+ (pH 2 – 6), Pb carbonate (pH 6 – 10), and Pb hydroxide (above pH 10).

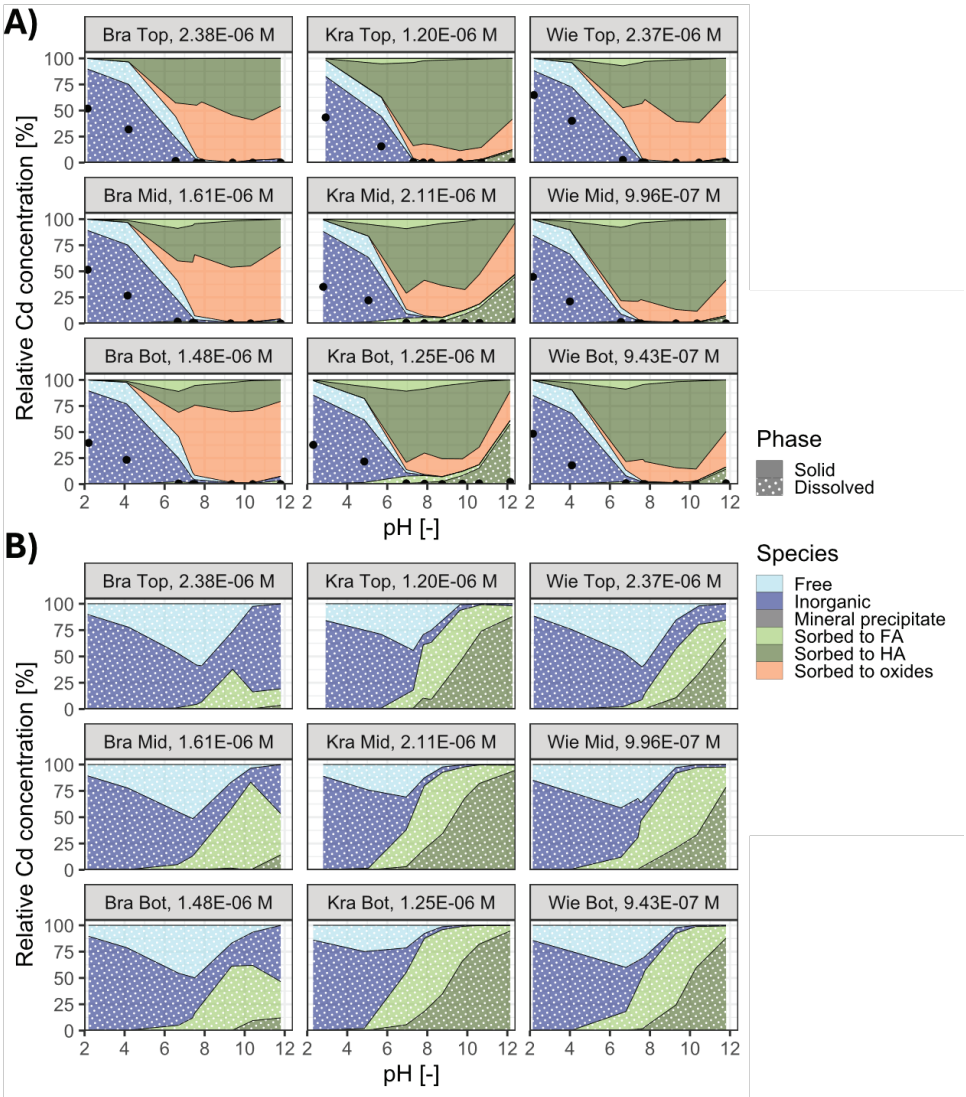


Figure S2.18 A) Model calculated solid and dissolved phase speciation of cadmium as a function of pH for all landfills and landfill layers. Measured dissolved concentrations are represented by the black circles; B) Dissolved phase speciation of cadmium as a function of pH for all landfills and landfill layers. Solid colours represent solid species, white-dotted colours represent dissolved species. Total concentrations used as model input are above each graph. Shown inorganic species are predominantly Cd-chloride complexes.

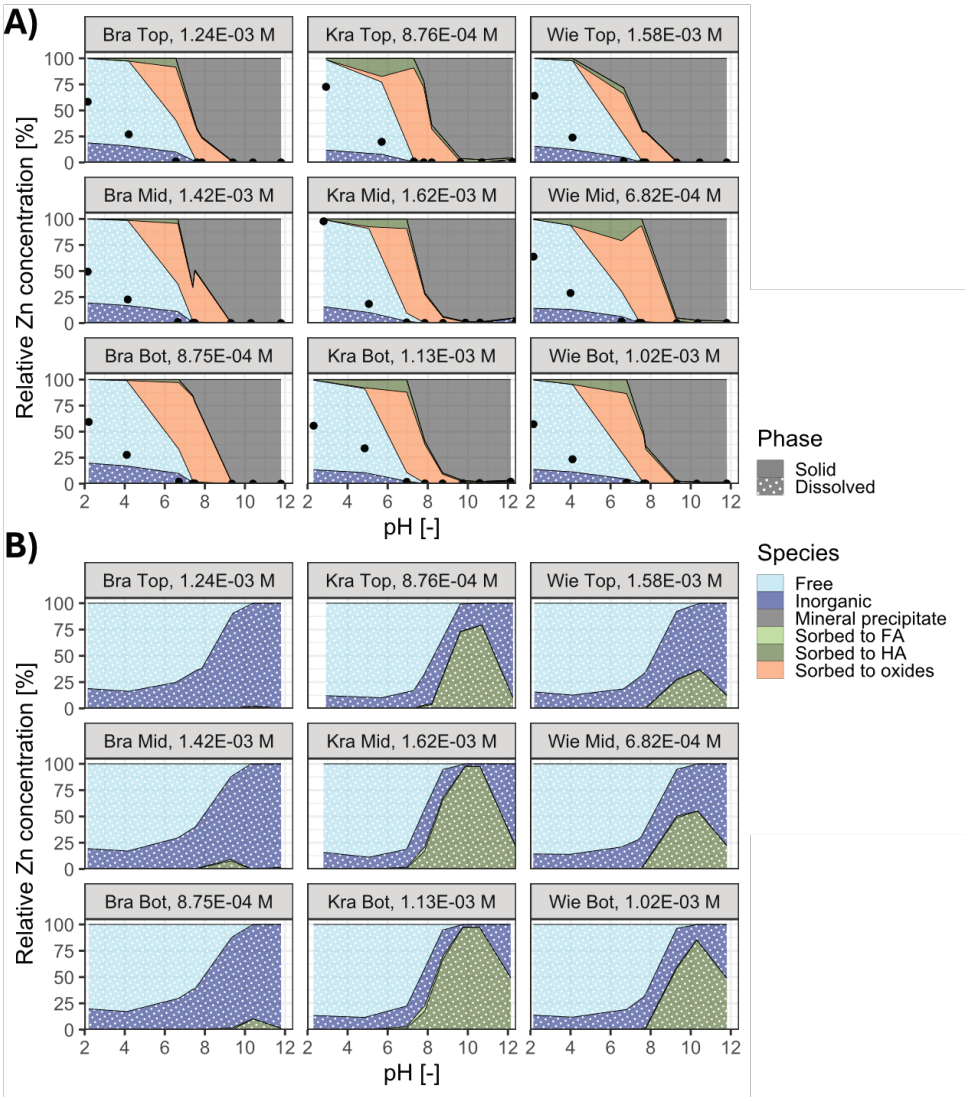


Figure S2.19 A) Model calculated solid and dissolved phase speciation of zinc as a function of pH for all landfills and landfill layers. Measured dissolved concentrations are represented by the black circles; B) Dissolved phase speciation of zinc as a function of pH for all landfills and landfill layers. Solid colours represent solid species, white-dotted colours represent dissolved species. Total concentrations used as model input are above each graph. Shown mineral precipitate is Willemite; shown inorganic species are predominantly ZnCl+ (pH 2 – 6), ZnSO4 (pH 6 – 8), and Zn hydroxides (above pH 8).

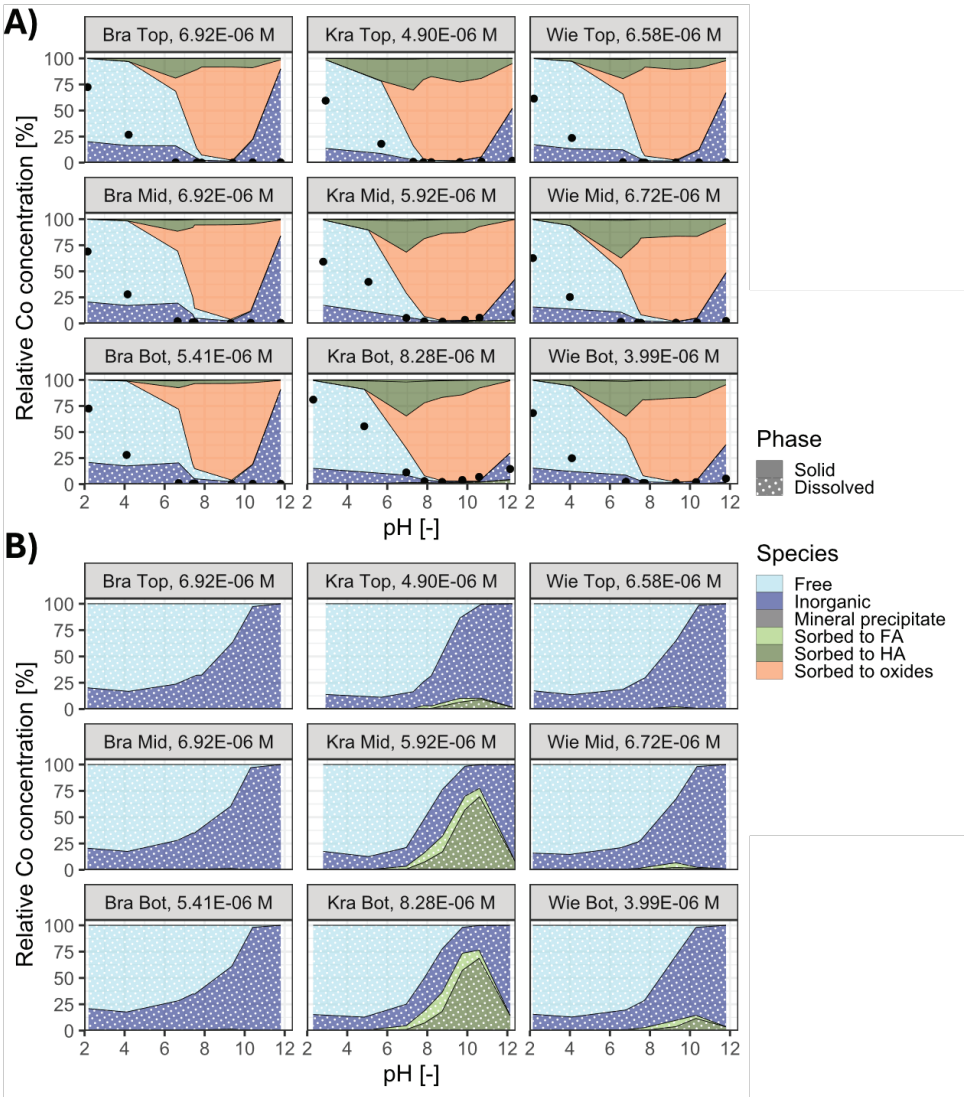


Figure S2.20 A) Model calculated solid and dissolved phase speciation of cobalt as a function of pH for all landfills and landfill layers. Measured dissolved concentrations are represented by the black circles; B) Dissolved phase speciation of cobalt as a function of pH for all landfills and landfill layers. Solid colours represent solid species, white-dotted colours represent dissolved species. Total concentrations used as model input are above each graph. Shown inorganic species are predominantly CoCl+ (pH 2 – 6), CoSO4 (pH 6 – 10), and Co hydroxides (above pH 10).

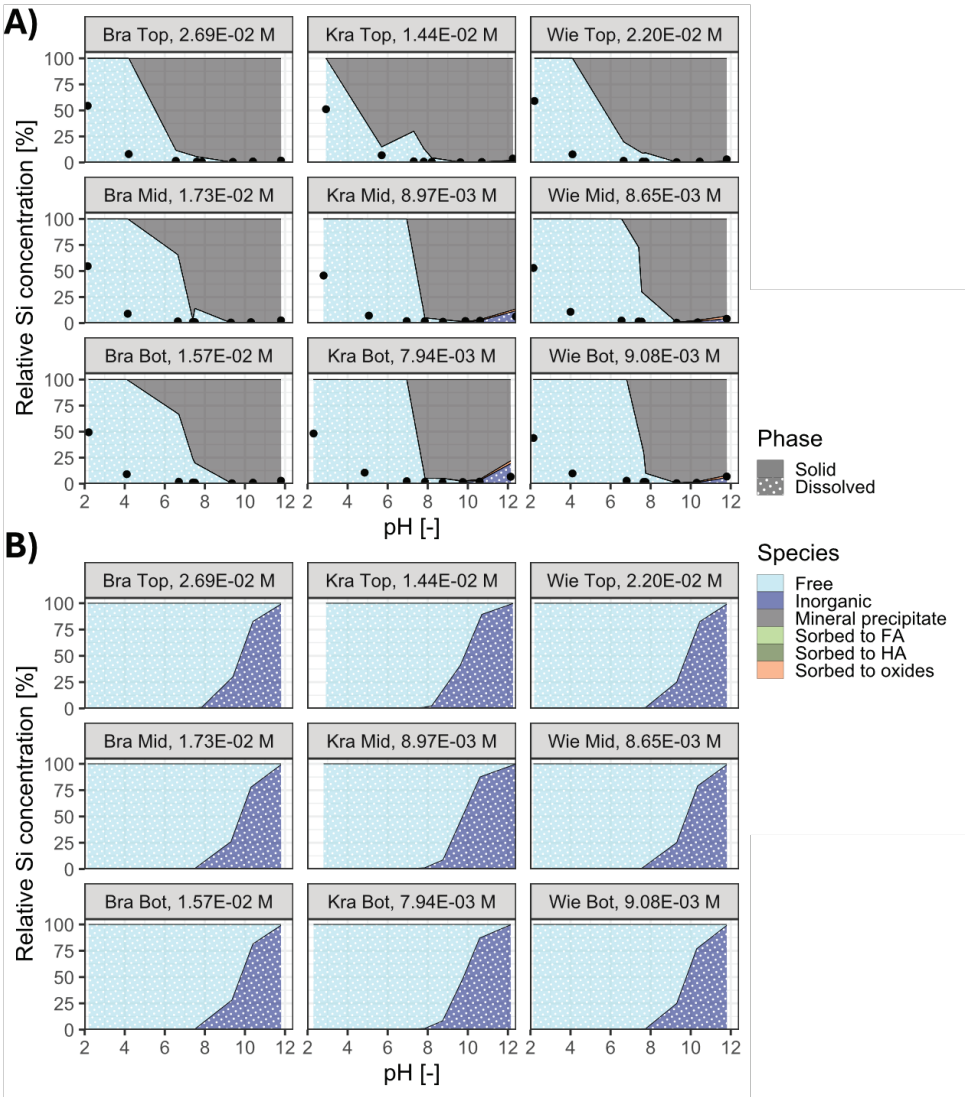


Figure S2.21 A) Model calculated solid and dissolved phase speciation of silicon as a function of pH for all landfills and landfill layers. Measured dissolved concentrations are represented by the black circles; B) Dissolved phase speciation of silicon as a function of pH for all landfills and landfill layers. Solid colours represent solid species, white-dotted colours represent dissolved species. Total concentrations used as model input are above each graph. Shown mineral precipitates are Wairakite (pH 6 – 8.5) and Sepiolite (above pH 8.5); shown inorganic species is predominantly H3SiO4-.

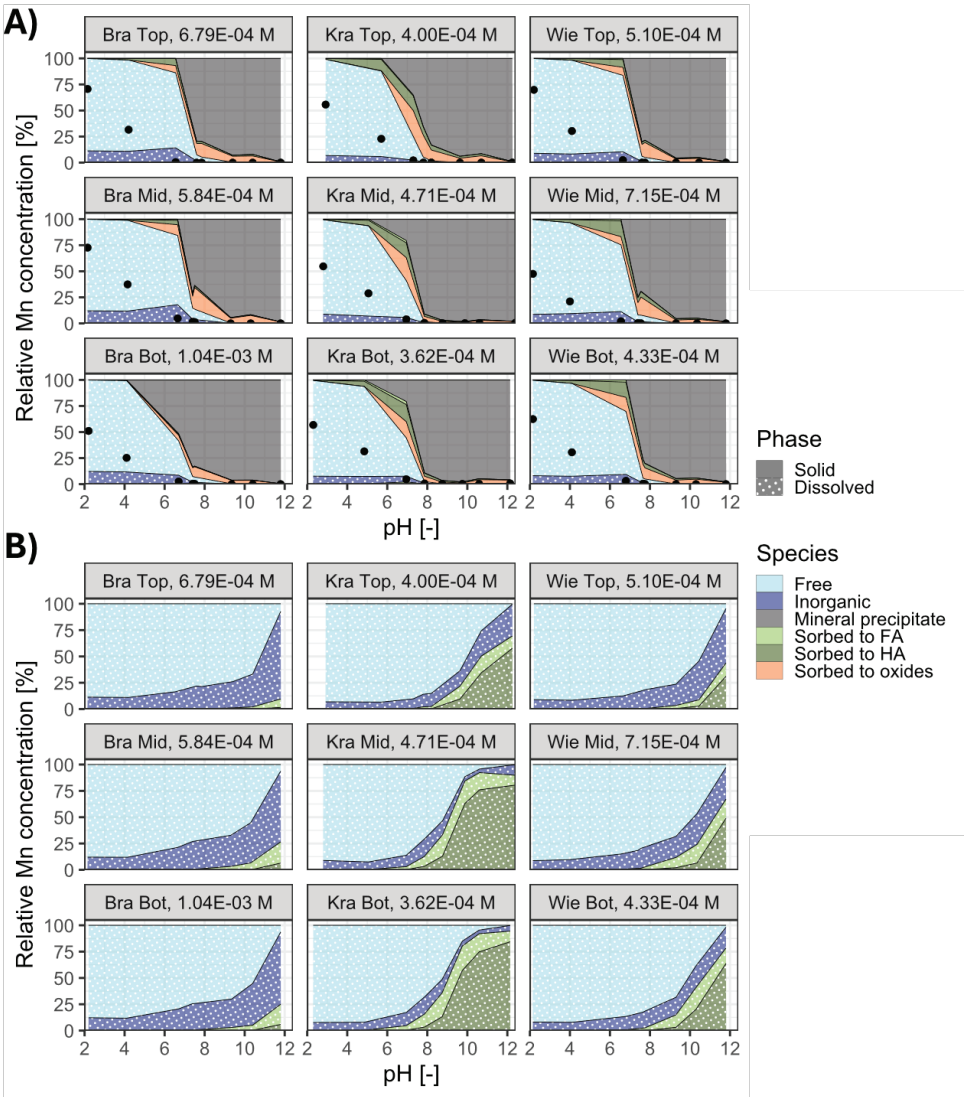


Figure S2.22 A) Model calculated solid and dissolved phase speciation of manganese as a function of pH for all landfills and landfill layers. Measured dissolved concentrations are represented by the black circles; B) Dissolved phase speciation of manganese as a function of pH for all landfills and landfill layers. Solid colours represent solid species, white-dotted colours represent dissolved species. Total concentrations used as input are above each graph. Shown minerals are Rhodochrosite (pH 6 – 10.5) and Pyrochroite (above pH 10.5); shown inorganic species are predominantly MnCl+ (pH 2 – 4), MnSO4 (pH 4 – 9.5), and MnOH+ (above pH 9.5).

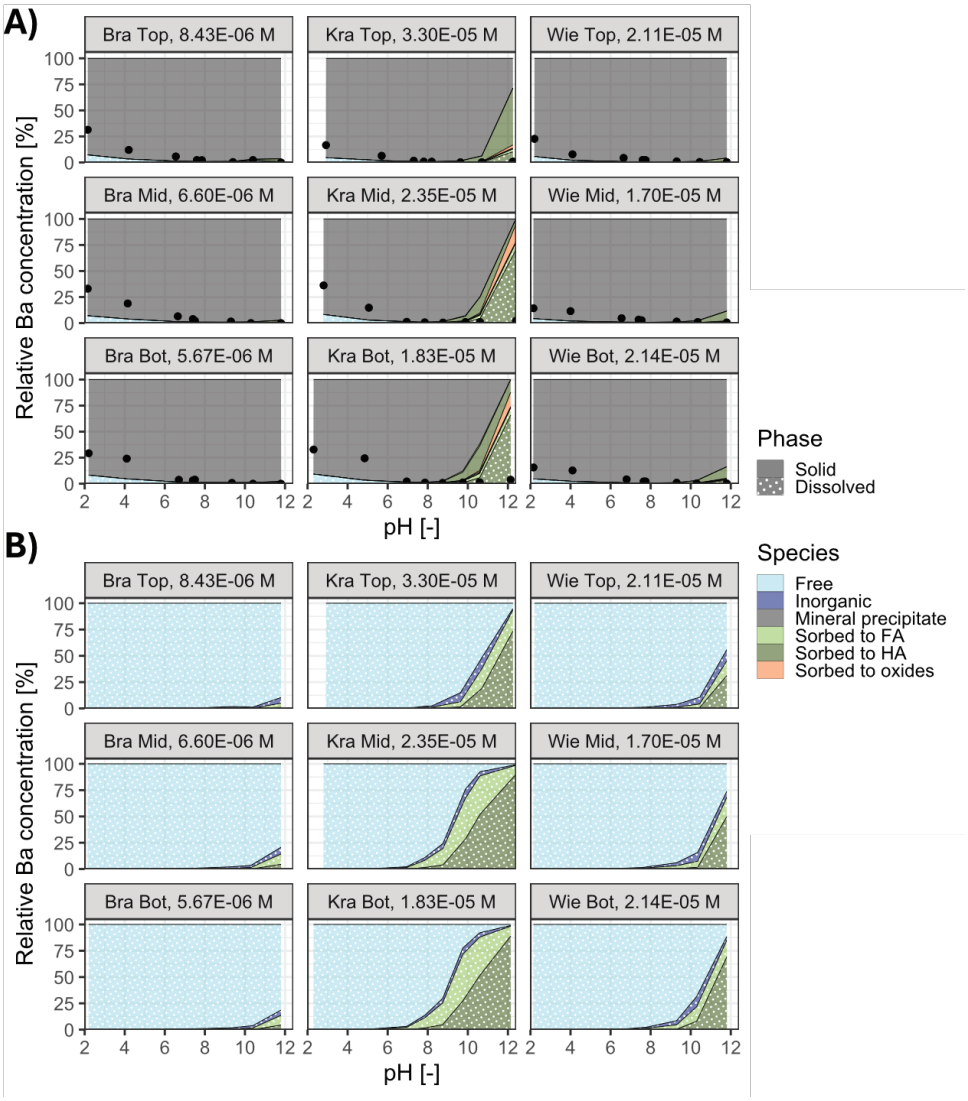


Figure S2.23 A) Model calculated solid and dissolved phase speciation of barium as a function of pH for all landfills and landfill layers. Measured dissolved concentrations are represented by the black circles; B) Dissolved phase speciation of barium as a function of pH for all landfills and landfill layers. Solid colours represent solid species, white-dotted colours represent dissolved species. Total concentrations used as model input are above each graph. Shown mineral precipitate is Barite.

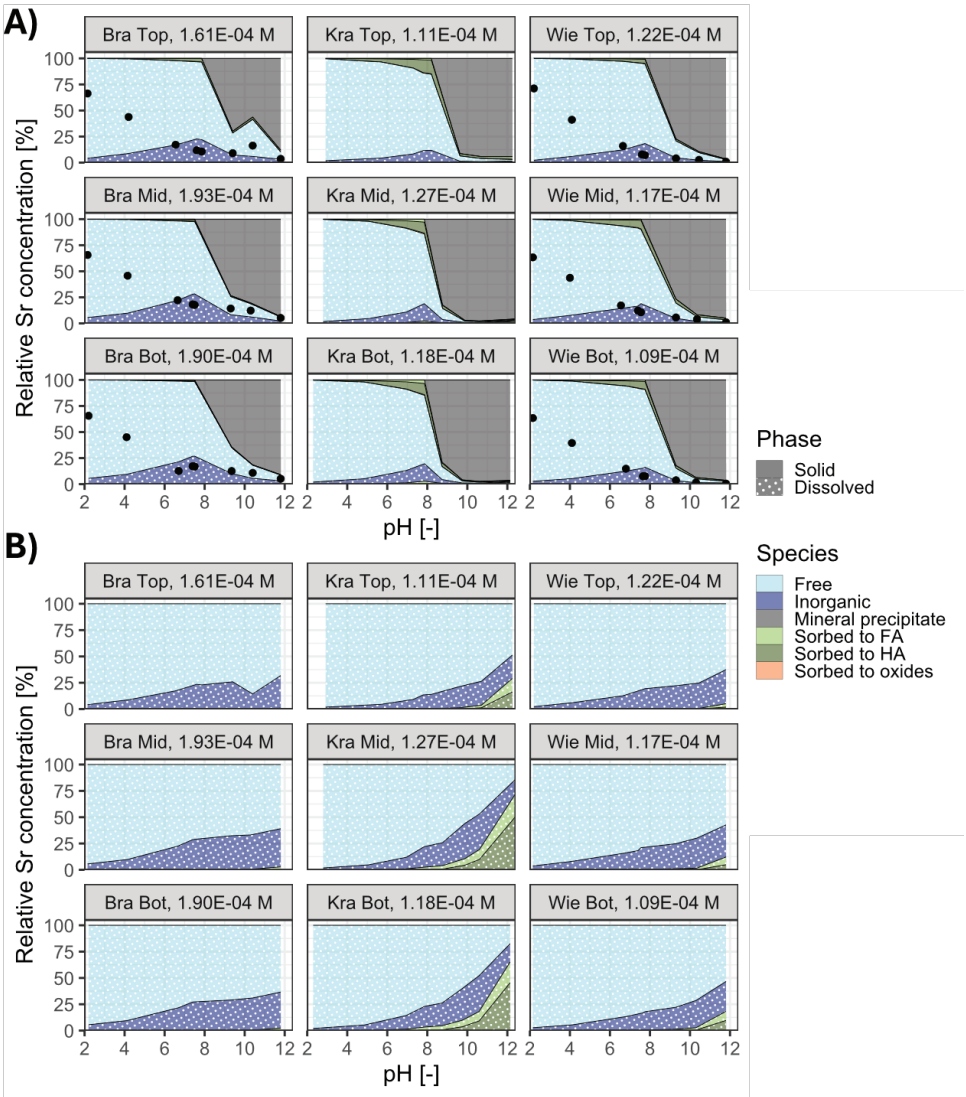


Figure S2.24 A) Model calculated solid and dissolved phase speciation of strontium as a function of pH for all landfills and landfill layers. Measured dissolved concentrations are represented by the black circles; B) Dissolved phase speciation of strontium as a function of pH for all landfills and landfill layers. Solid colours represent solid species, white-dotted colours represent dissolved species. Total concentrations used as model input are above each graph. Shown mineral precipitate is Strontianite; shown inorganic species are predominantly SrSO4 (pH 2 – 10) and SrCO3 (above pH 10).

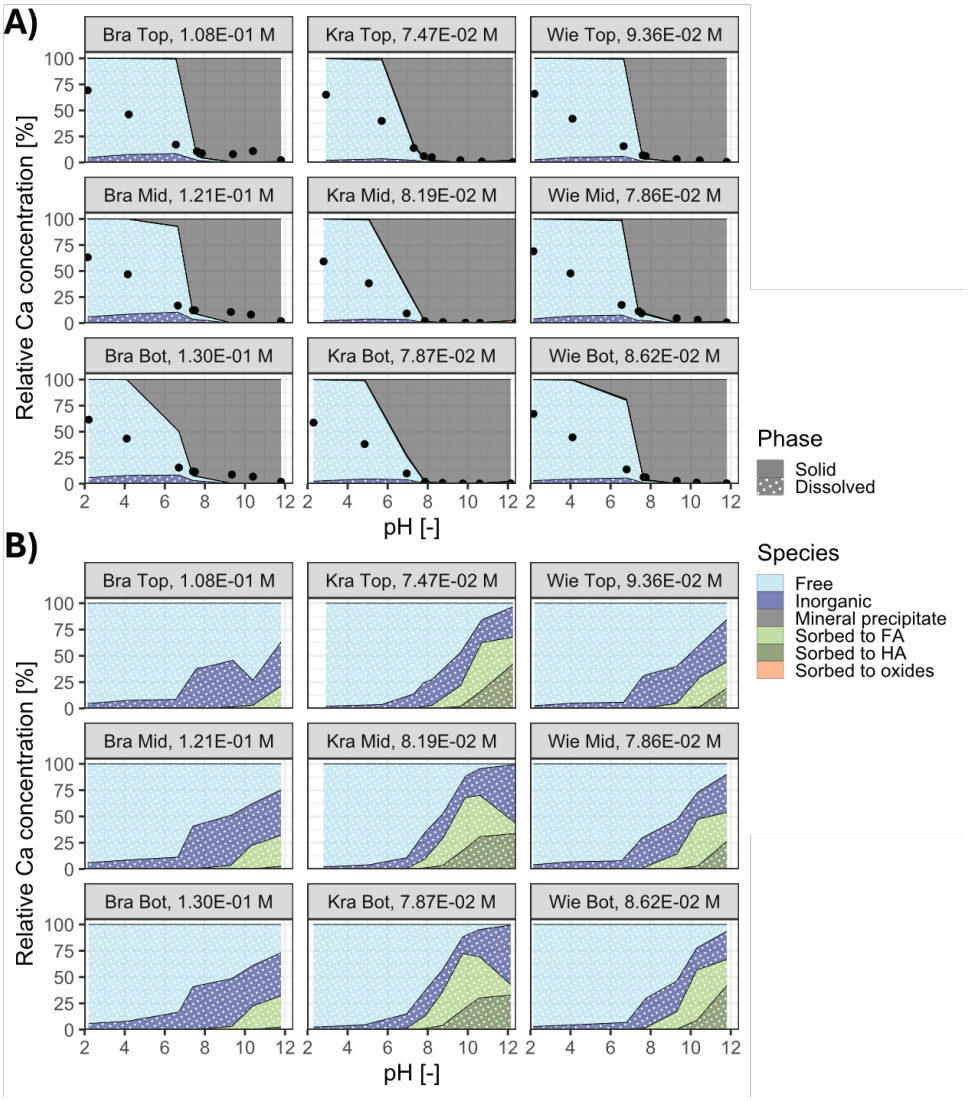


Figure S2.25 A) Model calculated solid and dissolved phase speciation of calcium as a function of pH for all landfills and landfill layers. Measured dissolved concentrations are represented by the black circles; B) Dissolved phase speciation of calcium as a function of pH for all landfills and landfill layers. Solid colours represent solid species, white-dotted colours represent dissolved species. Total concentrations used as model input are above each graph. Shown mineral precipitates are Ca4H(PO4)3 (pH 4 – 7) and Calcite (above pH 7); shown inorganic species are predominantly CaSO4 (pH 2 – 9.5), CaCO3 (pH 9.5 – 11), and CaPO4- (above pH 11).

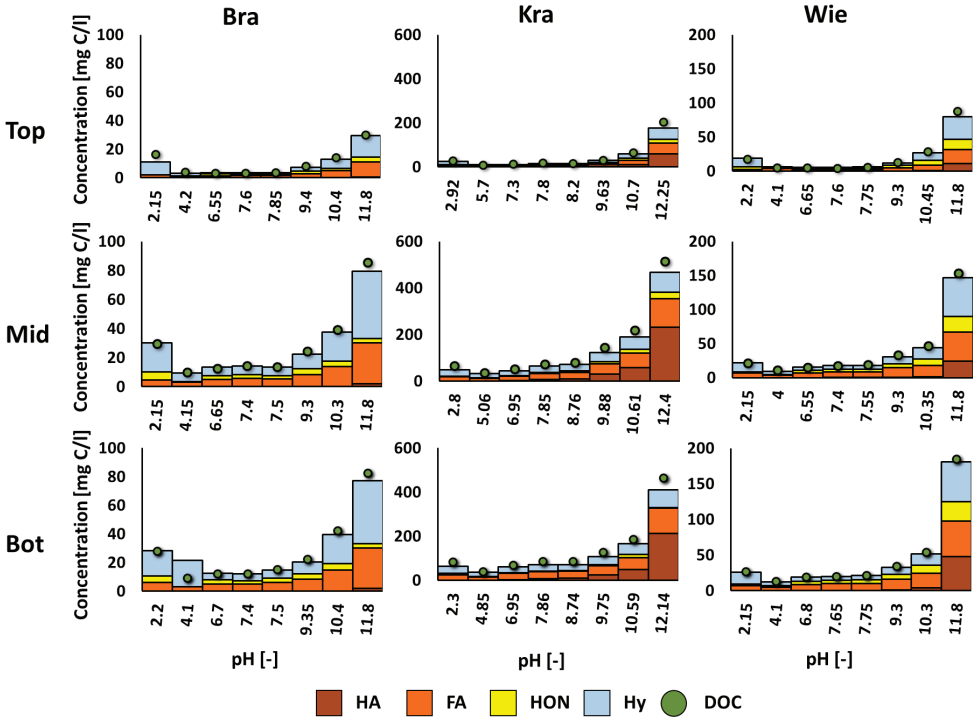


Figure S2.26 Concentration of dissolved organic matter and its subfractions as a function of pH for each landfill and each depth.

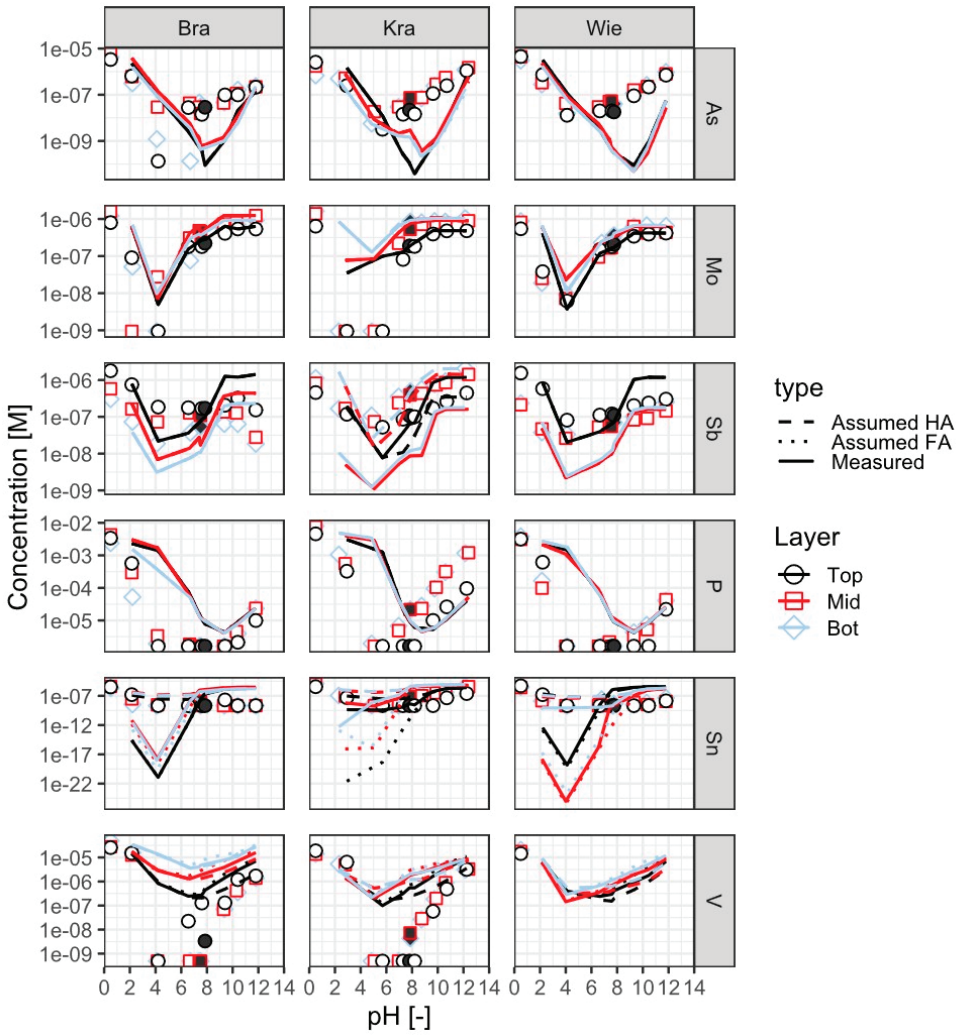


Figure S2.27 Concentrations of all elements as a function of pH for each landfill and each depth interval, measured experimentally (markers) and as calculated through multi-surface geochemical modelling using measured dissolved and solid HA and FA as input (solid lines), or assuming 50% of dissolved OM is HA (dashed lines) or FA (dotted lines). Unmanipulated samples are coloured dark grey.

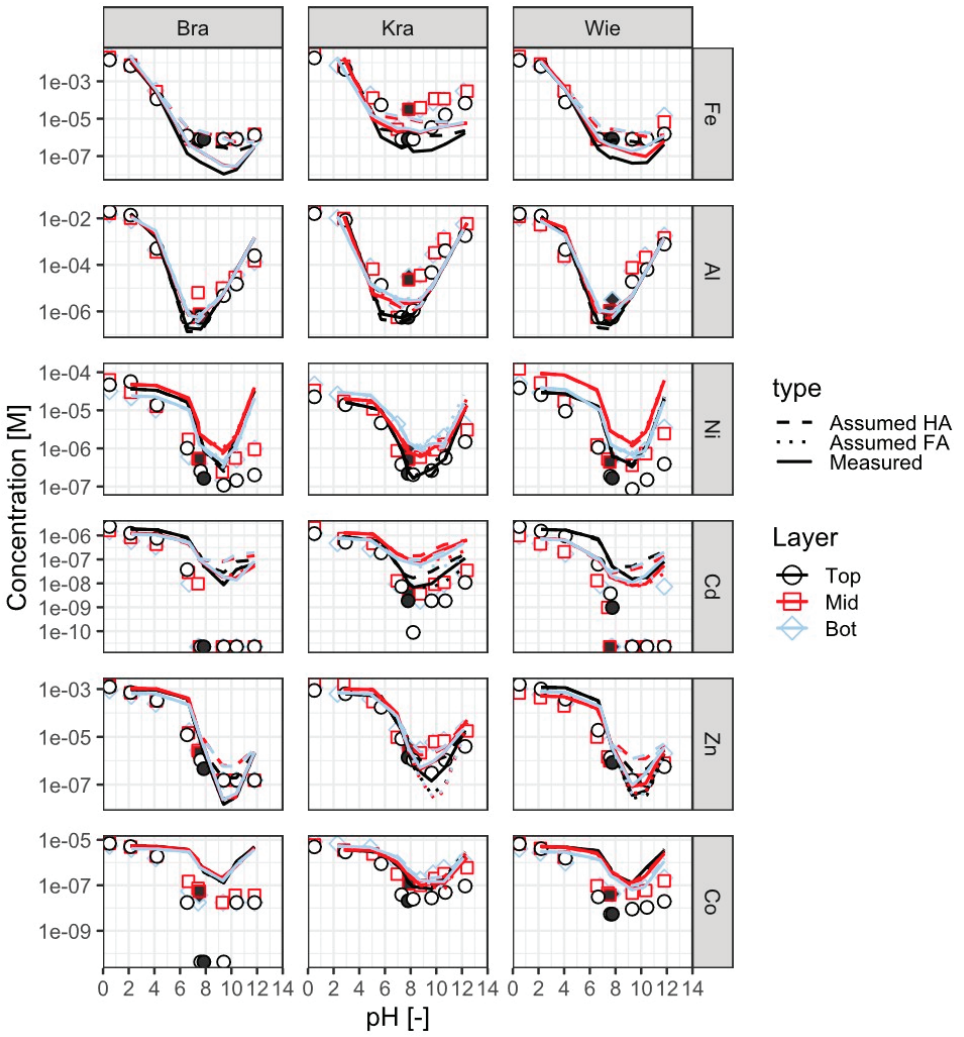


Figure S2.27 (continued)

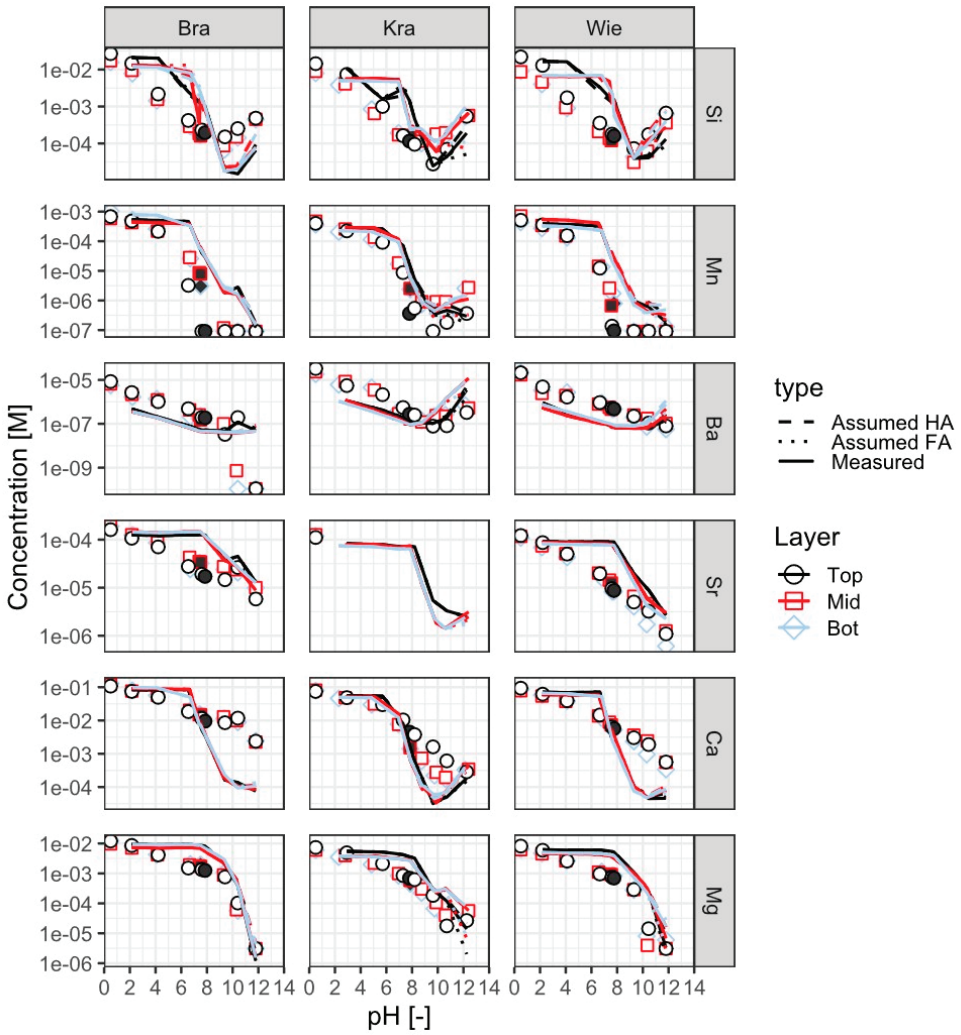


Figure S2.27 (continued)

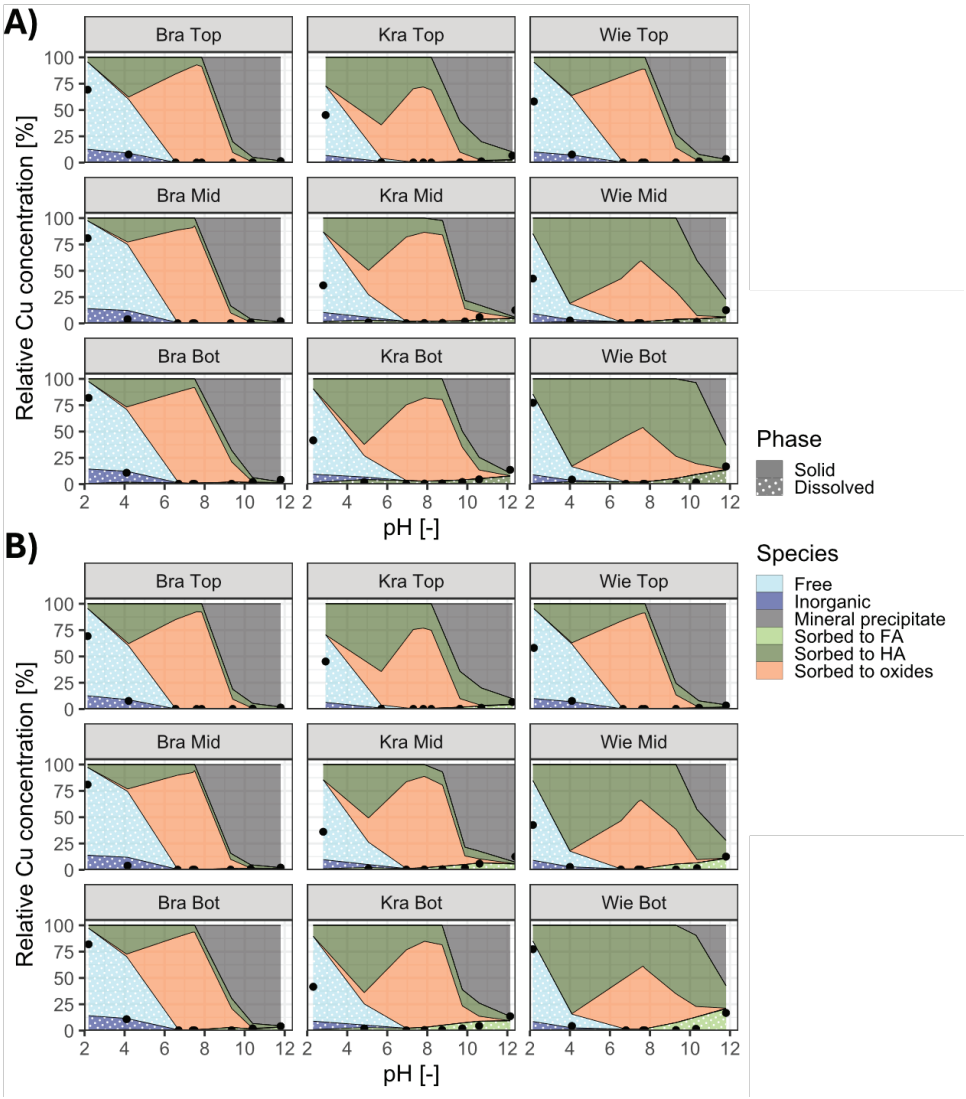


Figure S2.28 Model calculated solid and dissolved phase speciation of copper as a function of pH for all landfills and landfill layers, calculated assuming solid organic matter is 100% humic acid, and dissolved organic matter is A) 50 % humic acid; B) 50% fulvic acid. Shown mineral precipitate is Cu(OH)2.

Supplementary Tables

Table S2.1 Mineral reactions added to the MinteqV4 database in Orchestra format (reactions represent formation reactions and constants).

Reaction equation in ORCHESTRA	Source
@reaction(Analbite, 3.12E-04, -4.0, H+, -4.0, H2O, 1.0, Na+, 1.0, Al+3, 3.0, H4SiO4)	MinteqV1
@reaction(alpha-TCP, 2.45E-14, -4.0, H+, 3.0, Ca+2, 2.0, H2PO4-)	
@reaction(Albite[low], 2.56E-03, -4.0, H+, -4.0, H2O, 1.0, Na+, 1.0, Al+3, 3.0, H4SiO4)	MinteqV1
@reaction(Borax, 3.30E-26, 2.0, Na+, 4.0, H2BO3-, 2.0, H+, 1.0, H2O)	
@reaction(Ca_Vanadate, 1.48E-03, -2.0, H+, 0.5, Ca+2, 1.0, VO2+, 1.0, H2O)	MinteqV1
@reaction(Ca2Zn[PO4]2, 1.32E31, 2.0, Ca+2, 1.0, Zn+2, 2.0, PO4-3)	
@reaction(CaCu2[PO4]2, 5.89E35, 1.0, Ca+2, 2.0, Cu+2, 2.0, PO4-3)	
@reaction(CaZincate, 1.26E-44, -6.0, H+, 1.0, Ca+2, 2.0, Zn+2, 6.0, H2O)	
@reaction(Colemanite, 2.90E-18, 1.0, Ca+2, 3.0, H2BO3-, 1.0, H+, -4.0, H2O)	
@reaction(Diopside, 1.30E-20, -2.0, H2O, -4.0, H+, 1.0, Ca+2, 1.0, Mg+2, 2.0, H4SiO4)	MinteqV1
@reaction(Ettringite, 7.94E44, 6.0, Ca+2, 2.0, Al[OH]4-, 3.0, SO4-2, 4.0, OH-, 26.0, H2O)	
@reaction(Fe_Vanadate, 7.24E01, -2.0, H+, 0.5, Fe+2, 1.0, VO2+, 1.0, H2O)	MinteqV1
@reaction(Fe2[OH]4SeO3, 2.79E-02, -5.0, H+, 1.0, HSeO3-, 2.0, Fe+3, 4.0, H2O)	MinteqV1
@reaction(Franklinite, 1.41E-10, -8.0, H+, 1.0, Zn+2, 2.0, Fe+3, 4.0, H2O)	
@reaction(Illite[1], 6.05E-13, -2.0, H2O, -8.0, H+, 0.6, K+, 0.25, Mg+2, 2.3, Al+3, 3.5, H4SiO4)	
@reaction(Inderite, 1.40E-17, 1.0, Mg+2, 3.0, H2BO3-, 1.0, H+, 1.0, H2O	
@reaction(Inyoite, 2.90E-18, 1.0, Ca+2, 3.0, H2BO3-, 1.0, H+)	
@reaction(Koritnigite, 1.26E-22, 1.0, Zn+2, 1.0, AsO4-3, 1.0, H+, 1.0, H2O)	
@reaction(LDH_Ni, 6.46E-20 , 1.0, Al+3, 0.5, CO3-2, -6.0, H+, 1.0, H2O, 2.0, Ni+2)	
@reaction(LDH_Zn, 1.15e-20 , 1.0, Al+3, 0.5, CO3-2, -6.0, H+, 1.0, H2O, 2.0, Zn+2)	

Table S2.1 Mineral reactions added to the MinteqV4 database in Orchestra format (reactions represent formation reactions and constants). (*continued*)

Reaction equation in ORCHESTRA	Source
@reaction(Leucite, 3.78E-07, -2.0, H2O, -4.0, H+, 2.0, H4SiO4, 1.0, Al+3, 1.0, K+)	MinteqV1
@reaction(McAllisterite, 1.3E-46, 1.0, Mg+2, 6.0, H2BO3-, 4.0, H+, 7.0, H2O)	
@reaction(Nobleite, 1.7E-48, 1.0, Ca+2, 6.0, H2BO3-, 2.0, H+, 10.0, H2O)	
@reaction(PbMoO4[c], 6.30957E+15, 1.0, Pb+2, 1.0, MoO4-2)	
@reaction(Pinnoite, 2.5E-05, 1.0, Mg+2, 2.0, H2BO3-, -1.0, H2O)	
@reaction(Plgummite[2], 6.12E32, -5.0, H+, 1.0, Pb+2, 3.0, Al+3, 2.0, PO4-3, 6.0, H2O)	
@reaction(Struvite, 3.98E-7, -2.0, H+, 1.0, Mg+2, 1.0, NH4+, 1.0, H2PO4-, 6.0, H2O)	(Lindsay, 1979)
@reaction(Talc, 8.81E-24, -4.0, H2O, -6.0, H+, 3.0, Mg+2, 4.0, H4SiO4)	MinteqV1
@reaction(Wairakite, 1.35E-19, -8.0, H+, -2.0, H2O, 1.0, Ca+2, 2.0, Al+3, 4.0, H4SiO4)	MinteqV1
@reaction(Willemite_lindsay, 1.41254E+13, -4.0, H+, 2.0, Zn+2, 1.0, H4SiO4)	
@reaction(ZnSiO3, 1.17E-03, -2.0, H+, -1.0, H2O, 1.0, Zn+2, 1.0, H4SiO4)	MinteqV1

Table S2.2 Considered minerals and altered parameters for each element

Element	Minerals	Parameters
Al	Gibbsite	
As	-	
Ba	barite	
Ca	Calcite, $Ca_4H[PO4]_3$:3 H_2O	
Cd	$Cd[OH]_2$	
Co	-	
Cr	-	
C(Hiemstra & Van Riemsdijk, 2006) (Hiemstra & Van Riemsdijk, 2006), HFO (Appelo et al., 2002)		
K	-	
Li	-	
Mg	Brucite, Magnesite	
Mn	Rhodochrosite, Pyrochroite	
Mo	$PbMoO_4$	HFO (Gustafsson, 2003)
NH_4^+	-	
Ni	-	
Pb	$PbMoO_4$, $Pb[OH]_2$	HA & FA (Xiong et al., 2013), HFO (Meima & Comans, 1998a)
PO4	$Ca_4H[PO4]_3$:3 H_2O	
Sb	-	HFO (Meima & Comans, 1998b)
Si	Sepiolite, Wairakite	
Sn	-	
Sr	Strontianite	
SO4	-	
V	-	No formation of V(V) species (Dijkstra et al., 2009)
Zn	Willemite	



Supplementary information chapter 3

Chromium(III) Binding to Purified Fulvic and Humic Acid and its Solid Solution Partitioning and Speciation in Soil

SM3.1 Introduction of first hydroxy and dimeric Cr complex binding in ORCHESTRA

For scenario's 2 and 3 as described in the 'Optimization of NICA-Donnan parameters for HA and FA' section in the materials & methods, the first Cr-hydroxy species ($CrOH^{2+}$) and a dimeric Cr complex ($Cr_2(OH)_2^{4+}$) were introduced besides Cr^{3+} to calculate Cr binding to HS. $CrOH^{2+}$ is already defined within ORCHESTRA; inclusion solely required the formulation of two NICA species in the ORCHESTRA chemistry file: FA/HA1-CrOH and FA/HA2-CrOH, with the following definitions:

@nicaspecies(FA1-CrOH, FA1, Cr[OH]+2_FA_don, $n_{Cr1\ hyd}$, n_{h1}, $K_{Cr1\ hyd}$)

@nicaspecies(FA2-CrOH, FA1, Cr[OH]+2_FA_don, $n_{Cr2\ hyd}$, n_{h2}, $K_{Cr2\ hyd}$)

This also results in four additional parameters which are to be fitted: $n_{Cr1\ hyd}$, $n_{Cr2,\ hyd}$, $K_{Cr1\ hyd}$, and $K_{Cr2\ hyd}$.

Incorporation of $Cr_2(OH)_2^{4+}$ binding in ORCHESTRA first requires a definition of the species, as this is currently absent. Based on the information listed by Gustafsson et al. (2014), the following reaction was considered:

$$Cr_2(OH)_2^{4+} + 2\ H^+ \leftrightarrow 2\ Cr^{3+} + 2\ H_2O \qquad \text{Log K = -5}$$

This reaction was defined in the chemistry file in the following fashion:

@species(Cr2[OH]2+4, 4)

@reaction(Cr2[OH]2+4, 1.0E-5, 2.0, Cr+3, -2.0, H+, 2.0, H2O)

Following the species definition, incorporation into ORCHESTRA requires definition of a Donnan species and subsequently definition of the NICA species FA/HA1-Cr2[OH]2+4 and FA/HA2- Cr2[OH]2+4 similar to $Cr(OH)^{2+}$:

@donnanspecies(Cr2[OH]2+4_FA_don, FA_don, Cr2[OH]2+4, 4)

@nicaspecies(FA1- Cr2[OH]2+4, FA1, Cr2[OH]2+4 _FA_don, $n_{Cr1\ dim}$, n_{h1}, $K_{Cr1\ hyd}$)

@nicaspecies(FA2- Cr2[OH]2+4, FA1, Cr2[OH]2+4 _FA_don, $n_{Cr2\ hyd}$, n_{h2}, $K_{Cr2\ hyd}$)

Further incorporation is similar to the introduction of first hydroxy binding.

Supplementary Tables

Table S3.1 *Experimental conditions of the titration experiment with Suwannee river fulvic acid. SRFA concentration = 1002 mg L^{-1} (pH 3) or 334 mg L^{-1} (pH 4 & 5). Negative concentrations are set to 1E-20 in the modelling; sodium, calcium, and nitrate were assumed.* [a]based on an experimental concentration of 30 mM $NaNO_3$;[b]based on an experimental concentration of 2 mM $Ca(NO_3)_2$; [c]Based on an experimental concentration of 30 mM $NaNO_3$, 2 mM $Ca(NO_3)_2$, and a varying concentration of $Cr(NO_3)_3$.

Intended pH	Intended Cr	pH donor	pH acceptor	Cr donor	Cr acceptor	Assumed Na[a]	Assumed Ca[b]	Assumed NO3[c]
	[M]	[-]	[-]	[M]	[M]	[M]	[M]	[M]
3	1.00E-07	2.99	3.05	1.03E-07	1.35E-08	3.00E-02	2.00E-03	3.40E-02
		3.03	3.06	1.02E-07	1.44E-08	3.00E-02	2.00E-03	3.40E-02
	3.00E-07	3.02	3.03	2.44E-07	3.26E-08	3.00E-02	2.00E-03	3.40E-02
		3.01	3	2.37E-07	3.58E-08	3.00E-02	2.00E-03	3.40E-02
	1.00E-06	3.05	3.05	7.50E-07	1.05E-07	3.00E-02	2.00E-03	3.40E-02
		3.05	3.04	7.37E-07	1.08E-07	3.00E-02	2.00E-03	3.40E-02
	5.00E-06	3.02	3.02	3.53E-06	5.18E-07	3.00E-02	2.00E-03	3.40E-02
		3.03	3.01	3.47E-06	5.42E-07	3.00E-02	2.00E-03	3.40E-02
	5.00E-05	3.05	3.08	3.87E-05	7.86E-06	3.00E-02	2.00E-03	3.41E-02
		3.05	3.06	3.87E-05	8.34E-06	3.00E-02	2.00E-03	3.41E-02
	5.00E-04	2.99	3.01	4.36E-04	1.52E-04	3.00E-02	2.00E-03	3.53E-02
		3	3.01	4.36E-04	1.78E-04	3.00E-02	2.00E-03	3.53E-02
	5.00E-03	2.97	3.05	4.99E-03	1.91E-03	3.00E-02	2.00E-03	4.90E-02
		2.94	3.05	4.99E-03	1.95E-03	3.00E-02	2.00E-03	4.90E-02
4	5.00E-08	4.03	4.05	4.62E-08	2.33E-09	3.00E-02	2.00E-03	3.40E-02
		4.02	4.03	5.00E-08	-4.87E-09	3.00E-02	2.00E-03	3.40E-02
	1.00E-07	4.02	3.98	8.65E-08	5.29E-09	3.00E-02	2.00E-03	3.40E-02
		4.03	4	8.46E-08	5.08E-09	3.00E-02	2.00E-03	3.40E-02
	5.00E-07	4.05	4.02	4.38E-07	3.07E-08	3.00E-02	2.00E-03	3.40E-02
		4.04	4.02	4.27E-07	3.43E-08	3.00E-02	2.00E-03	3.40E-02
	1.00E-06	4.01	3.99	8.48E-07	6.20E-08	3.00E-02	2.00E-03	3.40E-02
		3.99	3.99	8.32E-07	6.60E-08	3.00E-02	2.00E-03	3.40E-02
	5.00E-06	4.04	4.04	4.70E-06	4.57E-07	3.00E-02	2.00E-03	3.40E-02
		4.03	4.05	4.65E-06	5.08E-07	3.00E-02	2.00E-03	3.40E-02
	1.00E-05	4.02	4.01	9.39E-06	9.18E-07	3.00E-02	2.00E-03	3.40E-02
		4.01	4.01	9.17E-06	9.99E-07	3.00E-02	2.00E-03	3.40E-02
	5.00E-05	3.97	4	4.81E-05	6.96E-06	3.00E-02	2.00E-03	3.41E-02
		3.99	4	4.78E-05	7.82E-06	3.00E-02	2.00E-03	3.41E-02
	5.00E-04	3.89	3.91	4.11E-04	1.48E-04	3.00E-02	2.00E-03	3.52E-02
		3.89	3.91	4.20E-04	1.72E-04	3.00E-02	2.00E-03	3.53E-02
5	1.00E-07	5.03	5.04	9.52E-08	2.54E-09	3.00E-02	2.00E-03	3.40E-02
		5.04	5.06	9.33E-08	1.27E-09	3.00E-02	2.00E-03	3.40E-02
	5.00E-07	5.01	4.96	4.38E-07	8.04E-09	3.00E-02	2.00E-03	3.40E-02
		5.03	5.01	4.44E-07	6.77E-09	3.00E-02	2.00E-03	3.40E-02
	1.00E-06	5.01	4.98	8.79E-07	1.63E-08	3.00E-02	2.00E-03	3.40E-02
		5.02	5.02	8.87E-07	1.52E-08	3.00E-02	2.00E-03	3.40E-02
	5.00E-06	4.97	4.96	4.20E-06	8.91E-08	3.00E-02	2.00E-03	3.40E-02
		4.97	4.96	4.17E-06	8.34E-08	3.00E-02	2.00E-03	3.40E-02
	1.00E-05	5.01	4.98	9.68E-06	2.20E-07	3.00E-02	2.00E-03	3.40E-02
		5.03	5.02	9.60E-06	2.08E-07	3.00E-02	2.00E-03	3.40E-02
	5.00E-05	5.04	5.03	4.89E-05	1.06E-06	3.00E-02	2.00E-03	3.41E-02
		5.05	5.06	4.89E-05	9.88E-07	3.00E-02	2.00E-03	3.41E-02
	1.00E-04	5.04	5.05	1.02E-04	1.71E-06	3.00E-02	2.00E-03	3.43E-02
		5.04	5.05	1.00E-04	1.58E-06	3.00E-02	2.00E-03	3.43E-02

Table S3.2 Experimental conditions of the titration experiment with Tongbersven Humic Acid. THA concentration = 167 mg L-1. Negative concentrations are set to 1E-20 in the modelling; chloride and nitrate were assumed. aBased on an experimental concentration of 2 mM CaCl2; aBased on an experimental concentration of 30 mM NaNO3 and a varying concentration of Cr(NO3)3.

Intended pH	Intended Cr	pH donor	pH acceptor	Cr donor	Cr acceptor	Na donor	Na acceptor	Ca donor	Ca acceptor	Assumed Cl^a	Assumed NO_3^b
	[M]	[-]	[-]	[M]	[M]	[M]	[M]	[M]	[M]	[M]	[M]
3	3.00E-07	3.22	3.13	1.15E-07	7.17E-08	3.11E-02	2.77E-02	2.04E-03	1.80E-03	4.00E-03	3.00E-02
		3.25	3.08	1.54E-07	8.84E-08	3.12E-02	2.88E-02	2.04E-03	1.90E-03	4.00E-03	3.00E-02
	5.00E-07	3.21	3.29	2.12E-07	7.64E-08	3.07E-02	2.80E-02	2.06E-03	1.83E-03	4.00E-03	3.00E-02
		3.11	3.12	2.69E-07	9.88E-08	3.09E-02	2.76E-02	2.04E-03	1.87E-03	4.00E-03	3.00E-02
	7.00E-07	3.09	3.09	3.85E-07	1.34E-07	3.17E-02	2.87E-02	2.10E-03	1.83E-03	4.00E-03	3.00E-02
		3.03	3.03	4.04E-07	1.64E-07	3.15E-02	2.83E-02	2.09E-03	1.80E-03	4.00E-03	3.00E-02
	4.50E-06	3.17	3.17	2.63E-06	8.99E-07	3.09E-02	2.82E-02	2.09E-03	1.85E-03	4.00E-03	3.00E-02
		3.1	3.11	2.67E-06	8.29E-07	3.14E-02	2.77E-02	2.11E-03	1.78E-03	4.00E-03	3.00E-02
	9.00E-06	3.23	3.28	2.40E-05	3.28E-06	3.11E-02	2.80E-02	2.07E-03	1.80E-03	4.00E-03	3.00E-02
		3.13	3.2	5.19E-06	1.98E-06	3.19E-02	2.81E-02	2.11E-03	1.78E-03	4.00E-03	3.00E-02
	9.50E-05	3.17	3.13	6.63E-05	3.18E-05	3.12E-02	2.77E-02	2.07E-03	1.84E-03	4.00E-03	3.03E-02
		3.04	3.07	7.33E-05	3.56E-05	3.18E-02	2.78E-02	2.14E-03	1.80E-03	4.00E-03	3.03E-02
	4.90E-04	3.14	3.11	4.56E-04	3.09E-04	3.11E-02	2.90E-02	2.17E-03	2.07E-03	4.00E-03	3.15E-02
		3.03	3.07	4.69E-04	2.78E-04	3.10E-02	2.77E-02	2.18E-03	1.86E-03	4.00E-03	3.15E-02
	2.90E-03	3.03	3.08	3.21E-03	1.91E-03	3.05E-02	2.44E-02	2.19E-03	1.56E-03	4.00E-03	3.87E-02
		2.96	3.01	3.33E-03	1.62E-03	3.10E-02	2.40E-02	2.20E-03	1.61E-03	4.00E-03	3.87E-02
4.5	7.60E-07	5.03	4.75	1.92E-07	3.58E-08	3.11E-02	2.83E-02	2.04E-03	1.83E-03	4.00E-03	3.00E-02
		5.31	5.27	2.12E-07	3.22E-08	3.19E-02	2.88E-02	2.04E-03	1.78E-03	4.00E-03	3.00E-02
	1.02E-06	4.37	4.34	4.42E-07	1.38E-08	3.13E-02	2.84E-02	2.05E-03	1.80E-03	4.00E-03	3.00E-02
		4.39	4.41	4.42E-07	1.12E-08	3.20E-02	2.87E-02	2.08E-03	1.75E-03	4.00E-03	3.00E-02
	4.26E-06	4.5	4.48	1.92E-06	1.26E-07	3.19E-02	2.88E-02	2.08E-03	1.78E-03	4.00E-03	3.00E-02
		4.42	4.4	1.87E-06	1.26E-07	3.22E-02	3.02E-02	2.06E-03	1.88E-03	4.00E-03	3.00E-02
	9.00E-06	4.6	4.56	4.29E-06	2.79E-07	3.10E-02	2.86E-02	2.07E-03	1.85E-03	4.00E-03	3.00E-02
		4.63	4.53	4.35E-06	1.69E-07	3.12E-02	2.93E-02	2.06E-03	1.85E-03	4.00E-03	3.00E-02
	4.50E-05	4.7	4.87	2.04E-05	4.06E-06	3.17E-02	2.91E-02	2.05E-03	1.87E-03	4.00E-03	3.00E-02

Table S3.2 Experimental conditions of the titration experiment with Tongbersven Humic Acid. THA concentration = 167 mg L-1. Negative concentrations are set to 1E-20 in the modelling; chloride and nitrate were assumed. aBased on an experimental concentration of 2 mM CaCl2; aBased on an experimental concentration of 30 mM NaNO3 and a varying concentration of Cr(NO3)3. (*continued*)

Intended pH	Intended Cr	pH donor	pH acceptor	Cr donor	Cr acceptor	Na donor	Na acceptor	Ca donor	Ca acceptor	Assumed Cl[a]	Assumed NO_3[b]
		4.75	5.07	1.96E-05	2.22E-06	3.17E-02	2.91E-02	2.03E-03	1.81E-03	4.00E-03	3.00E-02
	9.00E-05	4.2	4.2	4.00E-05	1.27E-05	3.13E-02	2.93E-02	2.08E-03	1.88E-03	4.00E-03	3.01E-02
		4.3	4.3	4.13E-05	6.68E-06	3.23E-02	2.95E-02	2.07E-03	1.86E-03	4.00E-03	3.01E-02
	4.50E-04	4.29	4.2	3.48E-04	1.43E-04	3.16E-02	2.83E-02	2.12E-03	1.88E-03	4.00E-03	3.03E-02
		4.33	4.25	3.19E-04	1.32E-04	3.20E-02	2.87E-02	2.12E-03	1.84E-03	4.00E-03	3.03E-02
	2.90E-03	4.08	3.93	2.87E-03	5.43E-04	3.33E-02	2.74E-02	2.06E-03	1.84E-03	4.00E-03	3.14E-02
		4.1	3.95	2.90E-03	5.46E-04	3.35E-02	2.72E-02	2.03E-03	1.79E-03	4.00E-03	3.14E-02
6	2.26E-06	6.54	7.1	4.81E-07	3.09E-08	3.22E-02	3.11E-02	2.03E-03	1.83E-03	4.00E-03	3.87E-02
		6.42	7.08	4.81E-07	3.38E-08	3.17E-02	2.89E-02	2.02E-03	1.70E-03	4.00E-03	3.87E-02
	4.52E-06	5.72	5.31	1.42E-06	8.04E-09	3.27E-02	2.83E-02	2.07E-03	1.63E-03	4.00E-03	3.00E-02
		6.02	6.1	1.44E-06	3.79E-07	3.21E-02	2.91E-02	2.04E-03	1.70E-03	4.00E-03	3.00E-02
	7.76E-06	6.63	6.06	2.60E-06	9.10E-09	3.17E-02	2.90E-02	2.05E-03	1.68E-03	4.00E-03	3.00E-02
		6.48	6.04	2.65E-06	1.04E-08	3.15E-02	2.90E-02	2.05E-03	1.73E-03	4.00E-03	3.00E-02
	4.55E-05	6.22	6.01	1.42E-05	3.28E-08	3.20E-02	2.90E-02	2.05E-03	1.73E-03	4.00E-03	3.00E-02
		6.17	5.89	1.43E-05	4.27E-08	3.12E-02	2.96E-02	2.04E-03	1.80E-03	4.00E-03	3.00E-02
	9.00E-05	6.05	6.06	2.04E-05	3.49E-07	3.23E-02	2.87E-02	2.03E-03	1.70E-03	4.00E-03	3.00E-02
		6.07	6.13	2.50E-05	3.62E-07	3.21E-02	2.93E-02	2.00E-03	1.75E-03	4.00E-03	3.00E-02
	4.50E-04	5.32	5.11	2.44E-04	9.46E-06	3.30E-02	2.90E-02	2.07E-03	1.69E-03	4.00E-03	3.01E-02
		5.55	5.26	2.60E-04	8.82E-06	3.26E-02	2.94E-02	2.03E-03	1.75E-03	4.00E-03	3.01E-02
	9.00E-04	5.85	5.12	7.38E-04	1.19E-06	3.38E-02	2.98E-02	2.02E-03	1.58E-03	4.00E-03	3.03E-02
		6.18	5.3	7.67E-04	1.13E-06	3.35E-02	2.97E-02	1.99E-03	1.63E-03	4.00E-03	3.03E-02
	4.50E-03	5.74	4.93	3.75E-03	4.42E-06	4.01E-02	3.07E-02	1.75E-03	1.12E-03	4.00E-03	3.14E-02
		5.59	5.09	3.73E-03	6.02E-06	3.98E-02	3.03E-02	1.74E-03	1.13E-03	4.00E-03	3.14E-02

Table S3.3 NICA-Donnan parameters used for the optimization of Cr parameters with generic HA, tongbersven HA, generic FA, and Suwannee river FA.

	Generic1 HA	Specific2 HA	Generic1 FA	Specific3 FA
adon	-	-	-	-
bdon	0.49	0.3	0.57	0.77
Qmax 1,H	3.15	2.3	5.88	5.36
p1	0.62	0.68	0.59	0.59
log K1, H	2.93	2.21	2.34	3.06
N1, H	0.81	0.78	0.66	0.73
log K1, Ca	-1.37	-3.86	-2.13	-2.13
N1, Ca	0.78	0.55	0.85	0.85
Qmax 2,H	2.55	3.92	1.86	3.08
p2	0.41	0.28	0.7	0.7
log K2,H	8	8.98	8.6	8.6
N2,H	0.63	0.61	0.76	0.83
log K2,Ca	-0.43	1.52	-3	-3
N2, Ca	0.75	0.79	0.8	0.8

1 - (Milne et al., 2003) Table 3

2 - (Kalis et al., 2006) Table S-3

3 - (Milne et al., 2001) Table 2 + 4 (FH-15)

Table S3.4 Inorganic chromium(III) equilibrium reactions used, as listed in the MINTEQV4 database.

Equation	Log K
$Cr^{3+} + H_2O \leftrightarrow CrOH^{2+} + H^+$	-3.66
$Cr^{3+} + 2\ H_2O \leftrightarrow Cr(OH)_2^+ + 2\ H^+$	-9.57
$Cr^{3+} + 3\ H_2O \leftrightarrow Cr(OH)_3^o + 3\ H^+$	-17.99
$Cr^{3+} + 4\ H_2O \leftrightarrow Cr(OH)_4^- + 4\ H^+$	-27.39
$2\ Cr^{3+} + 2\ H_2O \leftrightarrow Cr_2(OH)_2^{4+} + 2\ H^+$	-5

Table S3.5 Data of the chromium-humic acid binding experiment conducted by Fukushima et al. (1995) and used in this study to validate the newly optimized Cr parameters.

pH	DHA	Total Cr	Cl	Na	Formate	Bound Cr
[-]	[kg/l]	[M]	[M]	[M]	[M]	[M]
4.3	4.00E-05	4.99E-05	1.50E-04	1.00E-02	1.00E-02	3.50E-05
4.3	4.00E-05	4.37E-05	1.31E-04	1.00E-02	1.00E-02	3.31E-05
4.3	4.00E-05	3.88E-05	1.16E-04	1.00E-02	1.00E-02	3.09E-05
4.3	4.00E-05	3.49E-05	1.05E-04	1.00E-02	1.00E-02	2.77E-05
4.3	4.00E-05	2.98E-05	8.94E-05	1.00E-02	1.00E-02	2.46E-05
4.3	4.00E-05	2.51E-05	7.53E-05	1.00E-02	1.00E-02	2.11E-05
4.3	4.00E-05	2.04E-05	6.11E-05	1.00E-02	1.00E-02	1.71E-05
4.3	4.00E-05	1.52E-05	4.57E-05	1.00E-02	1.00E-02	1.30E-05
4.3	4.00E-05	6.22E-06	1.87E-05	1.00E-02	1.00E-02	5.12E-06
4.3	4.00E-05	2.79E-06	8.37E-06	1.00E-02	1.00E-02	2.78E-06
3.25	4.00E-05	4.94E-05	1.48E-04	1.00E-02	1.00E-02	8.12E-06
3.25	4.00E-05	4.45E-05	1.34E-04	1.00E-02	1.00E-02	7.72E-06
3.25	4.00E-05	3.64E-05	1.09E-04	1.00E-02	1.00E-02	6.90E-06
3.25	4.00E-05	3.13E-05	9.39E-05	1.00E-02	1.00E-02	6.06E-06
3.25	4.00E-05	2.49E-05	7.47E-05	1.00E-02	1.00E-02	4.59E-06
3.25	4.00E-05	2.09E-05	6.26E-05	1.00E-02	1.00E-02	5.04E-06
3.25	4.00E-05	1.58E-05	4.73E-05	1.00E-02	1.00E-02	3.99E-06
3.25	4.00E-05	1.09E-05	3.26E-05	1.00E-02	1.00E-02	2.52E-06
3.25	4.00E-05	4.68E-06	1.41E-05	1.00E-02	1.00E-02	8.35E-07
3.48	4.00E-05	5.01E-05	1.50E-04	1.00E-02	1.00E-02	1.57E-05
3.48	4.00E-05	4.00E-05	1.20E-04	1.00E-02	1.00E-02	1.46E-05
3.48	4.00E-05	3.06E-05	9.18E-05	1.00E-02	1.00E-02	1.25E-05
3.48	4.00E-05	2.10E-05	6.29E-05	1.00E-02	1.00E-02	1.00E-05
3.48	4.00E-05	1.07E-05	3.21E-05	1.00E-02	1.00E-02	5.96E-06
3.79	4.00E-05	5.01E-05	1.50E-04	1.00E-02	1.00E-02	1.89E-05
3.79	4.00E-05	4.11E-05	1.23E-04	1.00E-02	1.00E-02	1.70E-05
3.79	4.00E-05	3.13E-05	9.40E-05	1.00E-02	1.00E-02	1.49E-05
3.79	4.00E-05	2.09E-05	6.27E-05	1.00E-02	1.00E-02	1.17E-05
3.79	4.00E-05	1.09E-05	3.26E-05	1.00E-02	1.00E-02	6.82E-06
3.79	4.00E-05	6.19E-06	1.86E-05	1.00E-02	1.00E-02	3.84E-06

Table S3.6 pH, organic matter, and chromium data presented in Koopmans & Groenenberg (2011) and used in this study to validate the newly optimized Cr parameters.

Sample #	pH	DFA	DHA	Dissolved Cr	Free Cr
	[-]	[kg/l]	[kg/l]	[M]	[M]
1	5.06	1.52E-05	6.57E-07	3.31E-06	2.70E-09
2	5.1	1.64E-05	7.09E-07	3.38E-06	2.72E-09
3	4.46	7.91E-06	4.38E-07	2.75E-06	1.98E-08
4	4.43	7.15E-06	3.96E-07	2.65E-06	2.04E-08
5	5.53	1.39E-05	6.46E-07	1.55E-06	1.65E-10
6	5.65	1.33E-05	6.19E-07	1.53E-06	2.08E-10
7	4.52	3.58E-06	5.19E-07	1.21E-06	7.94E-09
8	4.6	3.12E-06	4.53E-07	1.13E-06	7.59E-09
9	5.27	1.54E-05	6.65E-07	2.52E-06	2.11E-09
10	5.19	1.69E-05	7.30E-07	2.56E-06	1.94E-09
11	4.57	8.28E-06	4.59E-07	2.31E-06	1.59E-08
12	4.58	7.36E-06	4.08E-07	2.29E-06	1.71E-08
13	5.66	1.42E-05	6.63E-07	1.26E-06	1.32E-10
14	5.72	1.37E-05	6.38E-07	1.24E-06	1.56E-10
15	4.76	3.68E-06	5.33E-07	1.04E-06	9.19E-09
16	4.66	3.22E-06	4.66E-07	9.65E-07	6.58E-09
17	4.64	4.74E-06	2.44E-07	2.29E-06	2.23E-09
18	4.64	4.56E-06	2.35E-07	2.17E-06	3.05E-09
19	4.21	8.31E-07	0.00E+00	1.55E-06	1.07E-08
20	4.2	8.48E-07	0.00E+00	1.43E-06	1.18E-08
21	5.18	8.17E-06	5.69E-07	1.15E-06	
22	5.16	8.44E-06	5.87E-07	1.29E-06	5.63E-10
23	4.38	1.66E-06	2.00E-07	6.23E-07	4.85E-09
24	4.35	1.96E-06	2.36E-07	6.44E-07	4.15E-09
25	4.87	4.56E-06	2.35E-07	1.96E-06	2.31E-09
26	4.87	4.69E-06	2.42E-07	1.92E-06	2.04E-09
27	4.46	8.61E-07	0.00E+00	1.32E-06	1.03E-08
28	4.43	9.02E-07	0.00E+00	1.25E-06	1.18E-08
29	5.36	8.92E-06	6.21E-07	1.11E-06	1.04E-09
30	4.55	2.05E-06	2.47E-07	6.06E-07	3.96E-09
31	4.53	2.00E-06	2.40E-07	6.29E-07	3.38E-09

Table S3.7 Dissolved concentrations of competing elements presented in Koopmans & Groenenberg (2011) and used in this study to validate the newly optimized Cr parameters.

Sample #	Na	Mg	Al	K	Ca	Mn	Fe	Ni	Cu	Zn	Cd	Cl	NO3-	PO4-3
	[M]	[M]	[M]	[M]	[M]	[M]	[M]	[M]	[M]	[M]	[M]	[M]	[M]	[M]
1	1.00E-03	1.34E-04	1.89E-05	1.48E-04	1.75E-03	1.95E-05	4.12E-06	7.55E-06	7.24E-07	3.61E-05	5.29E-08	1.00E-20	4.00E-03	7.41E-05
2	9.74E-04	1.38E-04	1.89E-05	1.59E-04	1.69E-03	1.97E-05	4.17E-06	7.60E-06	7.55E-07	3.64E-05	5.54E-08	1.00E-20	4.00E-03	7.44E-05
3	9.78E-04	8.39E-05	1.59E-05	1.97E-04	1.55E-03	1.05E-05	8.88E-06	4.04E-06	3.93E-07	1.62E-05	5.17E-08	1.00E-20	4.00E-03	1.05E-04
4	9.87E-04	8.02E-05	1.56E-05	1.89E-04	1.57E-03	1.02E-05	9.37E-06	3.94E-06	3.78E-07	1.57E-05	4.98E-08	1.00E-20	4.00E-03	1.03E-04
5	1.01E-03	1.70E-04	1.33E-05	1.48E-04	1.78E-03	1.01E-05	2.81E-06	1.35E-06	1.26E-07	7.83E-06	9.96E-09	1.00E-20	4.00E-03	3.61E-05
6	1.03E-03	1.70E-04	1.41E-05	1.43E-04	1.86E-03	1.04E-05	2.95E-06	1.37E-06	1.26E-07	8.24E-06	1.15E-08	1.00E-20	4.00E-03	3.47E-05
7	9.96E-04	4.90E-05	1.04E-05	5.88E-05	1.58E-03	3.79E-06	9.47E-06	1.32E-06	4.72E-08	4.04E-06	1.14E-08	1.00E-20	4.00E-03	4.62E-05
8	1.02E-03	4.57E-05	8.89E-06	5.37E-05	1.61E-03	3.49E-06	8.33E-06	9.97E-07	4.72E-08	3.70E-06	1.12E-08	1.00E-20	4.00E-03	4.19E-05
9	1.02E-03	1.31E-04	1.63E-05	1.51E-04	1.77E-03	1.89E-05	3.21E-06	7.33E-06	6.85E-07	3.49E-05	5.12E-08	1.00E-20	4.00E-03	7.41E-05
10	9.83E-04	1.34E-04	1.67E-05	1.53E-04	1.69E-03	1.89E-05	3.55E-06	7.29E-06	6.18E-07	3.46E-05	1.98E-08	1.00E-20	4.00E-03	7.44E-05
11	6.65E-04	5.43E-05	1.41E-05	1.30E-04	1.06E-03	1.02E-05	7.70E-06	3.92E-06	3.90E-07	1.56E-05	4.79E-08	1.00E-20	4.00E-03	1.05E-04
12	9.96E-04	7.78E-05	1.45E-05	1.87E-04	1.59E-03	9.96E-06	8.45E-06	3.85E-06	4.30E-07	1.54E-05	4.70E-08	1.00E-20	4.00E-03	1.03E-04
13	1.01E-03	1.65E-04	1.11E-05	1.48E-04	1.80E-03	9.85E-06	2.20E-06	1.35E-06	1.94E-07	7.67E-06	1.01E-08	1.00E-20	4.00E-03	3.61E-05
14	1.04E-03	1.64E-04	1.07E-05	1.38E-04	1.87E-03	1.01E-05	2.20E-06	1.36E-06	1.83E-07	8.01E-06	9.52E-09	1.00E-20	4.00E-03	3.47E-05
15	1.01E-03	4.77E-05	9.27E-06	5.88E-05	1.62E-03	3.68E-06	8.20E-06	1.34E-06	9.62E-08	3.96E-06	1.06E-08	1.00E-20	4.00E-03	4.62E-05
16	8.17E-04	3.46E-05	7.78E-06	4.09E-05	1.31E-03	3.39E-06	7.00E-06	9.75E-07	8.95E-08	3.65E-06	9.79E-09	1.00E-20	4.00E-03	4.19E-05
17	9.35E-04	1.16E-04	1.30E-05	1.20E-04	1.59E-03	1.77E-05	3.21E-06	6.13E-06	4.56E-07	3.33E-05	5.11E-08	1.00E-20	4.00E-03	4.67E-05
18	9.48E-04	1.17E-04	1.22E-05	1.23E-04	1.62E-03	1.75E-05	3.08E-06	6.13E-06	4.41E-07	3.35E-05	5.07E-08	1.00E-20	4.00E-03	4.54E-05
19	9.65E-04	7.32E-05	1.11E-05	1.87E-04	1.46E-03	9.90E-06	7.27E-06	3.24E-06	2.99E-07	1.37E-05	4.54E-08	1.00E-20	4.00E-03	6.29E-05
20	9.87E-04	7.49E-05	1.11E-05	1.89E-04	1.53E-03	9.96E-06	7.65E-06	3.36E-06	2.83E-07	1.39E-05	4.63E-08	1.00E-20	4.00E-03	6.12E-05

Table S3.7 Dissolved concentrations of competing elements presented in Koopmans & Groenenberg (2011) and used in this study to validate the newly optimized Cr parameters. *(continued)*

Sample #	Na	Mg	Al	K	Ca	Mn	Fe	Ni	Cu	Zn	Cd	Cl	NO3-	PO4-3
	[M]	[M]	[M]	[M]	[M]	[M]	[M]	[M]	[M]	[M]	[M]	[M]	[M]	[M]
21	9.96E-04	1.60E-04	1.11E-05	1.28E-04	1.77E-03	1.12E-05	2.85E-06	9.95E-07	1.42E-07	7.48E-06	9.96E-09	1.00E-20	4.00E-03	1.70E-05
22	1.01E-03	1.60E-04	1.33E-05	1.36E-04	1.74E-03	1.04E-05	3.26E-06	1.02E-06	1.57E-07	7.57E-06	1.13E-08	1.00E-20	4.00E-03	1.88E-05
23	9.96E-04	4.48E-05	7.04E-06	5.88E-05	1.64E-03	4.08E-06	8.60E-06	8.59E-07	6.29E-08	3.39E-06	9.79E-09	1.00E-20	4.00E-03	2.46E-05
24	1.00E-03	4.40E-05	7.41E-06	5.12E-05	1.61E-03	4.06E-06	8.88E-06	8.54E-07	6.29E-08	3.35E-06	9.79E-09	1.00E-20	4.00E-03	2.50E-05
25	9.44E-04	1.12E-04	1.26E-05	1.20E-04	1.61E-03	1.72E-05	2.99E-06	5.98E-06	2.82E-07	3.24E-05	4.02E-08	1.00E-20	4.00E-03	4.67E-05
26	9.52E-04	1.13E-04	1.26E-05	1.20E-04	1.64E-03	1.72E-05	2.88E-06	6.03E-06	3.30E-07	3.29E-05	5.06E-08	1.00E-20	4.00E-03	4.54E-05
27	9.61E-04	7.08E-05	1.00E-05	1.79E-04	1.49E-03	9.72E-06	5.98E-06	3.19E-06	1.94E-07	1.33E-05	4.18E-08	1.00E-20	4.00E-03	6.29E-05
28	9.83E-04	7.20E-05	1.00E-05	1.87E-04	1.55E-03	9.81E-06	6.11E-06	3.29E-06	2.03E-07	1.35E-05	4.53E-08	1.00E-20	4.00E-03	6.12E-05
29	1.01E-03	1.56E-04	1.33E-05	1.25E-04	1.76E-03	1.03E-05	3.26E-06	1.02E-06	1.21E-07	7.43E-06	1.10E-08	1.00E-20	4.00E-03	1.88E-05
30	9.96E-04	4.36E-05	7.04E-06	5.63E-05	1.67E-03	4.06E-06	7.97E-06	8.59E-07	5.57E-08	3.32E-06	1.01E-08	1.00E-20	4.00E-03	2.46E-05
31	9.96E-04	4.32E-05	7.41E-06	4.86E-05	1.63E-03	3.99E-06	8.24E-06	8.31E-07	6.23E-08	3.24E-06	9.87E-09	1.00E-20	4.00E-03	2.50E-05

Table S3.8 Soil data and dissolved phase concentrations measured in calcium chloride (CaCl2), pore water (PW), and acidified pore water (PW acid) extracts as listed in Groenenberg et al. (2012) and used in this study to validate the newly optimized Cr parameters.

Type	Depth	pH	DFA_kgl	DHA_ kgl	SFA_ kgkg	SHA_ kgkg	CLAY_ kgkg	HFO_ kgkg	Tot-Cr
	[cm - surface]	[-]	[kg l^{-1}]	[kg l^{-1}]	[kg kg^{-1}]	[kg kg^{-1}]	[kg kg^{-1}]	[kg kg^{-1}]	[M]
CaCl2	0 - 10	4.67	6.60E-07	2.22E-06	1.14E-03	4.57E-02	2.00E-02	1.04E-02	7.12E-04
CaCl2	20 - 30	4.67	1.84E-06	2.27E-06	7.55E-04	3.32E-02	2.00E-02	9.42E-03	5.64E-04
CaCl2	40 - 50	4.99	1.51E-06	1.03E-06	2.98E-04	9.22E-03	2.00E-02	4.16E-03	1.08E-04
CaCl2	70 -80	5.39	0.00E+00	3.99E-07	1.23E-04	1.93E-03	2.00E-02	3.27E-03	1.90E-05
CaCl2	100 - 110	5.68	0.00E+00	8.07E-07	1.18E-04	1.39E-03	2.00E-02	3.99E-03	6.47E-06
CaCl2	140 - 150	5.82	0.00E+00	1.34E-06	6.69E-05	1.56E-03	1.30E-01	4.34E-03	2.85E-06
PW	0 - 10	5.34	9.23E-05	3.58E-05	1.14E-03	4.57E-02	2.00E-02	1.04E-02	1.07E-02
PW	20 - 30	4.96	5.78E-05	1.92E-05	7.55E-04	3.32E-02	2.00E-02	9.42E-03	1.31E-02
PW	40 - 50	5.08	4.27E-05	1.05E-05	2.98E-04	9.22E-03	2.00E-02	4.16E-03	4.30E-03
PW	70 -80	5.79	3.30E-05	1.08E-05	1.23E-04	1.93E-03	2.00E-02	3.27E-03	7.59E-04
PW	100 - 110	5.86	2.53E-05	4.42E-06	1.18E-04	1.39E-03	2.00E-02	3.99E-03	2.59E-04
PW	140 - 150	6.08	1.50E-05	3.14E-06	6.69E-05	1.56E-03	1.30E-01	4.34E-03	1.25E-04
PW acid	0 - 10	5.37	6.70E-05	1.75E-05	1.14E-03	4.57E-02	2.00E-02	1.04E-02	1.13E-02
PW acid	20 - 30	4.52	5.96E-05	1.94E-05	7.55E-04	3.32E-02	2.00E-02	9.42E-03	1.91E-02
PW acid	40 - 50	5.41	4.63E-05	1.41E-05	2.98E-04	9.22E-03	2.00E-02	4.16E-03	4.39E-03
PW acid	70 -80	5.46	4.19E-05	4.92E-06	1.23E-04	1.93E-03	2.00E-02	3.27E-03	1.60E-03
PW acid	100 - 110	5.76	3.56E-05	3.32E-05	1.18E-04	1.39E-03	2.00E-02	3.99E-03	2.12E-04
PW acid	140 - 150	5.95	2.03E-05	1.74E-06	6.69E-05	1.56E-03	1.30E-01	4.34E-03	1.42E-04

Table S3.9 Dissolved concentrations of competing elements in the calcium chloride (CaCl2), pore water (PW), and acidified pore water (PW acid) as listed in Groenenberg et al. (2012) and used in this study to validate the newly optimized binding parameters.

Type	Depth		Ca	Cl	Al	Fe	As	Cd	Cr	Cu	Ni	Pb	Zn
	[cm - surface]		[M]	[M]	[M]	[M]	[M]	[M]	[M]	[M]	[M]	[M]	[M]
CaCl2		0 - 10	2.00E-03	4.00E-03	1.15E-05	2.33E-06	9.70E-08	4.93E-08	8.59E-07	2.02E-07	3.23E-06	7.50E-09	2.75E-06
CaCl2		20 - 30	2.00E-03	4.00E-03	1.52E-05	1.25E-06	1.20E-07	5.98E-08	6.06E-07	2.15E-07	6.28E-06	5.05E-09	3.84E-06
CaCl2		40 - 50	2.00E-03	4.00E-03	7.41E-06	3.58E-07	7.87E-08	3.46E-08	1.81E-07	9.71E-08	3.79E-06	1.21E-09	2.11E-06
CaCl2		70 -80	2.00E-03	4.00E-03	3.71E-07	-3.6E-07	6.90E-08	1.98E-08	5.15E-08	4.66E-08	2.05E-06	8.69E-11	1.02E-06
CaCl2		100 - 110	2.00E-03	4.00E-03	4.08E-06	2.15E-06	1.29E-07	8.98E-09	3.58E-08	4.14E-08	1.34E-06	2.41E-11	4.74E-07
CaCl2		140 - 150	2.00E-03	4.00E-03	1.37E-05	4.30E-06	1.60E-09	2.32E-09	1.51E-08	2.03E-08	1.73E-07	8.69E-11	1.53E-08
PW		0 - 10	1.18E-03	5.30E-04	5.86E-05	1.54E-05	4.30E-07	3.98E-08	8.33E-06	1.52E-06	4.96E-06	5.04E-08	2.84E-05
PW		20 - 30	1.25E-03	1.97E-04	5.74E-05	1.13E-05	5.98E-07	5.29E-08	7.20E-06	1.76E-06	9.15E-06	3.83E-08	4.57E-05
PW		40 - 50	8.91E-04	6.77E-04	4.86E-05	5.55E-06	7.26E-07	3.34E-08	5.02E-06	1.98E-06	7.85E-06	4.12E-08	2.86E-05
PW		70 -80	5.59E-04	6.37E-04	2.65E-04	7.97E-05	9.56E-07	1.73E-08	2.64E-06	1.42E-06	4.99E-06	2.55E-08	1.53E-05
PW		100 - 110	6.24E-04	7.50E-04	5.78E-05	5.19E-05	7.30E-07	8.45E-09	1.17E-06	9.13E-07	3.85E-06	5.41E-09	6.88E-06
PW		140 - 150	7.01E-04	2.20E-04	9.64E-06	3.76E-06	1.11E-08	2.22E-09	2.91E-07	3.35E-07	6.33E-07	1.69E-09	3.06E-07
PW acid		0 - 10	3.57E-04	4.40E-04	4.00E-05	1.31E-05	8.38E-07	2.22E-08	1.07E-05	1.53E-06	1.76E-06	6.99E-08	7.95E-06
PW acid		20 - 30	1.42E-03	4.88E-04	4.82E-05	1.04E-05	6.31E-07	9.07E-08	1.08E-05	1.92E-06	1.31E-05	5.90E-08	7.40E-05
PW acid		40 - 50	1.08E-03	4.65E-04	4.04E-05	8.42E-06	1.02E-06	3.57E-08	4.55E-06	1.59E-06	7.81E-06	3.28E-08	3.44E-05
PW acid		70 -80	8.98E-04	2.79E-04	4.56E-05	7.16E-06	9.66E-07	2.18E-08	3.03E-06	1.34E-06	6.74E-06	2.38E-08	2.77E-05
PW acid		100 - 110	5.08E-04	7.33E-04	1.32E-04	1.39E-04	2.90E-07	1.78E-08	1.06E-06	9.87E-07	5.19E-06	8.64E-08	2.16E-05
PW acid		140 - 150	9.16E-04	1.12E-03	8.89E-06	7.16E-06	1.01E-08	4.27E-09	1.99E-07	2.72E-07	8.59E-07	1.21E-09	1.68E-06

Table S3.9 Dissolved concentrations of competing elements in the calcium chloride (CaCl2), pore water (PW), and acidified pore water (PW acid) as listed in Groenenberg et al. (2012) and used in this study to validate the newly optimized binding parameters *(continued)*

Type	Depth	Ba	Co	Mo	Sb	Se	Sn	V	S	P
	[cm - surface]	[M]	[M]	[M]	[M]	[M]	[M]	[M]	[M]	[M]
CaCl2	0 - 10	1.17E-06	2.22E-08	3.32E-09	4.90E-09	1.47E-09	1.68E-09	2.85E-08	2.59E-05	5.17E-05
CaCl2	20 - 30	8.79E-07	2.15E-08	3.15E-09	5.72E-09	1.42E-09	8.09E-10	2.81E-08	2.15E-05	4.55E-05
CaCl2	40 - 50	2.67E-07	8.69E-09	4.25E-09	3.14E-09	6.84E-10	3.37E-11	2.45E-08	9.04E-06	2.74E-05
CaCl2	70 -80	2.48E-08	3.29E-09	1.78E-09	2.38E-09	3.04E-10	-3.37E-11	2.28E-08	5.30E-06	1.49E-05
CaCl2	100 - 110	1.59E-08	2.73E-09	2.89E-09	3.12E-09	6.84E-10	0.00E+00	2.20E-08	9.04E-06	4.84E-06
CaCl2	140 - 150	6.75E-08	1.37E-09	2.38E-09	2.16E-09	3.80E-11	0.00E+00	4.57E-09	9.98E-06	3.23E-07
PW	0 - 10	0.00E+00	1.08E-07	1.44E-08	3.51E-08	1.41E-08	1.19E-08	1.35E-07	5.15E-04	1.74E-04
PW	20 - 30	0.00E+00	5.43E-08	1.45E-08	4.14E-08	1.32E-08	8.85E-09	1.59E-07	5.21E-04	1.50E-04
PW	40 - 50	0.00E+00	2.44E-08	2.34E-08	4.13E-08	1.80E-08	6.40E-09	1.64E-07	3.77E-04	1.38E-04
PW	70 -80	0.00E+00	2.19E-08	2.73E-08	4.29E-08	1.30E-08	2.70E-09	2.51E-07	2.74E-04	1.79E-04
PW	100 - 110	0.00E+00	1.17E-08	3.07E-08	5.52E-08	9.75E-09	8.42E-10	1.83E-07	3.31E-04	1.65E-05
PW	140 - 150	0.00E+00	7.64E-09	9.59E-09	1.95E-08	3.80E-09	4.21E-10	2.45E-08	4.74E-04	1.61E-06
PW acid	0 - 10	0.00E+00	6.36E-08	7.92E-09	2.68E-08	9.37E-09	6.91E-09	1.67E-07	4.71E-04	2.66E-04
PW acid	20 - 30	0.00E+00	1.26E-07	7.61E-09	4.16E-08	1.11E-08	1.28E-08	1.17E-07	8.36E-04	1.74E-04
PW acid	40 - 50	0.00E+00	2.17E-08	1.25E-08	4.30E-08	1.03E-08	3.71E-09	1.80E-07	6.05E-04	1.40E-04
PW acid	70 -80	0.00E+00	2.22E-08	1.81E-08	4.98E-08	1.04E-08	1.60E-09	2.30E-07	6.42E-04	8.91E-05
PW acid	100 - 110	0.00E+00	2.71E-08	5.49E-08	6.69E-08	1.94E-08	2.11E-09	7.57E-07	4.93E-04	4.07E-05
PW acid	140 - 150	0.00E+00	1.07E-08	1.41E-08	1.93E-08	2.79E-09	2.53E-10	2.45E-08	6.70E-04	2.26E-06

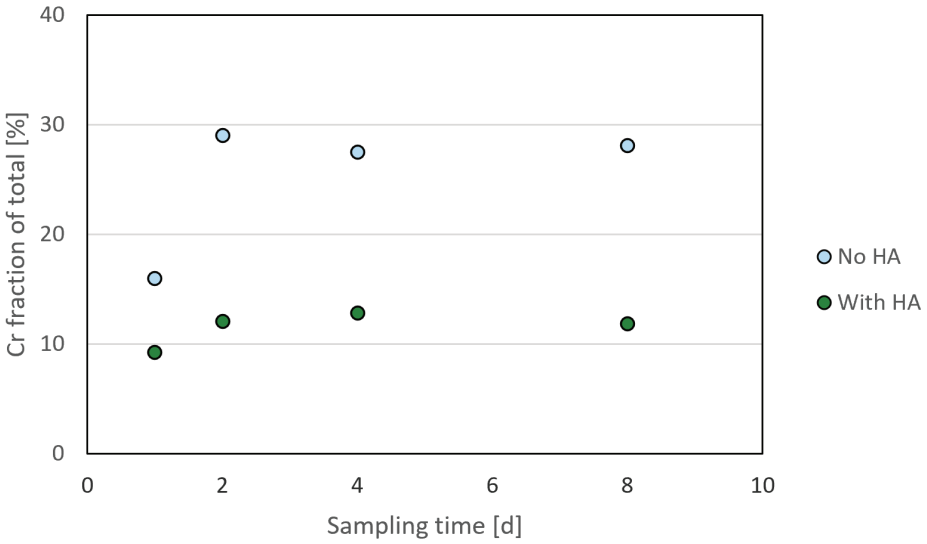


Figure S3.1 Chromium concentration in the acceptor cell as a function of time, in the absence and presence (167 mg L^{-1}) of humic acid in the donor cell. Initial donor solution contained a background concentration of 30 mM $NaNO_3$ and 2 mM $Ca(NO_3)_2$ at pH 3. Cr concentrations are 5.10^{-5} M in the presence of HA and 10^{-7} M in the absence of HA.

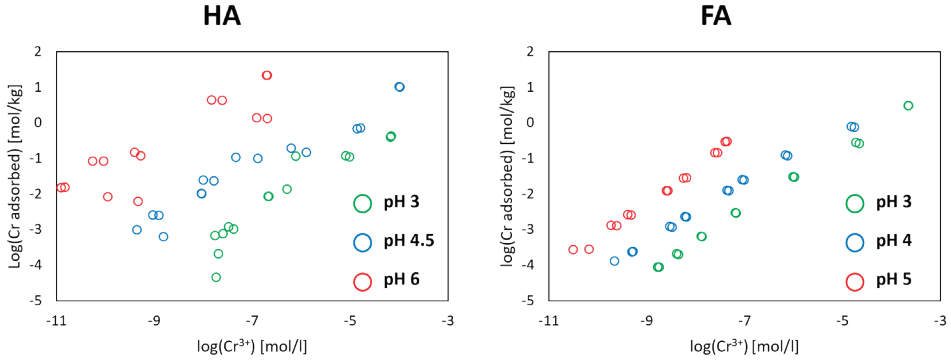


Figure S3.2 Cr adsorption to Tongbersven humic acid (left) and Suwannee River fulvic acid (right) at different pH levels and at different Cr^{3+} activities as measured in the DMT acceptor cells.

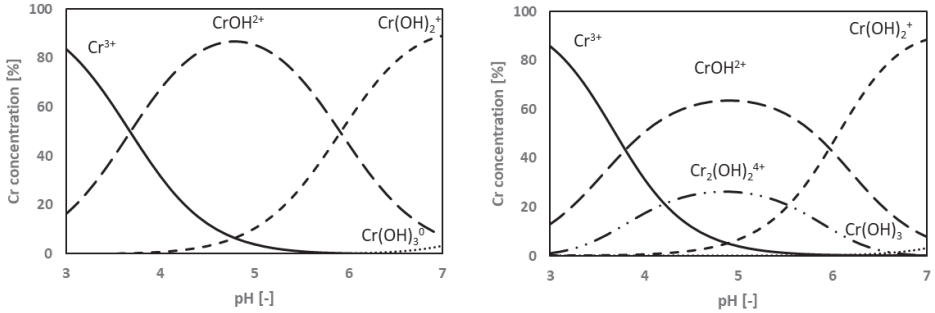


Figure S3.3 Inorganic Cr speciation as a function of pH at a total Cr concentration of 10-7 M (left) and 10-3 M (right).

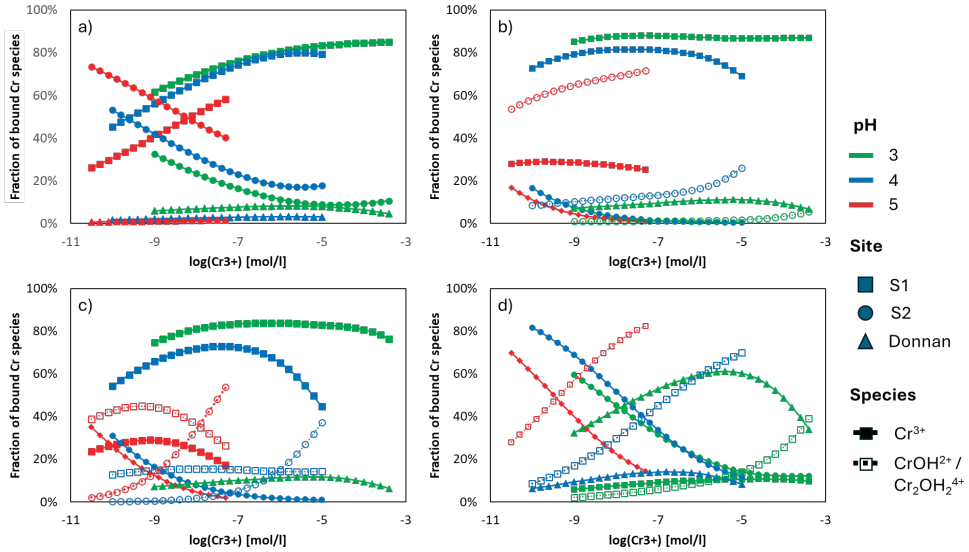


Figure S3.4 Distribution of Cr binding to SRFA across the carboxylic sites (S1), phenolic sites (S2), and the Donnan volume as a function of Cr^{3+} activity for different pH levels. Distributions are calculated using optimized Cr parameters fitted with specific SRFA proton parameters: a) fit solely considering Cr^{3+} adsorption; b) fit including adsorption of $CrOH^{2+}$; c) fit including adsorption of $Cr_2(OH)_2^{4+}$. For d), distributions are calculated using optimized parameters fitted with generic FA proton parameters considering Cr^{3+} adsorption and the adsorption of $Cr_2(OH)_2^{4+}$.

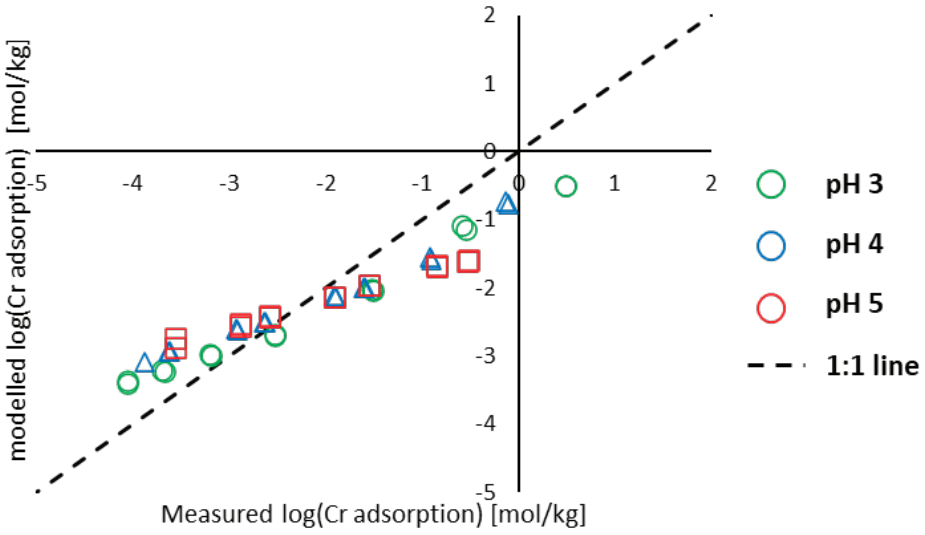


Figure S3.5 Optimized fit of Cr binding to SRFA using specific properties, solely considering Cr^{3+} adsorption. Fitted parameters n1 and n2 have been restricted between 0.2 – 0.4.

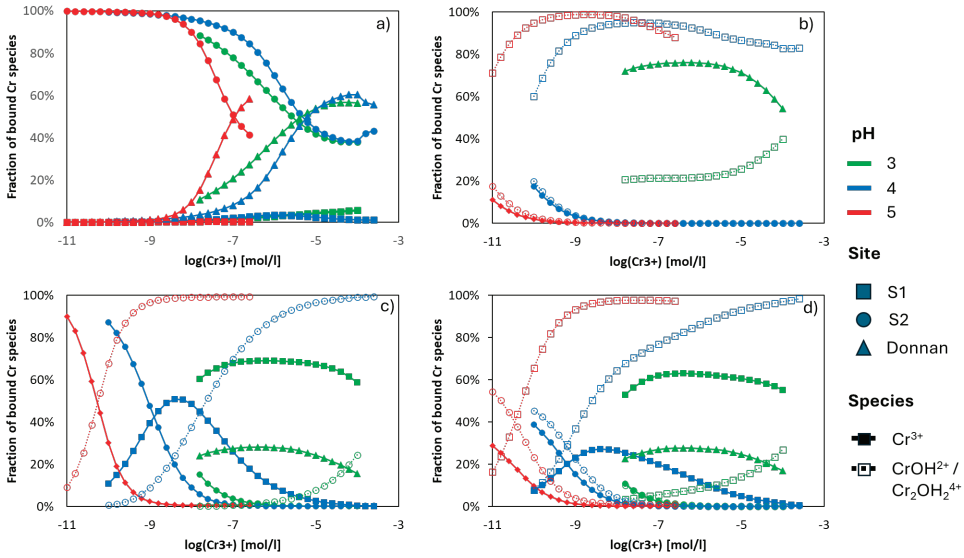


Figure S3.6 Distribution of Cr binding to THA across the carboxylic sites (S1), phenolic sites (S2), and the Donnan volume as a function of Cr^{3+} activity for different pH levels. Distributions are calculated using optimized Cr parameters fitted with specific THA proton parameters: a) fit solely considering Cr^{3+} adsorption; b) fit including adsorption of $CrOH^{2+}$; c) fit including adsorption of $Cr_2(OH)_2^{4+}$. For d), distributions are calculated using optimized parameters fitted with generic HA proton parameters considering Cr^{3+} adsorption and the adsorption of $Cr_2(OH)_2^{4+}$.

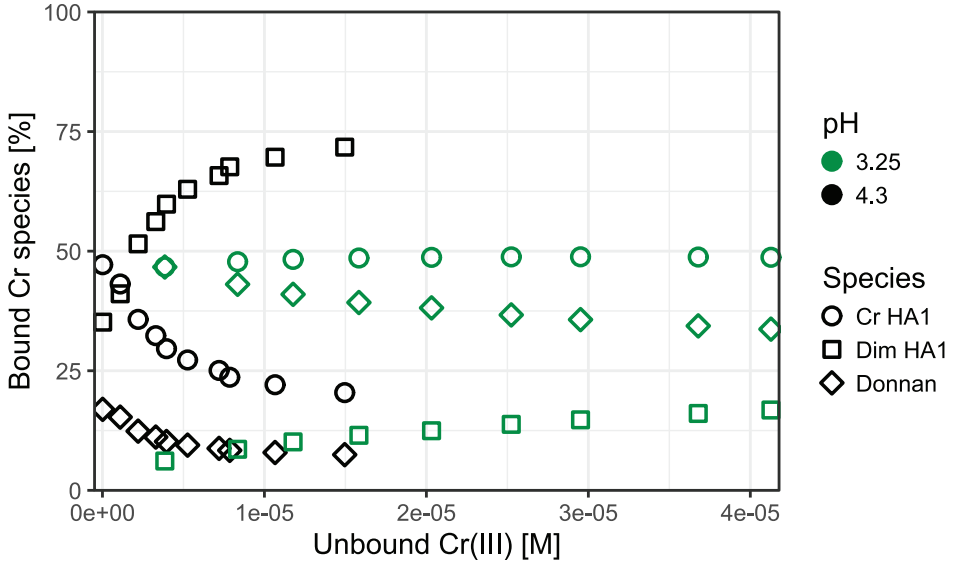


Figure S3.7 Distribution of Cr binding to humic acid calculated using the newly optimized parameters considering generic proton parameters and binding of Cr^{3+} and $Cr_2(OH)_2^{4+}$ for the dataset of Fukushima et al. (1995).

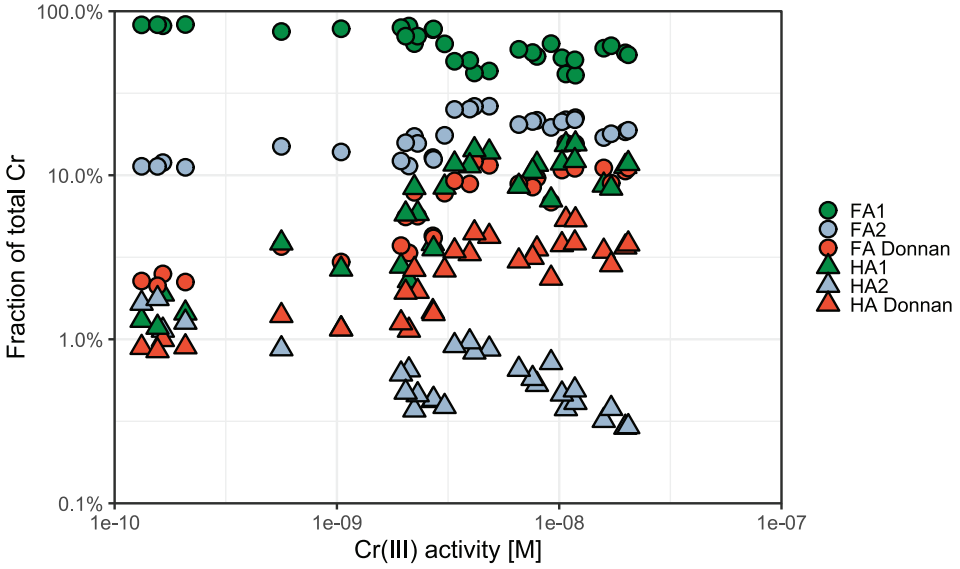


Figure S3.8 Distribution of Cr binding to humic acid and fulvic acid calculated using the newly optimized parameters considering generic proton parameters and binding of Cr^{3+} and $Cr_2(OH)_2^{4+}$ for the dataset of Koopmans & Groenenberg (2011).

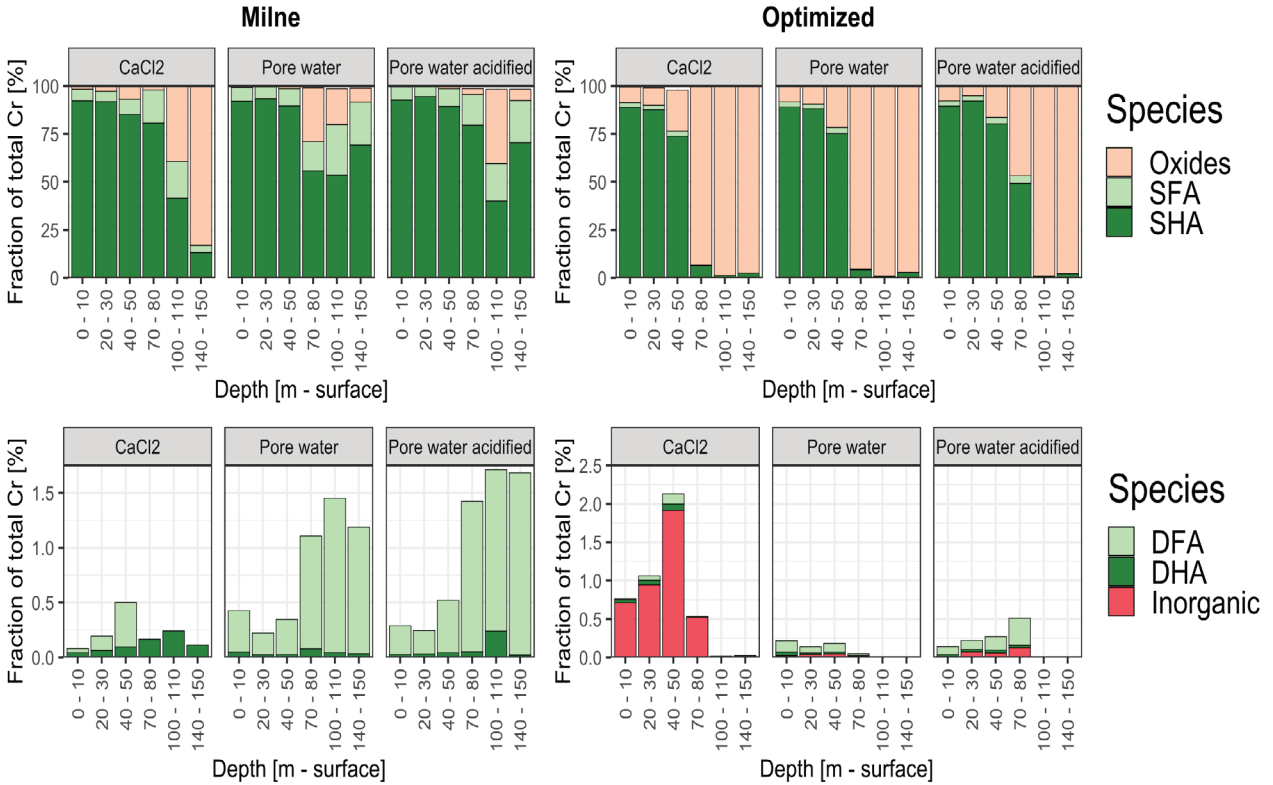


Figure S3.9 Cr speciation of the solid phase (top) and dissolved phase (bottom) in the calcium chloride ($CaCl_2$), pore water, and acidified pore water extracts from the dataset of Groenenberg et al. (2012). Binding to HA and FA is calculated using the generic parameters of Milne et al. (2003) (left) and the newly derived parameters of this paper (right).

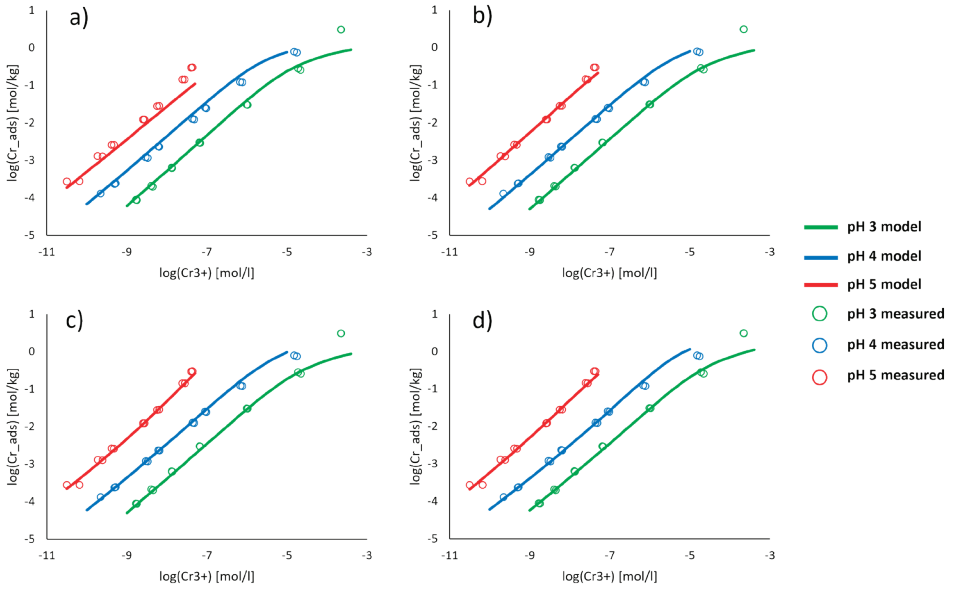


Figure S3.10 Optimized fits of Cr binding to SRFA using specific proton properties: a) fit solely considering Cr^{3+} adsorption; b) fit including adsorption of $Cr(OH)^{2+}$; c) fit including adsorption of $Cr_2(OH)_2^{4+}$; d) fit using the FA proton parameters of (Milne et al., 2001) including binding Cr^{3+} and $Cr_2(OH)_2^{4+}$.

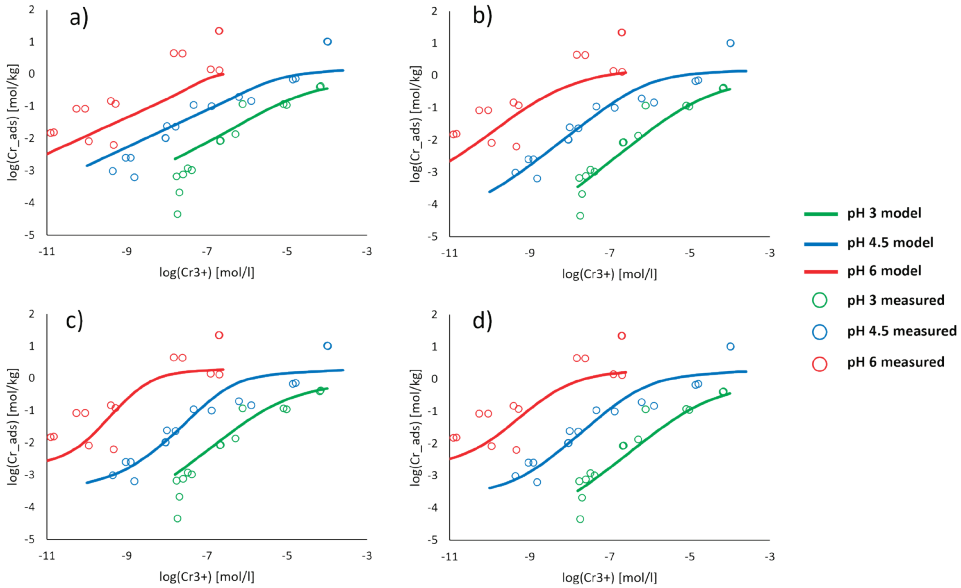


Figure S3.11 Optimized fits of Cr binding to THA using specific proton properties: a) fit solely considering Cr^{3+} adsorption; b) fit including adsorption of $Cr(OH)^{2+}$; c) fit including adsorption of $Cr_2(OH)_2^{4+}$; d) fit using the FA proton parameters of (Milne et al., 2001) including binding Cr^{3+} and $Cr_2(OH)_2^{4+}$.



Supplementary information chapter 4

Changing pH, organic matter, and redox state govern contaminant mobility during waste stabilization in landfill simulation reactors

Supplementary methods

SM4.1 pH dependent tests

Before filling of the LSRs, a representative fraction of the waste was investigated on pH dependent leaching of humic substances and inorganic elements in a similar set-up to van Raffe, Dijkstra, et al. (2025). Moist waste was extracted with ultrapure water with a liquid:solid ratio of 10 L/kg based on dry weight. A pH range of 2 – 12 was investigated through 9 simultaneous batch extractions, including one extraction at "native" (unaltered) pH. The pre-defined setpoint pH values were achieved through continuous pH measurements and automated addition of concentrated NaOH or HCl. Extractions were equilibrated for 48 hours following which suspensions were centrifuged and filtered over 0.45 µm cellulose filters. Part of the filtrate was acidified with 0.14 M HNO_3 and analysed on ICP-OES (Al, Ca, Cu, Fe, K, Mg, Mn, Na, P, Si, Z) and HR-ICP-MS (Al, As, Ba, Cd, Co, Cr, Cu, Fe, Mn, Ni, Sb, Sr, V, Zn); part of the filtrate was analysed (unacidified) for chloride (Cl) on a discrete analyser, and ammonium (NH_4^+), OC, and IC on the SFA. Remaining filtrate was further fractionated through rapid batch fractionation to analyse the dissolved HS (Van Zomeren & Comans, 2007).

SM4.2 Geochemical modelling

For the pH-dependent tests, total reactive surface inputs were based on the amounts measured before filling of the LSRs. The L/S was based on the final L/S (~10 l/kg). pH was directly measured, with pe calculated assuming moderately oxidizing conditions with a pH + pe of 12, based on the relation of van Raffe, Dijkstra, et al. (2025) which used similar samples and on an evaluation of the pH dependent leaching of the redox sensitive elements Fe and Mn. Assumed mineral forms and deviations from the generic parameter sets for the NICA-Donnan (Milne et al., 2001, 2003) and GTLM model (Dzombak & Morel, 1990) are listed in Table S4.1.

For the extracts of the solid waste in the mesh bags (hereafter "mesh bag extracts"), model inputs were similar to those used for the pH-dependent test, except for pe. Considering the different redox environments in the LSRs, both a pH + pe of 6 (reduced) and 12 (moderately oxidized) were used in the model, in order to evaluate the influence of redox potential on the partitioning of the elements under study. The used redox potentials are based on the potentials measured in the LSR, yet are slightly elevated to account for potential oxidation during sampling, storage, sample pre-treatment, and sample extraction. Considered mineral forms for the mesh bag extracts modelling are listed in Table S4.2, used binding parameters are identical to those used for the pH dependent test (Table S4.1).

Supplementary results

SR4.1 pH dependent leaching

The measured and modelled pH dependent solubility of elements show similarity for the waste sampled for the LSR study and for waste sampled from the same landfills in 2016 and 2017 prior to instigation of active treatment (T0; Figures S4.1 & S4.2). The T0 samples have previously been carefully investigated (van Raffe, Dijkstra, et al., 2025), and the identified general leaching patterns identified for the T0 samples are also observed for the LSR waste. The lack of a significant change in mechanisms after 7 years of active treatment is a potential indication of the limited effects of in-situ active treatment.

The pH-dependent leaching behaviour of reactive elements can be distinguished between anionic (As, Mo, P, and Sb) with a solubility minimum around pH 5, and cationic (Al, Ba, Ca, Cd, Co, Cr, Cu, Fe, Mg, Mn, Ni, Pb, Sn, Sr, V, Zn) with a variable pH of minimum solubility related to the affinity of the cation to bind to OM and the element's tendency to hydrolyze (van Raffe, Dijkstra, et al., 2025). For a detailed discussion on element behaviour and model performance, see van Raffe et al. (van Raffe, Dijkstra, et al., 2025). However, a significantly improved model description of Cr is achieved compared to van Raffe et al. (Figure S4.2), based on recently derived improved HS binding parameters for this metal (van Raffe, Comans, et al., 2025). Where Cr was predicted to be solely bound to HS in both the solid and dissolved phase in the T0 modelling (van Raffe, Dijkstra, et al., 2025), here Cr is predicted to be predominantly bound to Fe/Al (hydr)oxides in the solid phase and to occur as HA-bound and inorganic Cr-hydroxyl species in the dissolved phase (Figure S4.3).

Supplementary Tables

Table S4.1 Considered minerals and parameters differing from the generic parameter databases in the modelling of the pH dependent test

Element	Mineral	ND parameters	GTLM parameters
Al	Gibbsite, Wairakite		
As	-		
Ba	$BaSrSO_4$ [50% Ba], Barite		
Ca	Calcite, $Ca_4H[PO4]_3$:3 H_2O, Wairakite		
Cd	-	(Wiersma et al., 2025)	
Co	-		
Cr	-		
Cu	Tenorite	(Wiersma et al., 2025)	
Fe	Ferrihydrite	(Appelo et al., 2002)	
K	-		
Li	-		
Mg	Nesquehonite, struvite, brucite		
Mn	Rhodochrosite, pyro-chroite		
Mo	PbMoO4		
Na	-		
Ni	-		
NH_4^+	Struvite		
Pb	$PbMoO_4$, $Pb[OH]_2$		
P	Struvite, $Ca_4H[PO4]_3$:3 H_2O		
S	Barite, BaSrSO4		
Sb	-		
Si	Wairakite, Willemite, Sepiolite		
Sn	SnH2OH6-2		
Sr	BaSrSO4 , Strontianite		
Zn	Willemite		

Table S4.2 Minerals considered during the modelling of the water extracts and additional minerals added for the modelling of the LSR leachate.

Element	Minerals water extract	Minerals further added for LSR
Al	Gibbsite, Wairakite	
As	-	
Ba	$BaSrSO_4$ [50% Ba], Barite, Witherite	
Ca	Calcite, $Ca_3[PO_4]_2$, Wairakite	
Cd	$Cd[OH]_2$, Otavite	CdS[s]
Co	$CoCO_3$, Co_3O_4	
Cr	$CrOH_3$	
Cu	Tenorite, Chalcocite, Malachite	
Fe	Ferrihydrite, Greigite, Siderite	
K	-	
Li	-	
Mg	Brucite, Nesquehonite, Sepiolite, Struvite	
Mn	Rhodochrosite, Pyrochroite	
Mo	$PbMoO_4$	
Na	-	
Ni	-	
NH_4^+	Struvite	
Pb	$PbMoO_4$, $Pb[OH]_2$	Galena
P	Struvite, $Ca_4H[PO_4]_3$:3 H_2O	
S	Barite, $BaSrSO_4$, Chalcocite, Mackinawite	CdS[s] (F. Wang & Tessier, 1999), ZnS (am)
Sb	-	
Si	Wairakite, Willemite, Sepiolite	
Sn	$H_2Sn(OH)_6^{2-}$	
Sr	$BaSrSO_4$, Strontianite	
Zn	Willemite, Smithsonite	ZnS (am)

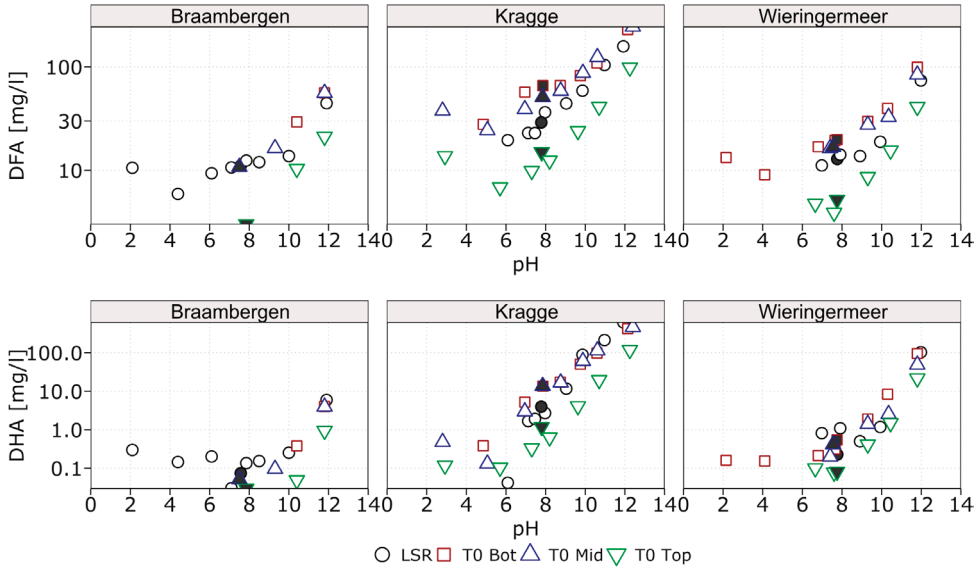


Figure S4.1 Concentration of dissolved fulvic acid (top) and dissolved humic acid (bottom) as a function of pH in UPW extracted solid waste sampled at different depths in a landfill before start of active treatment (top, mid, bot samples) or sampled across the entire landfill depth after ~6 years of active treatment (LSR).

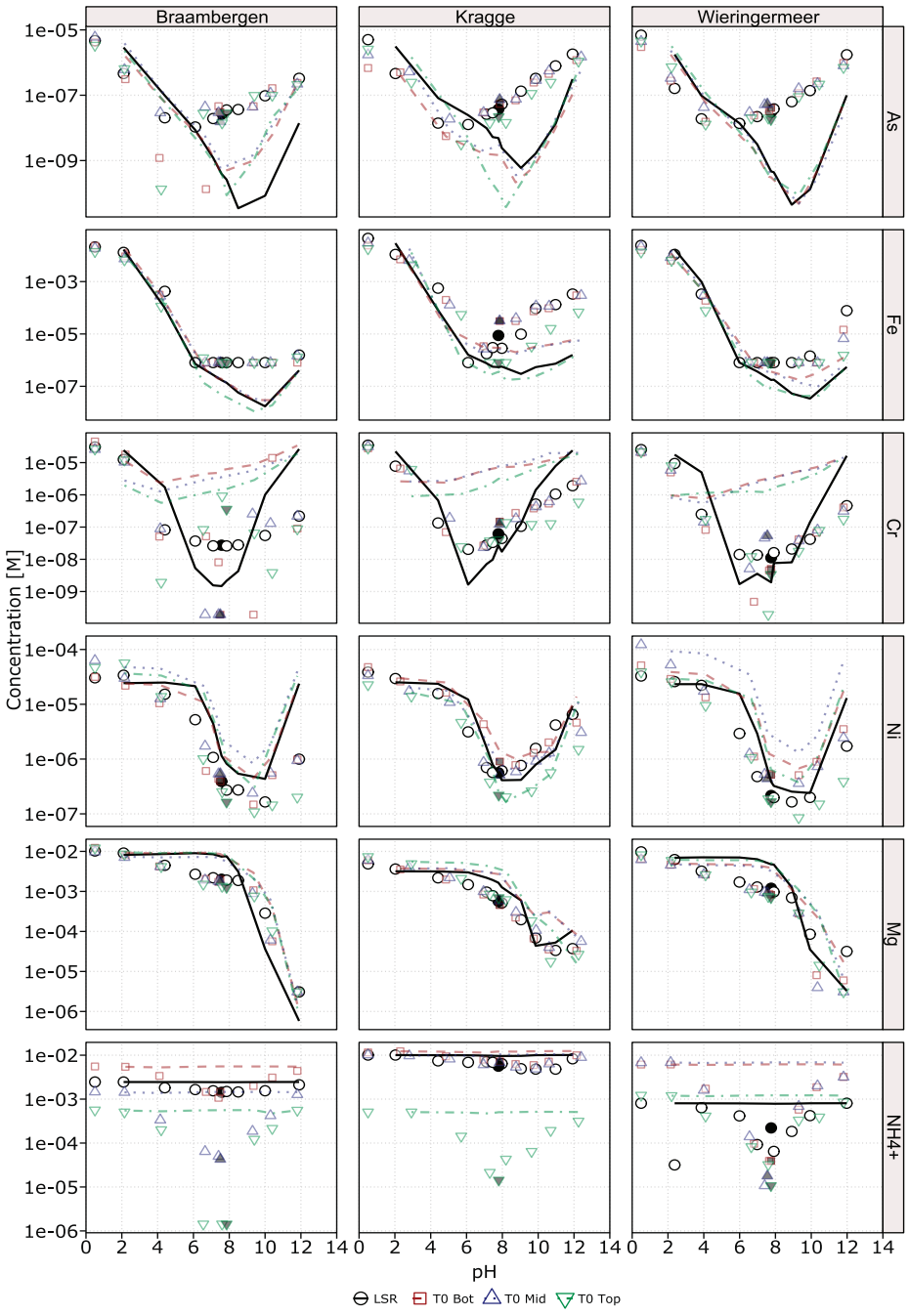


Figure S4.2 Measured (markers) and modelled (lines) concentrations of elements as a function of pH in ultrapure water extracts of solid waste sampled from three different landfill sites, Braambergen, Kragge, and Wieringermeer. Waste samples were sampled in 2016 and 2017 prior to field-scale active treatments at three different depths (T0-Top, -Mid and -Bottom, see also van Raffe, Dijkstra, et al. (2025)) and sampled at the same sites after 6 years of active treatment (LSR).

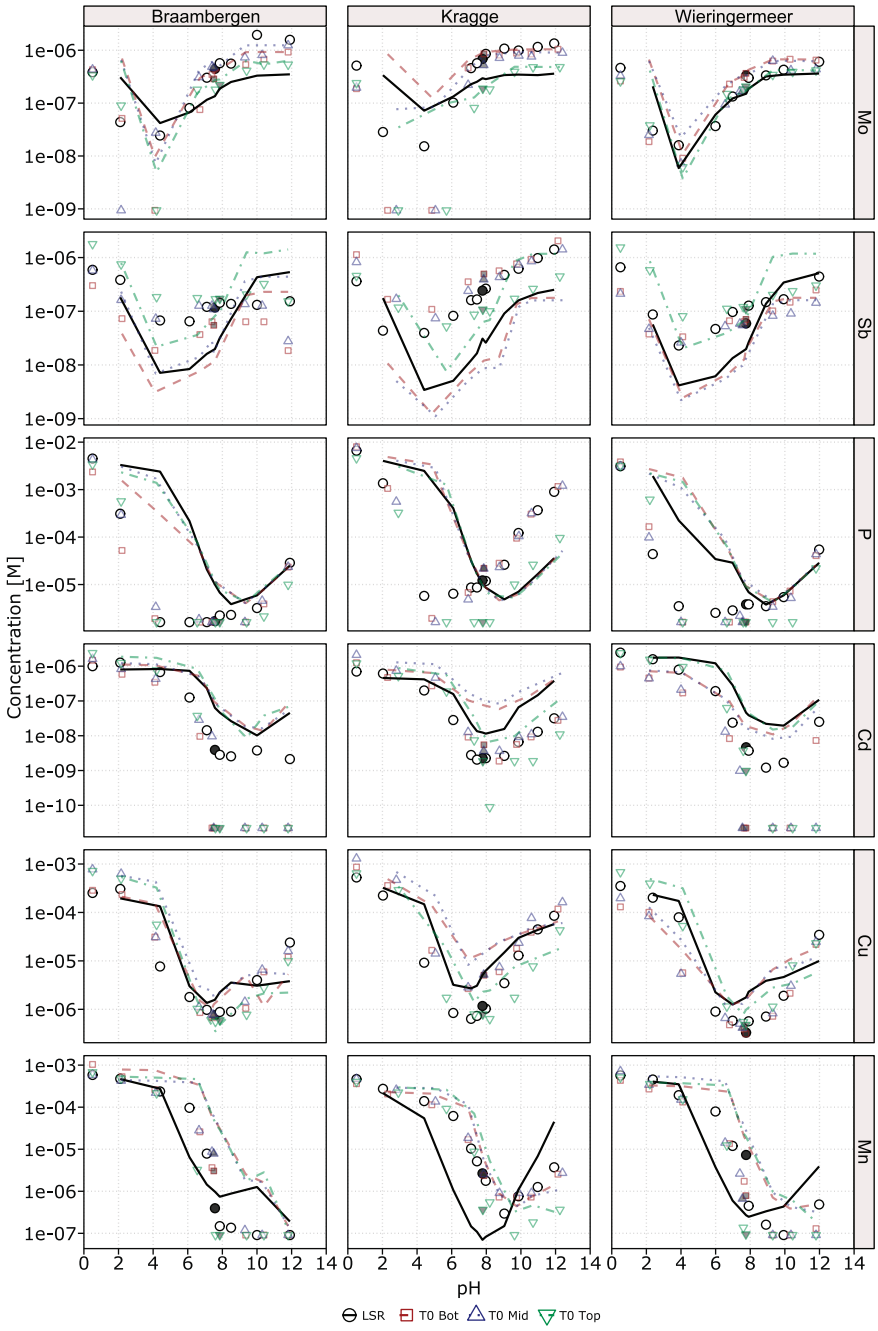


Figure S4.2 Measured (markers) and modelled (lines) concentrations of elements as a function of pH in ultrapure water extracts of solid waste sampled from three different landfill sites, Braambergen, Kragge, and Wieringermeer. Waste samples were sampled in 2016 and 2017 prior to field-scale active treatments at three different depths (T0-Top, -Mid and -Bottom, see also van Raffe, Dijkstra, et al. (2025)) and sampled at the same sites after 6 years of active treatment (LSR) *(Continued)*

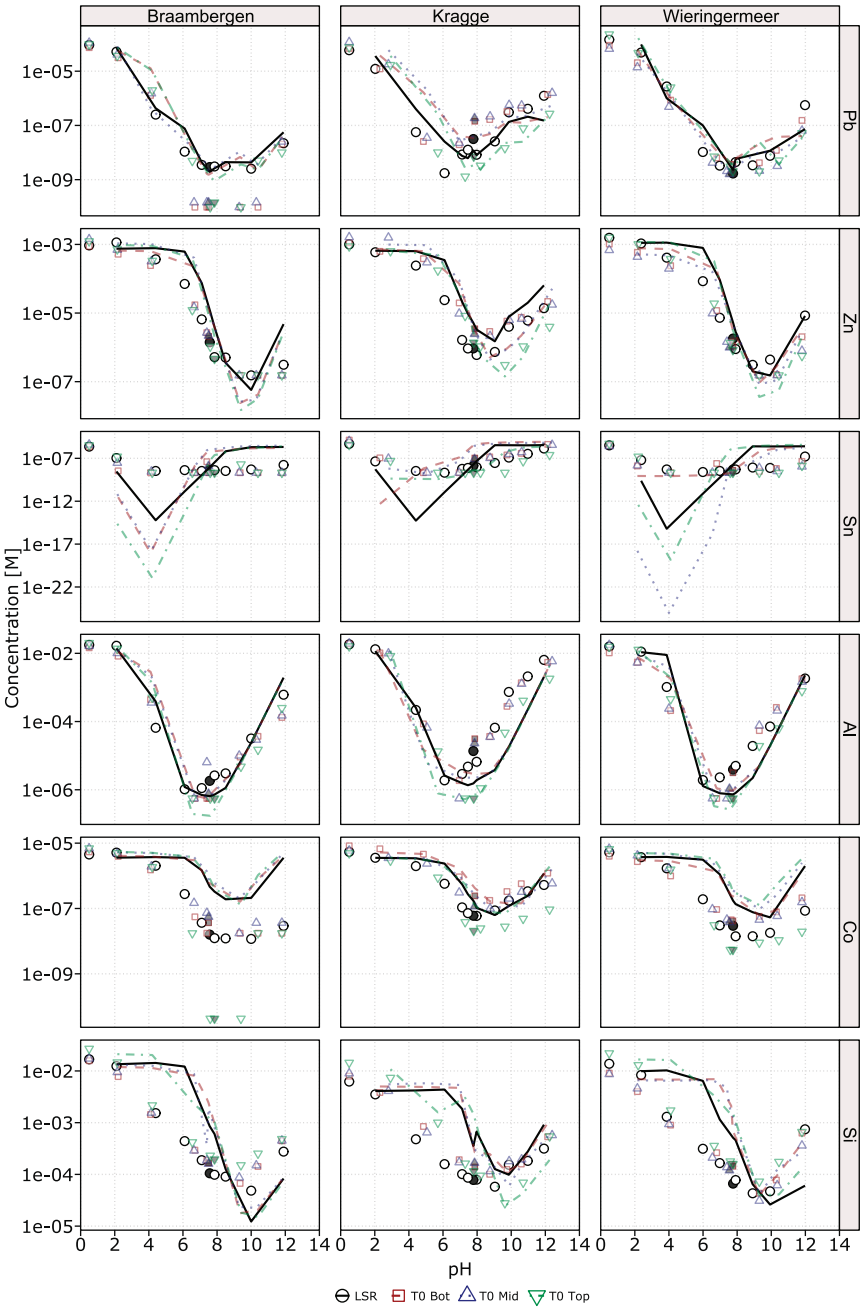


Figure S4.2 Measured (markers) and modelled (lines) concentrations of elements as a function of pH in ultrapure water extracts of solid waste sampled from three different landfill sites, Braambergen, Kragge, and Wieringermeer. Waste samples were sampled in 2016 and 2017 prior to field-scale active treatments at three different depths (T0-Top, -Mid and -Bottom, see also van Raffe, Dijkstra, et al. (2025)) and sampled at the same sites after 6 years of active treatment (LSR) *(Continued)*

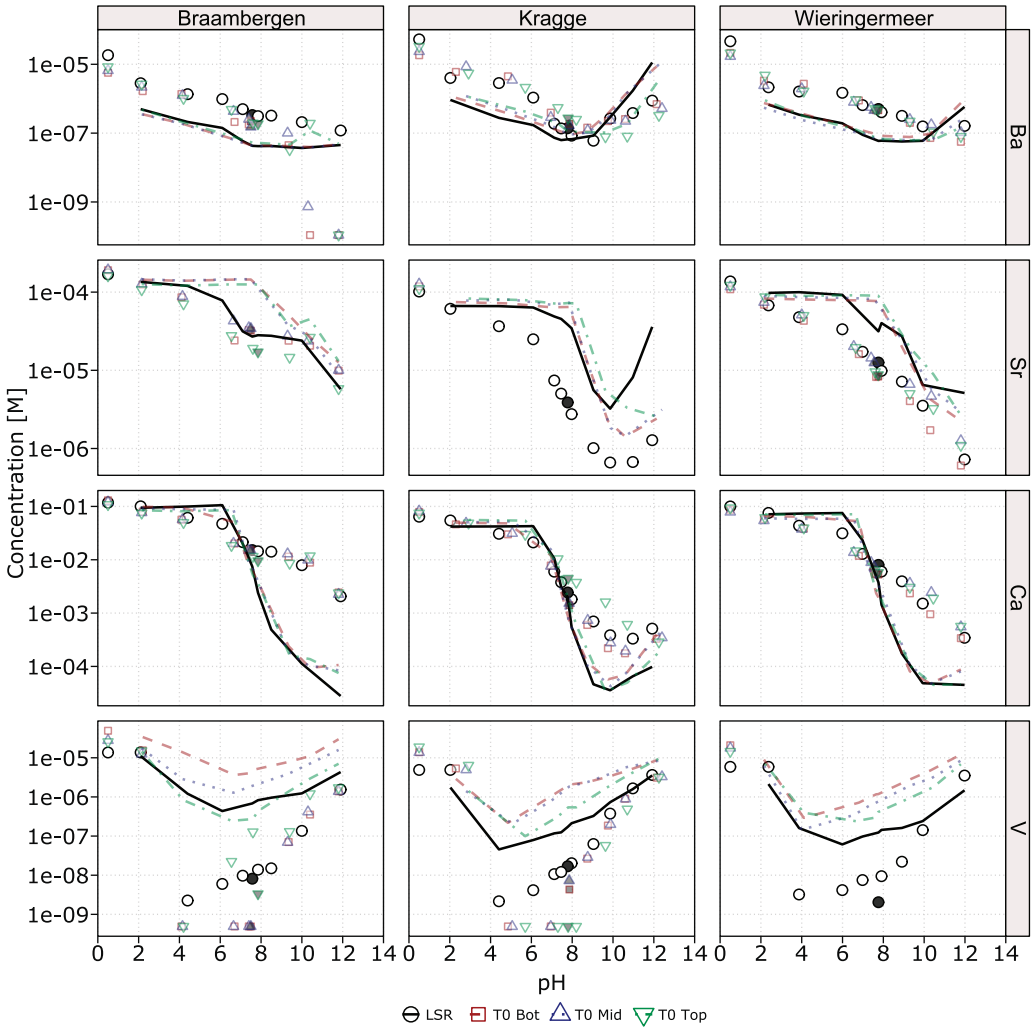


Figure S4.2 Measured (markers) and modelled (lines) concentrations of elements as a function of pH in ultrapure water extracts of solid waste sampled from three different landfill sites, Braambergen, Kragge, and Wieringermeer. Waste samples were sampled in 2016 and 2017 prior to field-scale active treatments at three different depths (T0-Top, -Mid and -Bottom, see also van Raffe, Dijkstra, et al. (2025)) and sampled at the same sites after 6 years of active treatment (LSR). (Continued)

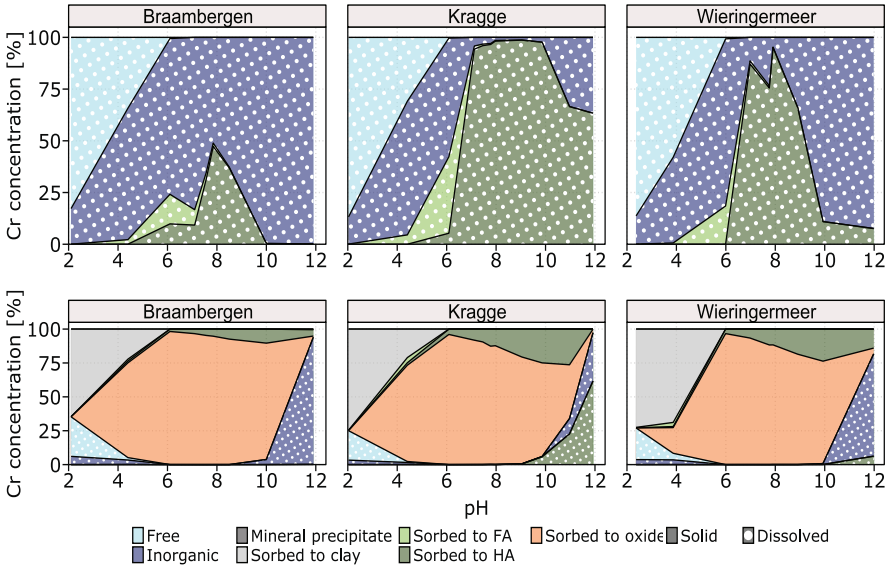


Figure S4.3 Model calculated dissolved phase speciation only (top) and combined solid and dissolved speciation (bottom) of Cr as a function of pH in UPW extracts of waste from three different landfills.

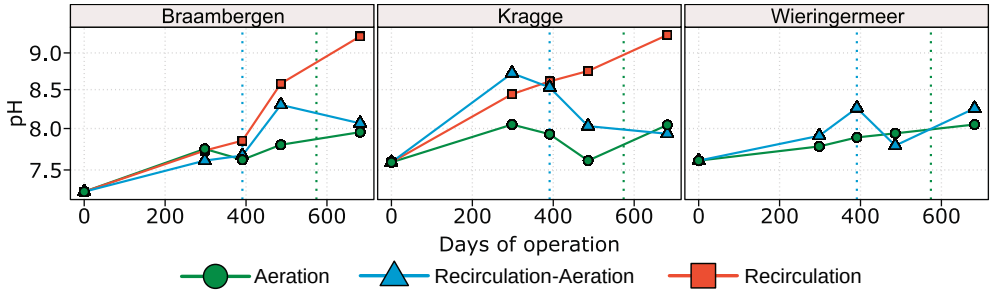


Figure S4.4 Trends in pH measured in UPW extracts of solid waste sampled at different times from landfill simulation reactors operated under different conditions. The vertical dotted lines indicate the date at which the Recirculation-Aeration LSR switched from recirculation to aeration (blue) and when the aeration LSRs of Braambergen and Kragge switched from aeration to anaerobic conditions (green).

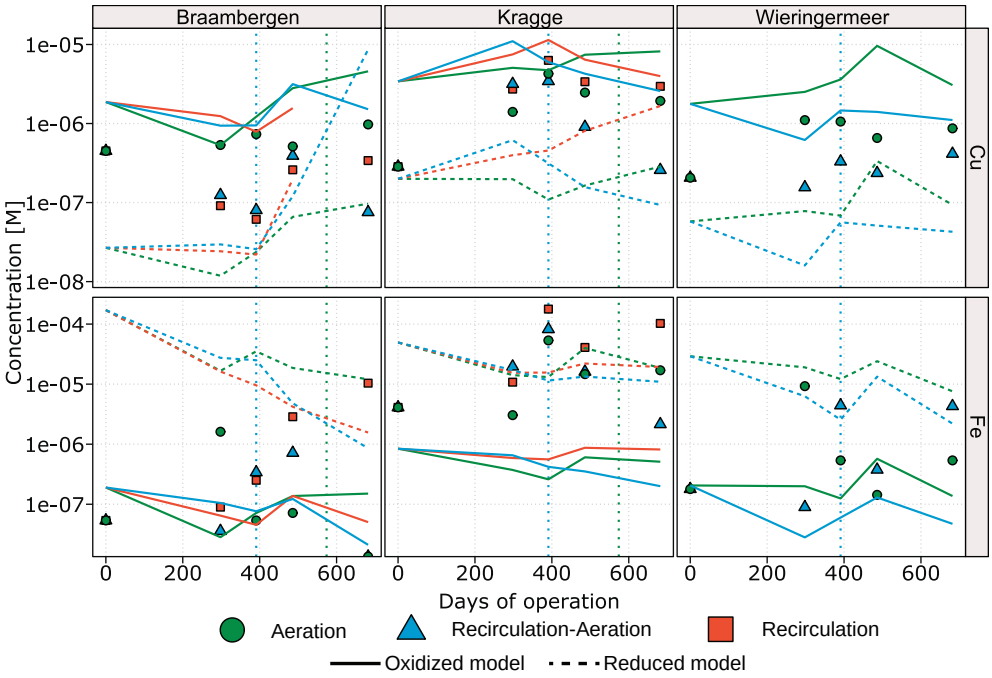


Figure S4.5 *Measured (markers) and modelled (lines) concentrations of Cu and Fe in UPW extract of solid waste sampled at different times from landfill simulation reactors operated under different conditions. The vertical dotted lines indicate the date at which the Recirculation-Aeration LSR switched from recirculation to aeration (blue) and when the aeration LSRs of Braambergen and Kragge switched from aeration to anaerobic conditions (green). For modelling calculations, redox conditions were assumed as pH + pe = 12 (oxidized, solid line) or pH + pe + 6 (reduced, dotted line).*

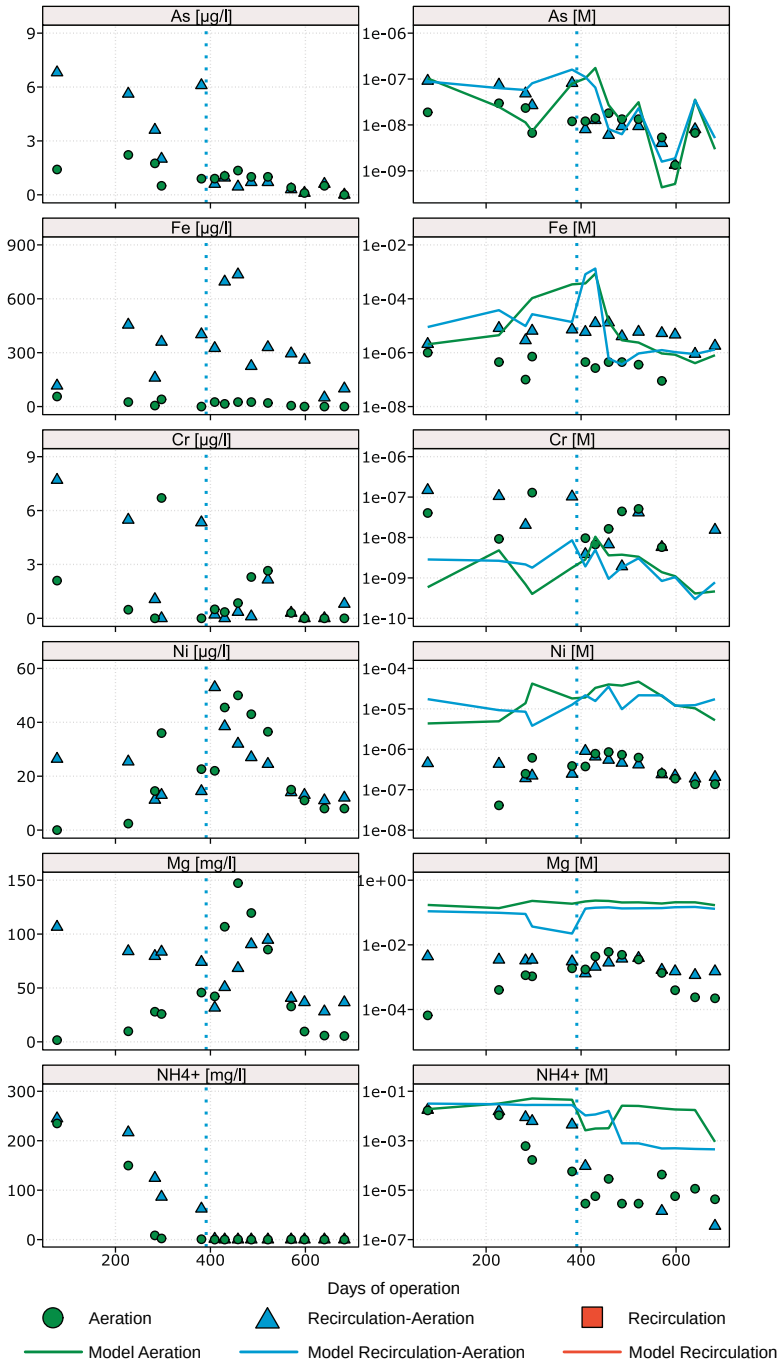


Figure S4.6 Measured (symbols) and modelled (lines) concentrations of contaminants in the leachate of the Wie LSR during operation under different operational conditions. The blue vertical dotted lines indicate the date at which the Recirculation-Aeration LSR switched from recirculation to aeration (blue) and when the aeration LSRs of Braambergen and Kragge switched from aeration to anaerobic conditions (green).

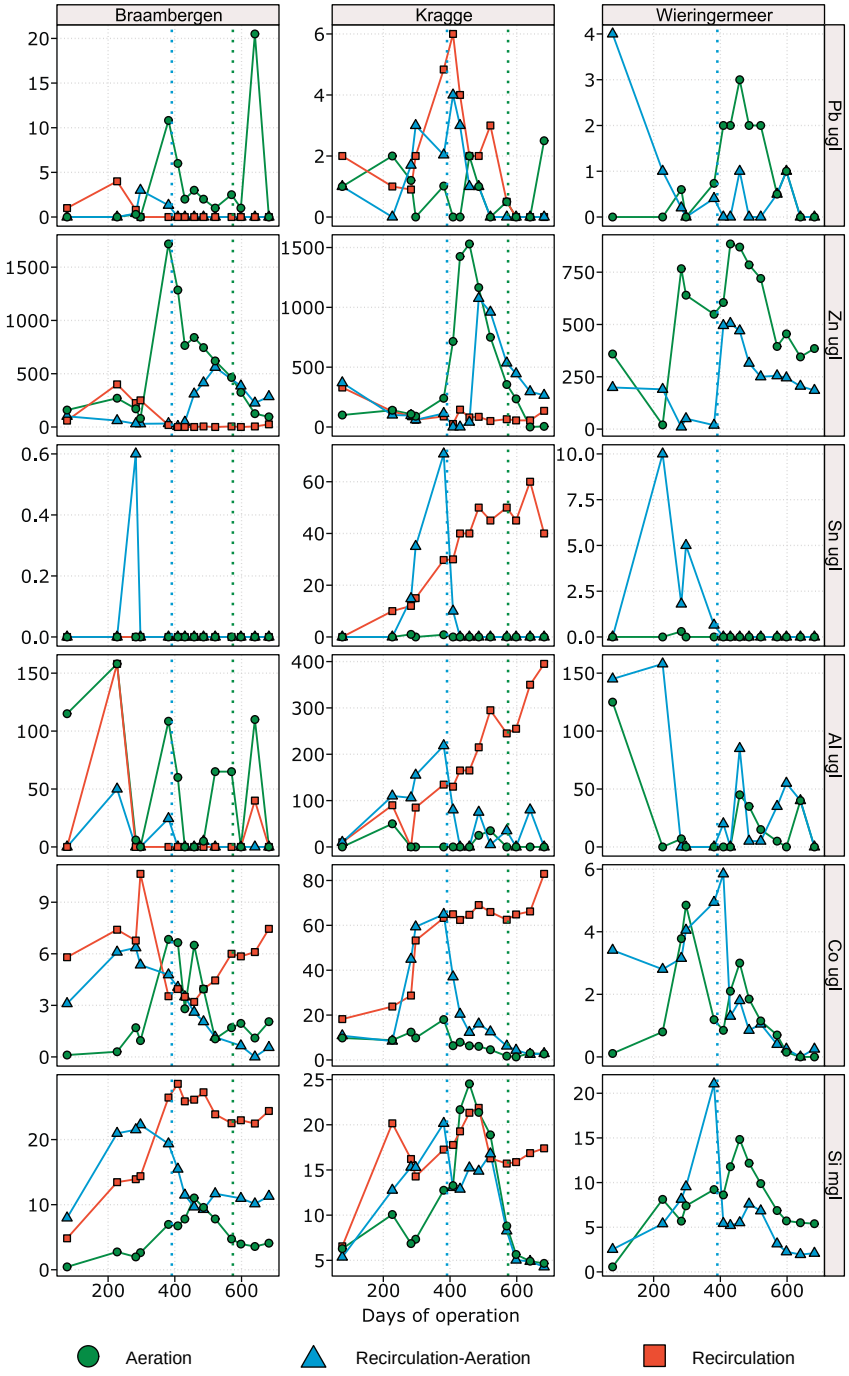


Figure S4.7 Measured concentrations of contaminants not listed in Figure 4.3 in the LSR leachate during LSR operation under different operational conditions. The vertical dotted lines indicate the date at which the Recirculation-Aeration LSR switched from recirculation to aeration (blue) and when the aeration LSRs of Braambergen and Kragge switched from aeration to anaerobic conditions (green).

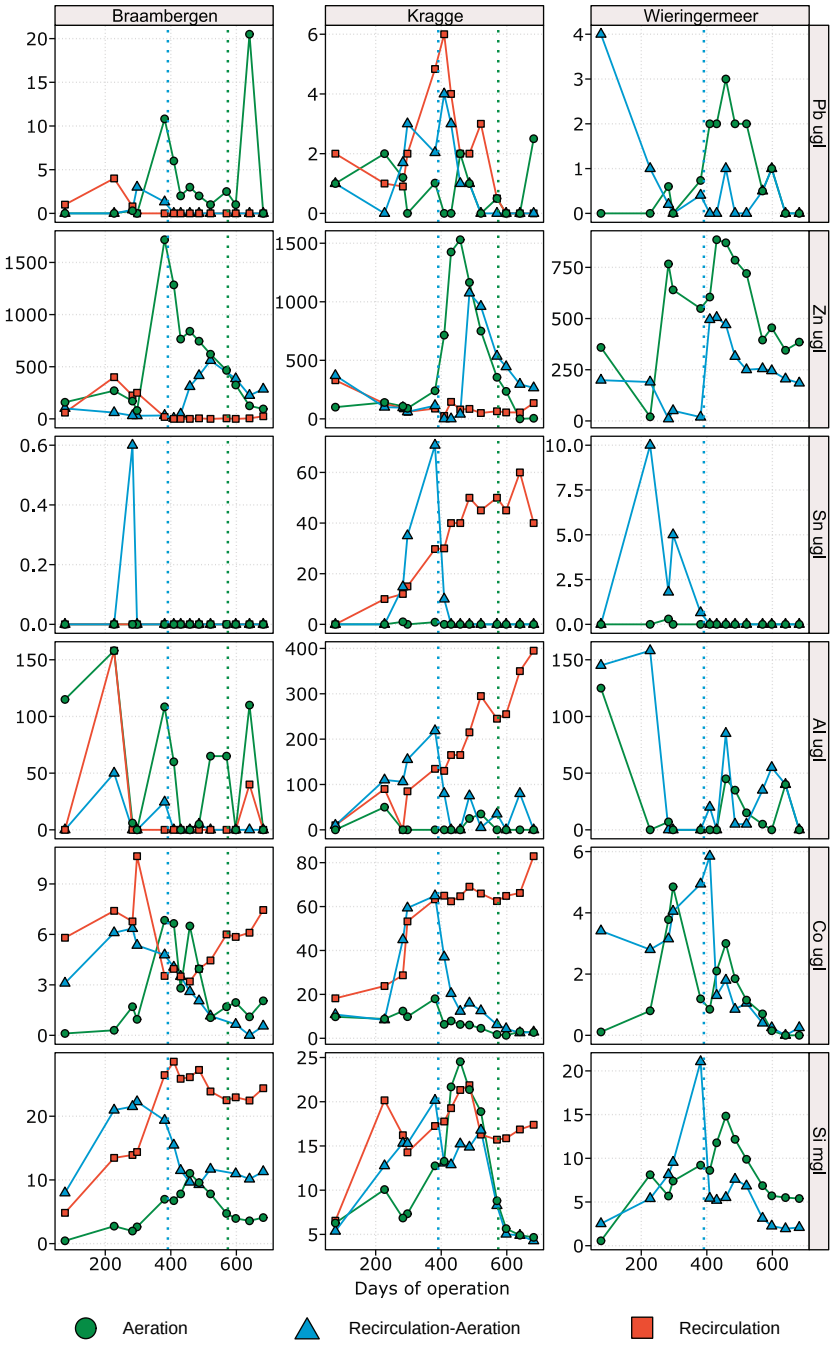


Figure S4.7 Measured concentrations of contaminants not listed in Figure 4.3 in the LSR leachate during LSR operation under different operational conditions. The vertical dotted lines indicate the date at which the Recirculation-Aeration LSR switched from recirculation to aeration (blue) and when the aeration LSRs of Braambergen and Kragge switched from aeration to anaerobic conditions (green). (Continued)

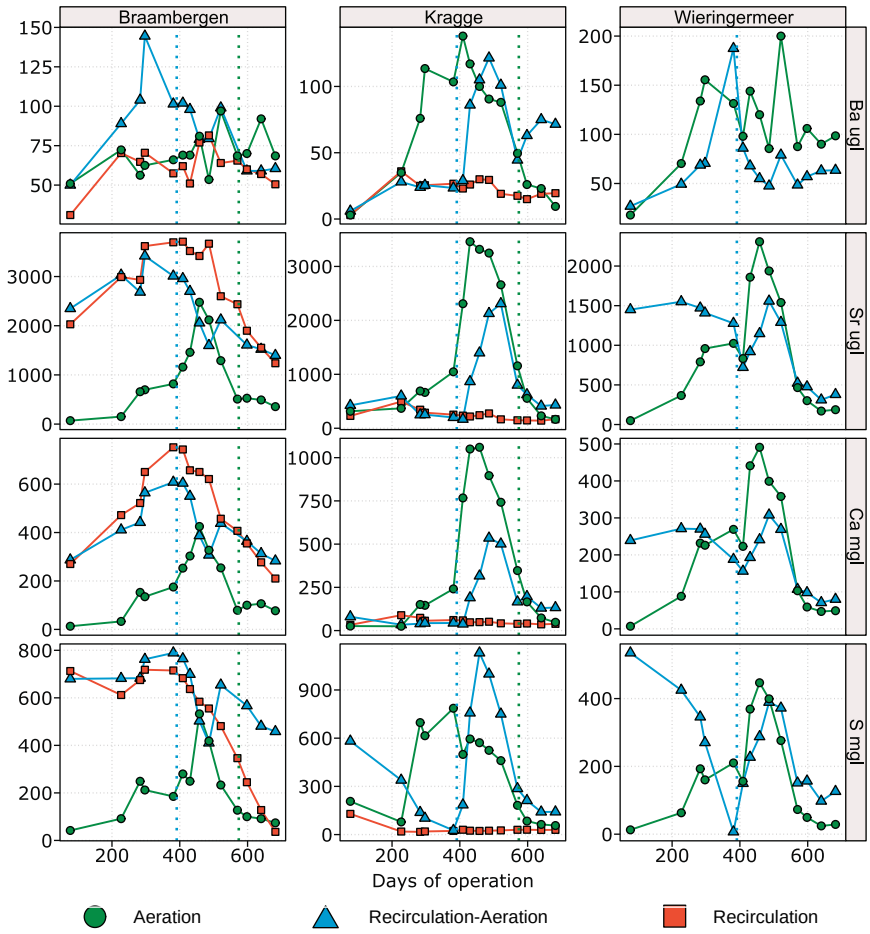


Figure S4.7 Measured concentrations of contaminants not listed in Figure 4.3 in the LSR leachate during LSR operation under different operational conditions. The vertical dotted lines indicate the date at which the Recirculation-Aeration LSR switched from recirculation to aeration (blue) and when the aeration LSRs of Braambergen and Kragge switched from aeration to anaerobic conditions (green).*(Continued)*

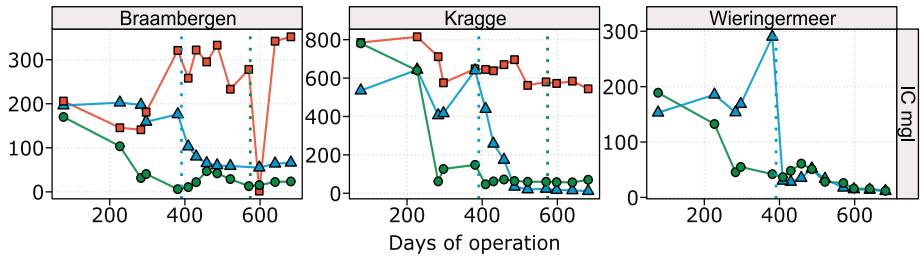


Figure S4.8 Measured concentrations of inorganic carbon in the LSR leachate during LSR operation under different operational conditions. The vertical dotted lines indicate the date at which the Recirculation-Aeration LSR switched from recirculation to aeration (blue) and when the aeration LSRs of Braambergen and Kragge switched from aeration to anaerobic conditions (green).

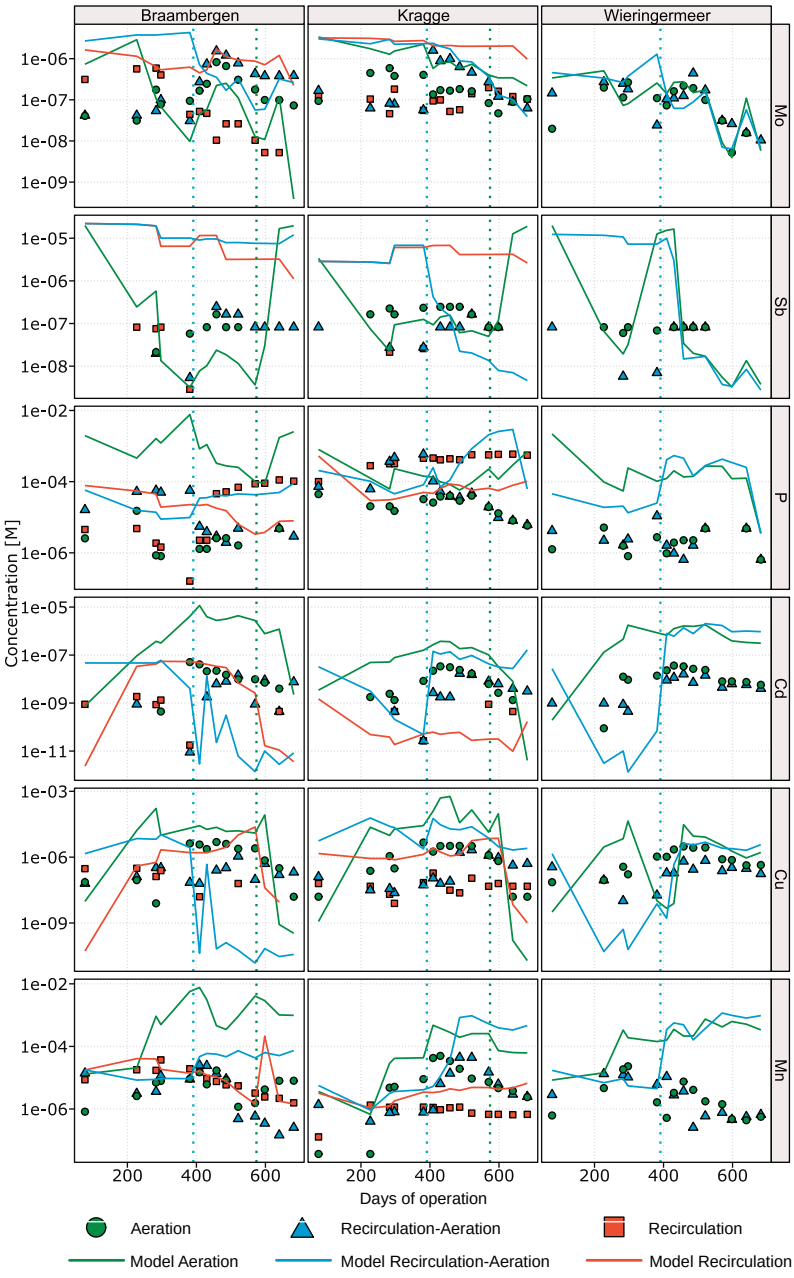


Figure S4.9 *Measured (symbols) and modelled (lines) concentrations of contaminants in the LSR leachates during LSR operation under different operational conditions. The vertical dotted lines indicate the date at which the Recirculation-Aeration LSR switched from recirculation to aeration (blue) and when the aeration LSRs of Braambergen and Kragge switched from aeration to anaerobic conditions (green).*

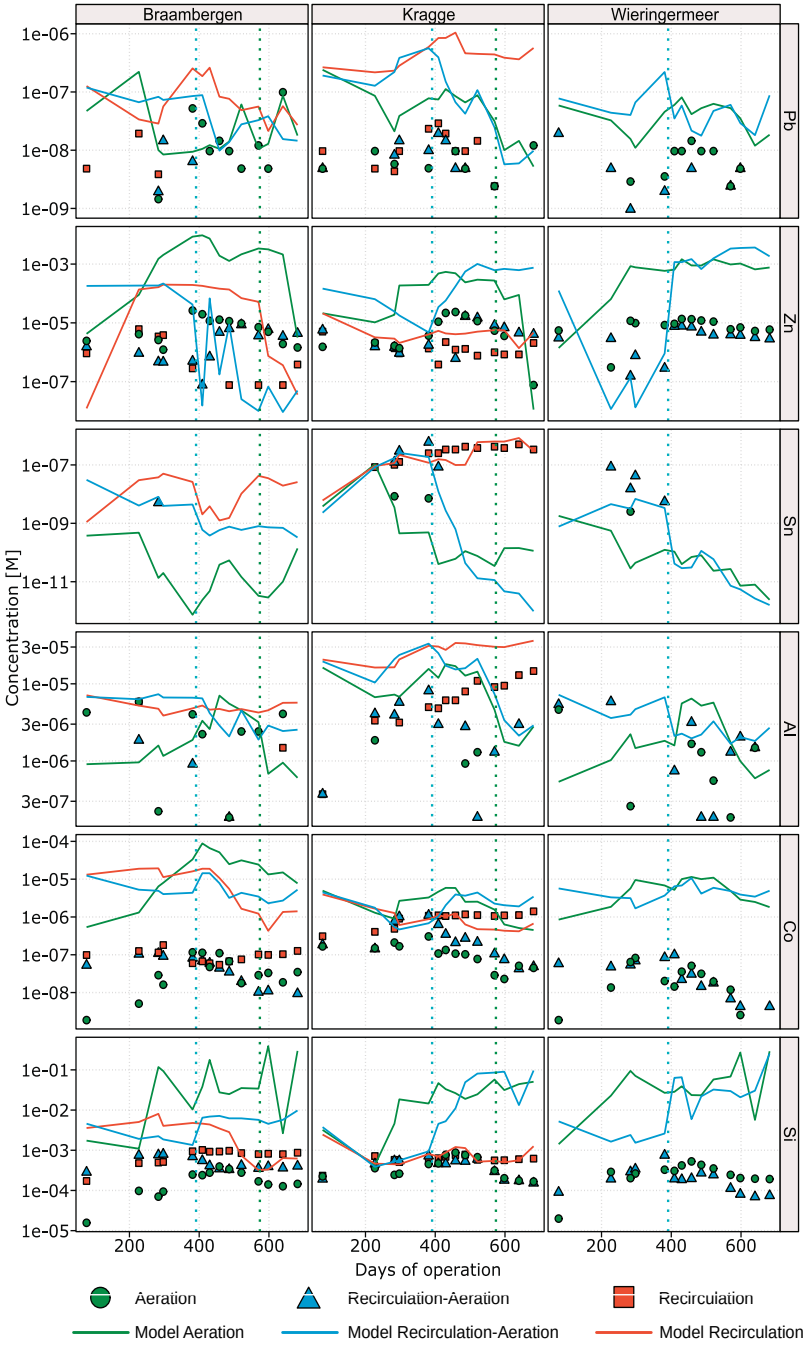


Figure S4.9 Measured (symbols) and modelled (lines) concentrations of contaminants in the LSR leachates during LSR operation under different operational conditions. The vertical dotted lines indicate the date at which the Recirculation-Aeration LSR switched from recirculation to aeration (blue) and when the aeration LSRs of Braambergen and Kragge switched from aeration to anaerobic conditions (green)**.** *(Continued)*

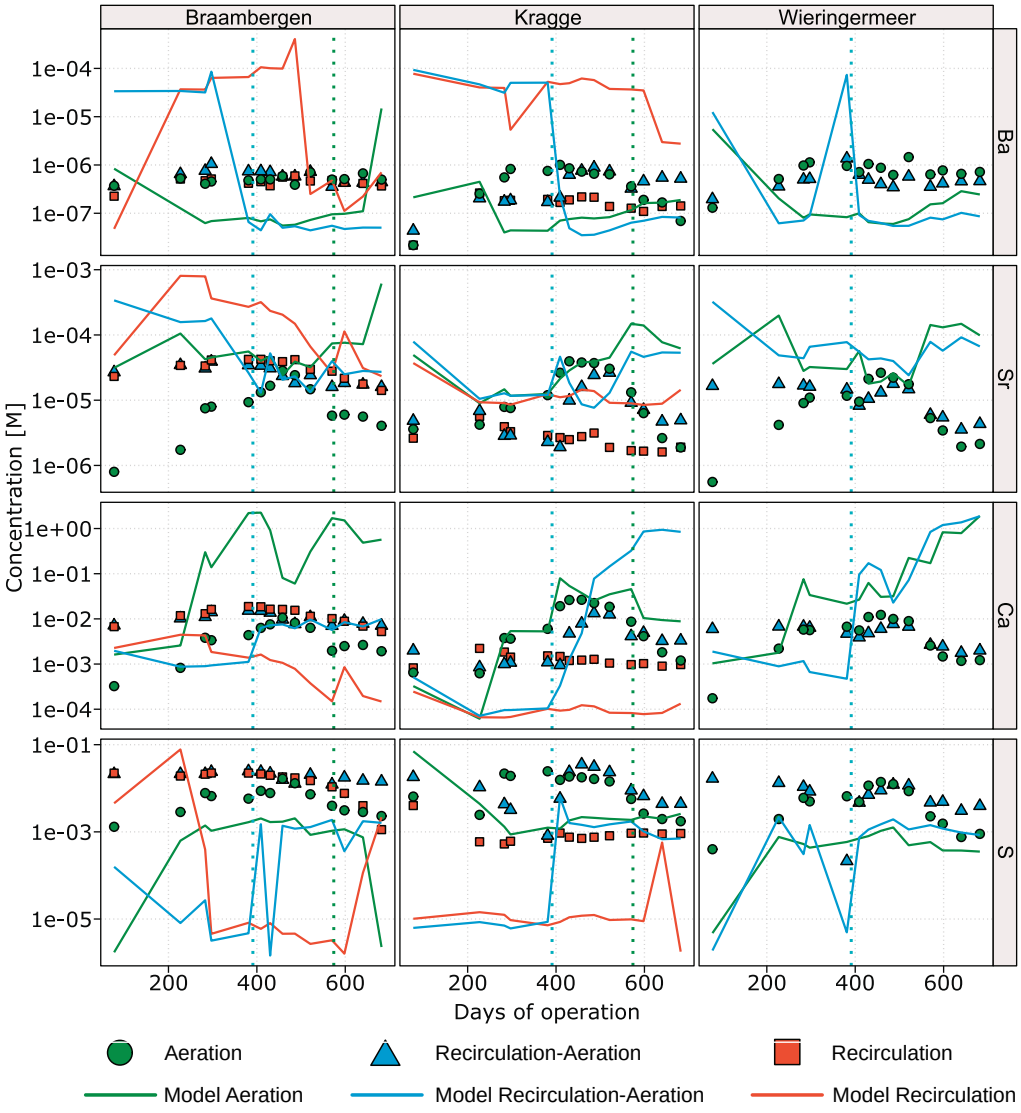


Figure S4.9 Measured (symbols) and modelled (lines) concentrations of contaminants in the LSR leachates during LSR operation under different operational conditions. The vertical dotted lines indicate the date at which the Recirculation-Aeration LSR switched from recirculation to aeration (blue) and when the aeration LSRs of Braambergen and Kragge switched from aeration to anaerobic conditions (green)**.** *(Continued)*

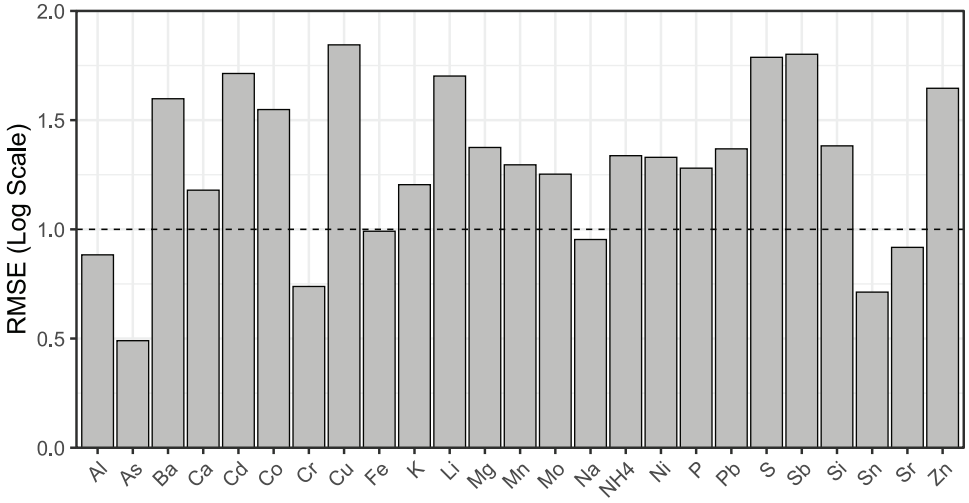


Figure S4.10 Root mean square error (RMSE) of the logarithmic difference between measured and modelled dissolved concentrations of elements in leachate of landfill simulation reactors operated under different conditions.

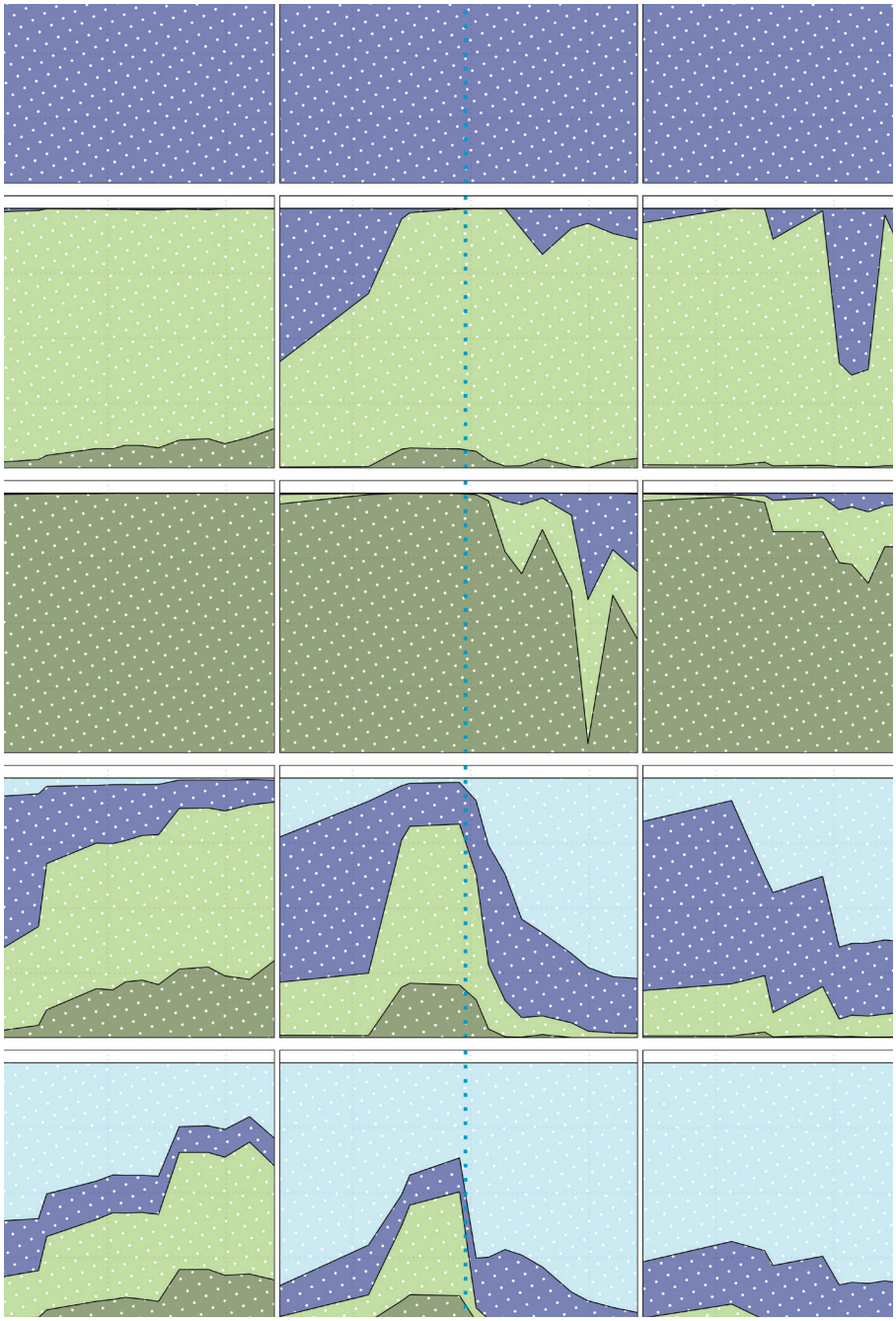


Figure S4.11 Model calculated dissolved phase speciation of contaminants in the Kragge LSRs as a function of time. The vertical dotted lines indicate the date at which the Recirculation-Aeration LSR switched from recirculation to aeration (blue) and when the aeration LSRs of Braambergen and Kragge switched from aeration to anaerobic conditions (green).

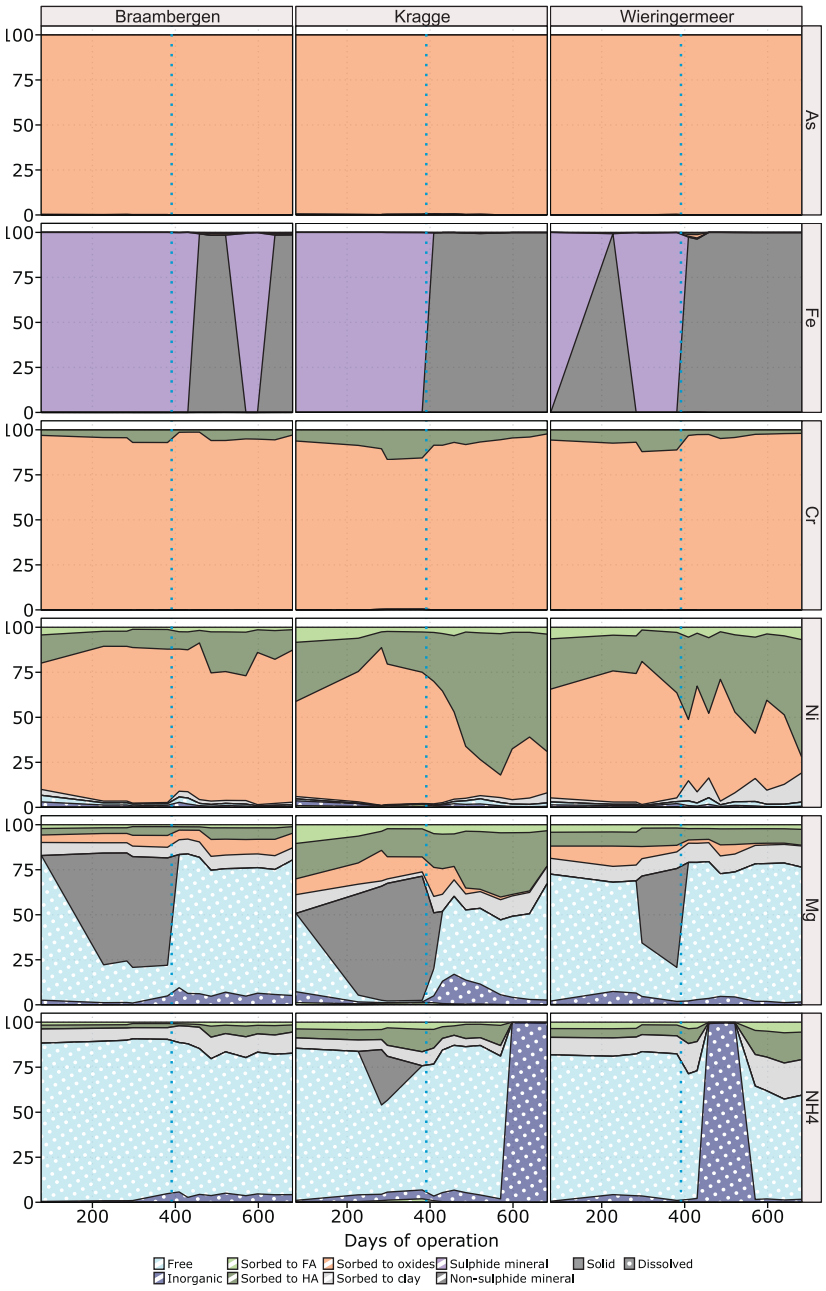


Figure S4.12 Model calculated solid and dissolved phase speciation of contaminants in all Recirculation-Aeration LSRs as a function of time. The blue vertical dotted lines indicate the date at which the Recirculation-Aeration LSR switched from recirculation to aeration.

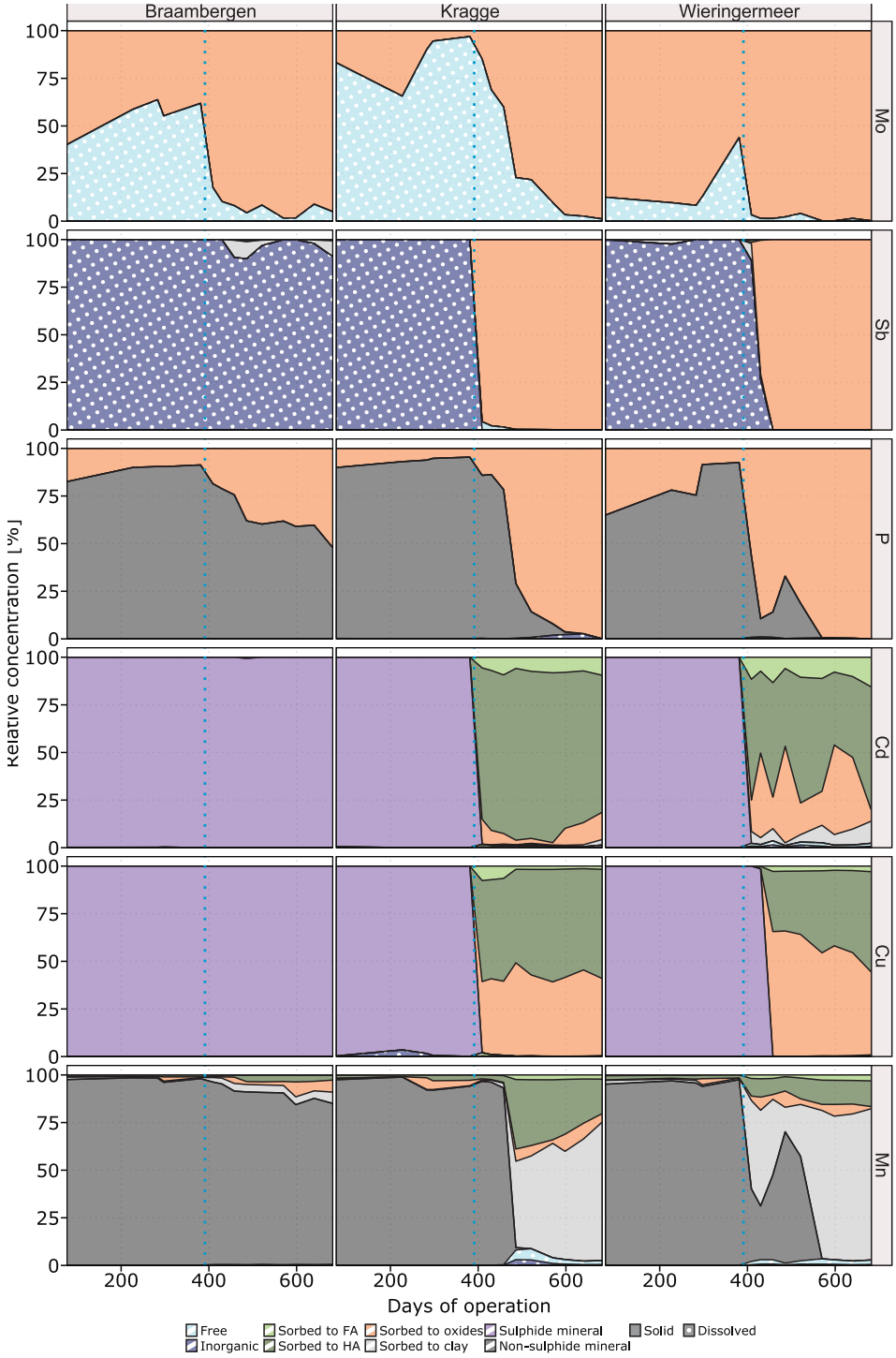


Figure S4.12 Model calculated solid and dissolved phase speciation of contaminants in all Recirculation-Aeration LSRs as a function of time. The blue vertical dotted lines indicate the date at which the Recirculation-Aeration LSR switched from recirculation to aeration *(Continued)*

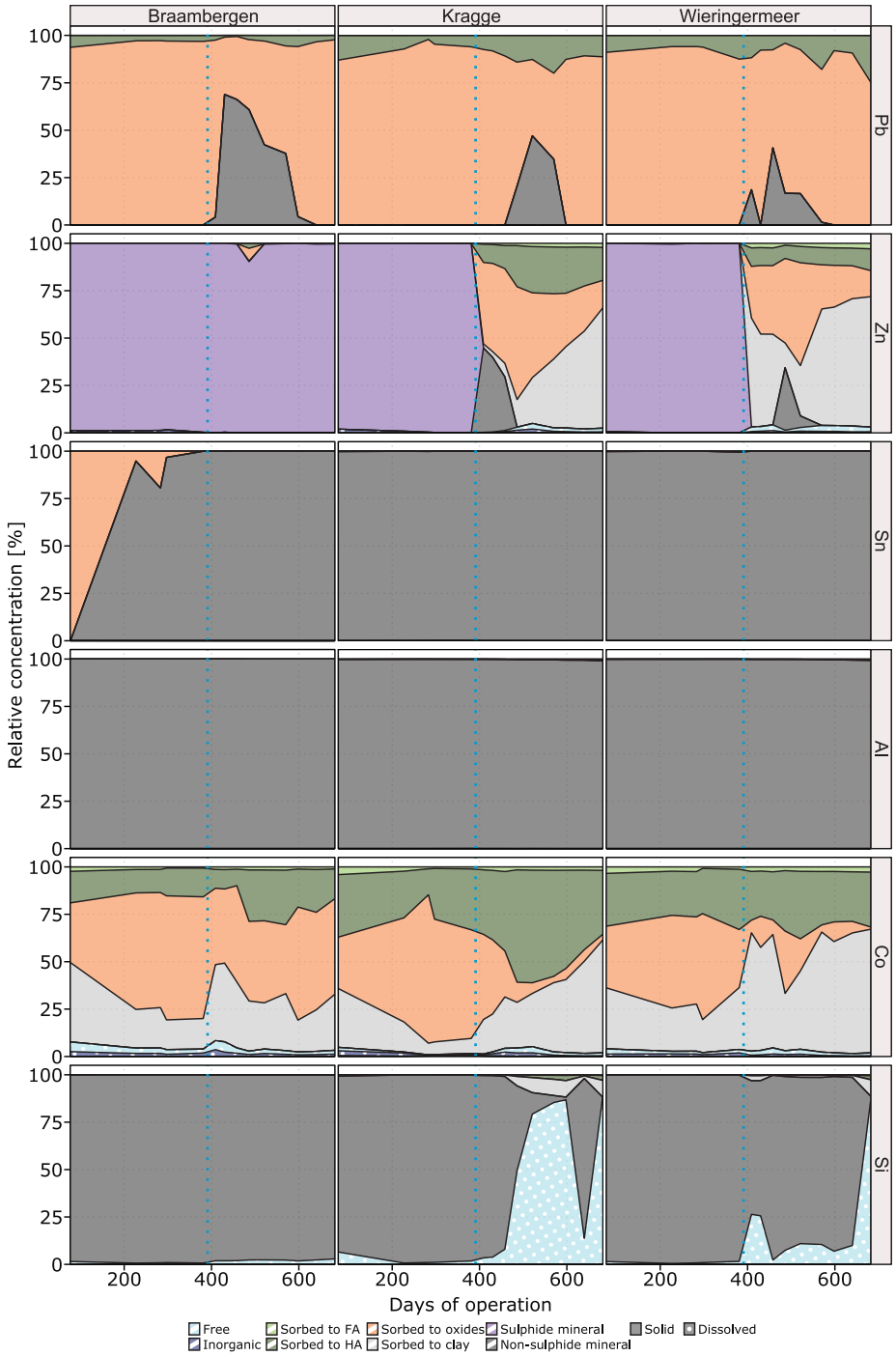


Figure S4.12 Model calculated solid and dissolved phase speciation of contaminants in all Recirculation-Aeration LSRs as a function of time. The blue vertical dotted lines indicate the date at which the Recirculation-Aeration LSR switched from recirculation to aeration *(Continued)*

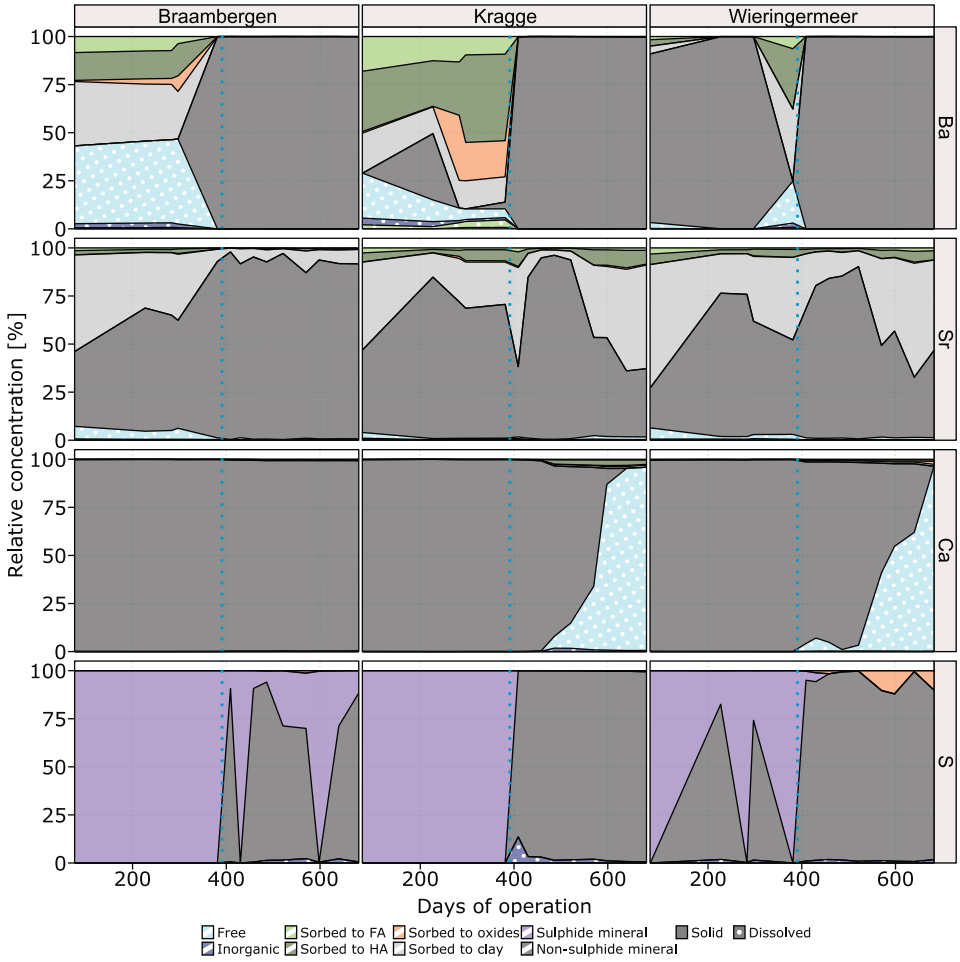


Figure S4.12 *Model calculated solid and dissolved phase speciation of contaminants in all Recirculation-Aeration LSRs as a function of time. The blue vertical dotted lines indicate the date at which the Recirculation-Aeration LSR switched from recirculation to aeration (Continued)*

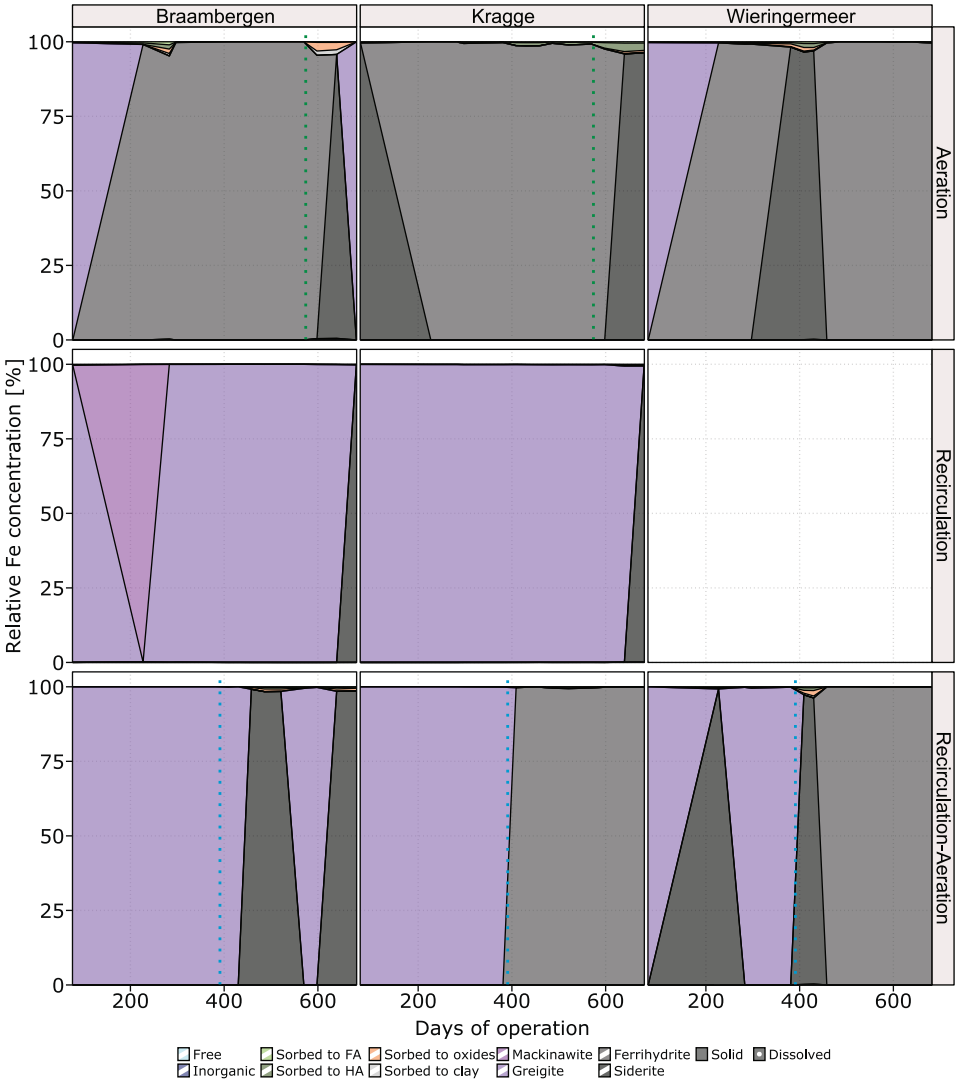


Figure S4.13 Model calculated solid and dissolved phase speciation of Fe in all LSRs as a function of time. The vertical dotted lines indicate the date at which the Recirculation-Aeration LSR switched from recirculation to aeration (blue) and when the aeration LSRs of Braambergen and Kragge switched from aeration to anaerobic conditions (green).

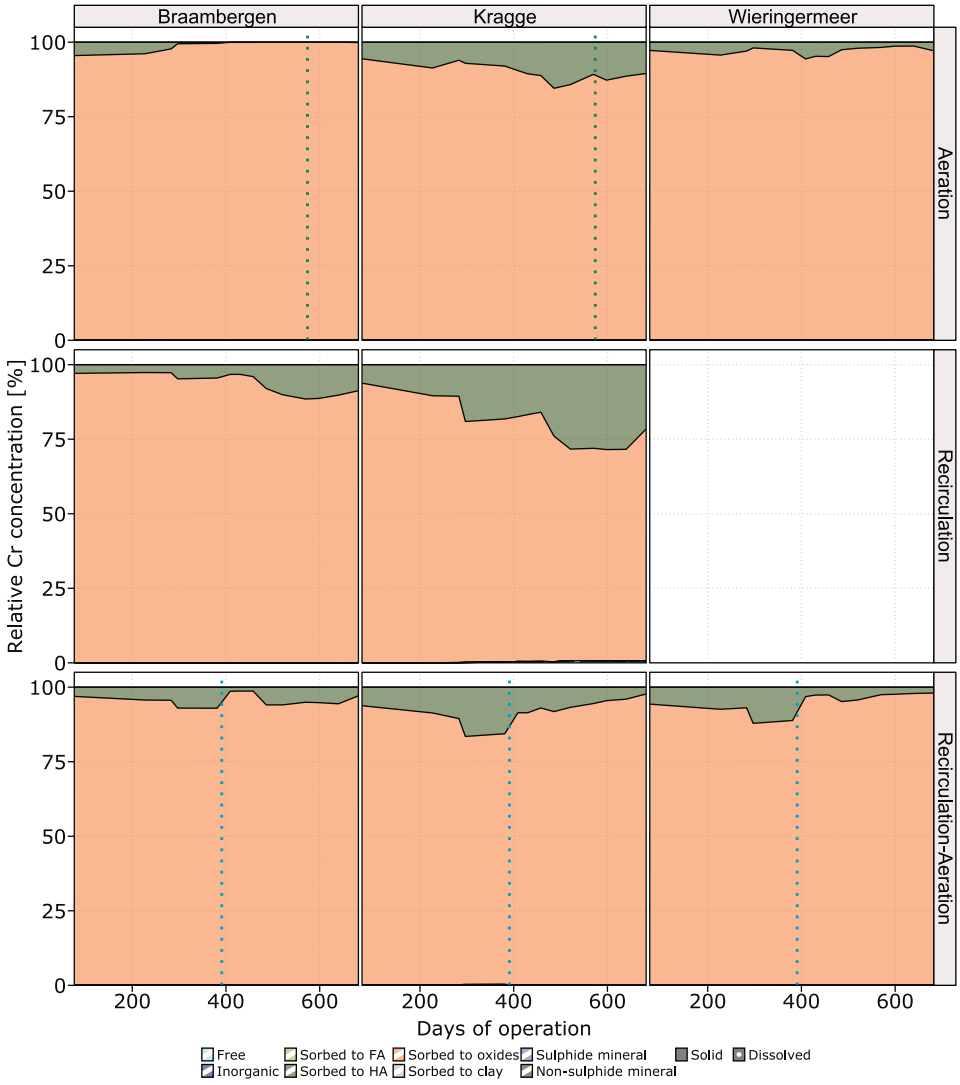


Figure S4.14 Model calculated solid and dissolved phase speciation of Cr in all LSRs as a function of time. The vertical dotted lines indicate the date at which the Recirculation-Aeration LSR switched from recirculation to aeration (blue) and when the aeration LSRs of Braambergen and Kragge switched from aeration to anaerobic conditions (green).

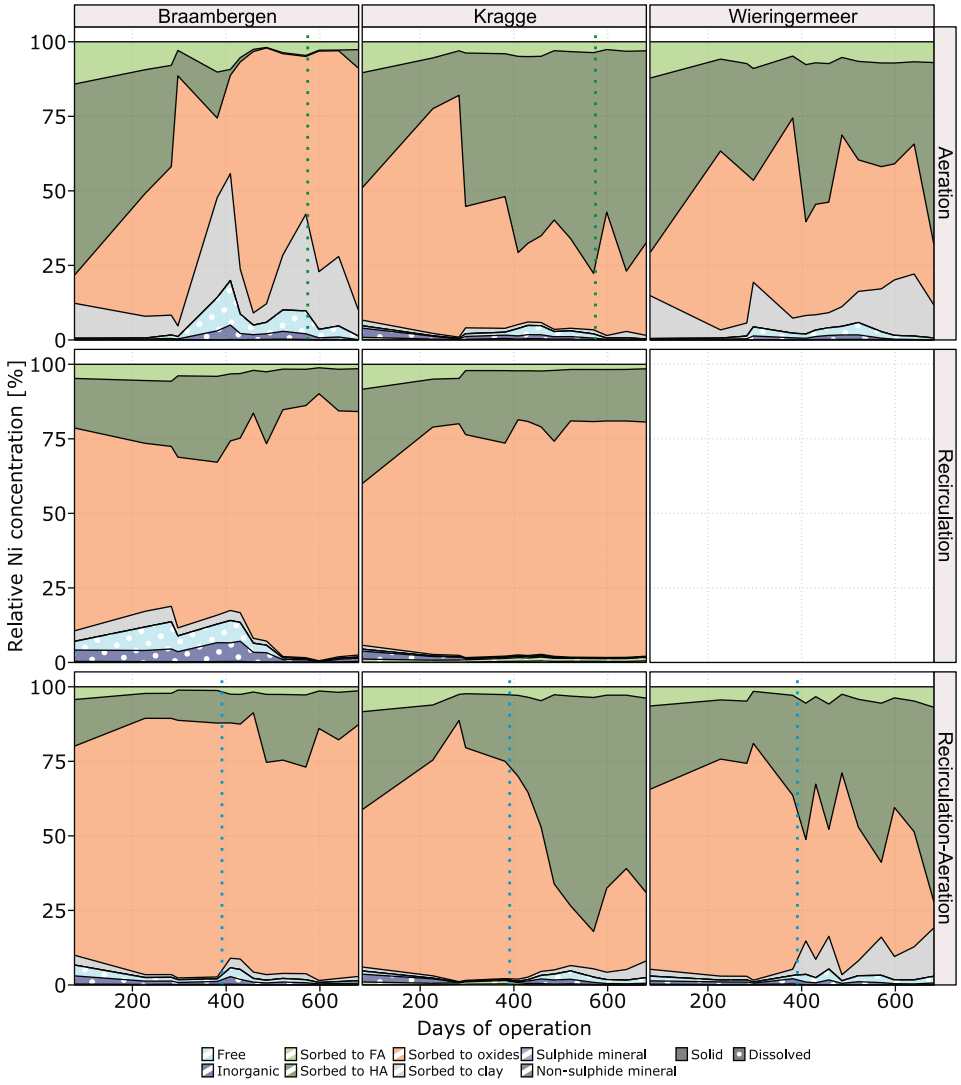


Figure S4.15 Model calculated solid and dissolved phase speciation of Ni in all LSRs as a function of time. The vertical dotted lines indicate the date at which the Recirculation-Aeration LSR switched from recirculation to aeration (blue) and when the aeration LSRs of Braambergen and Kragge switched from aeration to anaerobic conditions (green).

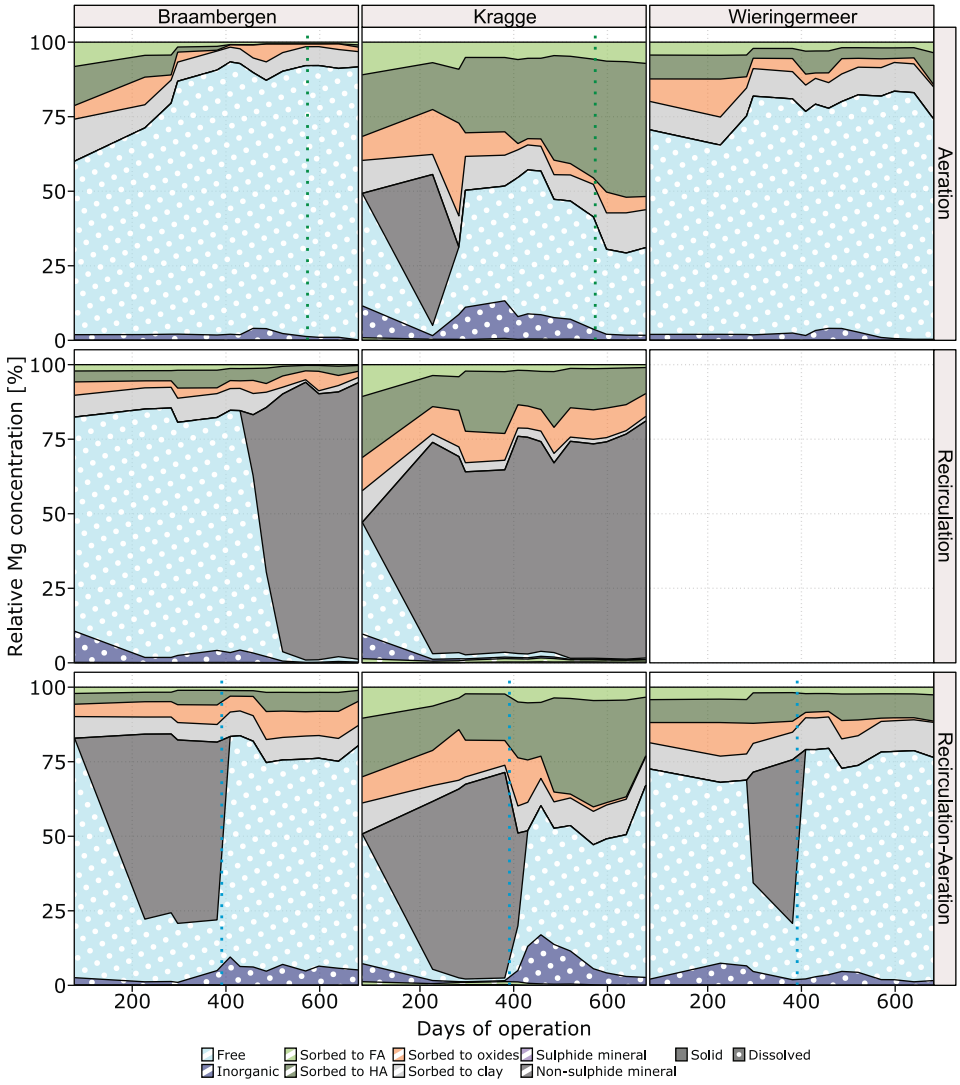


Figure S4.16 Model calculated solid and dissolved phase speciation of Mg in all LSRs as a function of time. The vertical dotted lines indicate the date at which the Recirculation-Aeration LSR switched from recirculation to aeration (blue) and when the aeration LSRs of Braambergen and Kragge switched from aeration to anaerobic conditions (green).

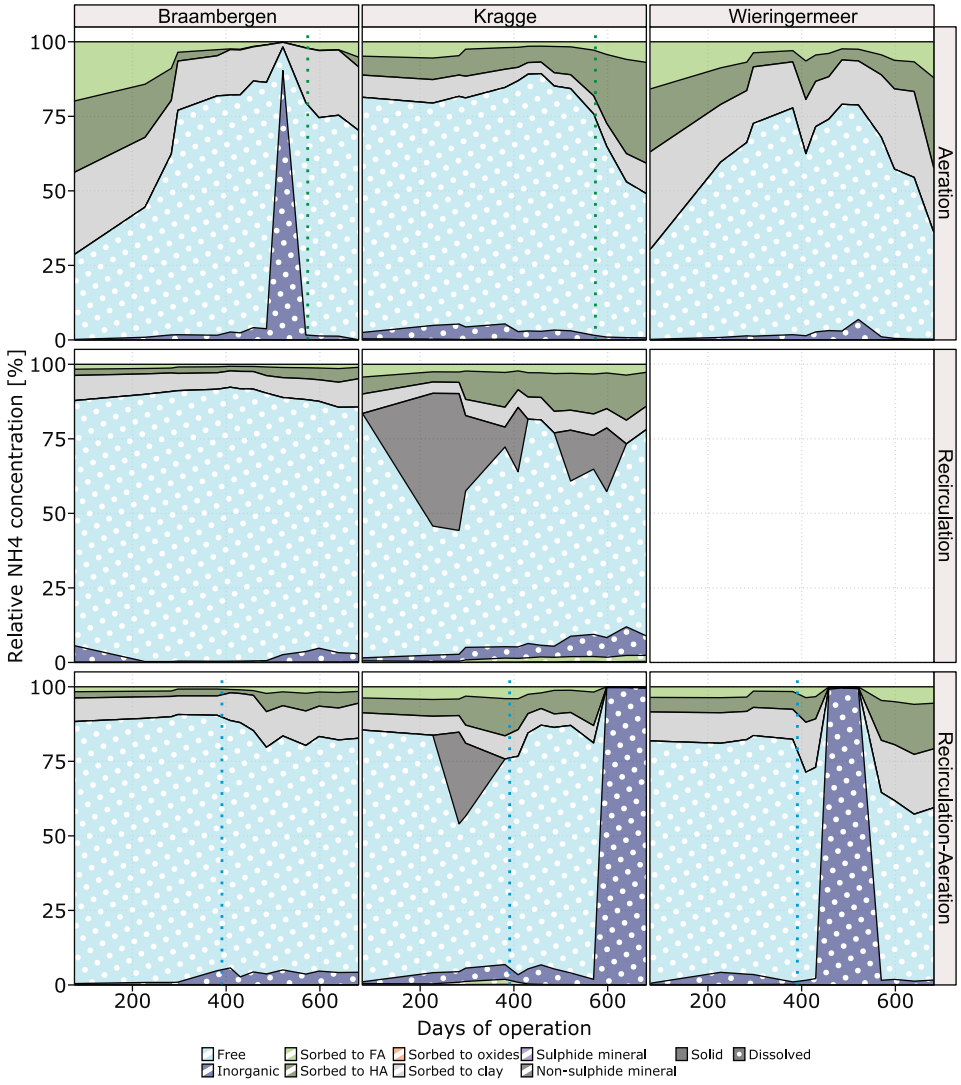


Figure S4.17 Model calculated solid and dissolved phase speciation of NH4+ in all LSRs as a function of time. The vertical dotted lines indicate the date at which the Recirculation-Aeration LSR switched from recirculation to aeration (blue) and when the aeration LSRs of Braambergen and Kragge switched from aeration to anaerobic conditions (green).



Supplementary information chapter 5

GEOCHEMICAL PROCESSES CONTROLLING IN-SITU CONTAMINANT SOLUBILITY IN LANDFILLS

SM5.1 Grout tests

The VMS were installed using a grout mixture to ensure there is proper contact between sampling ports and surrounding waste. Considering the found elevated pH values together with inconsistent contaminant concentrations measured in certain ports, there is a likelihood of grout leakage. The influence of this grout leakage on OM behaviour was investigated in two steps.

Firstly, batch leaching tests were conducted, in which solid waste samples were extracted with ultrapure water (UPW) at a L/S ratio of 10 in six parallel batches at different pH levels. To achieve this, pH was manipulated by adding the grout mixture as used during VMS installation. After 48 hours of equilibrium, the samples were centrifuged at 3750 RPM for 20 minutes and subsequently filtered over a 0.45 µm filter. The filtrate was further treated with rapid batch fractionation (van Zomeren & Comans, 2007).

Secondly, the effect of elevated Al concentrations found in the grout on the coagulation of HA and FA were investigated. Batch systems were created with either HA (300 mg C l^{-1}) or FA (100 mg C l^{-1}) and 40 ml of UPW or with the addition of 0.56 mM $AlCl_3{}^*6\ H_2O$. The solutions were raised to pH 12 either through addition of 1 M NaOH or through addition of the original grout mixture. The solutions were equilibrated end-over-end for 48 hours at 30 RPM, centrifuged for 20 minutes at 3750 RPM, and decanted. The supernatants were filtered over a 0.45 µm syringe filter and an aliquot was brought to pH 8.75 – 9.5 and measured for DOC. Remaining solution was once more subjected to rapid batch fractionation.

Supplementary Figures

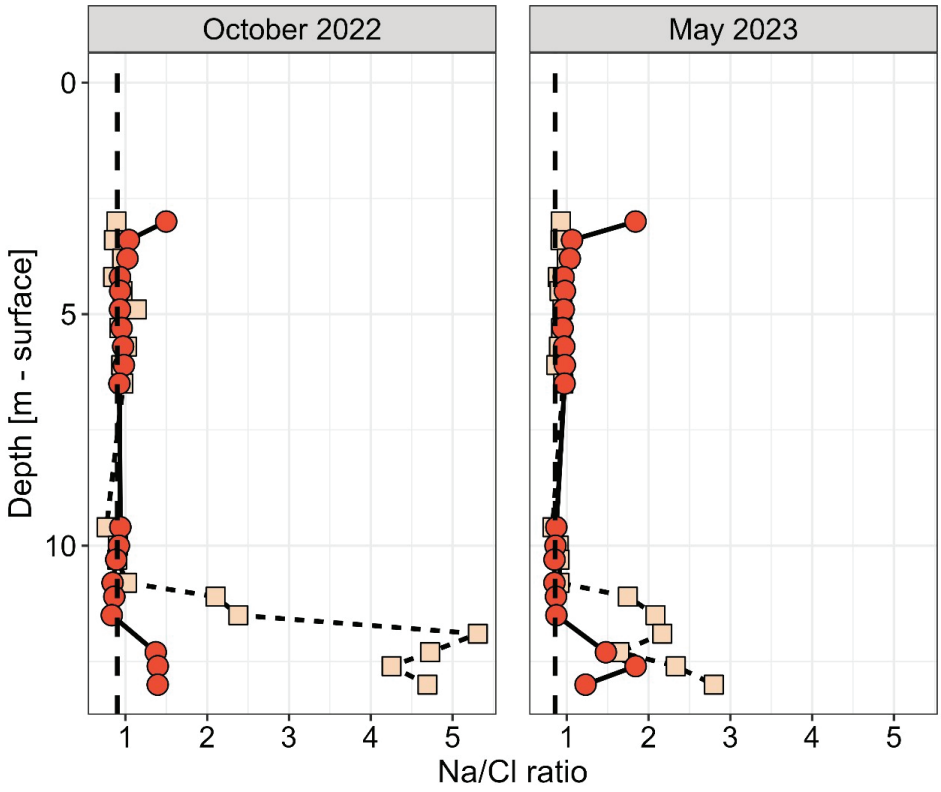


Figure S5.1 The sodium to chloride ratio as a function of depth in two vadose monitoring systems (VMS), VMS A (red circles), VMS B (beige squares), and leachate sampled simultaneously (dashed line) in October 2022 (left) and May 2023 (right).

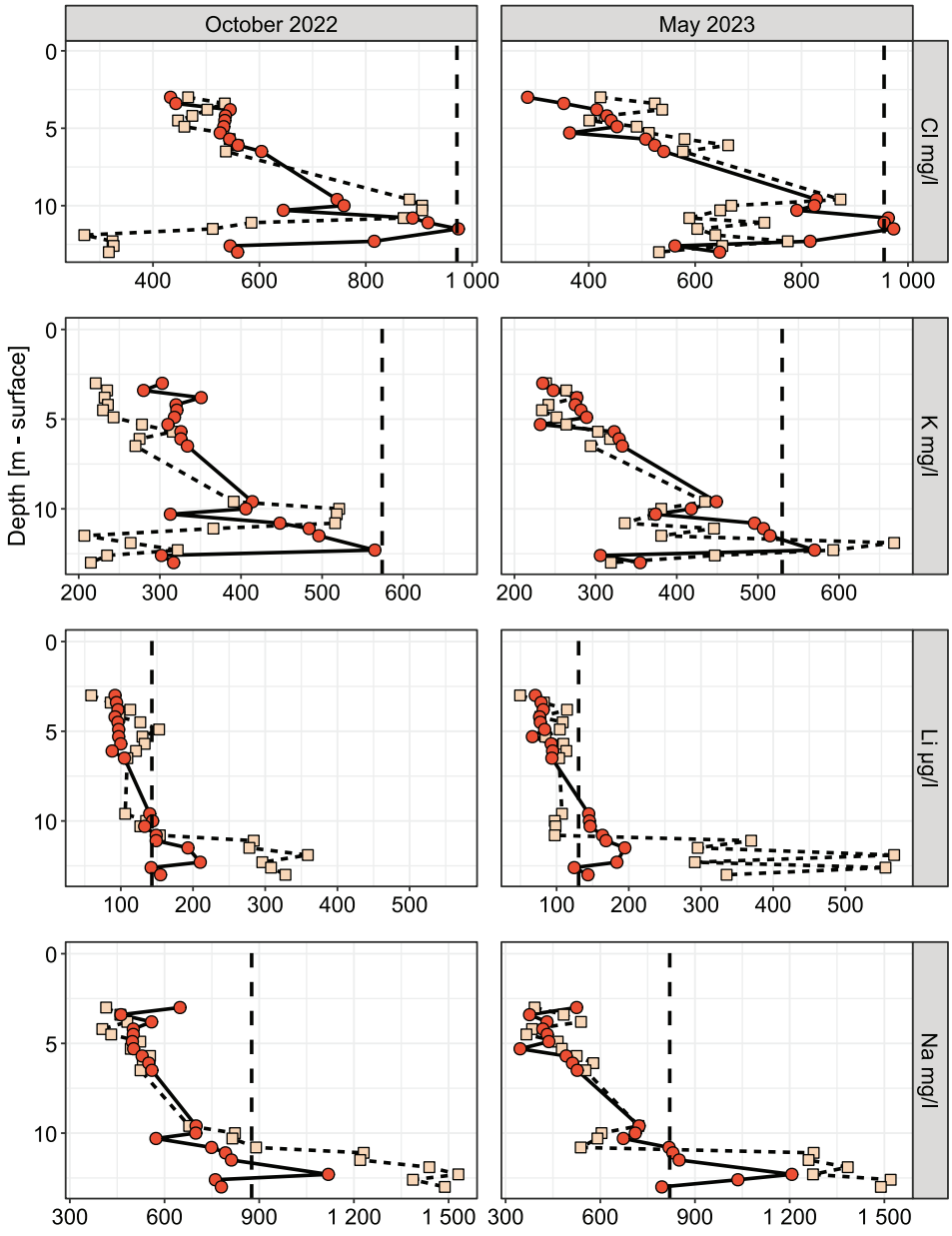


Figure S5.2 Measured concentrations of the non-reactive contaminant chloride (Cl), potassium (K), lithium (Li), and sodium (Na) as a function of depth in two vadose monitoring systems (VMS), VMS A (red circles), VMS B (beige squares), and leachate sampled simultaneously (dashed line) in October 2022 (left) and May 2023 (right).

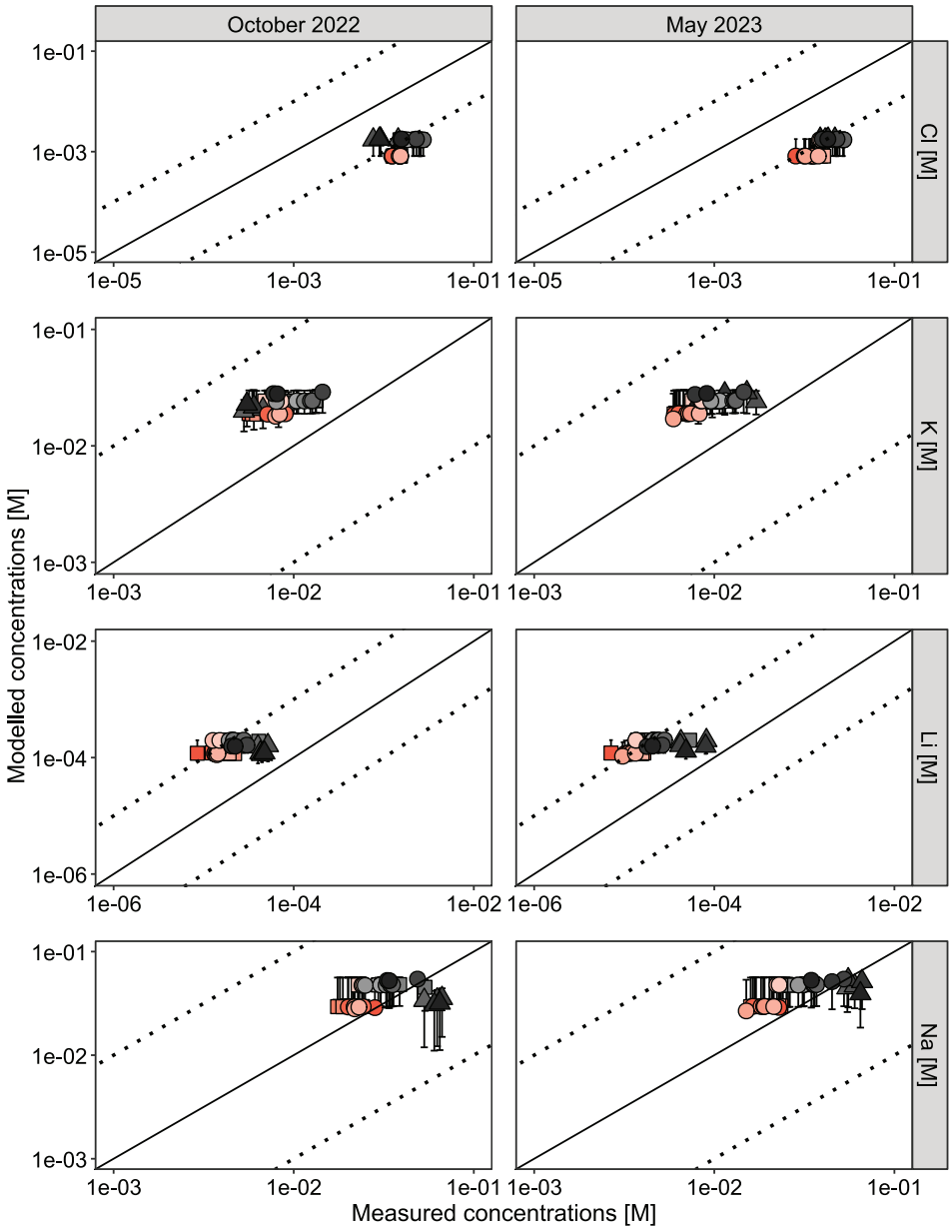


Figure S5.3 Measured pore water concentrations in VMS A (circles) and VMS B (squares) against model results of non-reactive contaminants in October 2022 (left) and May 2023 (right). The 1:1 line is represented by the solid line; 10 times higher and 10 times lower predicted concentrations are represented by dashed lines. VMS B ports influenced by grout leakage are marked by triangles. Sampling ports close to the surface are coloured red, deeper ports are coloured black.

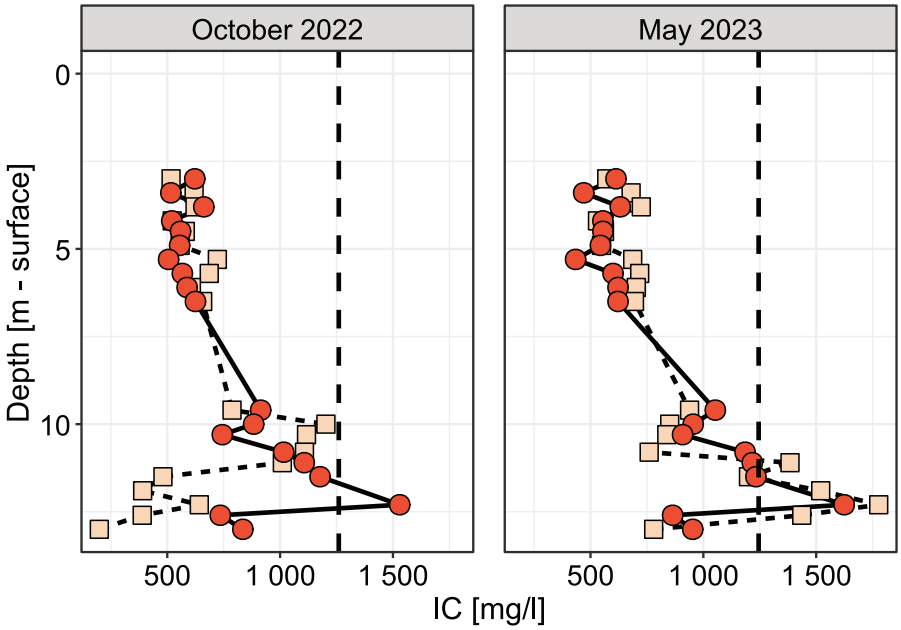


Figure S5.4 Measured inorganic carbon as a function of depth in two vadose monitoring systems (VMS), VMS A (red circles), VMS B (beige squares), and leachate sampled simultaneously (dashed line) in October 2022 (left) and May 2023 (right).

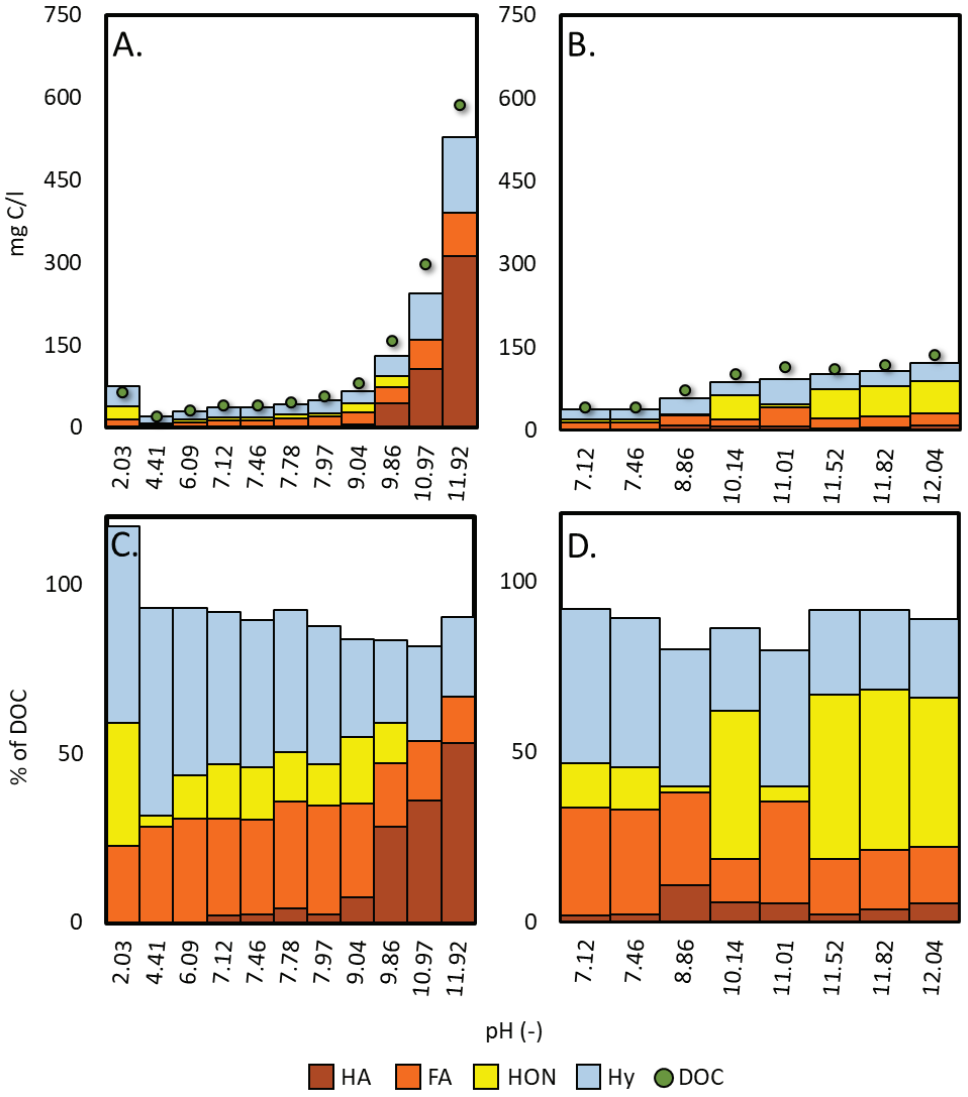


Figure S5.5 Humic substance fractions and total dissolved organic carbon measured in 1:10 water:waste solutions with solution pH adjusted using A) 0.1 M HCl and 0.1 M NaOH; B) grout used to fill the vadose monitoring systems. Relative amounts of humic substance fractions of DOC measured in 1:10 water:waste solutions with solution pH adjusted using C) 0.1 M HCl and 0.1 M NaOH; D) grout used to fill the vadose monitoring systems.

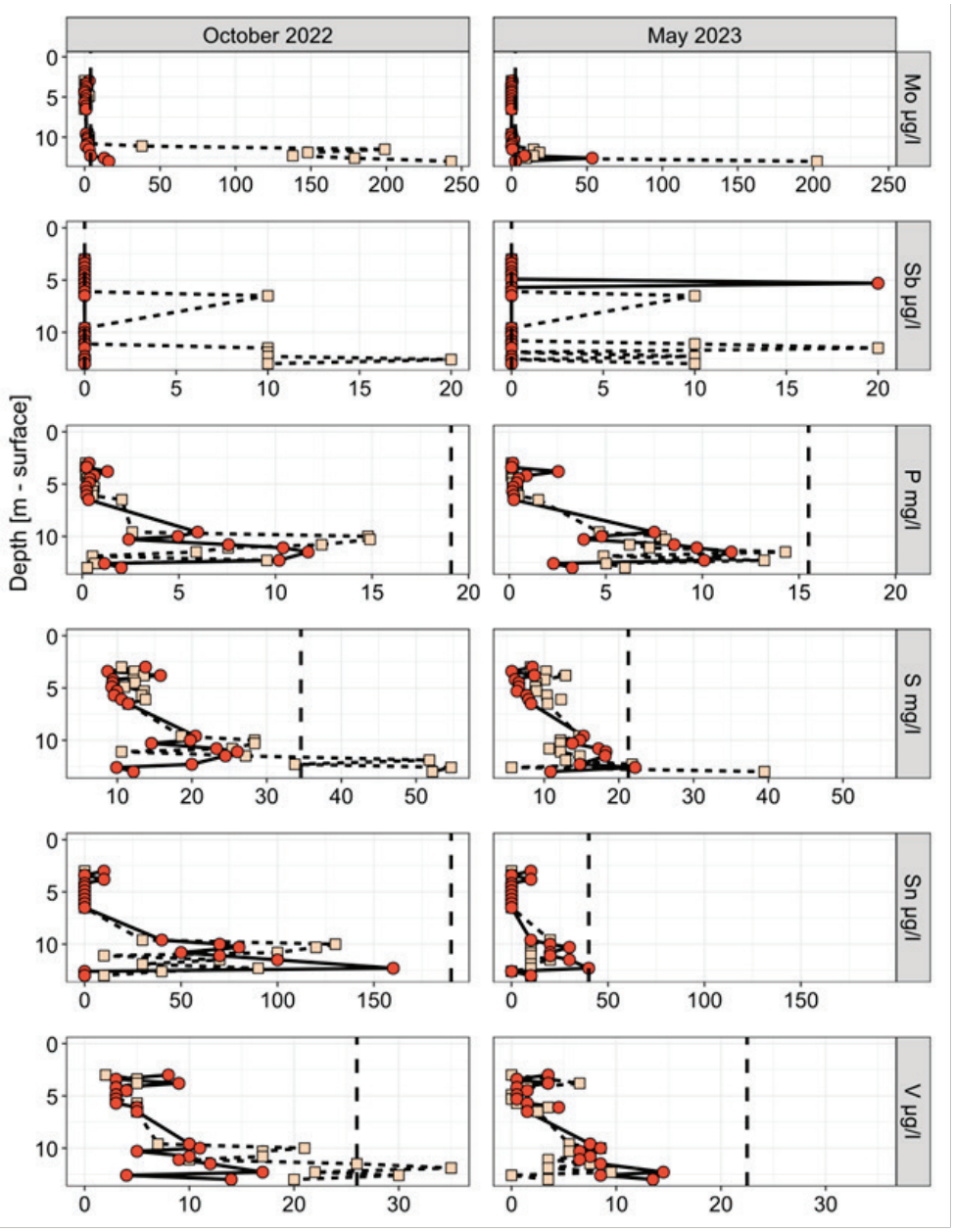


Figure S5.6 Measured concentrations of reactive ions as a function of depth in two vadose monitoring systems (VMS), VMS A (red circles), VMS B (beige squares), and leachate sampled simultaneously (dashed line) in October 2022 (left) and May 2023 (right).

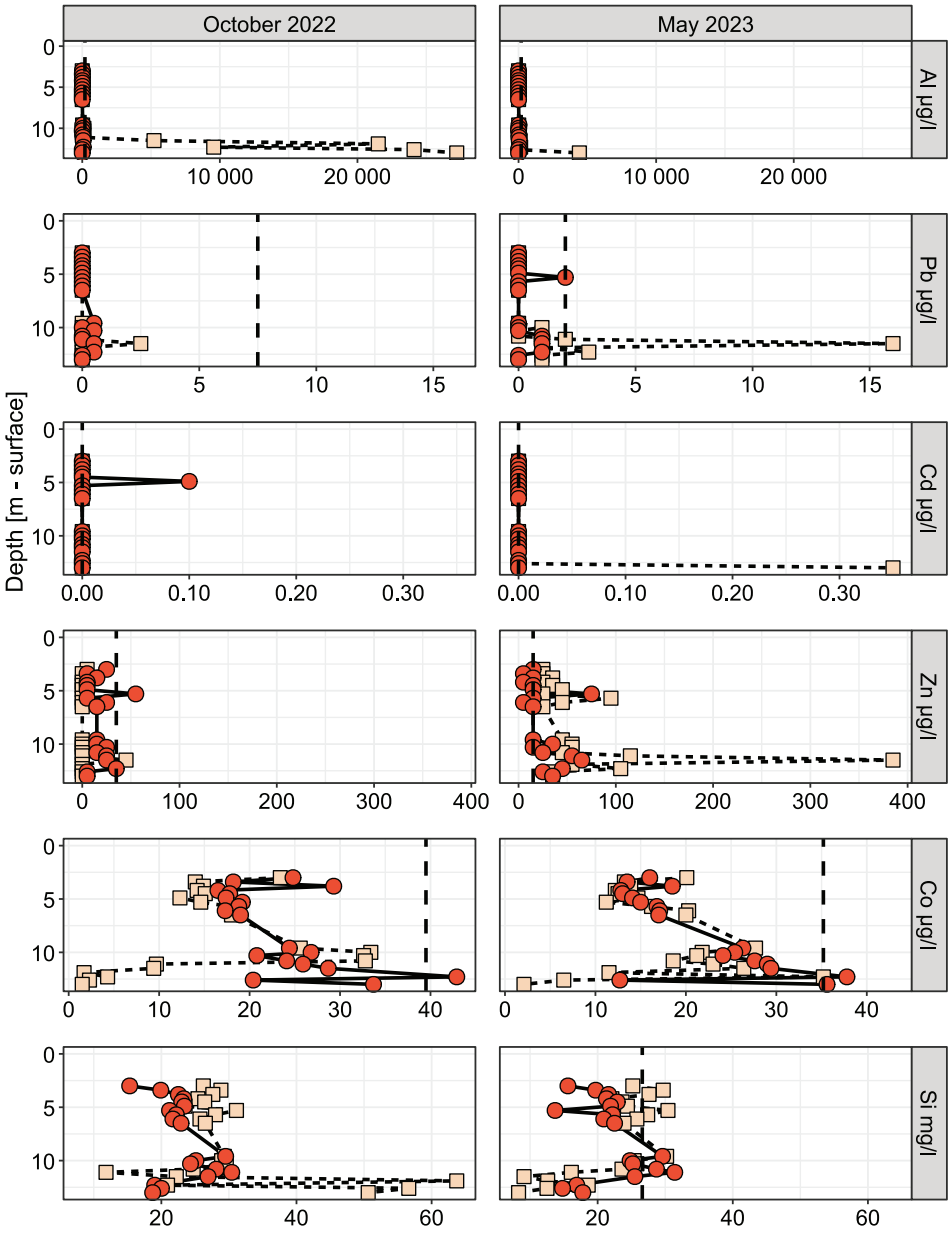


Figure S5.6 Measured concentrations of reactive ions as a function of depth in two vadose monitoring systems (VMS), VMS A (red circles), VMS B (beige squares), and leachate sampled simultaneously (dashed line) in October 2022 (left) and May 2023 (right). (*Continued*)

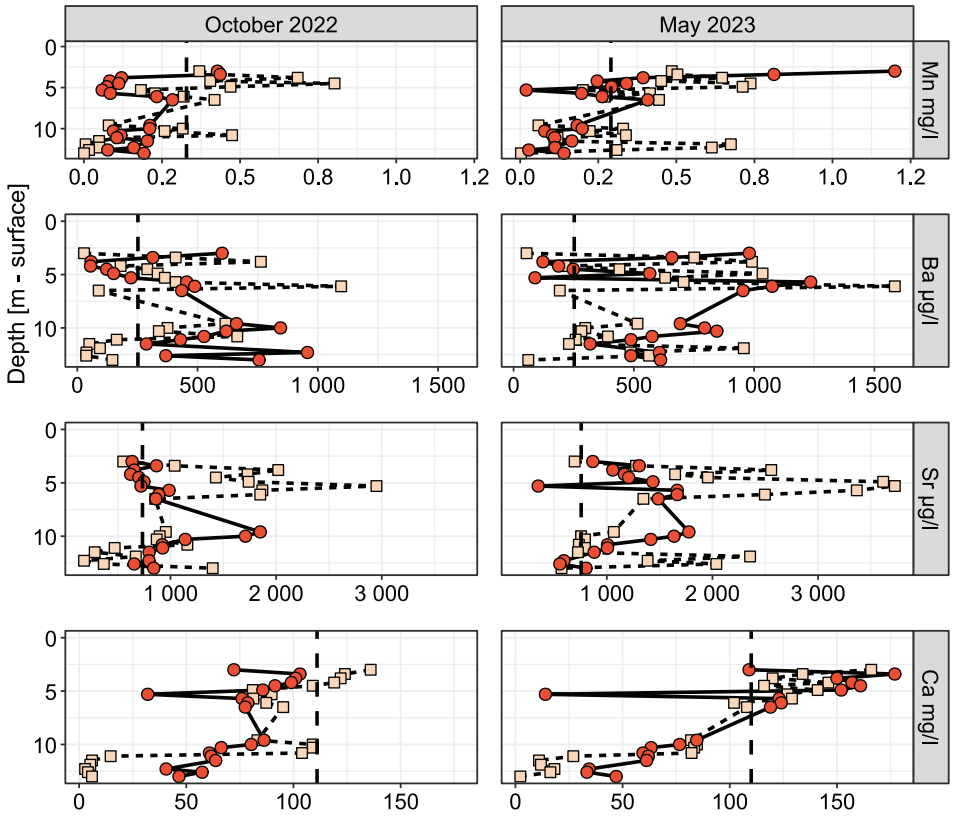


Figure S5.6 Measured concentrations of reactive ions as a function of depth in two vadose monitoring systems (VMS), VMS A (red circles), VMS B (beige squares), and leachate sampled simultaneously (dashed line) in October 2022 (left) and May 2023 (right). (*Continued*)

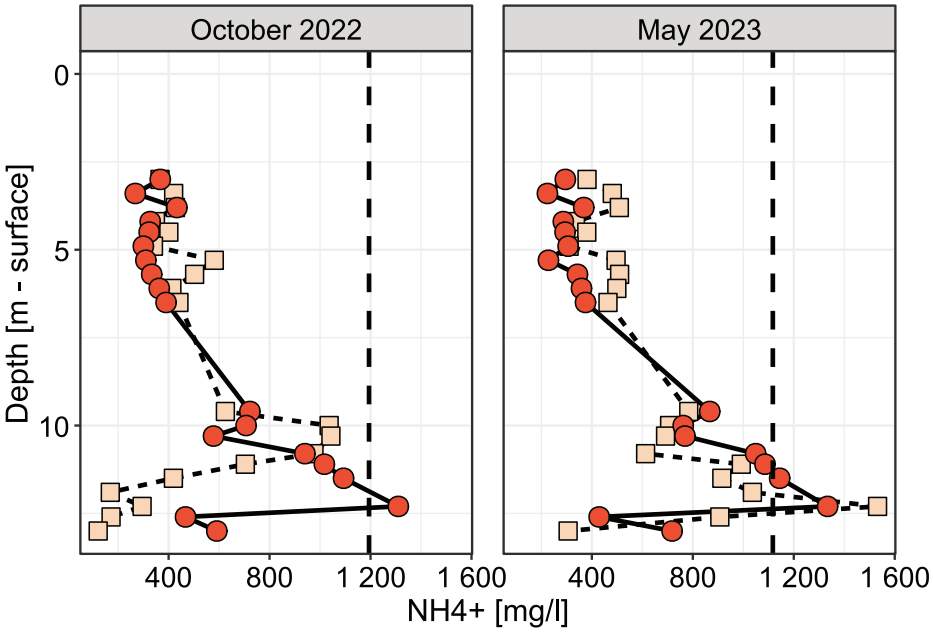


Figure S5.7 Ammonium concentration as a function of depth in two vadose monitoring systems (VMS), VMS A (red circles), VMS B (beige squares), and leachate sampled simultaneously (dashed line) in October 2022 (left) and May 2023 (right).

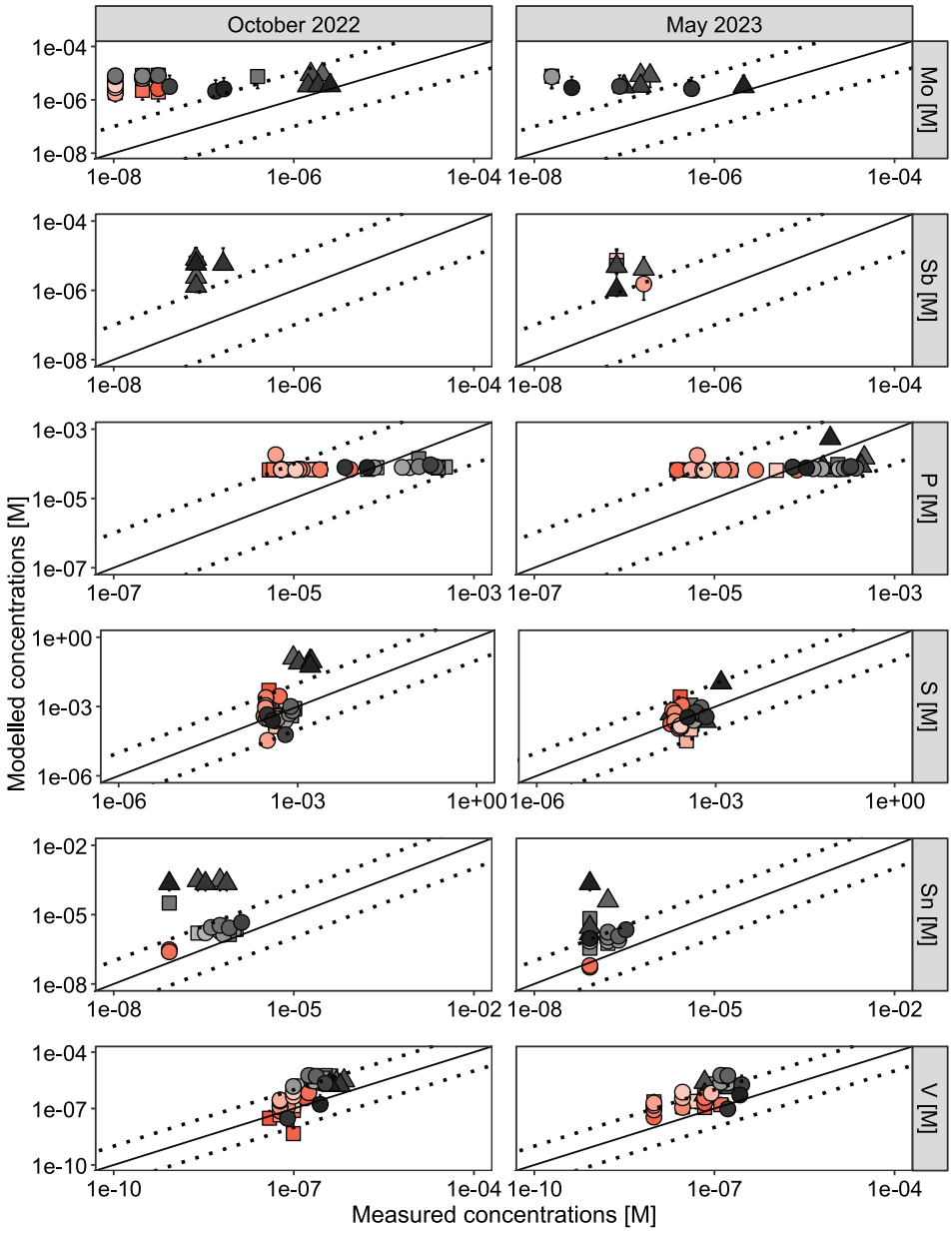


Figure S5.8 Measured pore water concentrations in VMS A (circles) and VMS B (squares) against model results of reactive contaminants in October 2022 (left) and May 2023 (right). The 1:1 line is represented by the solid line; 10 times higher and 10 times lower predicted concentrations are represented by dashed lines. VMS B ports influenced by grout leakage are marked by triangles. Sampling ports close to the surface are coloured red, deeper ports are coloured black.

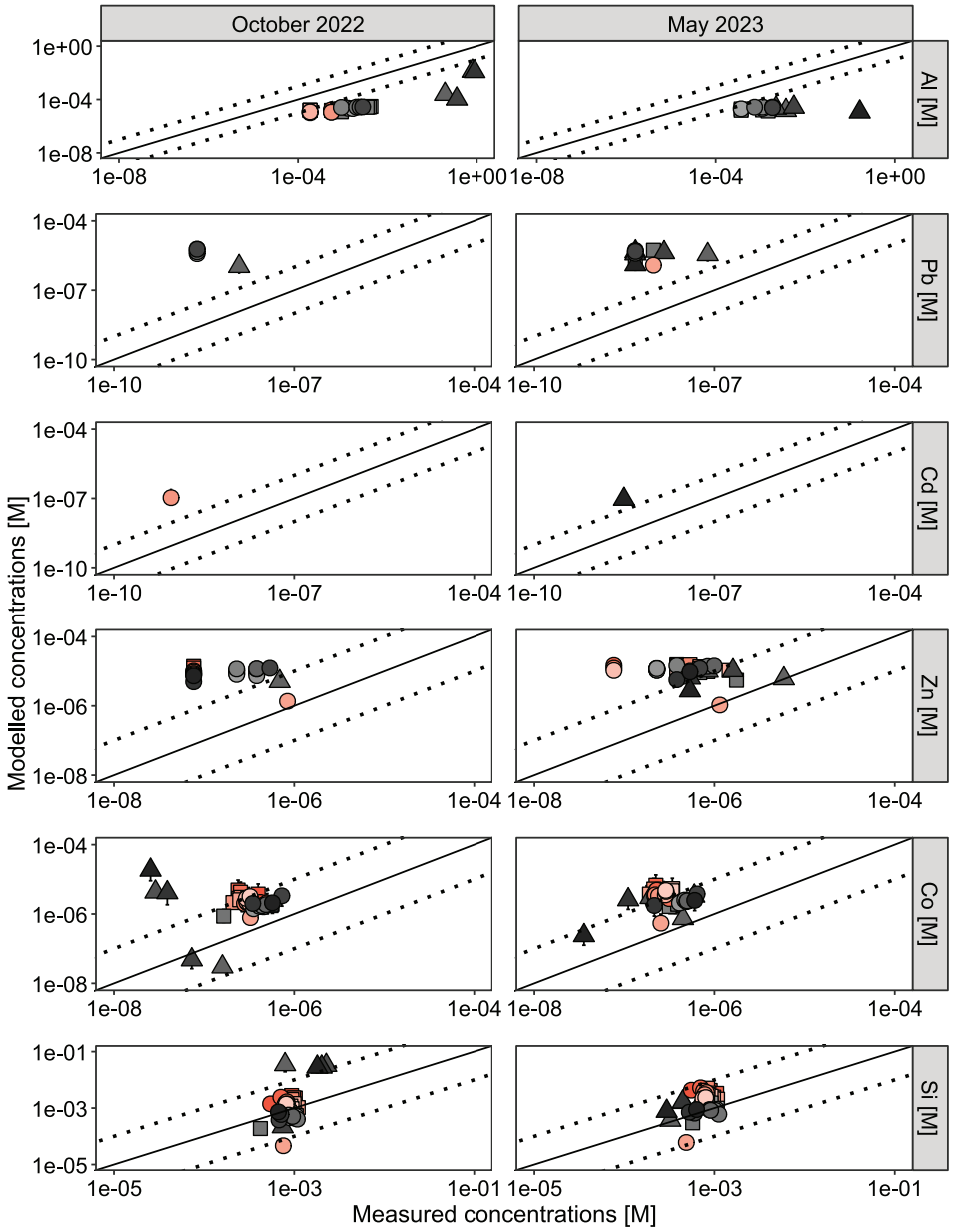


Figure S5.8 Measured pore water concentrations in VMS A (circles) and VMS B (squares) against model results of reactive contaminants in October 2022 (left) and May 2023 (right). The 1:1 line is represented by the solid line; 10 times higher and 10 times lower predicted concentrations are represented by dashed lines. VMS B ports influenced by grout leakage are marked by triangles. Sampling ports close to the surface are coloured red, deeper ports are coloured black. (*Continued*)

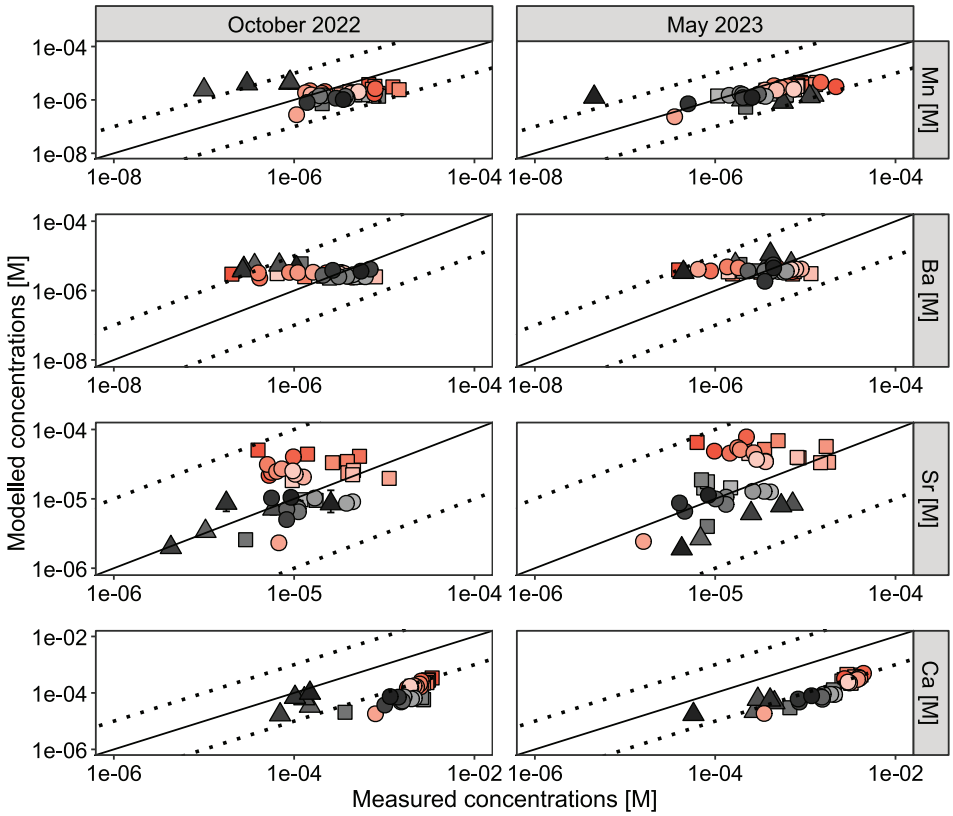


Figure S5.8 *Measured pore water concentrations in VMS A (circles) and VMS B (squares) against model results of reactive contaminants in October 2022 (left) and May 2023 (right). The 1:1 line is represented by the solid line; 10 times higher and 10 times lower predicted concentrations are represented by dashed lines. VMS B ports influenced by grout leakage are marked by triangles. Sampling ports close to the surface are coloured red, deeper ports are coloured black.* (Continued)

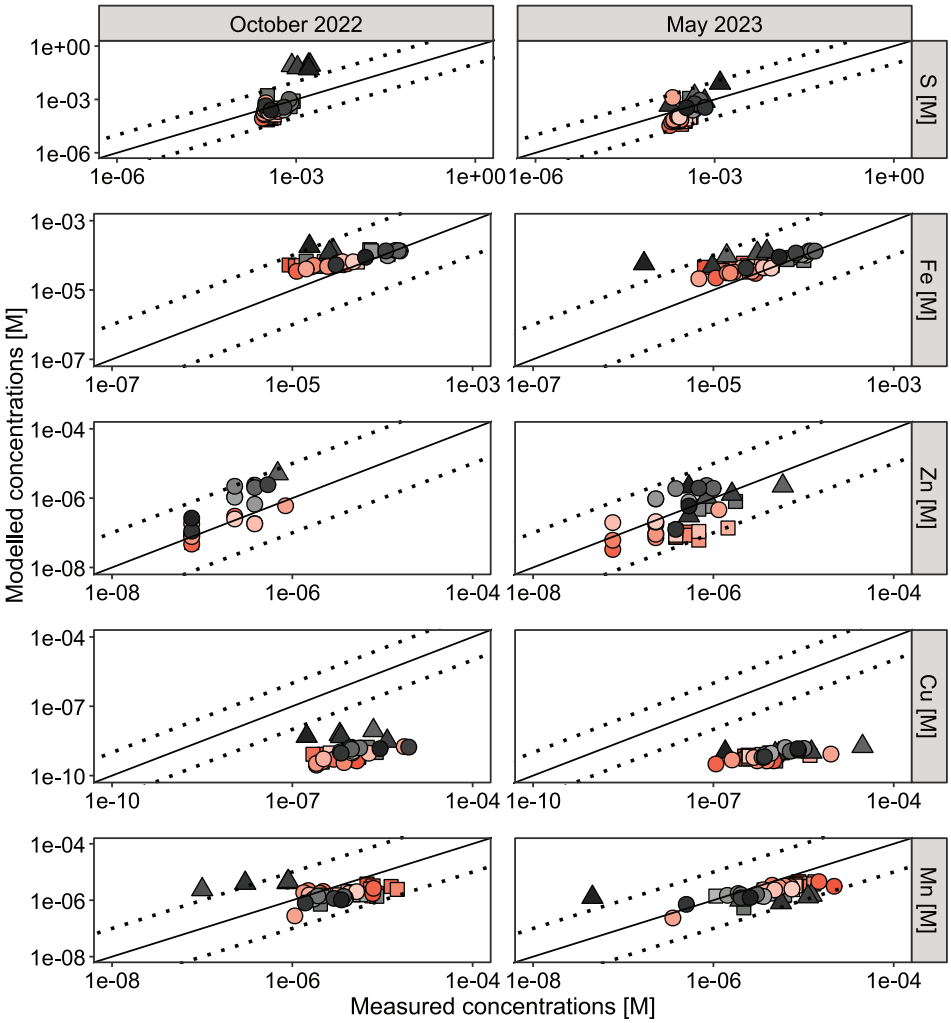


Figure S5.9 Measured pore water concentrations in VMS A (circles) and VMS B (squares) against model results at a more reduced condition of pH + pe = 4 of redox-sensitive contaminants, in October 2022 (left) and May 2023 (right). The 1:1 line is represented by the solid line; 10 times higher and 10 times lower predicted concentrations are represented by dashed lines. VMS B ports influenced by grout leakage are marked by triangles. Sampling ports close to the surface are coloured red, deeper ports are coloured black.

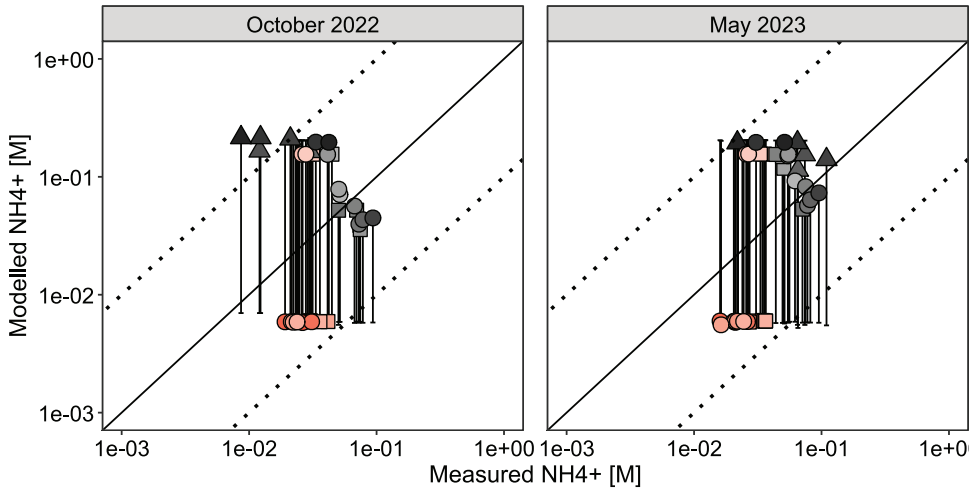


Figure S5.10 Measured pore water concentrations in VMS A (circles) and VMS B (squares) against model results of ammonium in October 2022 (left) and May 2023 (right). The 1:1 line is represented by the solid line; 10 times higher and 10 times lower predicted concentrations are represented by dashed lines. VMS B ports influenced by grout leakage are marked by triangles. Sampling ports close to the surface are coloured red, deeper ports are coloured black.

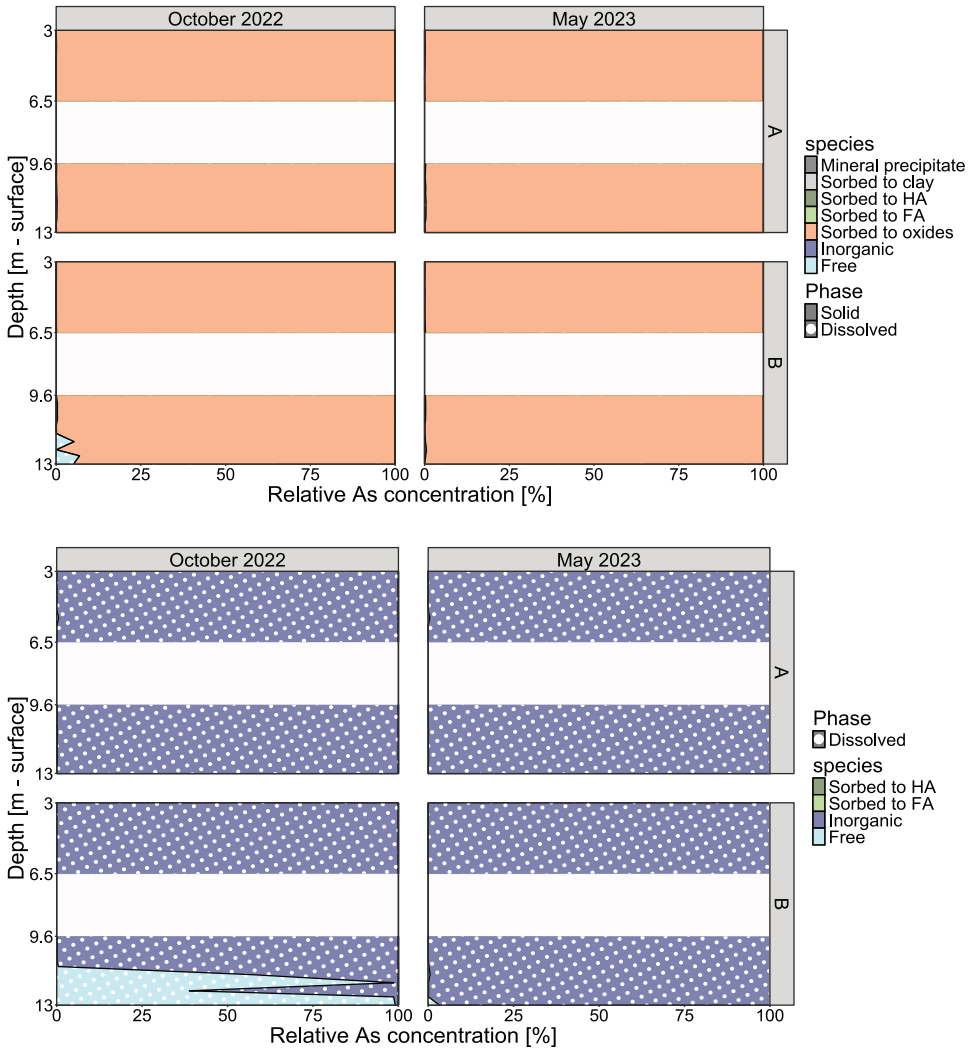


Figure S5.11 Geochemical model calculated solid phase (top) and dissolved phase (bottom) speciation of arsenic in landfill pore water as a function of depth in vadose monitoring systems (VMS) A and B in October 2022 and May 2023. Important to note model calculations below 11 metres for VMS B in October 2022 are inadequate.

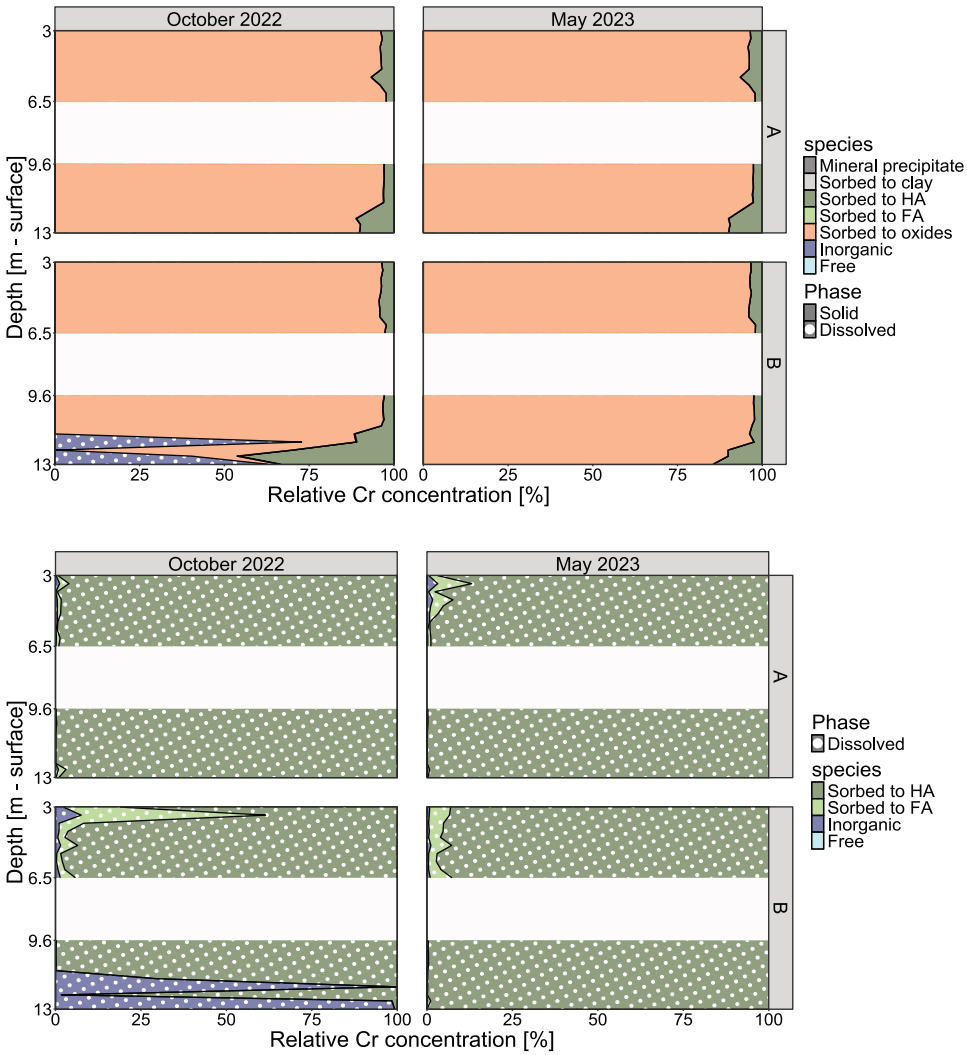


Figure S5.12 Geochemical model calculated solid phase (top) and dissolved phase (bottom) speciation of chromium in landfill pore water as a function of depth in vadose monitoring systems (VMS) A and B in October 2022 and May 2023. Important to note model calculations below 11 metres for VMS B in October 2022 are inadequate.

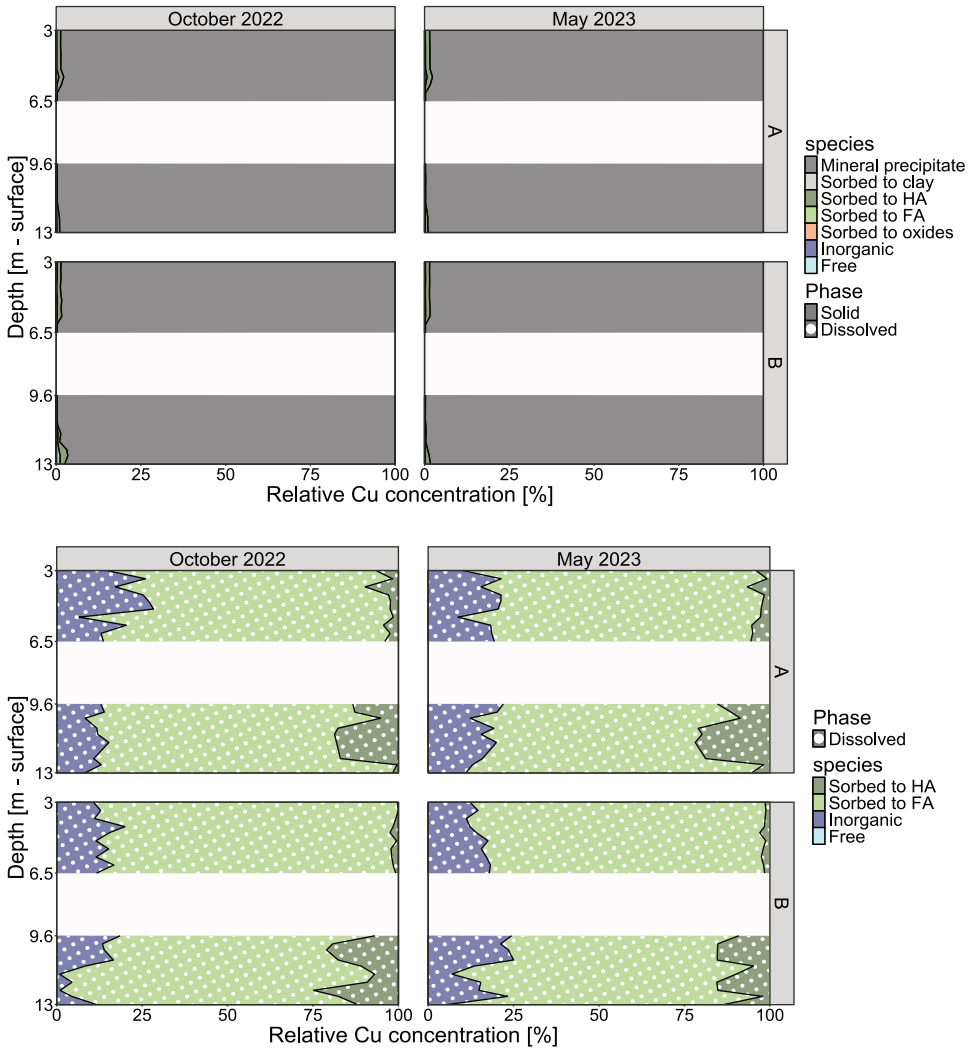


Figure S5.13 Geochemical model calculated solid phase (top) and dissolved phase (bottom) speciation of copper in landfill pore water as a function of depth in vadose monitoring systems (VMS) A and B in October 2022 and May 2023. Important to note model calculations below 11 metres for VMS B in October 2022 are inadequate.

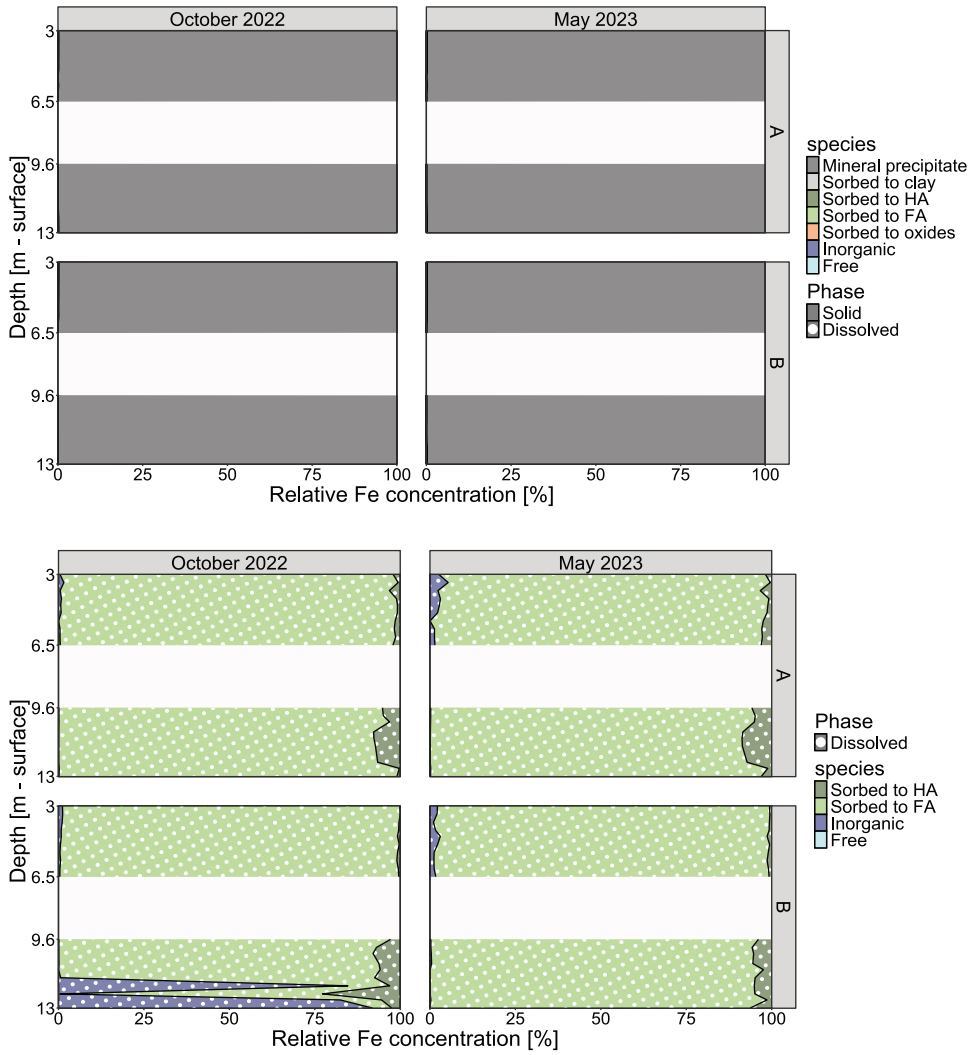


Figure S5.14 Geochemical model calculated solid phase (top) and dissolved phase (bottom) speciation of iron in landfill pore water as a function of depth in vadose monitoring systems (VMS) A and B in October 2022 and May 2023. Important to note model calculations below 11 metres for VMS B in October 2022 are inadequate.

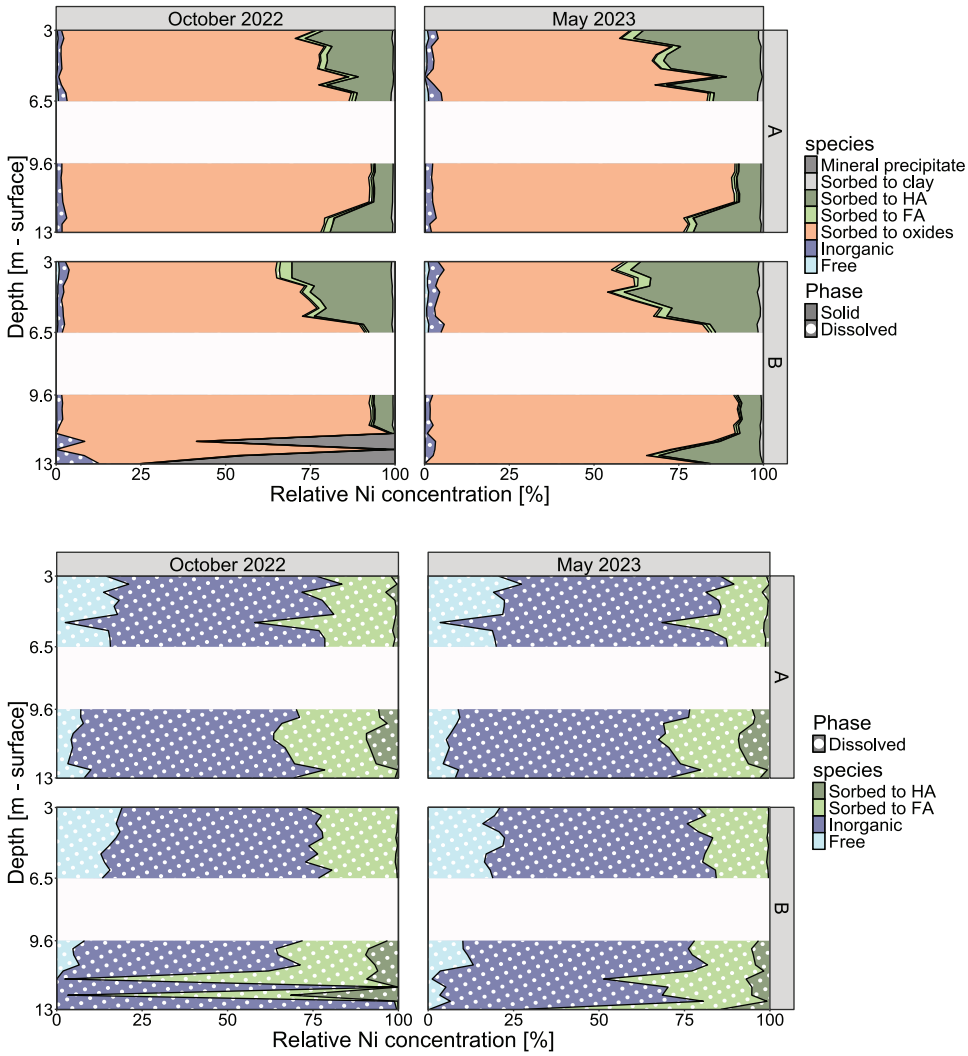


Figure S5.15 Geochemical model calculated solid phase (top) and dissolved phase (bottom) speciation of nickel in landfill pore water as a function of depth in vadose monitoring systems (VMS) A and B in October 2022 and May 2023. Important to note model calculations below 11 metres for VMS B in October 2022 are inadequate.

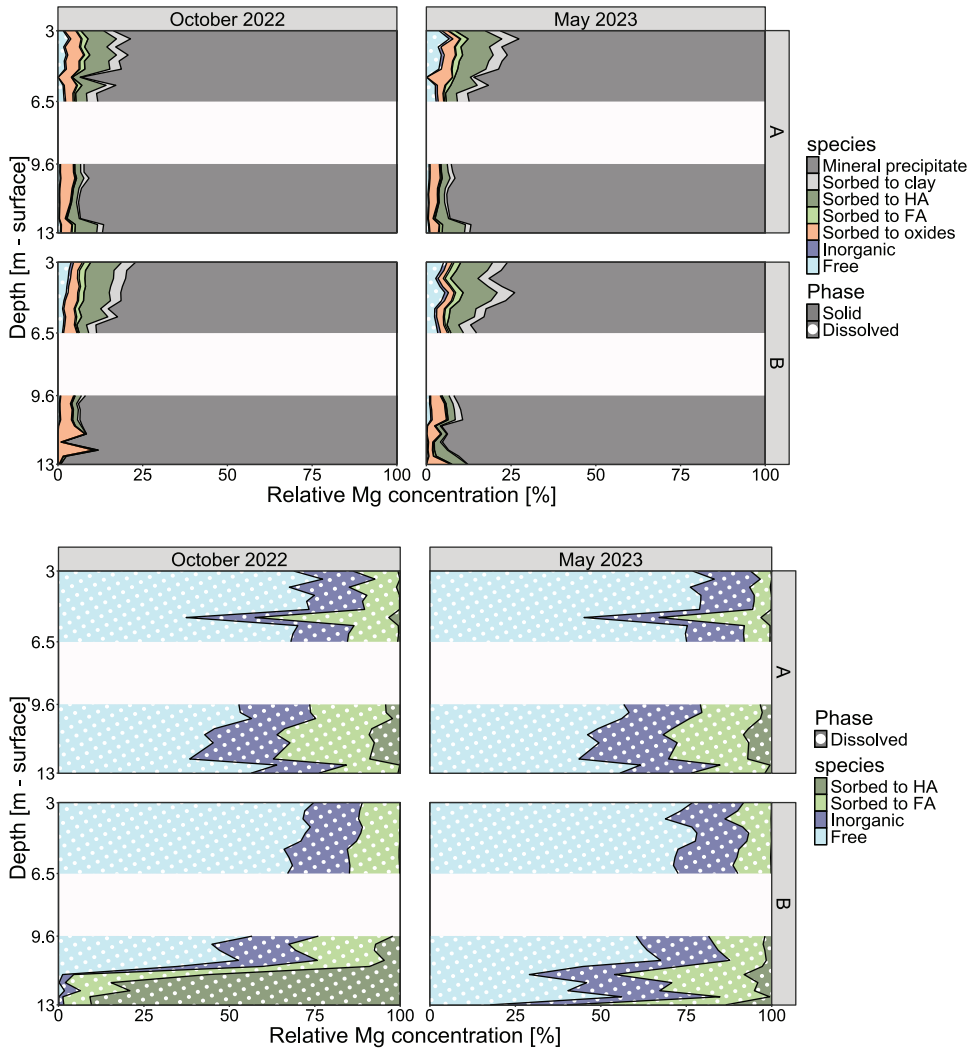


Figure S5.16 Geochemical model calculated solid phase (top) and dissolved phase (bottom) speciation of magnesium in landfill pore water as a function of depth in vadose monitoring systems (VMS) A and B in October 2022 and May 2023. Important to note model calculations below 11 metres for VMS B in October 2022 are inadequate.

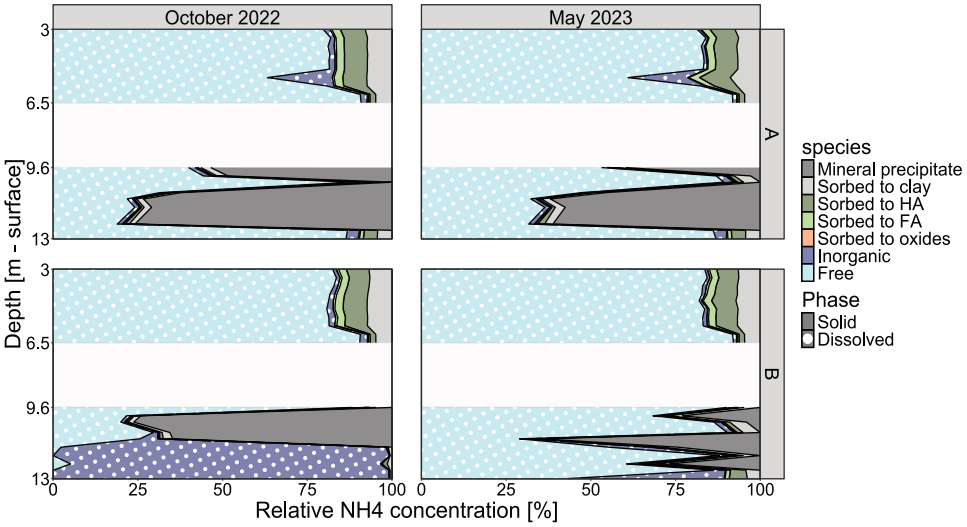


Figure S5.17 Geochemical model calculated speciation of ammonium in landfill pore water as a function of depth in vadose monitoring systems (VMS) A and B in October 2022 and May 2023.

Supplementary Tables

Table S5.1 Characteristics of the solid waste sampled around the VMS

Layer	Depth	SHA[a]	SHA[a]	Clay	Fe-Asc[b]	Al-AmOx[c]	Fe-DCB[d]	Al-DCB[d]
	[m - surface]	[g/kg]						
Top	0 - 6	5.06	0.93	53.32	11.49	4.23	26.96	5.53
Mid	6 - 12	2.09	0.29	53.32	10.18	1.96	22.01	2.03
Bot	12 - 18	5.16	0.79	53.32	6.12	3.15	14.94	3.51

[a]Solid humic acid and solid fulvic acid, determined according to (ISO 12782-4, 2012)

[b] Amorphous Fe, measured according to (ISO 12782-1, 2012)

[c] Amorphous Al, measured according to (ISO 12782-3, 2012)

[d] Crystalline iron- and aluminium (hydr)oxides, measured according to (ISO 12782-2, 2012)

Table S5.2 Elemental concentration of the grout used during installation of the VMS

	Cl (mg/l)	Li (mg/l)	Cr (mg/l)	Al (mg/l)	Ca (mg/l)	K (mg/l)	Na (mg/l)	pH (-)	EC (mS/cm)
Grout	299	0.4	1.3	18.3	4.9	379	2770	12.9	22.4

Table S5.3 Adaptations from generic binding parameters and relevant mineral forms of the model set-up of this paper.

Element	Minerals	Parameters
Al	Gibbsite	
As	-	
Ba	Barite	
Ca	Calcite	
Cd	**Otavite**	
Co	-	
Cr	-	
Cu	**Chalcocite**	
Fe	Ferrihydrite, **Franklinite, Siderity, (Pyrite)**	FA: (Hiemstra & van Riemsdijk, 2006) HFO (Fe^{2+}): (Appelo et al., 2002)
K	-	
Li	-	
Mg	**Magnesite**, Brucite	
Mn	Rhodocrhrosite, pyrochroite	
Mo	-	
NH4+	Struvite	
Ni	**$Ni[OH]_2$**	
P	**$CaHPO_4$**	
Pb	$Pb(OH)_2$	HFO: (Meima & Comans, 1998a), HA & FA: (Xiong et al., 2013)
S	**Barite, Chalcocite, (Sphalerite), (Pyrite)**	
Sb	-	
Si	Sepiolite	
Sn	$Sn[OH]_4$	
Sr	Strontianite	
V		
Zn	Willemite, **ZnCO3, (sphalerite)**	

Table S5.4 Calculated root mean square errors between the logarithm of model calculated and measured dissolved concentrations for each element, taking into account all samples (total), all except grout influenced samples (total - grout), only grout influenced samples (grout), all samples between 3 – 6.5 metres below the surface (top layer), all samples between 9.5 – 13 metres (Bottom layer), all samples between 9.5 – 13 metres except those influence by grout (Bot – grout). Samples considered to be inadequately modelled (RMSE > 1) are boldened.

	Al	Ba	Li	Mo	Sb	Sn	Sr	V	As	Ca	Co	Cr	Cu	Fe	K
Total	**1.41**	0.46	0.93	**1.68**	0.63	**1.05**	0.37	0.91	0.57	**1.16**	**1.02**	**1.28**	0.62	0.49	0.42
Total - grout	**1.15**	0.37	0.98	**1.76**	0.41	0.47	0.37	0.91	0.55	**1.22**	0.93	**1.25**	0.54	0.45	0.42
Top only	0.73	0.45	0.99	**1.43**	0.45	0.12	0.46	0.70	0.63	**1.09**	**1.08**	**1.49**	0.57	0.58	0.45
Bot only	**1.88**	0.47	0.85	**1.90**	0.78	**1.49**	0.25	**1.09**	0.51	**1.23**	0.95	**1.01**	0.66	0.39	0.40
Bot - grout	**1.60**	0.25	0.95	**2.12**	0.34	0.87	0.20	**1.16**	0.39	**1.38**	0.66	0.79	0.48	0.18	0.38

	Mg	Mn	Na	Ni	P	Pb	S	Si	Zn	Cl	NH4	Cu*	Fe*	Mn*	Zn*
Total	0.46	0.59	0.20	**1.36**	**1.07**	**1.31**	0.77	0.51	**1.37**	**1.11**	0.62	**3.03**	0.40	0.58	0.44
Total - grout	0.46	0.42	0.19	**1.31**	0.77	**1.21**	0.52	0.42	**1.45**	**1.14**	0.57	**3.06**	0.30	0.42	0.45
Top only	0.38	0.44	0.21	**1.41**	0.91	0.33	0.63	0.52	**1.55**	**1.17**	0.66	**3.04**	0.37	0.44	0.44
Bot only	0.54	0.71	0.18	**1.29**	**1.22**	**1.85**	0.90	0.50	**1.14**	**1.05**	0.57	**3.03**	0.42	0.71	0.44
Bot - grout	0.56	0.40	0.17	**1.14**	0.48	**1.83**	0.31	0.22	**1.27**	**1.10**	0.40	**3.09**	0.18	0.40	0.46

Table S5.5 Distribution of DOC fractions in batch systems at pH 12 (achieved with 1M NaOH) with HA (300 mg C/l) and ultrapure water (UPW) and pure FA (100 mg C/l) and UPW and batch systems in which Al was added at 15 mg/l. Additional systems (HA-grout & FA-grout) where pH 12 was achieved by adding grout solution.

	HA (mg C/l)	**FA (mg C/l)**	**Hy (mg C/l)**	**HON (mg C/l)**	**DOC (mg C/l)**	**Recovery (%)**
HA-UPW	251.0	11.7	4.0	7.3	295.3	92.8
HA-Al	254.5	12.2	4.0	4.5	288.3	95.4
HA-Grout	0.9	2.5	2.4	1.3	6.2	114.1
FA-UPW	2.2	73.6	3.2	13.7	99.0	93.6
FA-Al	2.5	74.0	3.5	4.1	99.0	84.9
FA-Grout	0.2	22.7	2.1	3.2	28.2	99.9

REFERENCE LIST

Adegoke, H. I., Adekola, F. A., Fatoki, O. S., & Ximba, B. J. (2013). Sorptive Interaction of Oxyanions with Iron Oxides: A Review. *Polish Journal of Environmental Studies*, *22*(1), 7–24.

Aeschbacher, M., Sander, M., & Schwarzenbach, R. P. (2010). Novel electrochemical approach to assess the redox properties of humic substances. *Environmental Science and Technology*, *44*(1), 87–93. https://doi.org/10.1021/ES902627P/SUPPL_FILE/ES902627P_SI_002.PDF

Aeschbacher, M., Vergari, D., Schwarzenbach, R. P., & Sander, M. (2011). Electrochemical analysis of proton and electron transfer equilibria of the reducible moieties in humic acids. *Environmental Science and Technology*, *45*(19), 8385–8394. https://doi.org/10.1021/ES201981G/SUPPL_FILE/ES201981G_SI_001.PDF

Aharoni, I., Dahan, O., & Siebner, H. (2022). Continuous monitoring of dissolved inorganic nitrogen (DIN) transformations along the waste-vadose zone - groundwater path of an uncontrolled landfill, using multiple N-species isotopic analysis. *Water Research*, *219*, 118508. https://doi.org/10.1016/J.WATRES.2022.118508

Aharoni, I., Siebner, H., & Dahan, O. (2017). Application of vadose-zone monitoring system for real-time characterization of leachate percolation in and under a municipal landfill. *Waste Management*, *67*, 203–213. https://doi.org/10.1016/J.WASMAN.2017.05.012

Aharoni, I., Siebner, H., Yogev, U., & Dahan, O. (2020). Holistic approach for evaluation of landfill leachate pollution potential – From the waste to the aquifer. *Science of The Total Environment*, *741*, 140367. https://doi.org/10.1016/J.SCITOTENV.2020.140367

Allen, H. E., Hall, R. H., & Brisbin, T. D. (1980). Metal Speciation. Effects on Aquatic Toxicity. *Environmental Science & Technology*, *14*(4), 441–443. https://pubs.acs.org/sharingguidelines

Alshameri, A., He, H., Zhu, J., Xi, Y., Zhu, R., Ma, L., & Tao, Q. (2017). Adsorption of ammonium by different natural clay minerals: Characterization, kinetics and adsorption isotherms. *Applied Clay Science*, *159*, 83–93. https://doi.org/10.1016/j.clay.2017.11.007

Antelo, J., Avena, M., Fiol, S., López, R., & Arce, F. (2005). Effects of pH and ionic strength on the adsorption of phosphate and arsenate at the goethite-water interface. *Journal of Colloid and Interface Science*, *285*(2), 476–486. https://doi.org/10.1016/j.jcis.2004.12.032

Appelo, C. A. J., Van Der Weiden, M. J. J., Tournassat, C., & Charlet, L. (2002). Surface complexation of ferrous iron and carbonate on ferrihydrite and the mobilization of arsenic. *Environmental Science and Technology*, *36*(14), 3096–3103. https://doi.org/10.1021/es010130n

Astrup, T., Dijkstra, J. J., Comans, R. N. J., Van Der Sloot, H. A., & Christensen, T. H. (2006). Geochemical modeling of leaching from MSWI air-pollution-control residues. *Environmental Science and Technology*, *40*(11), 3551–3557. https://doi.org/10.1021/es052250r

Baldermann, A., Mavromatis, V., Frick, P. M., & Dietzel, M. (2018). Effect of aqueous Si/Mg ratio and pH on the nucleation and growth of sepiolite at 25 °C. *Geochimica et Cosmochimica Acta*, *227*, 211–226. https://doi.org/10.1016/J.GCA.2018.02.027

Bao, Y., Bolan, N. S., Lai, J., Wang, Y., Jin, X., Kirkham, M. B., Wu, X., Fang, Z., Zhang, Y., & Wang, H. (2022). Interactions between organic matter and Fe (hydr)oxides and their influences on immobilization and remobilization of metal(loid)s: A review. *Critical Reviews in Environmental Science and Technology*, *52*(22), 4016–4037. https://doi.org/10.1080/10643389.2021.1974766

Bareither, C. A., Benson, C. H., Barlaz, M. A., Edil, T. B., & Tolaymat, T. M. (2010). Performance of North American Bioreactor Landfills. I: Leachate Hydrology and Waste Settlement. *Journal of Environmental Engineering*, *136*(8), 824–838. https://doi.org/10.1061/(ASCE)EE.1943-7870.0000219

Barré, P., Velde, B., & Abbadie, L. (2007). Dynamic role of "illite-like" clay minerals in temperate soils: Facts and hypotheses. *Biogeochemistry*, *82*(1), 77–88. https://doi.org/https://doi.org/10.1007/s10533-006-9054-2

Baun, D. L., & Christensen, T. H. (2004). Speciation of heavy metals in landfill leachate: A review. *Waste Management and Research*, *22*(1), 3–23. https://doi.org/10.1177/0734242X04042146

Benedetti, M. F., Van Riemsdijk, W. H., Koopal, L. K., Kinniburgh, D. G., Gooddy, D. C., & Milne, C. J. (1996). Metal ion binding by natural organic matter: From the model to the field. *Geochimica et Cosmochimica Acta*, *60*(14), 2503–2513. https://doi.org/10.1016/0016-7037(96)00113-5

Bennett, N. D., Croke, B. F. W., Guariso, G., Guillaume, J. H. A., Hamilton, S. H., Jakeman, A. J., Marsili-Libelli, S., Newham, L. T. H., Norton, J. P., Perrin, C., Pierce, S. A., Robson, B., Seppelt, R., Voinov, A. A., Fath, B. D., & Andreassian, V. (2013). Characterising performance of environmental models. *Environmental Modelling & Software*, *40*, 1–20. https://doi.org/10.1016/J.ENVSOFT.2012.09.011

Benson, C. H., Barlaz, M. A., Lane, D. T., & Rawe, J. M. (2007). Practice review of five bioreactor/recirculation landfills. *Waste Management*, *27*(1), 13–29. https://doi.org/10.1016/J.WASMAN.2006.04.005

Berge, N. D., Reinhart, D. R., & Batarseh, E. S. (2009). An assessment of bioreactor landfill costs and benefits. *Waste Management*, *29*(5), 1558–1567. https://doi.org/10.1016/j.wasman.2008.12.010

Berge, N. D., Reinhart, D. R., & Townsend, T. G. (2005). The fate of nitrogen in bioreactor landfills. *Critical Reviews in Environmental Science and Technology*, *35*(4), 365–399. https://doi.org/10.1080/10643380590945003

Bilgili, M. S., Demir, A., & Özkaya, B. (2007). Influence of leachate recirculation on aerobic and anaerobic decomposition of solid wastes. *Journal of Hazardous Materials*, *143*(1–2), 177–183. https://doi.org/10.1016/j.jhazmat.2006.09.012

Bolyard, S. C., & Reinhart, D. R. (2016). Application of landfill treatment approaches for stabilization of municipal solid waste. *Waste Management*, *55*, 22–30. https://doi.org/10.1016/J.WASMAN.2016.01.024

Borch, T., Kretzschmar, R., Skappler, A., Van Cappellen, P., Ginder-Vogel, M., Voegelin, A., & Campbell, K. (2010). Biogeochemical redox processes and their impact on contaminant dynamics. *Environmental Science and Technology*, *44*(1), 15–23. https://doi.org/https://doi.org/10.1021/es9026248

Borglin, S. E., Hazen, T. C., Oldenburg, C. M., & Zawislanski, P. T. (2004). Comparison of aerobic and anaerobic biotreatment of municipal solid waste. *Journal of the Air and Waste Management Association*, *54*(7), 815–822. https://doi.org/https://doi.org/10.1080/10473289.2004.10470951

Brand, E. (2014). *Development of emission testing values to assess sustainable landfill management on pilot landfills Phase 2: Proposals for testing values*.

Brand, E., De Nijs, T. C. M., Dijkstra, J. J., & Comans, R. N. J. (2016). A novel approach in calculating site-specific aftercare completion criteria for landfills in The Netherlands: Policy developments. *Waste Management*, *56*, 255–261. https://doi.org/10.1016/j.wasman.2016.07.038

Brand, J. H., & Spencer, K. L. (2024). Potential pollution risks of historic landfills in England: Further analysis of climate change impacts. *Wiley Interdisciplinary Reviews: Water*, *11*(3). https://doi.org/https://doi.org/10.1002/wat2.1706

Brandely, M., Coussy, S., Blanc-Biscarat, D., & Gourdon, R. (2022). Assessment of Molybdenum and Antimony speciation in excavated rocks and soils from the Parisian basin using mineralogical and chemical analyses coupled to geochemical modelling. *Applied Geochemistry*, *136*. https://doi.org/10.1016/j.apgeochem.2021.105129

Brandstätter, C., Laner, D., & Fellner, J. (2015a). Carbon pools and flows during lab-scale degradation of old landfilled waste under different oxygen and water regimes. *Waste Management*, *40*, 100–111. https://doi.org/10.1016/j.wasman.2015.03.011

Brandstätter, C., Laner, D., & Fellner, J. (2015b). Nitrogen pools and flows during lab-scale degradation of old landfilled waste under different oxygen and water regimes. *Biodegradation*, *26*(5), 399–414. https://doi.org/10.1007/s10532-015-9742-5

Brandstätter, C., Prantl, R., & Fellner, J. (2020). Performance assessment of landfill in-situ aeration – A case study. *Waste Management*, *101*, 231–240. https://doi.org/10.1016/J.WASMAN.2019.10.022

Bruggenwert, M. G. M., & Kamphorst, A. (1979). Survey of Experimental Information on Cation Exchange in Soil Systems. In *Developments in Soil Science* (Vol. 5, Number PART B, pp. 141–203). Elsevier Ltd. https://doi.org/10.1016/S0166-2481(08)70660-3

Burns, R. G., & Burns, V. M. (1979). Manganese Oxides. In *Marine Minerals* (pp. 1–46). https://doi.org/10.1515/9781501508646-005

Butera, S., Christensen, T. H., & Astrup, T. F. (2014). Composition and leaching of construction and demolition waste: Inorganic elements and organic compounds. *Journal of Hazardous Materials*, *276*, 302–311. https://doi.org/10.1016/J.JHAZMAT.2014.05.033

Caille, N., Tiffreau, C., Leyval, C., & Morel, J. L. (2003). Solubility of metals in an anoxic sediment during prolonged aeration. *Science of The Total Environment*, *301*(1–3), 239–250. https://doi.org/10.1016/S0048-9697(02)00289-9

Canavan, R. W., Van Cappellen, P., Zwolsman, J. J. G., van den Berg, G. A., & Slomp, C. P. (2007). Geochemistry of trace metals in a fresh water sediment: Field results and diagenetic modeling. *Science of The Total Environment*, *381*(1–3), 263–279. https://doi.org/10.1016/J.SCITOTENV.2007.04.001

Capozzi, S. L., Leang, A. L., Rodenburg, L. A., Chandramouli, B., Delistraty, D. A., & Carter, C. H. (2023). PFAS in municipal landfill leachate: Occurrence, transformation, and sources. *Chemosphere*, *334*, 138924. https://doi.org/10.1016/J.CHEMOSPHERE.2023.138924

Cappuyns, V., & Swennen, R. (2008). The application of pHstat leaching tests to assess the pH-dependent release of trace metals from soils, sediments and waste materials. *Journal of Hazardous Materials*, *158*(1), 185–195. https://doi.org/10.1016/j.jhazmat.2008.01.058

Carbonaro, R. F., & Di Toro, D. M. (2007). Linear free energy relationships for metal-ligand complexation: Monodentate binding to negatively-charged oxygen donor atoms. *Geochimica et Cosmochimica Acta*, *71*(16), 3958–3968. https://doi.org/10.1016/j.gca.2007.06.005

Carter, C. M., Van Der Sloot, H. A., & Cooling, D. (2009). pH-dependent extraction of soil and soil amendments to understand the factors controlling element mobility. *European Journal of Soil Science*, *60*(4), 622–637. https://doi.org/10.1111/j.1365-2389.2009.01139.x

Cerminara, G., Raga, R., Hirata, O., & Pivato, A. (2020). Denitrification of low C/N landfill leachate in lab-scale landfill simulation bioreactors. *Waste Management*, *113*, 236–243. https://doi.org/10.1016/J.WASMAN.2020.05.041

Charriau, A., Lesven, L., Gao, Y., Leermakers, M., Baeyens, W., Ouddane, B., & Billon, G. (2011). Trace metal behaviour in riverine sediments: Role of organic matter and sulfides. *Applied Geochemistry*, *26*(1), 80–90. https://doi.org/10.1016/J.APGEOCHEM.2010.11.005

Chen, J., Gu, B., Royer, R. A., & Burgos, W. D. (2003). The roles of natural organic matter in chemical and microbial reduction of ferric iron. *Science of The Total Environment*, *307*(1–3), 167–178. https://doi.org/10.1016/S0048-9697(02)00538-7

Choppala, G., Kunhikrishnan, A., Seshadri, B., Park, J. H., Bush, R., & Bolan, N. (2018). Comparative sorption of chromium species as influenced by pH, surface charge and organic matter content in contaminated soils. *Journal of Geochemical Exploration*, *184*, 255–260. https://doi.org/10.1016/j.gexplo.2016.07.012

Christensen, T. H., Kjeldsen, P., Bjerg, P. L., Jensen, D. L., Christensen, J. B., Baun, A., Albrechtsen, H.-J., & Heron, G. (2001). Biogeochemistry of landfill leachate plumes. *Applied Geochemistry*, *16*, 659–718. www.elsevier.com/locate/apgeochem

Chung, J., Kim, S., Baek, S., Lee, N. H., Park, S., Lee, J., Lee, H., & Bae, W. (2015). Acceleration of aged-landfill stabilization by combining partial nitrification and leachate recirculation: A field-scale study. *Journal of Hazardous Materials*, *285*, 436–444. https://doi.org/10.1016/J.JHAZMAT.2014.12.013

Coetzee, J. J., Bansal, N., & Chirwa, E. M. N. (2020). Chromium in Environment, Its Toxic Effect from Chromite-Mining and Ferrochrome Industries, and Its Possible Bioremediation. In *Exposure and Health* (Vol. 12, Number 1, pp. 51–62). Springer. https://doi.org/10.1007/s12403-018-0284-z

Conlan, M. J. W., Mayer, K. U., Blaskovich, R., & Beckie, R. D. (2012). Solubility controls for molybdenum in neutral rock drainage. *Geochemistry: Exploration, Environment, Analysis*, *12*(1), 21–32. https://doi.org/10.1144/1467-7873/10-RA-043

Cornelis, G., Johnson, C. A., Gerven, T. Van, & Vandecasteele, C. (2008). Leaching mechanisms of oxyanionic metalloid and metal species in alkaline solid wastes: A review. *Applied Geochemistry*, *23*(5), 955–976. https://doi.org/10.1016/j.apgeochem.2008.02.001

Cossu, R., Morello, L., Raga, R., & Cerminara, G. (2016). Biogas production enhancement using semi-aerobic pre-aeration in a hybrid bioreactor landfill. *Waste Management*, *55*, 83–92. https://doi.org/10.1016/J.WASMAN.2015.10.025

Council of the European Union. (1999). Directive 1999/31/EC of 26 April 1999 on the landfill of waste. *Official Journal of the European Union*.

Couture, R. M., Rose, J., Kumar, N., Mitchell, K., Wallschläger, D., & Van Cappellen, P. (2013). Sorption of arsenite, arsenate, and thioarsenates to iron oxides and iron sulfides: A kinetic and spectroscopic investigation. *Environmental Science and Technology*, *47*(11), 5652–5659. https://doi.org/https://doi.org/10.1021/es3049724

Crannell, B. S., Taylor Eighmy, T., Krzanowski, J. E., Dykstra Eusden Jr, J., Shaw, E. L., & Francis, C. A. (2000). Heavy metal stabilization in municipal solid waste combustion bottom ash using soluble phosphate. *Waste Management*, 135–148. www.elsevier.nl/locate/wasman

Craven, A. M., Aiken, G. R., & Ryan, J. N. (2012). Copper(II) binding by dissolved organic matter: Importance of the copper-to-dissolved organic matter ratio and implications for the biotic ligand model. *Environmental Science and Technology*, *46*(18), 9948–9954. https://doi.org/10.1021/ES301015P/SUPPL_FILE/ES301015P_SI_001.PDF

Curtin, D., Peterson, M. E., & Anderson, C. R. (2016). pH-dependence of organic matter solubility: Base type effects on dissolved organic C, N, P, and S in soils with contrasting mineralogy. *Geoderma*, *271*, 161–172. https://doi.org/10.1016/J.GEODERMA.2016.02.009

Dagwar, P. P., & Dutta, D. (2024). Landfill leachate a potential challenge towards sustainable environmental management. *Science of The Total Environment*, *926*, 171668. https://doi.org/10.1016/J.SCITOTENV.2024.171668

Dahan, O., Talby, R., Yechieli, Y., Adar, E., Lazarovitch, N., & Enzel, Y. (2009). In Situ Monitoring of Water Percolation and Solute Transport Using a Vadose Zone Monitoring System. *Vadose Zone Journal*, *8*(4), 916–925. https://doi.org/10.2136/vzj2008.0134

Dang, Q., Zhao, X., Xi, B., Zhang, C., & He, L. (2023). The key role of denitrification and dissimilatory nitrate reduction in nitrogen pollution along vertical landfill profiles from metagenomic perspective. *Journal of Environmental Management*, *342*, 118300. https://doi.org/10.1016/J.JENVMAN.2023.118300

Das, S., Lee, S. H., Kumar, P., Kim, K. H., Lee, S. S., & Bhattacharya, S. S. (2019). Solid waste management: Scope and the challenge of sustainability. *Journal of Cleaner Production*, *228*, 658–678. https://doi.org/10.1016/j.jclepro.2019.04.323

Davies, C. W. (1938). Extent of Dissociation of Salts in Water. Part VIII. An equation for the mean ionic activity coefficient of an electrolyte in water, and a revision of the dissociation constants of some sulphates. *Journal of the Chemical Society*, 2093–2098.

Dewey, C., Juillot, F., Fendorf, S., & Bargar, J. R. (2023). Seasonal Oxygenation of Contaminated Floodplain Soil Releases Zn to Porewater. *Environmental Science and Technology*, *57*(12), 4841–4851. https://doi.org/https://doi.org/10.1021/acs.est.2c08764

Di Bonito, M., Lofts, S., & Groenenberg, J. E. (2024). Models of Geochemical Speciation: Structure and Applications. In *Environmental Geochemistry: Site Characterization, Data Analysis and Case Histories: Second Edition* (pp. 329–419). Elsevier. https://doi.org/https://doi.org/10.1016/B978-0-443-13801-0.00017-7

Diab, S., Kochba, M., & Avnimelech, Y. (1993). Nitrification pattern in a fluctuating anaerobic-aerobic pond environment. *Water Research*, *27*(9), 1469–1475. https://doi.org/10.1016/0043-1354(93)90027-F

Dijkstra, J. J., Meeussen, J. C. L., & Comans, R. N. J. (2004). Leaching of heavy metals from contaminated soils: An experimental and modeling study. *Environmental Science and Technology*, *38*(16), 4390–4395. https://doi.org/10.1021/es049885v

Dijkstra, J. J., Meeussen, J. C. L., & Comans, R. N. J. (2009). Evaluation of a generic multisurface sorption model for inorganic soil contaminants. *Environmental Science and Technology*, *43*(16), 6196–6201. https://doi.org/10.1021/es900555g

Dijkstra, J. J., Van Der Sloot, H. A., & Comans, R. N. J. (2006). The leaching of major and trace elements from MSWI bottom ash as a function of pH and time. *Applied Geochemistry*, *21*(2), 335–351. https://doi.org/10.1016/j.apgeochem.2005.11.003

Dijkstra, J. J., Van Zomeren, A., Brand, E., & Comans, R. N. J. (2018). Site-specific aftercare completion criteria for sustainable landfilling in the Netherlands: Geochemical modelling and sensitivity analysis. *Waste Management*, *75*, 407–414. https://doi.org/10.1016/J.WASMAN.2018.02.002

Dijkstra, J. J., Van Zomeren, A., Meeussen, J. C. L., & Comans, R. N. J. (2006). Effect of accelerated aging of MSWI bottom ash on the leaching mechanisms of copper and molybdenum. *Environmental Science and Technology*, *40*(14), 4481–4487. https://doi.org/10.1021/es052214s

Dixit, S., & Hering, J. G. (2003). Comparison of arsenic(V) and arsenic(III) sorption onto iron oxide minerals: Implications for arsenic mobility. *Environmental Science & Technology*, *37*(18), 4182–4189. https://doi.org/https://doi.org/10.1021/es030309t

Doherty, J. (2023). *PEST: Model-Independent Parameter Estimation and Uncertainty Analysis*. https://pesthomepage.org/

Dzombak, D. A., & Morel, F. (1990). *Surface complexation modeling: hydrous ferric oxide*. John Wiley & Sons.

EEA. (2024, August). *EEA greenhouse gases — data viewer | European Environment Agency's home page*. https://www.eea.europa.eu/en/analysis/maps-and-charts/greenhouse-gases-viewer-data-viewers

Eggen, T., Moeder, M., & Arukwe, A. (2010). Municipal landfill leachates: A significant source for new and emerging pollutants. *Science of The Total Environment*, *408*(21), 5147–5157. https://doi.org/10.1016/J.SCITOTENV.2010.07.049

Erses, A. S., & Onay, T. T. (2003). In situ heavy metal attenuation in landfills under methanogenic conditions. *Journal of Hazardous Materials*, *99*(2), 159–175. https://doi.org/10.1016/S0304-3894(02)00354-0

Erses, A. S., Onay, T. T., & Yenigun, O. (2008). Comparison of aerobic and anaerobic degradation of municipal solid waste in bioreactor landfills. *Bioresource Technology*, *99*(13), 5418–5426. https://doi.org/10.1016/J.BIORTECH.2007.11.008

Essington, M. E. (1992). Fluorine and Molybdenum Solubility Relationships in Combusted Oil Shale. *Journal of Environmental Science and Health. Part a: Environmental Science and Engineering and Toxicology*, *27*(2), 547–564. https://doi.org/10.1080/10934529209375744

European Parliament and Council of the European Union. (2008). Directive 2008/98/EC of 19 November 2008 on waste and repealing certain Directives. *Official Journal of the European Union*, 3–30.

Evangelou, V. P., & Lumbanraja, J. (2002). Ammonium–Potassium–Calcium Exchange on Vermiculite and Hydroxy-aluminum Vermiculite. *Soil Science Society of America Journal*, *66*(2), 445–455. https://doi.org/10.2136/sssaj2002.4450

Evangelou, V. P., & Phillips, R. E. (2018). Cation Exchange in Soils. *Chemical Processes in Soils*, 343–410. https://doi.org/10.2136/SSSABOOKSER8.C7

Fannin, C. A., & Roberts, R. D. (2006). Mature landfill waste geochemical characteristics and implications for long-term secondary substance release. *Geochemistry: Exploration, Environment, Analysis*, *6*(4), 369–378. https://doi.org/10.1144/1467-7873/06-103

Fellner, J., & Brunner, P. H. (2010). Modeling of leachate generation from MSW landfills by a 2-dimensional 2-domain approach. *Waste Management*, *30*(11), 2084–2095. https://doi.org/10.1016/J.WASMAN.2010.03.020

Fetting, C. (2020). The European Green Deal. *ESDN Report, December 2020, ESDN Office, Vienna*.

Flyhammar, P. (1997). Estimation of heavy metal transformations in municipal solid waste. *Science of The Total Environment*, *198*(2), 123–133. https://doi.org/10.1016/S0048-9697(97)05439-9

Fricko, N., Brandstätter, C., & Fellner, J. (2021a). Enduring reduction of carbon and nitrogen emissions from landfills due to aeration? *Waste Management*, *135*, 457–466. https://doi.org/10.1016/j.wasman.2021.09.024

Fricko, N., Brandstätter, C., & Fellner, J. (2021b). Enduring reduction of carbon and nitrogen emissions from landfills due to aeration? *Waste Management*, *135*, 457–466. https://doi.org/10.1016/J.WASMAN.2021.09.024

Frost, R. L., & Palmer, S. J. (2011). Thermal stability of the 'cave' mineral brushite CaHPO4·2H2O – Mechanism of formation and decomposition. *Thermochimica Acta*, *521*(1–2), 14–17. https://doi.org/10.1016/J.TCA.2011.03.035

Fukushima, M., Nakayasu, K., Tanaka, S., & Nakamura, H. (1995). Chromium(III) binding abilities of humic acids. *Analytica Chimica Acta*, *317*(1–3), 195–206. https://doi.org/https://doi.org/10.1016/0003-2670(95)00410-6

Gao, H., Weng, L., Comans, R. N. J., & Koopmans, G. F. (2025). Dual-Domain Regulation of Dissolved Organic Matter Release in Soil: The Role of pH and Calcium. *ACS Earth and Space Chemistry*, *2025*, 1377–1391. https://doi.org/10.1021/acsearthspacechem.4c00377

Gao, J., Oloibiri, V., Chys, M., Audenaert, W., Decostere, B., He, Y., Van Langenhove, H., Demeestere, K., & Van Hulle, S. W. H. (2015). The present status of landfill leachate treatment and its development trend from a technological point of view. *Reviews in Environmental Science and Biotechnology*, *14*(1), 93–122. https://doi.org/10.1007/S11157-014-9349-Z/TABLES/11

Garrabrants, A. C., Kosson, D. S., Brown, K. G., Fagnant, D. P., Helms, G., & Thorneloe, S. A. (2021a). Demonstration of the use of test results from the Leaching Environmental Assessment Framework (LEAF) to develop screening-level leaching assessments. *Waste Management*, *121*, 226–236. https://doi.org/10.1016/J.WASMAN.2020.12.016

Garrabrants, A. C., Kosson, D. S., Brown, K. G., Fagnant, D. P., Helms, G., & Thorneloe, S. A. (2021b). Methodology for scenario-based assessments and demonstration of treatment effectiveness

using the Leaching Environmental Assessment Framework (LEAF). *Journal of Hazardous Materials*, *406*, 124635. https://doi.org/10.1016/J.JHAZMAT.2020.124635

Ghosh, A., Mukiibi, M., Sáez, A. E., & Ela, W. P. (2006). Leaching of arsenic from granular ferric hydroxide residuals under mature landfill conditions. *Environmental Science & Technology*, *40*(19), 6070–6075. https://doi.org/https://doi.org/10.1021/es060561b

Giannis, A., Makripodis, G., Simantiraki, F., Somara, M., & Gidarakos, E. (2008). Monitoring operational and leachate characteristics of an aerobic simulated landfill bioreactor. *Waste Management*, *28*(8), 1346–1354. https://doi.org/10.1016/J.WASMAN.2007.06.024

GodvinSharmila, V., Shanmugavel, S. P., Tyagi, V. K., & Rajesh Banu, J. (2023). Microplastics as emergent contaminants in landfill leachate: Source, potential impact and remediation technologies. *Journal of Environmental Management*, *343*, 118240. https://doi.org/10.1016/J.JENVMAN.2023.118240

Groenenberg, J. E., Dijkstra, J. J., Bonten, L. T. C., De Vries, W., & Comans, R. N. J. (2012). Evaluation of the performance and limitations of empirical partition-relations and process based multisurface models to predict trace element solubility in soils. *Environmental Pollution*, *166*, 98–107. https://doi.org/10.1016/j.envpol.2012.03.011

Groenenberg, J. E., Koopmans, G. F., & Comans, R. N. J. (2010). Uncertainty analysis of the nonideal competitive adsorption - Donnan model: Effects of dissolved organic matter variability on predicted metal speciation in soil solution. *Environmental Science and Technology*, *44*(4), 1340–1346. https://doi.org/10.1021/es902615w

Groenenberg, J. E., & Lofts, S. (2014). The use of assemblage models to describe trace element partitioning, speciation, and fate: A review. *Environmental Toxicology and Chemistry*, *33*(10), 2181–2196. https://doi.org/10.1002/etc.2642

Groenenberg, J. E., Römkens, P. F. A. M., Zomeren, A. Van, Rodrigues, S. M., & Comans, R. N. J. (2017). Evaluation of the Single Dilute (0.43 M) Nitric Acid Extraction to Determine Geochemically Reactive Elements in Soil. *Environmental Science and Technology*, *51*(4), 2246–2253. https://doi.org/10.1021/acs.est.6b05151

Gu, X., & Evans, L. J. (2007). Modelling the adsorption of Cd(II), Cu(II), Ni(II), Pb(II), and Zn(II) onto Fithian illite. *Journal of Colloid and Interface Science*, *307*(2), 317–325. https://doi.org/10.1016/J.JCIS.2006.11.022

Gustafsson, J. P. (2001). Modeling the acid-base properties and metal complexation of humic substances with the Stockholm Humic Model. *Journal of Colloid and Interface Science*, *244*(1), 102–112. https://doi.org/10.1006/jcis.2001.7871

Gustafsson, J. P. (2003). Modelling molybdate and tungstate adsorption to ferrihydrite. *Chemical Geology*, *200*(1–2), 105–115. https://doi.org/10.1016/S0009-2541(03)00161-X

Gustafsson, J. P. (2019). Vanadium geochemistry in the biogeosphere –speciation, solid-solution interactions, and ecotoxicity. *Applied Geochemistry*, *102*, 1–25. https://doi.org/10.1016/j.apgeochem.2018.12.027

Gustafsson, J. P. (2022). *Visual MINTEQ version 4.0. http://vminteq.com*.

Gustafsson, J. P., & Antelo, J. (2022). Competitive Arsenate and Phosphate Adsorption on Ferrihydrite as Described by the CD-MUSIC Model. *ACS Earth and Space Chemistry*. https://doi.org/10.1021/acsearthspacechem.2c00081

Gustafsson, J. P., Persson, I., Oromieh, A. G., Van Schaik, J. W. J., Sjöstedt, C., & Kleja, D. B. (2014). Chromium(III) complexation to natural organic matter: Mechanisms and modeling. *Environmental Science and Technology*, *48*(3), 1753–1761. https://doi.org/10.1021/es404557e

Hanor, J. S. (2000). Barite-celestine geochemistry and environments of formation. *Reviews in Mineralogy and Geochemistry*, *40*(1), 193–275. https://doi.org/10.2138/rmg.2000.40.4

Hao, Y. J., Ji, M., Chen, Y. X., Wu, W. X., Zhang, S. G., & Liu, H. Q. (2010). The pathway of in-situ ammonium removal from aerated municipal solid waste bioreactor: nitrification/denitrification or air stripping? *Waste Management & Research*, *28*(12), 1057–1064. https://doi.org/10.1177/0734242X09355182

Hayes, M. H. B., & Swift, R. S. (2020). Vindication of humic substances as a key component of organic matter in soil and water. In *Advances in Agronomy* (Vol. 163, pp. 1–37). Academic Press Inc. https://doi.org/10.1016/bs.agron.2020.05.001

He, P., Chen, L., Shao, L., Zhang, H., & Lü, F. (2019). Municipal solid waste (MSW) landfill: A source of microplastics? -Evidence of microplastics in landfill leachate. *Water Research*, *159*, 38–45. https://doi.org/10.1016/J.WATRES.2019.04.060

He, P. J., Xue, J. F., Shao, L. M., Li, G. J., & Lee, D. J. (2006). Dissolved organic matter (DOM) in recycled leachate of bioreactor landfill. *Water Research*, *40*(7), 1465–1473. https://doi.org/10.1016/j.watres.2006.01.048

Helz, G. R., & Holland, H. D. (1965). The solubility and geologic occurrence of strontianite. *Geochimica et Cosmochimica Acta*, *29*(12), 1303–1315. https://doi.org/10.1016/0016-7037(65)90008-6

Hemond, H. F., & Fechner, E. J. (2022). *Chemical Fate and Transport in the Environment*. Academic press.

Hernandez-Soriano, M. C., & Jimenez-Lopez, J. C. (2012). Effects of soil water content and organic matter addition on the speciation and bioavailability of heavy metals. *Science of The Total Environment*, *423*, 55–61. https://doi.org/10.1016/J.SCITOTENV.2012.02.033

Hiemstra, T. (2013). Surface and mineral structure of ferrihydrite. *Geochimica et Cosmochimica Acta*, *105*, 316–325. https://doi.org/10.1016/j.gca.2012.12.002

Hiemstra, T., & Van Riemsdijk, W. H. (1996). A Surface Structural Approach to Ion Adsorption: The Charge Distribution (CD) Model. *Journal of Colloid and Interface Science*, *179*(2), 488–508. https://doi.org/10.1006/JCIS.1996.0242

Hiemstra, T., & Van Riemsdijk, W. H. (1999). Surface Structural Ion Adsorption Modeling of Competitive Binding of Oxyanions by Metal (Hydr)oxides. *Journal of Colloid and Interface Science*, *210*(1), 182–193. https://doi.org/10.1006/JCIS.1998.5904

Hiemstra, T., & Van Riemsdijk, W. H. (2006). Biogeochemical speciation of Fe in ocean water. *Marine Chemistry*, *102*(3–4), 181–197. https://doi.org/10.1016/j.marchem.2006.03.008

Hiemstra, T., & Van Riemsdijk, W. H. (2009). A surface structural model for ferrihydrite I: Sites related to primary charge, molar mass, and mass density. *Geochimica et Cosmochimica Acta*, *73*(15), 4423–4436. https://doi.org/10.1016/j.gca.2009.04.032

Hongshao, Z., & Stanforth, R. (2001). Competitive adsorption of phosphate and arsenate on goethite. *Environmental Science & Technology*, *35*(24), 4753–4757. https://doi.org/https://doi.org/10.1021/es010890y

Hoornweg, D., & Bhada-Tata, P. (2012). A Global Review of Solid Waste Management - Review, Global Management, Solid Waste. *World Bank Urban Development Series Knowledge Papers*, *1*(11), 1–116.

Houba, V. J. G., Novozamsky, I., & van der Lee, J. (1995). *Soil analysis procedures: other procedures* (6th ed.). Agricultural University, Wageningen . https://library.wur.nl/WebQuery/titel/2258936

Hrad, M., Gamperling, O., & Huber-Humer, M. (2013). Comparison between lab- and full-scale applications of in situ aeration of an old landfill and assessment of long-term emission development after completion. *Waste Management*, *33*(10), 2061–2073. https://doi.org/10.1016/j.wasman.2013.01.027

Hyks, J., Astrup, T., & Christensen, T. H. (2009). Long-term leaching from MSWI air-pollution-control residues: Leaching characterization and modeling. *Journal of Hazardous Materials*, *162*(1), 80–91. https://doi.org/10.1016/j.jhazmat.2008.05.011

Ionas, A. C., Dirtu, A. C., Anthonissen, T., Neels, H., & Covaci, A. (2014). Downsides of the recycling process: Harmful organic chemicals in children's toys. *Environment International*, *65*, 54–62. https://doi.org/10.1016/J.ENVINT.2013.12.019

ISO 12782-1. (2012). *Soil quality — Parameters for geochemical modelling of leaching and speciation of constituents in soils and materials — Part 1: Extraction of amorphous iron oxides and hydroxides with ascorbic acid.*

ISO 12782-2. (2012). *Soil quality -- Parameters for geochemical modelling of leaching and speciation of constituents in soils and materials -- Part 2: Extraction of crystalline iron oxides and hydroxides with dithionite.*

ISO 12782-3. (2012). *Soil quality -- Parameters for geochemical modelling of leaching and speciation of constituents in soils and materials -- Part 3: Extraction of aluminium oxides and hydroxides with ammonium oxalate/oxalic acid.*

ISO 12782-4. (2012). *Soil quality — Parameters for geochemical modelling of leaching and speciation of constituents in soils and materials — Part 4: Extraction of humic substances from solid samples*.

ISO 12782-5. (2012). *Soil quality — Parameters for geochemical modelling of leaching and speciation of constituents in soils and materials — Part 5: Extraction of humic substances from aqueous samples*.

ISO 17586. (2016). *Soil quality — Extraction of trace elements using dilute nitric acid*.

ISO 21268-3. (2019). *Soil quality — Leaching procedures for subsequent chemical and ecotoxicological testing of soil and soil-like materials — Part 3: Up-flow percolation test.*

Iván, D., Iván, I., Ortiz, B., Fr´, F., Fréd´, F., Thalasso, F., De, F., Cuervo, M., Opez, L. ´, & Texier, A.-C. (2013). Inhibitory effect of sulfide on the nitrifying respiratory process. *Journal of Chemical Technology & Biotechnology*, *88*(7), 1344–1349. https://doi.org/10.1002/JCTB.3982

Janot, N., Groenenberg, J. E., Otero-Fariña, A., & Pinheiro, J. P. (2021). Free Eu(III) Determination by Donnan Membrane Technique with Electrochemical Detection: Implementation and Evaluation. *Aquatic Geochemistry*, *27*(2), 127–140. https://doi.org/10.1007/s10498-021-09392-4

Janot, N., Pinheiro, J. P., Botero, W. G., Meeussen, J. C. L., & Groenenberg, J. E. (2017). PEST-ORCHESTRA, a tool for optimising advanced ion-binding model parameters: Derivation of NICA-Donnan model parameters for humic substances reactivity. *Environmental Chemistry*, *14*(1), 31–38. https://doi.org/10.1071/EN16039

Jardine, P. M., Mehlhorn, T. L., Bailey, W. B., Brooks, S. C., Fendorf, S., Gentry, R. W., Phelps, T. J., & Saiers, J. E. (2011). Geochemical Processes Governing the Fate and Transport of Chromium(III) and Chromium(VI) in Soils. *Vadose Zone Journal*, *10*(3), 1058–1070. https://doi.org/10.2136/vzj2010.0102

Jardine, P. M., Stewart, M. A., Barnett, M. O., Basta, N. T., Brooks, S. C., Fendorf, S., & Mehlhorn, T. L. (2013). Influence of soil geochemical and physical properties on chromium(VI) sorption and bioaccessibility. *Environmental Science and Technology*, *47*(19), 11241–11248. https://doi.org/10.1021/es401611h

Jean, G. E., & Bancroft, G. M. (1986). Heavy metal adsorption by sulphide mineral surfaces. *Geochimica et Cosmochimica Acta*, *50*(7), 1455–1463. https://doi.org/10.1016/0016-7037(86)90319-4

Jensen, D. L., Boddum, J. K., Tjell, J. C., & Christensen, T. H. (2002). The solubility of rhodochrosite (MnCO3) and siderite (FeCO3) in anaerobic aquatic environments. *Applied Geochemistry*, *17*(4), 503–511. https://doi.org/10.1016/S0883-2927(01)00118-4

Jianlong, W., & Ning, Y. (2004). Partial nitrification under limited dissolved oxygen conditions. *Process Biochemistry*, *39*(10), 1223–1229. https://doi.org/10.1016/S0032-9592(03)00249-8

Jin, Z., Ci, M., Yang, W., Shen, D., Hu, L., Fang, C., & Long, Y. (2020). Sulfate reduction behavior in the leachate saturated zone of landfill sites. *Science of The Total Environment*, *730*, 138946. https://doi.org/10.1016/J.SCITOTENV.2020.138946

Johnson, C. A., & Glasser, F. P. (2003). Hydrotalcite-like minerals (M2Al(OH 6(CO3)0.5XH2O, where M = Mg, Zn, Co, Ni) in the environment: Synthesis, characterization and thermodynamic stability. *Clays and Clay Minerals*, *51*(1), 1–8. https://doi.org/10.1346/CCMN.2003.510101

Jones, B. F., & Conko, K. M. (2011). Environmental influences on the occurrences of sepiolite and palygorskite: A brief review. In *Developments in Clay Science* (Vol. 3, pp. 69–83). Elsevier B.V. https://doi.org/10.1016/B978-0-444-53607-5.00003-7

Kalbitz, K., & Wennrich, R. (1998). Mobilization of heavy metals and arsenic in polluted wetland soils and its dependence on dissolved organic matter. *Science of The Total Environment*, *209*(1), 27–39. https://doi.org/10.1016/S0048-9697(97)00302-1

Kalis, E. J. J., Weng, L., Dousma, F., Temminghoff, E. J. M., & Van Riemsdijk, W. H. (2006). Measuring free metal ion concentrations in situ in natural waters using the Donnan Membrane Technique. *Environmental Science and Technology*, *40*(3), 955–961. https://doi.org/10.1021/es051435v

Karamalidis, A. K., & Dzombak, D. A. (2010). *Surface complexation modelling: gibbsite*. John Wiley & Sons.

Keith, M., Haase, K. M., Schwarz-Schampera, U., Klemd, R., Petersen, S., & Bach, W. (2014). Effects of temperature, sulfur, and oxygen fugacity on the composition of sphalerite from submarine hydrothermal vents. *Geology*, *42*(8), 699–702. https://doi.org/10.1130/G35655.1

Kim, D., Ryu, H. D., Kim, M. S., Kim, J., & Lee, S. I. (2007). Enhancing struvite precipitation potential for ammonia nitrogen removal in municipal landfill leachate. *Journal of Hazardous Materials*, *146*(1–2), 81–85. https://doi.org/10.1016/j.jhazmat.2006.11.054

Kim, H., Jang, Y. C., & Townsend, T. (2011). The behavior and long-term fate of metals in simulated landfill bioreactors under aerobic and anaerobic conditions. *Journal of Hazardous Materials*, *194*, 369–377. https://doi.org/10.1016/J.JHAZMAT.2011.07.119

Kinniburgh, D. G., Milne, C. J., Benedetti, M. F., Pinheiro, J. P., Filius, J., Koopal, L. K., & Van Riemsdijk, W. H. (1996). Metal ion binding by humic acid: Application of the NICA-Donnan model. *Environmental Science and Technology*, *30*(5), 1687–1698. https://doi.org/https://doi.org/10.1021/es950695h

Kinniburgh, D. G., Van Riemsdijk, W. H., Koopal, L. K., Borkovec, M., Benedetti, M. F., & Avena, M. J. (1999). Ion binding to natural organic matter: competition, heterogeneity, stoichiometry and thermodynamic consistency. *Colloids and Surfaces A: Physicochemical and Engineering Aspects*, *151*(1–2), 147–166. https://doi.org/https://doi.org/10.1016/S0927-7757(98)00637-2

Kjeldsen, P., Barlaz, M. A., Rooker, A. P., Baun, A., Ledin, A., & Christensen, T. H. (2002). Present and long-term composition of MSW landfill leachate: A review. *Critical Reviews in Environmental Science and Technology*, *32*(4), 297–336. https://doi.org/10.1080/10643380290813462

Kleber, M., & Lehmann, J. (2019). Humic Substances Extracted by Alkali Are Invalid Proxies for the Dynamics and Functions of Organic Matter in Terrestrial and Aquatic Ecosystems. *Journal of Environmental Quality*, *48*(2), 207–216. https://doi.org/10.2134/jeq2019.01.0036

Klinkert, S., & Comans, R. N. J. (2020). Geochemical Multisurface Modeling of Reactive Zinc Speciation in Compost as Influenced by Extraction Conditions. *Environmental Science and Technology*, *54*(4), 2467–2475. https://doi.org/10.1021/acs.est.9b04104

Kloster, N., Brigante, M., Zanini, G., & Avena, M. (2013). Aggregation kinetics of humic acids in the presence of calcium ions. *Colloids and Surfaces A: Physicochemical and Engineering Aspects*, *427*, 76–82. https://doi.org/10.1016/j.colsurfa.2013.03.030

Komonweeraket, K., Cetin, B., Aydilek, A. H., Benson, C. H., & Edil, T. B. (2015). Effects of pH on the leaching mechanisms of elements from fly ash mixed soils. *Fuel*, *140*, 788–802. https://doi.org/10.1016/j.fuel.2014.09.068

Konstantaki, L. A., Ghose, R., Draganov, D., & Heimovaara, T. (2016). Wet and gassy zones in a municipal landfill from P- and S-wave velocity fields. *Geophysics*, *81*(6), 75–86. https://doi.org/https://doi.org/10.1190/GEO2015-0581.1

Koo, T. H., & Kim, J. (2020). Controls on the Formation and Stability of Siderite (FeCO3) and Chukanovite (Fe2(CO3)(OH)2) in Reducing Environment. *Minerals*, *10*(2), 156. https://doi.org/10.3390/MIN10020156

Koopal, L. K., Saito, T., & Avena, M. (2025). Modified Donnan model for ion binding to small soft nano particles. *Colloids and Surfaces A: Physicochemical and Engineering Aspects*, *705*, 135665. https://doi.org/10.1016/J.COLSURFA.2024.135665

Koopal, L. K., Saito, T., Pinheiro, J. P., & Van Riemsdijk, W. H. (2005). Ion binding to natural organic matter: General considerations and the NICA–Donnan model. *Colloids and Surfaces A: Physicochemical and Engineering Aspects*, *265*(1–3), 40–54. https://doi.org/10.1016/J.COLSURFA.2004.11.050

Koopal, L., Tan, W., & Avena, M. (2020). Equilibrium mono- and multicomponent adsorption models: From homogeneous ideal to heterogeneous non-ideal binding. In *Advances in Colloid and Interface Science* (Vol. 280). Elsevier B.V. https://doi.org/10.1016/j.cis.2020.102138

Koopmans, G. F., & Groenenberg, J. E. (2011). Effects of soil oven-drying on concentrations and speciation of trace metals and dissolved organic matter in soil solution extracts of sandy soils. *Geoderma*, *161*(3–4), 147–158. https://doi.org/10.1016/j.geoderma.2010.12.012

Kosmulski, M. (2016). Isoelectric points and points of zero charge of metal (hydr)oxides: 50 years after Parks' review. *Advances in Colloid and Interface Science*, *238*, 1–61. https://doi.org/10.1016/j.cis.2016.10.005

Kosson, D. S., Van Der Sloot, H. A., & Eighmy, T. T. (1996). An approach for estimation of contaminant release during utilization and disposal of municipal waste combustion residues. *Journal of Hazardous Materials*, *47*(1–3), 43–75. https://doi.org/10.1016/0304-3894(95)00109-3

Kristensen, E., Ahmed, S. I., & Devol, A. H. (1995). Aerobic and anaerobic decomposition of organic matter in marine sediment: Which is fastest? *Limnology and Oceanography*, *40*(8), 1430–1437. https://doi.org/https://doi.org/10.4319/lo.1995.40.8.1430

Krupka, K. M., Erikson, R. L., Mattigod, S. V, Schramke, J. A., & Cowan, C. E. (1988). *Thermochemical data used by the FASTCHEM package: Final report*.

Kumar, B. (2025). Waste: Challenges and Opportunities. *Global Waste Management*, 15–27. https://doi.org/10.1002/9781394318414.CH2;PAGEGROUP:STRING:PUBLICATION

Kumar, M., & Lin, J. G. (2010). Co-existence of anammox and denitrification for simultaneous nitrogen and carbon removal-Strategies and issues. In *Journal of Hazardous Materials* (Vol. 178, Numbers 1–3, pp. 1–9). https://doi.org/10.1016/j.jhazmat.2010.01.077

Kumar, R., & Pal, P. (2015). Assessing the feasibility of N and P recovery by struvite precipitation from nutrient-rich wastewater: a review. *Environmental Science and Pollution Research*, *22*(22), 17453–17464. https://doi.org/10.1007/s11356-015-5450-2

Labrenz, M., Druschel, G. K., Thomsen-Ebert, T., Gilbert, B., Welch, S. A., Kemner, K. M., Logan, G. A., Summons, R. E., De Stasio, G., Bond, P. L., Lai, B., Kelly, S. D., & Banfield, J. F. (2000). Formation of sphalerite (ZnS) deposits in natural biofilms of sulfate-reducing bacteria. *Science*, *290*(5497), 1744–1747. https://doi.org/10.1126/science.290.5497.1744

Ladd, J. N., & Jackson, R. B. (1982). Biochemistry of ammonification. In *Nitrogen in Agricultural Soils* (Vol. 22, pp. 173–228). wiley. https://doi.org/10.2134/AGRONMONOGR22.C5

Lammen, H., Van Zomeren, A., Dijkstra, J. J., & Comans, R. N. J. (2019). Susainable landfill management: solid waste sampling and geochemical characterization prior to (an)aerobic stabilization of three old landfills. *17th International Symposium on Waste Management, Resource Recovery and Sustainable Landfilling, 2019*. www.cisapublisher.com

Laner, D., Crest, M., Scharff, H., Morris, J. W. F., & Barlaz, M. A. (2012). A review of approaches for the long-term management of municipal solid waste landfills. *Waste Management*, *32*(3), 498–512. https://doi.org/10.1016/j.wasman.2011.11.010

Lang, J. R., Allred, B. M. K., Field, J. A., Levis, J. W., & Barlaz, M. A. (2017). National Estimate of Per- and Polyfluoroalkyl Substance (PFAS) Release to U.S. Municipal Landfill Leachate. *Environmental Science and Technology*, *51*(4), 2197–2205. https://doi.org/https://doi.org/10.1021/acs.est.6b05005

Lee, J., Pedersen, A. B., & Thomsen, M. (2014). Are the resource strategies for sustainable development sustainable? Downside of a zero waste society with circular resource flows. *Environmental Technology & Innovation*, *1–2*(C), 46–54. https://doi.org/10.1016/J.ETI.2014.10.002

Lehmann, J., & Kleber, M. (2015). The contentious nature of soil organic matter. *Nature 2015 528:7580*, *528*(7580), 60–68. https://doi.org/10.1038/nature16069

Li, G., Jaisi, D. P., Wang, M., Yan, F., Zhang, X., Jin, Y., Zheng, Z., & Feng, X. (2024). Zeolite facilitates sequestration of heavy metals via lagged Fe(II) oxidation during sediment aeration. *Journal of Hazardous Materials*, *469*, 133961. https://doi.org/10.1016/J.JHAZMAT.2024.133961

Liang, Z., & Liu, J. (2008). Landfill leachate treatment with a novel process: Anaerobic ammonium oxidation (Anammox) combined with soil infiltration system. *Journal of Hazardous Materials*, *151*(1), 202–212. https://doi.org/10.1016/J.JHAZMAT.2007.05.068

Lindsay, W. L. (1979). *Chemical equilibria in soils*.

Linggi, L., Berlin, M., & Mallik, M. (2021). Experimental investigation on the effects of clay colloid-facilitated ammonium transport through saturated porous media under variable transport conditions. *Chemical Papers*, *75*(7), 3411–3420. https://doi.org/10.1007/s11696-021-01570-6

Liu, L., Xiong, H., Ma, J., Ge, S., Yu, X., & Zeng, G. (2018). Leachate Recirculation for Enhancing Methane Generation within Field Site in China. *Journal of Chemistry*, *1*. https://doi.org/10.1155/2018/9056561

Liu, X., & Millero, F. J. (1999). The solubility of iron hydroxide in sodium chloride solutions. *Geochimica et Cosmochimica Acta*, *63*(19–20), 3487–3497. https://doi.org/10.1016/S0016-7037(99)00270-7

Loncnar, M., Mladenovič, A., Zalar Serjun, V., Zupančič, M., & van der Sloot, H. A. (2022). Leaching and Geochemical Modelling of an Electric Arc Furnace (EAF) and Ladle Slag Heap. *Toxics*, *10*(1). https://doi.org/10.3390/toxics10010010

Loncnar, M., van der Sloot, H. A., Mladenovič, A., Zupančič, M., Kobal, L., & Bukovec, P. (2016). Study of the leaching behaviour of ladle slags by means of leaching tests combined with geochemical modelling and mineralogical investigations. *Journal of Hazardous Materials*, *317*, 147–157. https://doi.org/10.1016/J.JHAZMAT.2016.05.046

Long, Y., Liu, D., Xu, J., Fang, Y., Du, Y., & Shen, D. (2018). Release behavior of chloride from MSW landfill simulation reactors with different operation modes. *Waste Management*, *77*, 350–355. https://doi.org/10.1016/J.WASMAN.2018.04.018

Löv, Å., Sjöstedt, C., Larsbo, M., Persson, I., Gustafsson, J. P., Cornelis, G., & Kleja, D. B. (2017). Solubility and transport of Cr(III) in a historically contaminated soil – Evidence of a rapidly reacting dimeric Cr(III) organic matter complex. *Chemosphere*, *189*, 709–716. https://doi.org/10.1016/j.chemosphere.2017.09.088

Lu, M. C., Chen, Y. Y., Chiou, M. R., Chen, M. Y., & Fan, H. J. (2016). Occurrence and treatment efficiency of pharmaceuticals in landfill leachates. *Waste Management*, *55*, 257–264. https://doi.org/10.1016/J.WASMAN.2016.03.029

Luo, H., Cheng, Y., He, D., & Yang, E. H. (2019). Review of leaching behavior of municipal solid waste incineration (MSWI) ash. *Science of the Total Environment*, *668*, 90–103. https://doi.org/10.1016/j.scitotenv.2019.03.004

Luther, G. W., & Rickard, D. T. (2005). Metal sulfide cluster complexes and their biogeochemical importance in the environment. *Journal of Nanoparticle Research*, *7*(4–5), 389–407. https://doi.org/10.1007/S11051-005-4272-4/METRICS

Ma, J., Li, Y., & Li, Y. (2021). Effects of leachate recirculation quantity and aeration on leachate quality and municipal solid waste stabilization in semi-aerobic landfills. *Environmental Technology and Innovation*, *21*(19), 101353. https://doi.org/10.1016/j.eti.2021.101353

Maguire, M., Slaved, J., Vimpany, I., Higginsonh, F. R., & Pickering, W. F. (1981). Influence of pH on copper and zinc uptake by soil clays. *Soil Research*, *19*(3), 217–229. https://doi.org/10.1071/SR9810217

Manheim, D. C., Yeşiller, N., & Hanson, J. L. (2021). Gas Emissions from Municipal Solid Waste Landfills: A Comprehensive Review and Analysis of Global Data. *Journal of the Indian Institute of Science 2021 101:4*, *101*(4), 625–657. https://doi.org/10.1007/S41745-021-00234-4

Manning, D. A. C. (2001). Calcite precipitation in landfills: an essential product of waste stabilization. *Mineralogical Magazine*, *65*(5), 603–610. https://doi.org/https://doi.org/10.1180/002646101317018424

Marttinen, S. K., Kettunen, R. H., & Rintala, J. A. (2003). Occurrence and removal of organic pollutants in sewages and landfill leachates. *Science of The Total Environment*, *301*(1–3), 1–12. https://doi.org/10.1016/S0048-9697(02)00302-9

Masoner, J. R., Kolpin, D. W., Furlong, E. T., Cozzarelli, I. M., & Gray, J. L. (2016). Landfill leachate as a mirror of today's disposable society: Pharmaceuticals and other contaminants of emerging concern in final leachate from landfills in the conterminous United States. *Environmental Toxicology and Chemistry*, *35*(4), 906–918. https://doi.org/10.1002/ETC.3219

Mathur, S. S., & Dzombak, D. A. (2006). Surface complexation modelling: goethite. In *Surface Complexation Modelling* (Vol. 11). Elsevier.

Mavromatis, V., Harrison, A. L., Eisenhauer, A., & Dietzel, M. (2017). Strontium isotope fractionation during strontianite (SrCO3) dissolution, precipitation and at equilibrium. *Geochimica et Cosmochimica Acta*, *218*, 201–214. https://doi.org/10.1016/J.GCA.2017.08.039

McGrath, S. P. (1982). The uptake and translocation of tri-valent and hexa-valent chromium and effects on the growth of oat in flowing nutrient solution and in soil. *New Phytologist*, *92*(3), 381–390. https://doi.org/10.1111/j.1469-8137.1982.tb03395.x

McLaren, T. I., Smernik, R. J., McLaughlin, M. J., McBeath, T. M., Kirby, J. K., Simpson, R. J., Guppy, C. N., Doolette, A. L., & Richardson, A. E. (2015). Complex Forms of Soil Organic Phosphorus-A Major Component of Soil Phosphorus. *Environmental Science and Technology*, *49*(22), 13238–13245. https://doi.org/https://doi.org/10.1021/acs.est.5b02948

Meeussen, J. C. L. (2003). Orchestra: An object-oriented framework for implementing chemical equilibrium models. *Environmental Science and Technology*, *37*(6), 1175–1182. https://doi.org/10.1021/es025597s

Meima, J. A., & Comans, R. N. J. (1997). Geochemical modeling of weathering reactions in municipal solid waste incinerator bottom ash. *Environmental Science and Technology*, *31*(5), 1269–1276. https://doi.org/10.1021/es9603158

Meima, J. A., & Comans, R. N. J. (1998a). Application of Surface Complexation/ Precipitation Modeling to Contaminant Leaching from Weathered Municipal Solid Waste Incinerator Bottom Ash. *Environmental Science & Technology*, 688–693. https://pubs.acs.org/sharingguidelines

Meima, J. A., & Comans, R. N. J. (1998b). Reducing Sb-leaching from municipal solid waste incinerator bottom ash by addition of sorbent minerals. *Journal of Geochemical Exploration*, *62*, 299–304. https://doi.org/https://doi.org/10.1016/S0375-6742(97)00044-7

Meima, J. A., & Comans, R. N. J. (1999). The leaching of trace elements from municipal solid waste incinerator bottom ash at different stages of weathering. *Applied Geochemistry*, *14*, 159–171. https://doi.org/10.1016/S0883-2927(98)00047-X

Mendez, J. C., & Hiemstra, T. (2020). Ternary Complex Formation of Phosphate with Ca and Mg Ions Binding to Ferrihydrite: Experiments and Mechanisms. *ACS Earth and Space Chemistry*, *4*(4), 545–557. https://doi.org/10.1021/ACSEARTHSPACECHEM.9B00320

Mertoglu, B., Calli, B., Inanc, B., & Ozturk, I. (2006). Evaluation of in situ ammonia removal in an aerated landfill bioreactor. *Process Biochemistry*, *41*(12), 2359–2366. https://doi.org/10.1016/J.PROCBIO.2006.06.014

Milne, C. J., Kinniburgh, D. G., & Tipping, E. (2001). Generic NICA-Donnan model parameters for proton binding by humic substances. *Environmental Science and Technology*, *35*(10), 2049–2059. https://doi.org/10.1021/es000123j

Milne, C. J., Kinniburgh, D. G., Van Riemsdijk, W. H., & Tipping, E. (2003). Generic NICA - Donnan model parameters for metal-ion binding by humic substances. *Environmental Science and Technology*, *37*(5), 958–971. https://doi.org/10.1021/es0258879

Moody, C. M., & Townsend, T. G. (2017). A comparison of landfill leachates based on waste composition. *Waste Management*, *63*, 267–274. https://doi.org/10.1016/j.wasman.2016.09.020

Morello, L., Cossu, R., Raga, R., Pivato, A., & Lavagnolo, M. C. (2016). Recirculation of reverse osmosis concentrate in lab-scale anaerobic and aerobic landfill simulation reactors. *Waste Management*, *56*, 262–270. https://doi.org/10.1016/J.WASMAN.2016.07.030

Morris, J. W. F., Vasuki, N. C., Baker, J. A., & Pendleton, C. H. (2003). Findings from long-term monitoring studies at MSW landfill facilities with leachate recirculation. *Waste Management*, *23*(7), 653–666. https://doi.org/10.1016/S0956-053X(03)00098-9

Nag, M., Shimaoka, T., & Komiya, T. (2018). Influence of operations on leachate characteristics in the Aerobic-Anaerobic Landfill Method. *Waste Management*, *78*, 698–707. https://doi.org/10.1016/J.WASMAN.2018.06.044

NEN-EN 14997. (2015). *Characterization of waste - leaching behaviour test - Influence of pH on leaching with continuous pH control*.

Nicholls, R. J., Beaven, R. P., Stringfellow, A., Monfort, D., Le Cozannet, G., Wahl, T., Gebert, J., Wadey, M., Arns, A., Spencer, K. L., Reinhart, D., Heimovaara, T., Santos, V. M., Enríquez, A. R., & Cope, S. (2021). Coastal Landfills and Rising Sea Levels: A Challenge for the 21st Century. *Frontiers in Marine Science*, *8*, 710342. https://doi.org/https://doi.org/10.3389/fmars.2021.710342

Nieder, R., Benbi, D. K., & Scherer, H. W. (2011). Fixation and defixation of ammonium in soils: a review. *Biology and Fertility of Soils*, *47*, 1–14. https://doi.org/10.1007/s00374-010-0506-4

Nikolaou, A., Giannis, A., & Gidarakos, E. (2010). Comparative studies of aerobic and anaerobic treatment of MSW organic fraction in landfill bioreactors. *Environmental Technology*, *31*(12), 1381–1389. https://doi.org/10.1080/09593331003743104

Nommik, H. (1965). Ammonium fixation and other reactions involving a nonenzymatic immobilization of mineral nitrogen in soil. In W. V. Bartholomew & F. E. Clark (Eds.), *Soil Nitrogen* (Vol. 10, pp. 198–258). Wiley Blackwell. https://doi.org/10.2134/AGRONMONOGR10.C5

Nommik, H. (1970). Non-exchangeable binding of ammonium and amino nitrogen by Norway spruce raw humus. *Plant and Soll*, *33*, 1344. https://doi.org/https://doi.org/10.1007/BF01378248

Nommik, H., & Ahtras, K. V. (1982). Retention and Fixation of Ammonium and Ammonia in Soils. In *Nitrogen in Agricultural soils* (Vol. 22, 4). https://doi.org/https://doi.org/10.2134/agronmonogr22.c4

Ohta, A., Kagi, H., Tsuno, H., Nomure, M., & Okai, T. (2012). Speciation study of Cr(VI/III) reacting with humic substances and determination of local structure of Cr binding humic substances

using XAFS spectroscopy. *Geochemical Journal*, *46*, 409–420. https://doi.org/https://doi.org/10.2343/geochemj.2.0222

Olk, D. C., Bloom, P. R., Perdue, E. M., McKnight, D. M., Chen, Y., Farenhorst, A., Senesi, N., Chin, Y.-P., Schmitt-Kopplin, P., Hertkorn, N., & Harir, M. (2019). Environmental and Agricultural Relevance of Humic Fractions Extracted by Alkali from Soils and Natural Waters. *Journal of Environmental Quality*, *48*(2), 217–232. https://doi.org/10.2134/jeq2019.02.0041

Oonk, H., Zomeren, A. van, Rees-White, T. C., Beaven, R. P., Hoekstra, N., Luning, L., Hannen, M., Hermkes, H., & Woelders, H. (2013). Enhanced biodegradation at the Landgraaf bioreactor test-cell. *Waste Management*, *33*(10), 2048–2060. https://doi.org/10.1016/J.WASMAN.2013.03.003

Oste, L. A., Temminghoff, E. J. M., Lexmond, T. M., & Van Riemsdijk, W. H. (2002). Measuring and modeling zinc and cadmium binding by humic acid. *Analytical Chemistry*, *74*(4), 856–862. https://doi.org/10.1021/ac0105080

Östman, M., Wahlberg, O., Ågren, S., & Mårtensson, A. (2006). Metal and organic matter contents in a combined household and industrial landfill. *Waste Management*, *26*(1), 29–40. https://doi.org/10.1016/J.WASMAN.2005.01.012

Östman, M., Wahlberg, O., & Mårtensson, A. (2008). Leachability and metal-binding capacity in ageing landfill material. *Waste Management*, *28*(1), 142–150. https://doi.org/10.1016/J.WASMAN.2006.11.003

Otero-Fariña, A., Janot, N., Marsac, R., Catrouillet, C., & Groenenberg, J. E. (2023). Rare earth elements binding humic acids: NICA–Donnan modelling. *Environmental Chemistry*, *21*(1), NULL-NULL. https://doi.org/10.1071/EN23049

Paleari, S. (2022). The Impact of the European Green Deal on EU Environmental Policy. *Journal of Environment and Development*, *31*(2), 196–220. https://doi.org/https://doi.org/10.1177/10704965221082

Pan, C., Troyer, L. D., Liao, P., Catalano, J. G., Li, W., & Giammar, D. E. (2017). Effect of Humic Acid on the Removal of Chromium(VI) and the Production of Solids in Iron Electrocoagulation. *Environmental Science and Technology*, *51*(11), 6308–6318. https://doi.org/10.1021/acs.est.7b00371

Pan, Y., Bonten, L. T. C., Koopmans, G. F., Song, J., Luo, Y., Temminghoff, E. J. M., & Comans, R. N. J. (2016). Solubility of trace metals in two contaminated paddy soils exposed to alternating flooding and drainage. *Geoderma*, *261*, 59–69. https://doi.org/10.1016/j.geoderma.2015.07.011

Pan, Y., Koopmans, G. F., Bonten, L. T. C., Song, J., Luo, Y., Temminghoff, E. J. M., & Comans, R. N. J. (2014). Influence of pH on the redox chemistry of metal (hydr)oxides and organic matter in paddy soils. *Journal of Soils and Sediments*, *14*(10), 1713–1726. https://doi.org/10.1007/S11368-014-0919-Z/FIGURES/5

Papassiopi, N., Vaxevanidou, K., Christou, C., Karagianni, E., & Antipas, G. S. E. (2014). Synthesis, characterization and stability of Cr(III) and Fe(III) hydroxides. *Journal of Hazardous Materials*, *264*, 490–497. https://doi.org/10.1016/j.jhazmat.2013.09.058

Parker, D. R., Chaney, R. L., & Norvell, W. A. (1995). Chemical Equilibrium Models: Applications to Plant Nutrition Research. In *Chemical equilibrium and reaction models* (Vol. 42, pp. 163–200).

Parks, J. L., & Edwards, M. (2005). Boron in the environment. In *Critical Reviews in Environmental Science and Technology* (Vol. 35, Number 2, pp. 81–114). https://doi.org/10.1080/10643380590900200

Pereira, A. D., Cabezas, A., Etchebehere, C., Chernicharo, C. A. de L., & de Araújo, J. C. (2017). Microbial communities in anammox reactors: a review. *Environmental Technology Reviews*, *6*(1), 74–93. https://doi.org/10.1080/21622515.2017.1304457

Perkins, R. B., & Palmer, C. D. (1999). *Solubility of ettringite (Ca 6 [Al(OH) 6] 2 (SO 4) 3 26H 2 O) at 5-75°C*.

Pham, A. N., Rose, A. L., & Waite, T. D. (2012). Kinetics of Cu(II) reduction by natural organic matter. *Journal of Physical Chemistry A*, *116*(25), 6590–6599. https://doi.org/10.1021/JP300995H/SUPPL_FILE/JP300995H_SI_001.PDF

Pinheiro, J. P., Rotureau, E., & Duval, J. F. L. (2021). Addressing the electrostatic component of protons binding to aquatic nanoparticles beyond the Non-Ideal Competitive Adsorption (NICA)-Donnan level: Theory and application to analysis of proton titration data for humic matter. *Journal of Colloid and Interface Science*, *583*, 642–651. https://doi.org/10.1016/j.jcis.2020.09.059

Pires, A., & Martinho, G. (2019). Waste hierarchy index for circular economy in waste management. *Waste Management*, *95*, 298–305. https://doi.org/10.1016/J.WASMAN.2019.06.014

Pokrovsky, O. S., & Schott, J. (2004). Experimental study of brucite dissolution and precipitation in aqueous solutions: surface speciation and chemical affinity control. *Geochimica et Cosmochimica Acta*, *68*(1), 31–45. https://doi.org/10.1016/S0016-7037(03)00238-2

Ponthieu, M., Juillot, F., Hiemstra, T., van Riemsdijk, W. H., & Benedetti, M. F. (2006). Metal ion binding to iron oxides. *Geochimica et Cosmochimica Acta*, *70*(11), 2679–2698. https://doi.org/10.1016/J.GCA.2006.02.021

Powell, J. T., Townsend, T. G., & Zimmerman, J. B. (2016). Estimates of solid waste disposal rates and reduction targets for landfill gas emissions. *Nature Climate Change*, *6*(2), 162–165. https://doi.org/10.1038/nclimate2804

Power, I. M., Kenward, P. A., Dipple, G. M., & Raudsepp, M. (2017). Room Temperature Magnesite Precipitation. *Crystal Growth and Design*, *17*(11), 5652–5659. https://doi.org/https://doi.org/10.1021/acs.cgd.7b00311

Prantl, R., Tesar, M., Huber-Humer, M., & Lechner, P. (2006). Changes in carbon and nitrogen pool during in-situ aeration of old landfills under varying conditions. *Waste Management*, *26*(4), 373–380. https://doi.org/10.1016/J.WASMAN.2005.11.010

Pribyl, D. W. (2010). A critical review of the conventional SOC to SOM conversion factor. *Geoderma*, *156*(3–4), 75–83. https://doi.org/10.1016/j.geoderma.2010.02.003

Prosser, J. I. (2007). The Ecology of Nitrifying Bacteria. *Biology of the Nitrogen Cycle*, 223–243. https://doi.org/10.1016/B978-044452857-5.50016-3

Qafoku, O., Dixon, D. A., Rosso, K. M., Schaef, H. T., Bowden, M. E., Arey, B. W., & Felmy, A. R. (2015). Dynamics of Magnesite Formation at Low Temperature and High pCO2 in Aqueous Solution. *Environmental Science & Technology*, *49*(17), 10736–10744. https://doi.org/10.1021/acs.est.5b02588

Qiao, W., Guo, H., He, C., Shi, Q., Xiu, W., & Zhao, B. (2020). Molecular Evidence of Arsenic Mobility Linked to Biodegradable Organic Matter. *Environmental Science and Technology*, *54*(12), 7280–7290. https://doi.org/10.1021/ACS.EST.0C00737/ASSET/IMAGES/LARGE/ES0C00737_0006.JPEG

Qin, F., Wen, B., Shan, X. Q., Xie, Y. N., Liu, T., Zhang, S. Z., & Khan, S. U. (2006). Mechanisms of competitive adsorption of Pb, Cu, and Cd on peat. *Environmental Pollution*, *144*(2), 669–680. https://doi.org/10.1016/J.ENVPOL.2005.12.036

Quina, M. J., Bordado, J. C. M., & Quinta-Ferreira, R. M. (2009). The influence of pH on the leaching behaviour of inorganic components from municipal solid waste APC residues. *Waste Management*, *29*(9), 2483–2493. https://doi.org/10.1016/j.wasman.2009.05.012

Raffe, F. van, Comans, R. N. J., & Groenenberg, J. E. (2025). Chromium(III) Binding to Purified Fulvic and Humic Acids and Their Solid-Solution Partitioning and Speciation in Soil. *ACS Earth and Space Chemistry*. https://doi.org/10.1021/ACSEARTHSPACECHEM.5C00075

Raga, R., & Cossu, R. (2013). Bioreactor tests preliminary to landfill in situ aeration: A case study. *Waste Management*, *33*(4), 871–880. https://doi.org/10.1016/J.WASMAN.2012.11.014

Raga, R., Cossu, R., Heerenklage, J., Pivato, A., & Ritzkowski, M. (2015). Landfill aeration for emission control before and during landfill mining. *Waste Management*, *46*, 420–429. https://doi.org/10.1016/J.WASMAN.2015.09.037

Rai, D., Eary, L. E., & Zachara, J. M. (1989). Environmental chemistry of chromium. *The Science of the Total Environment*, *86*(1–2), 15–23. https://doi.org/https://doi.org/10.1016/0048-9697(89)90189-7

Rai, D., Sass, B. M., & Moore, D. A. (1987). Chromium(III) Hydrolysis Constants and Solubility of Chromium(III) Hydroxide. *Inorganic Chemistry*, *26*(3), 345–349. https://doi.org/https://doi.org/10.1021/ic00250a002

Rasmussen, L. (1990). *Nitrification in Forest Soils: Effects from Nitrogen Deposition on Soil Acidification and Aluminum Release*. https://doi.org/https://doi.org/10.1007/978-1-4612-3366-4_1

Reijonen, I., & Hartikainen, H. (2016). Oxidation mechanisms and chemical bioavailability of chromium in agricultural soil – pH as the master variable. *Applied Geochemistry*, *74*, 84–93. https://doi.org/10.1016/j.apgeochem.2016.08.017

Reinhart, D. R. (1996). Full-Scale Experiences With Leachate Recirculating Landfills: Case Studies. *Waste Management & Research*, *14*(4), 347–365. https://doi.org/10.1177/0734242X9601400403

Reinhart, D. R., & Al-Yousfi, A. B. (1996). The impact of leachate recirculation on municipal solid waste landfill operating characteristics. *Waste Management & Research*, *14*, 337–346. https://doi.org/https://doi.org/10.1006/wmre.1996.0035

Renou, S., Givaudan, J. G., Poulain, S., Dirassouyan, F., & Moulin, P. (2008). Landfill leachate treatment: Review and opportunity. *Journal of Hazardous Materials*, *150*(3), 468–493. https://doi.org/10.1016/j.jhazmat.2007.09.077

Rich, C., Gronow, J., & Voulvoulis, N. (2008). The potential for aeration of MSW landfills to accelerate completion. *Waste Management*, *28*(6), 1039–1048. https://doi.org/10.1016/j.wasman.2007.03.022

Ritzkowski, M., Heyer, K. U., & Stegmann, R. (2006). Fundamental processes and implications during in situ aeration of old landfills. *Waste Management*, *26*(4), 356–372. https://doi.org/10.1016/j.wasman.2005.11.009

Ritzkowski, M., & Stegmann, R. (2007). Controlling greenhouse gas emissions through landfill in situ aeration. *International Journal of Greenhouse Gas Control*, *1*(3), 281–288. https://doi.org/10.1016/S1750-5836(07)00029-1

Ritzkowski, M., & Stegmann, R. (2012). Landfill aeration worldwide: Concepts, indications and findings. *Waste Management*, *32*(7), 1411–1419. https://doi.org/10.1016/j.wasman.2012.02.020

Rodrigues, C. C., de Moraes, D., da Nóbrega, S. W., & Barboza, M. G. (2007). Ammonia adsorption in a fixed bed of activated carbon. *Bioresource Technology*, *98*(4), 886–891. https://doi.org/10.1016/J.BIORTECH.2006.03.024

Roy, S. (1968). Mineralogy of the Different Genetic Types of Manganese Deposits. *Economic Geology*, *63*, 760–786.

Sabba, F., Kassar, C., Zeng, T., Mallick, S. P., Downing, L., & McNamara, P. (2025). PFAS in landfill leachate: Practical considerations for treatment and characterization. *Journal of Hazardous Materials*, *481*, 136685. https://doi.org/10.1016/J.JHAZMAT.2024.136685

Sahrawat, K. L. (2008). Factors affecting nitrification in soils. *Communications in Soil Science and Plant Analysis*, *39*(9–10), 1436–1446. https://doi.org/10.1080/00103620802004235

Samson, E., Lemaire, G., Marchand, J., & Beaudoin, J. J. (1999). Modeling chemical activity effects in strong ionic solutions. *Computational Materials Science*, *15*(3), 285–294. https://doi.org/10.1016/S0927-0256(99)00017-8

Šan, I., & Onay, T. T. (2001). Impact of various leachate recirculation regimes on municipal solid waste degradation. *Journal of Hazardous Materials*, *87*, 259–271.

Sanphoti, N., Towprayoon, S., Chaiprasert, P., & Nopharatana, A. (2006). The effects of leachate recirculation with supplemental water addition on methane production and waste decomposition in a simulated tropical landfill. *Journal of Environmental Management*, *81*(1), 27–35. https://doi.org/10.1016/J.JENVMAN.2005.10.015

Schalk, T., Marx, C., Haupt, A., Kühn, V., & Krebs, P. (2019). Long-Term Effects of Sulfide on Ammonia Oxidation and Nitrite Accumulation in a Seasonally Loaded Vertical Flow Constructed Wetland. *Wetlands 2019 40:2*, *40*(2), 205–222. https://doi.org/10.1007/S13157-019-01185-4

Scharff, H. (2014). Landfill reduction experience in The Netherlands. *Waste Management*, *34*(11), 2218–2224. https://doi.org/10.1016/j.wasman.2014.05.019

Scharff, H., Van Zomeren, A., & Van Der Sloot, H. A. (2011). Landfill sustainability and aftercare completion criteria. *Waste Management and Research*, *29*(1), 30–40. https://doi.org/10.1177/0734242X10384310

Schellekens, J., Buurman, P., Kalbitz, K., Zomeren, A. Van, Vidal-Torrado, P., Cerli, C., & Comans, R. N. J. (2017). Molecular Features of Humic Acids and Fulvic Acids from Contrasting Environments. *Environmental Science and Technology*, *51*(3), 1330–1339. https://doi.org/10.1021/acs.est.6b03925

Schwab, A. P., & Lindsay, W. L. (1983). Effect of Redox on the Solubility and Availability of Iron. *Soil Science Society of America Journal*, *47*(2), 201–205. https://doi.org/10.2136/sssaj1983.03615995004700020005x

Séby, F., Potin-Gautier, M., Giffaut, E., & Donard, O. F. X. (2001). A critical review of thermodynamic data for inorganic tin species. *Geochimica et Cosmochimica Acta*, *65*(18), 3041–3053. https://doi.org/10.1016/S0016-7037(01)00645-7

Shammas, N. (1986). Interactions of Temperature, pH, and Biomass on the Nitrification Process. *Water Pollution Control Federation*, *58*(1), 52–59.

Shi, Z., Wang, P., Peng, L., Lin, Z., & Dang, Z. (2016). Kinetics of Heavy Metal Dissociation from Natural Organic Matter: Roles of the Carboxylic and Phenolic Sites. *Environmental Science and Technology*, *50*(19), 10476–10484. https://doi.org/10.1021/ACS.EST.6B01809

Siddiqua, A., Hahladakis, J. N., & Al-Attiya, W. A. K. A. (2022). An overview of the environmental pollution and health effects associated with waste landfilling and open dumping. *Environmental Science and Pollution Research*, *29*(39), 58514–58536. https://doi.org/10.1007/S11356-022-21578-Z

Sinan Bilgili, M., Demir, A., Ince, M., & Özkaya, B. (2007). Metal concentrations of simulated aerobic and anaerobic pilot scale landfill reactors. *Journal of Hazardous Materials*, *145*(1–2), 186–194. https://doi.org/10.1016/j.jhazmat.2006.11.014

Sjöstedt, C., Kristofferson, Å., Gustafsson, J. P., Heldele, A. S., Kessler, V., & Kleja, D. B. (2022). Evidence of the mineral ZnHAsO4·H2O, koritnigite, controlling As(V) and Zn(II) solubility in a multi-contaminated soil. *Applied Geochemistry*, *140*. https://doi.org/10.1016/j.apgeochem.2022.105301

Slezak, R., Krzystek, L., & Ledakowicz, S. (2009). Simulation of aerobic landfill in laboratory scale lysimeters — effect of aeration rate. *Chemical Papers 2009 64:2*, *64*(2), 223–229. https://doi.org/10.2478/S11696-009-0113-8

Slezak, R., Krzystek, L., & Ledakowicz, S. (2015). Degradation of municipal solid waste in simulated landfill bioreactors under aerobic conditions. *Waste Management*, *43*, 293–299. https://doi.org/10.1016/J.WASMAN.2015.06.017

Smith, D. S., Bell, R. A., & Kramer, J. R. (2002). Metal speciation in natural waters with emphasis on reduced sulfur groups as strong metal binding sites. *Comparative Biochemistry and Physiology Part C: Toxicology & Pharmacology*, *133*(1–2), 65–74. https://doi.org/10.1016/S1532-0456(02)00108-4

Sohoo, I., Ritzkowski, M., & Kuchta, K. (2021). Influence of moisture content and leachate recirculation on oxygen consumption and waste stabilization in post aeration phase of landfill operation. *Science of the Total Environment*, *773*. https://doi.org/10.1016/j.scitotenv.2021.145584

Song, J., Townsend, T., Solo-Gabriele, H., & Jang, Y. C. (2006). Hexavalent chromium reduction in soils contaminated with chromated copper arsenate preservative. *Soil and Sediment Contamination*, *15*(4), 387–399. https://doi.org/10.1080/15320380600751751

Stark, J. M. (1996). Modeling the temperature response of nitrification. *Biogeochemistry*, *35*(3), 433–445. https://doi.org/10.1007/BF02183035/METRICS

Stefánsson, A. (2007). Iron(III) hydrolysis and solubility at 25°C. *Environmental Science and Technology*, *41*(17), 6117–6123. https://doi.org/10.1021/ES070174H/SUPPL_FILE/ES070174HSI20070503_115412.PDF

Sternbeck, J. (1997). Kinetics of rhodochrosite crystal growth at 25°C: The role of surface speciation. *Geochimica et Cosmochimica Acta*, *61*(4), 785–793. https://doi.org/10.1016/S0016-7037(96)00379-1

Stewart, M. A., Jardine, P. M., Brandt, C. C., Barnett, M. O., Fendorf, S. E., McKay, L. D., Mehlhorn, T. L., & Paul, K. (2003). Effects of contaminant concentration, aging, and soil properties on the bioaccessibility of Cr(III) and Cr(VI) in soil. *Soil and Sediment Contamination*, *12*(1), 1–21. https://doi.org/10.1080/713610958

Stringfellow, A., Beaven, R., Rees-White, T., Smethurst, J., Powrie, W., & Kanen, T. (2023). Installation of a vadose zone monitoring system for tracer testing in a municipal solid waste landfill subject to leachate recirculation. *19th International Symposium on Waste Management, Resource Recovery and Sustainable Landfilling*.

Stuenzi, H., Spiccia, L., Rotzinger, F. P., & Marty, W. (1989). Early Stages of the Hydrolysis of Chromium(III) in Aqueous Solution. 4. Stability Constants of the Hydrolytic Dimer, Trimer, and Tetramer at 25 °C and I = 1.0 M. *Inorganic Chemistry*, *28*(1), 66–71. https://doi.org/doi:10.1021/ic00300a015

Sundberg, C., Smårs, S., & Jönsson, H. (2004). Low pH as an inhibiting factor in the transition from mesophilic to thermophilic phase in composting. *Bioresource Technology*, *95*(2), 145–150. https://doi.org/10.1016/J.BIORTECH.2004.01.016

Suter, D., Banwart, S., & Stumm, W. (1991). Dissolution of Hydrous Iron(III) Oxides by Reductive Mechanisms. *C. Ber. Bunsen-Ges. Phys. Chem*, *7*(1), 333. https://pubs.acs.org/sharingguidelines

Swift, R. S. (1996). Organic Matter Characterization. *Methods of Soil Analysis, Part 3: Chemical Methods*, 1011–1069. https://doi.org/10.2136/SSSABOOKSER5.3.C35

Tansel, B., Lunn, G., & Monje, O. (2018). Struvite formation and decomposition characteristics for ammonia and phosphorus recovery: A review of magnesium-ammonia-phosphate interactions. *Chemosphere*, *194*, 504–514. https://doi.org/10.1016/J.CHEMOSPHERE.2017.12.004

Temminghoff, E. J. M., Plette, A. C., Van Eck, R., & Van Riemsdijk, W. H. (2000). Determination of the chemical speciation of trace metals in aqueous systems by the Wageningen Donnan Membrane Technique. *Analytica Chimica Acta*, *417*(2). https://doi.org/https://doi.org/10.1016/S0003-2670(00)00935-1

Temminghoff, E. J. M., Van der Zee, S., & De Haan, F. (1997). Copper Mobility in a Copper-Contaminated Sandy Soil as Affected by pH and Solid and Dissolved Organic Matter. *Environmental Science & Technology*, *31*, 1109–1115. https://doi.org/doi:10.1021/es9606236

Teng, C., Zhou, K., Peng, C., & Chen, W. (2021). Characterization and treatment of landfill leachate: A review. *Water Research*, *203*, 117525. https://doi.org/10.1016/J.WATRES.2021.117525

Tiberg, C., Sjöstedt, C., Eriksson, A. K., Klysubun, W., & Gustafsson, J. P. (2020). Phosphate competition with arsenate on poorly crystalline iron and aluminum (hydr)oxide mixtures. *Chemosphere*, *255*. https://doi.org/10.1016/j.chemosphere.2020.126937

Tipping, E. (1998). Humic Ion-Binding Model VI: An Improved Description of the Interactions of Protons and Metal Ions with Humic Substances. *Aquatic Geochemistry*, *4*, 3–47. https://doi.org/https://doi.org/10.1023/A:1009627214459

Tipping, E., Lofts, S., & Sonke, J. E. (2011). Humic Ion-Binding Model VII: A revised parameterisation of cation-binding by humic substances. *Environmental Chemistry*, *8*(3), 225–235. https://doi.org/10.1071/EN11016

Tiwari, M. K., Bajpai, S., Dewangan, U. K., & Tamrakar, R. K. (2015). Suitability of leaching test methods for fly ash and slag: A review. *Journal of Radiation Research and Applied Sciences*, *8*(4), 523–537. https://doi.org/10.1016/j.jrras.2015.06.003

Tong, H., Yin, K., Giannis, A., Ge, L., & Wang, J. Y. (2015). Influence of temperature on carbon and nitrogen dynamics during in situ aeration of aged waste in simulated landfill bioreactors. *Bioresource Technology*, *192*, 149–156. https://doi.org/10.1016/j.biortech.2015.05.049

Town, R. M., Van Leeuwen, H. P., & Duval, J. F. L. (2019). Rigorous Physicochemical Framework for Metal Ion Binding by Aqueous Nanoparticulate Humic Substances: Implications for Speciation Modeling by the NICA-Donnan and WHAM Codes. *Environmental Science and Technology*, *53*(15), 8516–8532. https://doi.org/10.1021/acs.est.9b00624

Tumolo, M., Ancona, V., De Paola, D., Losacco, D., Campanale, C., Massarelli, C., & Uricchio, V. F. (2020). Chromium pollution in European water, sources, health risk, and remediation strategies: An overview. *International Journal of Environmental Research and Public Health*, *17*(15), 1–25. https://doi.org/10.3390/ijerph17155438

Turner, D. A., Beaven, R. P., & Woodman, N. D. (2017). Evaluating landfill aftercare strategies: A life cycle assessment approach. *Waste Management*, *63*, 417–431. https://doi.org/10.1016/J.WASMAN.2016.12.005

Uddh-Söderberg, T., Augustsson, A., Kleja, D. B., Jarsjö, J., Fröberg, M., Åström, M., & Gustafsson, J. P. (2024). Challenges in geochemical modelling of metal(loid) solubility and binding mechanisms along a soil profile at a multi-contaminated site. *Applied Geochemistry*, *170*. https://doi.org/10.1016/j.apgeochem.2024.106063

United Nations Environment Programme. (2024). *Global Waste Management Outlook 2024: Beyond and age of waste - Turning rubbish into a resource*. https://wedocs.unep.org/20.500.11822/44939

US EPA. (1999). *MINTEQA2/PRODEFA2, A Geochemical assessment model for environmental systems: user manual supplement for versio 4.0*.

US EPA. (2009). *Description of input and examples for PHREEQC version 3: a computer program for speciation, batch-reaction, one-dimensional transport, and inverse geochemical calculations*.

Valencia, R., Zon, W. van der, Woelders, H., Lubberding, H. J., & Gijzen, H. J. (2011). Anammox: An option for ammonium removal in bioreactor landfills. *Waste Management*, *31*(11), 2287–2293. https://doi.org/10.1016/j.wasman.2011.06.012

Van Breukelen, B. M., & Griffioen, J. (2004). Biogeochemical processes at the fringe of a landfill leachate pollution plume: potential for dissolved organic carbon, Fe(II), Mn(II), NH4, and CH4 oxidation. *Journal of Contaminant Hydrology*, *73*(1–4), 181–205. https://doi.org/10.1016/J.JCONHYD.2004.01.001

Van Breukelen, B. M., Griffioen, J., Röling, W. F. M., & Van Verseveld, H. W. (2004). Reactive transport modelling of biogeochemical processes and carbon isotope geochemistry inside a landfill leachate plume. *Journal of Contaminant Hydrology*, *70*(3–4), 249–269. https://doi.org/10.1016/J.JCONHYD.2003.09.003

Van Der Salm, C., Köhlenberg, L., & De Vries, W. (1998). Assessment of weathering rates in Dutch loess and river-clay soils at pH 3.5, using laboratory experiments. *Geoderma*, *85*(1), 41–62. https://doi.org/10.1016/S0016-7061(98)00024-X

Van Der Sloot, H. A., & Dijkstra, J. J. (2004). *Development of horizontally standardized leaching tests for construction materials: a material based or release based approach? Identical leaching mechanisms for different materials*.

Van Der Sloot, H. A., Kosson, D. S., & Van Zomeren, A. (2017). Leaching, geochemical modelling and field verification of a municipal solid waste and a predominantly non-degradable waste landfill. *Waste Management*, *63*, 74–95. https://doi.org/10.1016/j.wasman.2016.07.032

Van Eynde, E., Weng, L., & Comans, R. N. J. (2020). Boron speciation and extractability in temperate and tropical soils: A multi-surface modeling approach. *Applied Geochemistry*, *123*, 104797. https://doi.org/10.1016/J.APGEOCHEM.2020.104797

van Raffe, F., Comans, R. N. J., & Groenenberg, J. E. (2025). Chromium(III) Binding to Purified Fulvic and Humic Acids and Their Solid-Solution Partitioning and Speciation in Soil. *ACS Earth and Space Chemistry*. https://doi.org/10.1021/acsearthspacechem.5c00075

van Raffe, F., Dijkstra, J. J., & Comans, R. N. J. (2025). Mechanisms controlling the release of inorganic contaminants, organic matter fractions, and ammonium from solid landfill waste: pH dependent leaching experiments and geochemical modelling. *Applied Geochemistry*, *190*, 106503. https://doi.org/10.1016/j.apgeochem.2025.106503

Van Raffe, F., Jin, R., Lammen, H., Dijkstra, J. J., & Comans, R. N. J. (2021). Sustainable landfill management in the Netherlands: application of geochemical modelling to characterise solid waste prior to (an)aerobic stabilization. *18th International Symposium on Waste Management, Resource Recovery and Sustainable Landfilling, 2021*. www.cisapublisher.com

Van Raffe, F., Quist, N., Kanen, T., & Comans, R. N. J. (2023). Sustainable landfill management in the Netherlands: Long term changes in landfill leachate quality during (an)aerobic in-situ stabilization. *19th International Symposium on Waste Management, Resource Recovery and Sustainable Landfilling, 2023*. www.cisapublisher.com

van Raffe, F., Quist, N., Rees-White, T. C., & Comans, R. N. J. (2026). Geochemical Processes Controlling In Situ Contaminant Solubility in Landfills. *ACS ES and T Water*, *6*(3), 1481–1490. https://doi.org/10.1021/acsestwater.5c00840

van Turnhout, A. G., Brandstätter, C., Kleerebezem, R., Fellner, J., & Heimovaara, T. J. (2018). Theoretical analysis of municipal solid waste treatment by leachate recirculation under anaerobic and aerobic conditions. *Waste Management*, *71*, 246–254. https://doi.org/10.1016/j.wasman.2017.09.034

Van Zomeren, A., & Comans, R. N. J. (2007). Measurement of humic and fulvic acid concentrations and dissolution properties by a rapid batch procedure. *Environmental Science and Technology*, *41*(19), 6755–6761. https://doi.org/10.1021/es0709223

van Zomeren, A., & Comans, R. N. J. (2007). Measurement of humic and fulvic acid concentrations and dissolution properties by a rapid batch procedure. *Environmental Science & Technology*, *41*(19), 6755–6761. https://doi.org/10.1021/es0709223

Van Zomeren, A., & Comans, R. N. J. (2009). Carbon speciation in municipal solid waste incinerator (MSWI) bottom ash in relation to facilitated metal leaching. *Waste Management*, *29*(7), 2059–2064. https://doi.org/10.1016/j.wasman.2009.01.005

Van Zomeren, A., Costa, A., Pinheiro, J. P., & Comans, R. N. J. (2009). Proton binding properties of humic substances originating from natural and contaminated materials. *Environmental Science and Technology*, *43*(5), 1393–1399. https://doi.org/10.1021/es801924x

Vaverková, M. D. (2019). Landfill impacts on the environment— review. In *Geosciences (Switzerland)* (Vol. 9, Number 10). MDPI AG. https://doi.org/10.3390/geosciences9100431

Vink, J. P. M., Harmsen, J., & Rijnaarts, H. (2010). Delayed immobilization of heavy metals in soils and sediments under reducing and anaerobic conditions; consequences for flooding and storage. *Journal of Soils and Sediments*, *10*(8), 1633–1645. https://doi.org/https://doi.org/10.1007/s11368-010-0296-1

Vink, J. P. M., van Zomeren, A., Dijkstra, J. J., & Comans, R. N. J. (2017). When soils become sediments: Large-scale storage of soils in sandpits and lakes and the impact of reduction kinetics on

heavy metals and arsenic release to groundwater. *Environmental Pollution*, *227*, 146–156. https://doi.org/10.1016/J.ENVPOL.2017.04.016

Vinokurov, E. G., & Bondar', V. V. (2003). Prediction of Stability Constants for Cr(III) and Cr(II) Complexes. *Russian Journal of Coordination Chemistry/Koordinatsionnaya Khimiya*, *29*(1), 66–72. https://doi.org/10.1023/A:1021851219309

Vlek, P. L. G., & Lindsay, W. L. (1977). Thermodynamic Stability and Solubility of Molybdenum Minerals in Soils. *Soil Science Society of America Journal*, *41*(1), 42–46. https://doi.org/10.2136/sssaj1977.03615995004100010016x

Wall, N. A., & Choppin, G. R. (2003). Humic acids coagulation: Influence of divalent cations. *Applied Geochemistry*, *18*(10), 1573–1582. https://doi.org/10.1016/S0883-2927(03)00046-5

Wang, F., & Tessier, A. (1999). Cadmium complexation with bisulfide. *Environmental Science and Technology*, *33*(23), 4270–4277. https://doi.org/10.1021/ES990283Z/SUPPL_FILE/ES990283Z_S.PDF

Wang, H., Yuan, Y., Tan, W., Zhang, J., Gong, X., Li, Y., Hui, K., Chen, H., & Xi, B. (2024). New insight into the functional group mechanism and structure-activity relationship of the complexation between DOM and Cr(III) in landfill leachate. *Journal of Hazardous Materials*, *466*, 133210. https://doi.org/10.1016/J.JHAZMAT.2023.133210

Wang, L., & Heimovaara, T. J. (2025). Quantifying Landfill Emission Potential Using a Weakly Coupled Particle Filter. *Water Resources Research*, *61*(2), e2023WR036549. https://doi.org/10.1029/2023WR036549

Wang, L. W. (2012). High chalcocite Cu 2S: A solid-liquid hybrid phase. *Physical Review Letters*, *108*(8). https://doi.org/10.1103/PhysRevLett.108.085703

Wang, Q., Zhu, C., Yun, J., & Yang, G. (2017). Isomorphic Substitutions in Clay Materials and Adsorption of Metal Ions onto External Surfaces: A DFT Investigation. *Journal of Physical Chemistry C*, *121*(48), 26722–26732. https://doi.org/https://doi.org/10.1021/acs.jpcc.7b03488

Wen, J., Li, Z., Huang, B., Luo, N., Huang, M., Yang, R., Zhang, Q., Zhai, X., & Zeng, G. (2018). The complexation of rhizosphere and nonrhizosphere soil organic matter with chromium: Using elemental analysis combined with FTIR spectroscopy. *Ecotoxicology and Environmental Safety*, *154*, 52–58. https://doi.org/10.1016/j.ecoenv.2018.02.014

Weng, L., Temminghoff, E. J. M., Lofts, S., Tipping, E., & Van Riemsdijk, W. H. (2002). Complexation with dissolved organic matter and solubility control of heavy metals in a sandy soil. *Environmental Science and Technology*, *36*(22), 4804–4810. https://doi.org/10.1021/ES0200084/SUPPL_FILE/ES0200084_S.PDF

Weng, L., Temminghoff, E. J. M., & Van Riemsdijk, W. H. (2001). Contribution of individual sorbents to the control of heavy metal activity in sandy soil. *Environmental Science and Technology*, *35*(22), 4436–4443. https://doi.org/10.1021/ES010085J/SUPPL_FILE/ES010085J_S.PDF

Weng, L., Temminghoff, E. J. M., & Van Riemsdijk, W. H. (2002a). Aluminum speciation in natural waters: measurement using Donnan membrane technique and modeling using NICA-Donnan. *Water Research*, *36*, 4215–4226. https://doi.org/https://doi.org/10.1016/S0043-1354(02)00166-5

Weng, L., Temminghoff, E. J. M., & Van Riemsdijk, W. H. (2002b). Interpretation of humic acid coagulation and soluble soil organic matter using a calculated electrostatic potential. *European Journal of Soil Science*, *53*(4), 575–588. https://doi.org/10.1046/j.1365-2389.2002.00455.x

Weng, L., Van Riemsdijk, W. H., & Temminghoff, E. J. M. (2005). Kinetic aspects of Donnan membrane technique for measuring free trace cation concentration. *Analytical Chemistry*, *77*(9), 2852–2861. https://doi.org/10.1021/ac0485435

Weng, L., Vega, F. A., & Van Riemsdijk, W. H. (2011). Competitive and synergistic effects in pH dependent phosphate adsorption in soils: LCD modeling. *Environmental Science and Technology*, *45*(19), 8420–8428. https://doi.org/10.1021/es201844d

White, J. K., Beaven, R. P., Powrie, W., & Knox, K. (2011). Leachate recirculation in a landfill: Some insights obtained from the development of a simple 1-D model. *Waste Management*, *31*(6), 1210–1221. https://doi.org/10.1016/j.wasman.2010.10.022

Whitworth, T. M. (1998). Clay minerals: Ion exchange. *Geochemistry*, 85–87. https://doi.org/10.1007/1-4020-4496-8_56

Wiersma, W., Van Eynde, E., Comans, R. N. J., & Groenenberg, J. E. (2025). Quantifying the Accuracy, Uncertainty, and Sensitivity of Soil Geochemical Multisurface Models. *Environmental Science and Technology*. https://doi.org/10.1021/acs.est.4c04812

Wijekoon, P., Koliyabandara, P. A., Cooray, A. T., Lam, S. S., Athapattu, B. C. L., & Vithanage, M. (2022). Progress and prospects in mitigation of landfill leachate pollution: Risk, pollution potential, treatment and challenges. *Journal of Hazardous Materials*, *421*, 126627. https://doi.org/10.1016/J.JHAZMAT.2021.126627

Wolkersdorfer, C. (2008). Water management at abandoned flooded underground mines: Fundamentals, tracer tests, modelling, water treatment. In *Water Management at Abandoned Flooded Underground Mines: Fundamentals, Tracer Tests, Modelling, Water Treatment*. Springer Berlin Heidelberg. https://doi.org/10.1007/978-3-540-77331-3

Wu, C., Shimaoka, T., Nakayama, H., Komiya, T., Chai, X., & Hao, Y. (2014). Influence of aeration modes on leachate characteristic of landfills that adopt the aerobic–anaerobic landfill method. *Waste Management*, *34*(1), 101–111. https://doi.org/10.1016/J.WASMAN.2013.10.015

Xiao, F., Zhang, B., & Lee, C. (2008). Effects of low temperature on aluminum(III) hydrolysis: Theoretical and experimental studies. *Journal of Environmental Sciences*, *20*(8), 907–914. https://doi.org/10.1016/S1001-0742(08)62185-3

Xiong, J., Koopal, L. K., Tan, W., Fang, L., Wang, M., Zhao, W., Liu, F., Zhang, J., & Weng, L. (2013). Lead binding to soil fulvic and humic acids: NICA-donnan modeling and XAFS spectroscopy. *Environmental Science and Technology*, *47*(20), 11634–11642. https://doi.org/10.1021/es402123v

Xu, J., Tan, W., Xiong, J., Wang, M., Fang, L., & Koopal, L. K. (2016). Copper binding to soil fulvic and humic acids: NICA-Donnan modeling and conditional affinity spectra. *Journal of Colloid and Interface Science*, *473*, 141–151. https://doi.org/10.1016/J.JCIS.2016.03.066

Xu, Y., Bai, Y., Hiemstra, T., Tan, W., & Weng, L. (2020). Resolving humic and fulvic acids in binary systems influenced by adsorptive fractionation to Fe-(hydr)oxide with focus on UV–Vis analysis. *Chemical Engineering Journal*, *389*. https://doi.org/10.1016/j.cej.2020.124380

Yan, M., Ma, J., & Ji, G. (2016). Examination of effects of Cu(II) and Cr(III) on Al(III) binding by dissolved organic matter using absorbance spectroscopy. *Water Research*, *93*, 84–90. https://doi.org/10.1016/j.watres.2016.02.017

Yan, Y., Wan, B., Jiang, R., Wang, X., Wang, H., Lan, S., Zhang, Q., & Feng, X. (2023). Interactions of organic phosphorus with soil minerals and the associated environmental impacts: A review. *Pedosphere*, *33*(1), 74–92. https://doi.org/10.1016/J.PEDSPH.2022.08.001

Yang, S., & Yang, G. (2024). Selective adsorption and release of the ammonium ion (NH4+) at smectites/water interfaces. *Separation and Purification Technology*, *339*(6568), 126662. https://doi.org/10.1016/j.seppur.2024.126662

Yang, Z., Zhang, X., Jiang, Z., Li, Q., Huang, P., Zheng, C., Liao, Q., & Yang, W. (2021). Reductive materials for remediation of hexavalent chromium contaminated soil – A review. *Science of the Total Environment*, *773*. https://doi.org/10.1016/j.scitotenv.2021.145654

Yechiel, A., & Shevah, Y. (2016). Optimization of energy generation using landfill biogas. *Journal of Energy Storage*, *7*, 93–98. https://doi.org/10.1016/J.EST.2016.05.002

Yi, S., Meza, N., & Gebert, J. (2025). Application of the nitrogen-to-argon ratio to understand nitrogen transformation pathways in landfills under in-situ stabilization. *Waste Management*, *194*, 13–23. https://doi.org/10.1016/j.wasman.2024.12.042

Yin, Q., Si, L., Wang, R., Zhao, Z., & Li, H. (2022). Influence of the defect of carbonaceous surface on ammonium adsorption: A DFT study. *Fuel*, *325*. https://doi.org/10.1016/j.fuel.2022.124873

Yu, Z. G., Göttlicher, J., Steininger, R., & Knorr, K. H. (2016). Organic sulfur and organic matter redox processes contribute to electron flow in anoxic incubations of peat. *Environmental Chemistry*, *13*(5), 816–825. https://doi.org/10.1071/EN15091

Zeng, Y., De Guardia, A., Ziebal, C., De Macedo, F. J., & Dabert, P. (2012). Nitrification and microbiological evolution during aerobic treatment of municipal solid wastes. *Bioresource Technology*, *110*, 144–152. https://doi.org/10.1016/J.BIORTECH.2012.01.135

Zhang, H., He, P. J., Shao, L. M., & Li, X. J. (2008). Leaching behavior of heavy metals from municipal solid waste incineration bottom ash and its geochemical modeling. *Journal of Material Cycles and Waste Management*, *10*(1), 7–13. https://doi.org/10.1007/S10163-007-0191-Z/METRICS

Zhang, L., Wang, S., Jiao, L., Li, Y., Yang, J., Zhang, R., Feng, S., & Wang, J. (2016). Effects of organic matter content and composition on ammonium adsorption in lake sediments. *Environmental Science and Pollution Research*, *23*(7), 6179–6187. https://doi.org/10.1007/s11356-015-5820-9

Zhao, S., Zheng, Q., Wang, H., & Fan, X. (2024). Nitrogen in landfills: Sources, environmental impacts and novel treatment approaches. *Science of The Total Environment*, *924*, 171725. https://doi.org/10.1016/J.SCITOTENV.2024.171725

Ziegler, F., & Johnson, C. A. (2001). *The solubility of calcium zincate (CaZn2(OH)6*2H2O)*.

SUMMARY

Waste generation is increasing globally. Governments are striving to manage the generated waste via sustainable strategies such as recycling, yet a share of (untreatable) waste needs to be landfilled. Landfilled waste may lead to adverse impacts on human health and the environment, as landfills are a significant source of the greenhouse gas methane and of leachate rich in contaminants. Such adverse impacts are traditionally reduced via sealing of the waste with impermeable barriers together with capture and treatment of the gas and leachate; an effective method, yet in which degradation processes are halted and the potential to pollute remains. Consequently, costs of replacing the barrier and treating the leachate are shifted to future generations. A potentially more sustainable method of landfill management is to instead actively stabilize the waste via active introduction of air (aeration) or recirculation of the leachate (leachate recirculation). This so-called 'active treatment' intends to either degrade, flush, or retain contaminants, to a point where the waste ultimately no longer poses a threat to the environment.

To assess the potential of active treatment, three Dutch landfill-scale pilots were instigated with the infrastructure to extensively monitor changes in gas quality, leachate quality, and changes in the solid waste. This thesis specifically focused on changes in leachate quality during active treatment and aimed to elucidate the underlying geochemical mechanisms. This was done by conducting experiments from the lab- to the field scale, for each scale identifying the main controlling parameters. The lab experiments were supported by multi-surface geochemical model calculations – calculations which combine models predicting ion-binding to reactive surfaces (clay, metal (hydr)oxides, organic matter) with a thermodynamic database to calculate inorganic speciation and mineral precipitation. Thus, the distribution of contaminants across different chemical species could be identified, which can be linked to processes controlling contaminant solubility.

Mechanisms were first identified in chapter 2 in the most well-defined lab set-up: the pH-dependent test. The pH-dependent solubility of contaminants was determined experimentally, which was supported by geochemical model calculations to identify three distinct contaminant groups: non-reactive contaminants, reactive anions, and reactive cations. Non-reactive contaminants had only limited interaction with the solid waste and did not show any pH-dependent solubility. Reactive ions did have a pH-dependent solubility, with a maximum solubility around the upper and lower ends of the pH range. Reactive anions had a minimum solubility around pH 5, steered by binding to metal (hydr) oxides. Reactive cations had a minimum solubility at varying pH, based on the cations' tendency to hydrolyse (resulting in a solubility minimum at higher pH) and their affinity to bind to organic matter (OM) (resulting in a solubility minimum at lower pH). The mechanisms steering solubility varied between reactive cations and included binding to OM, binding to metal (hydr)oxides, and the formation of mineral precipitates. Ammonium

(NH_4^+) surprisingly showed behaviour akin to a reactive cation with a solubility minimum around pH 8. The distinction between non-reactive contaminants, reactive anions, and reactive cations formed the basis of contaminant behaviour interpretation in the next chapters. Additionally, a discrepancy was observed between geochemical model calculations and experimental results for NH_4^+, due to the absence of binding parameters, and chromium (Cr), likely due to poor OM-binding parameters.

A first step in improving model calculations was taken in chapter 3, where new OM-binding parameters were derived for Cr. Adsorption experiments were conducted where at different pH levels and in the presence of humic- or fulvic acid, the solution was titrated with Cr and free Cr was measured to determine total adsorption. This data was used to fit NICA-Donnan parameters, which could only be done by considering the binding of the free Cr^{3+} species and the binding of $Cr_2(OH)_2^{4+}$. The derived parameters were compared against the originally existing parameters using three independent datasets. The newly derived parameters showed a significant improvement in predicting Cr binding to specific OM fractions, and in predicting free Cr concentrations. However, in soil samples marked with low amounts of (dissolved) OM, binding of Cr was underestimated and the prediction of dissolved Cr worsened when compared to predictions using the original parameter set. It was thus concluded that the newly derived Cr parameters were a significant improvement in predicting environmental Cr speciation, yet that care should be taken when applying the parameters to low OM environments.

On a larger scale than the pH-dependent test, 60L landfill simulation reactors containing waste from all three landfills were applied to identify effects of leachate recirculation, aeration, and their combination on contaminant solubility in chapter 4. Leachate recirculation was marked by strongly reduced conditions, where dissolved OM concentrations were stable and pH increased. Based on their identified pH-dependent solubility, the change in pH resulted in an increase for most contaminants due to hydrolyzation and mineral dissolution. Contrary to the pH-dependent test, the landfill simulation reactors supported by geochemical modelling identified that for several contaminants, i.e. Cd, Cu, Fe, Mn, and Zn, their solubility was steered by the formation of sulphide minerals. Aeration resulted in oxidized conditions, decreased dissolved OM, and decreased pH. The oxidized conditions led to a dissolution of sulphide minerals with a corresponding increased solubility of associated elements, which subsequently decreased as other mineral precipitates were formed or the elements bound to different reactive surfaces. Ammonium concentrations strongly decreased during aeration as the presence of oxygen allowed for the process of nitrification and NH_4^+ was transformed to nitrate. The landfill simulation reactors ultimately showed the importance of redox conditions, and that in active treatment there is a precarious balance, and switching treatments and changing redox conditions may lead to a decrease in some contaminants and an increase in others.

Solubility of contaminants was finally explored on the landfill scale in chapter 5 by sampling pore water from one of the landfills using vadose monitoring systems. A high covariance could be observed between the different parameters. Concentrations of dissolved OM and contaminants increased with depth yet sharply decreased below 12 metres, likely due to the presence of an impermeable layer. By combining the insights of the previous chapters and estimating solid waste properties based on solid waste extractions, the geochemical model could capture these trends well for most contaminants. Thus, the importance of binding to specific reactive surfaces, formation of minerals, and importance of redox could be coupled to specific contaminants, and their concentrations could be well-predicted based mostly on measurements of pH and dissolved OM. This shows the applicability of geochemical models to identify contaminant speciation even in such complex systems.

Finally, all content chapters were synthesized in chapter 6, and their findings were outlined against the overall research goal of elucidating mechanisms underlying contaminant solubility in landfills. A reflection was made of the used methodologies in this thesis, particularly regarding the investigation of the different scales (what scales tell what) and the different assumptions made and problems encountered when applying the multi-surface model. Considering the poor model description of NH_4^+ in the different content chapters, an attempt was made at improving this description by performing NH_4^+-OM adsorption experiments and by modelling pH-dependent NH_4^+ solubility considering selective binding to clay; particularly the latter proved promising for future studies. The implications of this thesis' findings for active treatment were discussed by interpreting changes in leachate quality of the full treated landfills and by discussing the criteria for when a landfill can be considered safe for the environment. Ultimately, this thesis' findings show the potential and the pitfalls when actively treating landfill waste to reduce contaminant emissions.

AUTHORSHIP STATEMENT

Chapter 1: I was introduced to sustainable landfilling by my promotor (Rob N.J. Comans). I developed an understanding of the issues regarding sustainable landfilling together with him and my colleague PhD in the project (Nick Quist). I wrote the initial draft, and revised the general introduction once after comments of my promotor.

Chapter 2: Following from previous research conducted by TNO, and a model set-up devised together with a MSc student I supervised (Runwen Jin), I set up a new experiment together with my co-author (Joris J. Dijkstra) and promotor (Rob N.J. Comans) and following their advice conducted the new experimental work and modelling implementation myself. I wrote the initial draft myself, and revised the text several times after feedback of both co-authors.

Chapter 3: The original set-up and idea of the experiments were set up by my co-author and co-supervisor (Jan E. Groenenberg). Following the initial experimental set-up, I set-up the model to conduct model fits and performed the data analysis. I wrote the first draft alone, and revise the draft twice based on feedback from both co-authors (Jan E. Groenenberg and Rob N.J. Comans).

Chapter 4: Experimental set-up was designed by co-author (Nick Quist), with contribution from me and co-author Rob N.J. Comans). Experimental work was conducted by co-author (Nick Quist) with assistance from me. I conducted the modelling work, wrote the original draft with first major feedback from co-author (Nick Quist). The draft was revised twice by me and co-author (Nick Quist) following feedback from co-authors (Joris J. Dijkstra and Rob N.J. Comans).

Chapter 5: Original pore water sampling infrastructure was placed by co-author (Tristan C. Rees-White). Sampling and sample analysis were conducted by me and co-author (Nick Quist). I conducted the modelling, and data analysis and writing of initial draft were conducted by me and co-author (Nick Quist). The initial draft was revised twice after feedback from co-author (Rob Comans).

Chapter 6: I conducted experimental work of ammonium adsorption experiment, modelled results, and conducted data analysis throughout the general discussion. I wrote the initial draft, which was revised once after feedback from supervisor (Rob N.J. Comans).

AFFILIATION OF CO-AUTHORS

The affiliation of the co-authors of the various chapters of this thesis at the time of their contribution are:

Nick Quist

Soil Chemistry Group, Wageningen University & Research, 6708 PB Wageningen, The Netherlands

Rob N.J. Comans

Soil Chemistry Group, Wageningen University & Research, 6708 PB Wageningen, The Netherlands

Jan E. Groenenberg

Soil Chemistry Group, Wageningen University & Research, 6708 PB Wageningen, The Netherlands

Joris J. Dijkstra

Netherlands Organisation for Applied Scientific Research, Geological Survey of the Netherlands, 3508 TA Utrecht, the Netherlands

Tristan C. Rees-White

Faculty of Engineering and Physical Sciences, University of Southampton, SO16 7QF Southampton, United Kingdom

ACKNOWLEDGEMENTS

Creating this thesis was a journey of many years, and one that I am confident I would not have finished if I had to do it all by myself. I therefore want to express my sincerest gratitude to everyone who accompanied me along the way.

I would firstly like to thank my supervisory team for their guidance and instruction. Rob, thank you for all the detailed discussions, for all the inspiration, and for allowing me to take up a significant teaching portion for the entire duration. I really appreciate how you both tried to push me to make the most out of my PhD and simultaneously took care that I was not straining myself too far. A thank you also to Timo; even if I somehow managed to avoid you for most of my PhD, I still want to thank you for your initial trust and the interesting discussions and inputs you gave me throughout the years. Thank you, Bert-Jan, for guiding me along the modelling components of my PhD. You taught me a lot, and I was happy to be teaching the Applications course together for the past years. Finally, while not an official part of my supervisory team, I also want to thank Joris for contributing to two very important papers and always being willing and excited to discuss geochemistry and modelling.

Next, I would like to thank all the colleagues at the soil chemistry chair group. The PhD's, for the inspiring discussions about soil chemistry and all sorts of other topics, the fun lunches, and for all the other social activities to make the tough PhD life a lot more bearable. The staff, who accepted me in their midst and allowed me to follow my passion of teaching already during the PhD. The lab staff, who were always keen to help during all the data collection, even if I probably sent some of the most difficult samples to analyse (I promise I will do no further pH-dependent tests). A specific shoutout to my office roommates during the PhD. Maarten, thank you for being an amazing student and an even better colleague; you make me feel impressively stupid by your amount of knowledge on virtually everything. And of course, thank you Nick. We already had some excellent group work together during our studies, and I am happy that could be extended throughout our PhDs. It made these past years a lot more social, productive, hectic, and most of all enjoyable. I hope you are as proud of the work we achieved together as I am.

A big thank you to everyone associated with CURE and iDS. For making this entire research possible. For travelling to the Sardinia conferences together; they were always a blast. For all the discussions on landfills, the on-going research, but also all sorts of other titbits. It was a joy working together with all of you over the past years on this enormous project.

For the final work-related thank you's, I want to thank my newest colleagues at NMI. Thank you for providing me with a new adventure following my PhD (even when my PhD

had not finished yet). I am excited to see where that adventure will take me in the coming years.

Thankfully, these past years were not only dedicated to the PhD and work. Therefore I also want to thank all those who made the days more pleasant outside of working hours.

A major thank you to everyone at the Bongerd, where I spent an unhealthy amount of time during- and outside of working hours. To all the teachers for organizing amazing sports classes, and for the other regulars who joined the classes; the enthusiasm made for a perfect (and tiring) break from all the modelling, lab, and writing work.

Another thank you to the education and volunteering crew at Burgers Zoo, for providing an outlet for me to share trivia about animals to unsuspecting victims. A specific shoutout to the Ede carpool gang enduring my tagging along and me always being two minutes late, the rides there and back are always a ton of fun. And of course a shoutout to the bus gang, even if the bus travel has ceded quite a while ago. Our zoo trips are some of the most fun parts of my year, even considering all the clumsiness and gift shops. So many gift shops.

Of course a big thanks to all the friends who are not really a part of any specific group. I would like to thank you for all the time you spent with me playing board games, doing sports, or going on random trips visiting museums, zoos, natural areas, and all sorts of other stuff. A particularly big thanks to Aafke. We started our PhD journey and our cycling career together. I hope you will soon finish your journey also, and that we can ride our bike a lot more in the future.

Aside from my friends, I also want to thank my family. Thank you mom and dad, for putting up with all my nonsense and supporting me through thick and thin. We are not a very expressive sort, but it really means the world to me to know that there is always someone to rely one when things do not work out. And also that every weekend and every vacation period you are open (and enthusiastic) to undertake all sorts of random activities. And of course thank you JJ, for always being there to help out when needed, for being very reticent, but also very open to undertake random adventures.

And finally thank you Lotte. I am very happy we got to know each other. It was already a great friendship during our studies, and I am grateful for all the support you gave me through the hard times and all the joy you gave me during the happy times.

To the unmentioned people who played a role in my life, for good or for bad, I am grateful, as it shaped me to be the person I am now.

ABOUT THE AUTHOR

Frank van Raffe was born in Wageningen, the Netherlands, on September 19th 1996. In an endeavour to see as little of the world as possible, Frank finished his primary and secondary school in Wageningen and subsequently started the BSc "Soil, Water, Atmosphere" in Wageningen. While there was a short detour to Sweden for a minor in Geology at Gothenburg University, Frank continued his education following the MSc "Earth & Environment", taking courses focused specifically on chemical quality of soil and water. He was particularly interested in geochemical modelling and chemical speciation calculations, and this interest was furthered by his MSc thesis. There, he explored how variations in the experimental procedure of the calcium chloride extraction influenced extractability of copper and zinc, with a specific focus on geochemical modelling. During his MSc, Frank additionally took part in the WIMEK honours programme and wrote a research proposal on sustainable landfilling that would sadly not be granted. Luckily, funding was available from the soil chemistry group, and Frank started his PhD on his proposal topic at the end of 2019, just before the COVID-19 outbreak. One year later, the PhD was transformed and Frank stepped into the CURE project, embedding the original topic into a larger research project which would ultimately lead to this dissertation. In addition to the laborious PhD work, Frank spent time teaching several BSc and MSc courses and taking up the role as a PhD representative in the soil chemistry group. Starting from 2025, Frank works as a lecturer at the soil chemistry group and as a project lead at the Nutrient Management Institute.

Netherlands Research School for the
Socio-Economic and Natural Sciences of the Environment

D I P L O M A

for specialised PhD training

The Netherlands research school for the
Socio-Economic and Natural Sciences of the Environment
(SENSE) declares that

Frank van Raffe

born on 1996-09-19 in Wageningen, the Netherlands

has successfully fulfilled all requirements of the
educational PhD programme of SENSE.

Wageningen, 8 October 2026

SENSE coordinator PhD education



Dr Ir Peter Vermeulen

The SENSE Director



Dr Jampel Dell'Angelo

The SENSE Research School declares that **Frank van Raffe** has successfully fulfilled all requirements of the educational PhD programme of SENSE with a workload of **39.6 ECTS**, including the following activities:

Academic knowledge and skills

o Ecotoxicology (2021)	University of Amsterdam and WUR
o Speciation and bioavailability of metals, organics, and nanoparticles (2022)	University of Antwerp and WUR
o Oral Presentation: Sustainable landfill management in the Netherlands: application of geochemical modelling to characterise solid waste prior to (an)aerobic stabilization (2021)	8th international symposium on waste management and sustainable landfilling, Cagliari, Italy
o Oral presentation: pH dependent tests & Geochemical modelling to predict contaminant mobilization (2023)	Landfill In-situ stabilization workshop, Wageningen
o Oral presentation: Vertical heterogeneity of contaminants in the pore water of a municipal solid waste landfill subject to leachate recirculation (2023)	9th international symposium on waste management and sustainable landfilling, Cagliari, Italy
o Oral presentation: Cr3+ binding to purified fulvic and humic acid and its solid-solution partitioning and speciation in soils (2024)	Interfaces against pollution, Turin, Italy
o Poster presentation: The effect of pH on dissolved organic matter and associated contaminants in solid waste (2023)	Wageningen Soil Conference
o Poster presentation: Long term changes in landfill leachate quality during (an)aerobic in-situ stabilization (2023)	9th international symposium on waste management and sustainable landfilling, Cagliari, Italy

Effective research management (including Integrity and Ethics)

o Critical Thinking and Argumentation (2021)	WUR

Transferable Professional Skills

o Environmental Research in Context (2020)	WUR
o Effective behaviour in your professional surroundings (2021)	WUR
o Supervising BSc and MSc students (2022)	WUR
o Organizsation of stakeholder workshop (2023)	

Societal impact

o A2: pathways to impact (2025)	WUR
o Supervising two Msc students (2020-2022) and one BSc student with thesis Sc thesis (2023)	WUR
o Teaching course Soil Quality (2020 - 2023)	WUR
o Teaching Chemical processes in soil, water, atmosphere (2020 - 2023)	WUR
o Teaching Applications in Soil and Water Chemistry (2020 - 2026)	WUR

Career perspectives

o Career perspectives (2024)	WUR

The research described in this thesis was financially supported by the Dutch National Science Foundation (NWO) under project no. OCENW.GROOT.2019.O92.

Financial support from Wageningen University for printing this thesis is gratefully acknowledged.

Cover design by Lotte Stokkermans

Layout and printing by proefschriftmaken.nl

